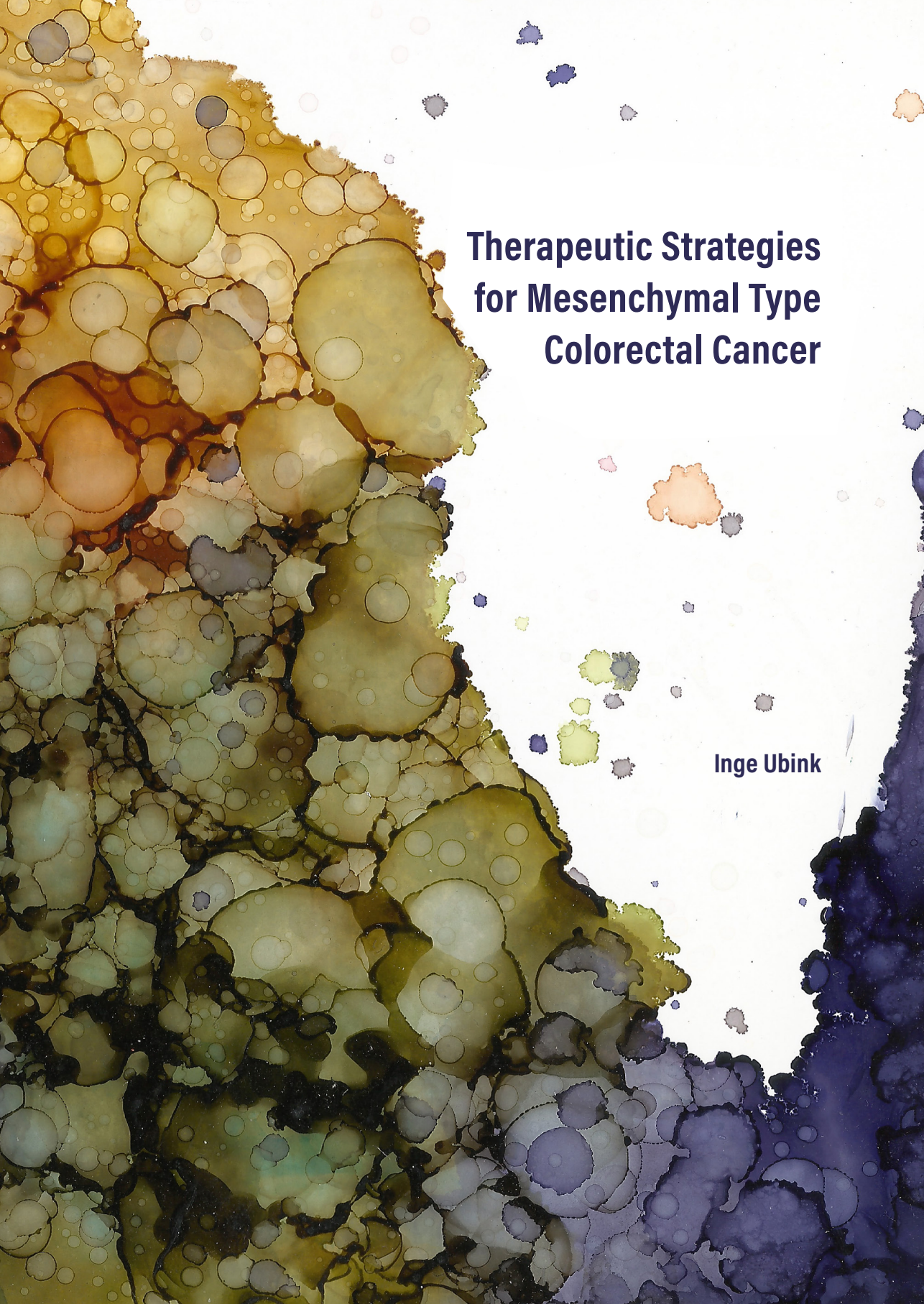

Therapeutic Strategies for Mesenchymal Type Colorectal Cancer

Inge Ubink

Therapeutic Strategies for Mesenchymal Type Colorectal Cancer

Inge Ubink

Therapeutic Strategies for Mesenchymal Type Colorectal Cancer

ISBN/EAN: 978-94-6380-729-6

Cover art by Daphne Costopoulos, DC Artwork
Layout by Wendy Schoneveld || www.wenzid.nl
Printed by ProefschriftMaken || proefschriftmaken.nl

The research presented in this thesis was financially supported by the Dutch Cancer Society (KWF grant UU2014-6617) and ZonMw (PTO 95104001).

Financial support for printing of this thesis was kindly provided by UMCU Cancer Center, Chirurgie Jeroen Bosch Ziekenhuis and IF.

Therapeutic Strategies for Mesenchymal Type Colorectal Cancer

Strategieën voor de behandeling van
dikke darmkanker van het mesenchymale subtype

(met een samenvatting in het Nederlands)

Proefschrift

ter verkrijging van de graad van doctor aan de Universiteit Utrecht
op gezag van de rector magnificus, prof.dr. H.R.B.M. Kummeling,
ingevolge het besluit van het college voor promoties
in het openbaar te verdedigen op

donderdag 12 maart 2020 des middags te 2.30 uur

door

Inge Ubink

geboren op 9 juni 1988
te Leiderdorp

Promotoren
Prof. dr. I.H.M. Borel Rinkes
Prof. dr. O.W. Kranenburg

Copromotoren
Dr. S.G. Elias
Dr. J. Hagendoorn

Table of Contents

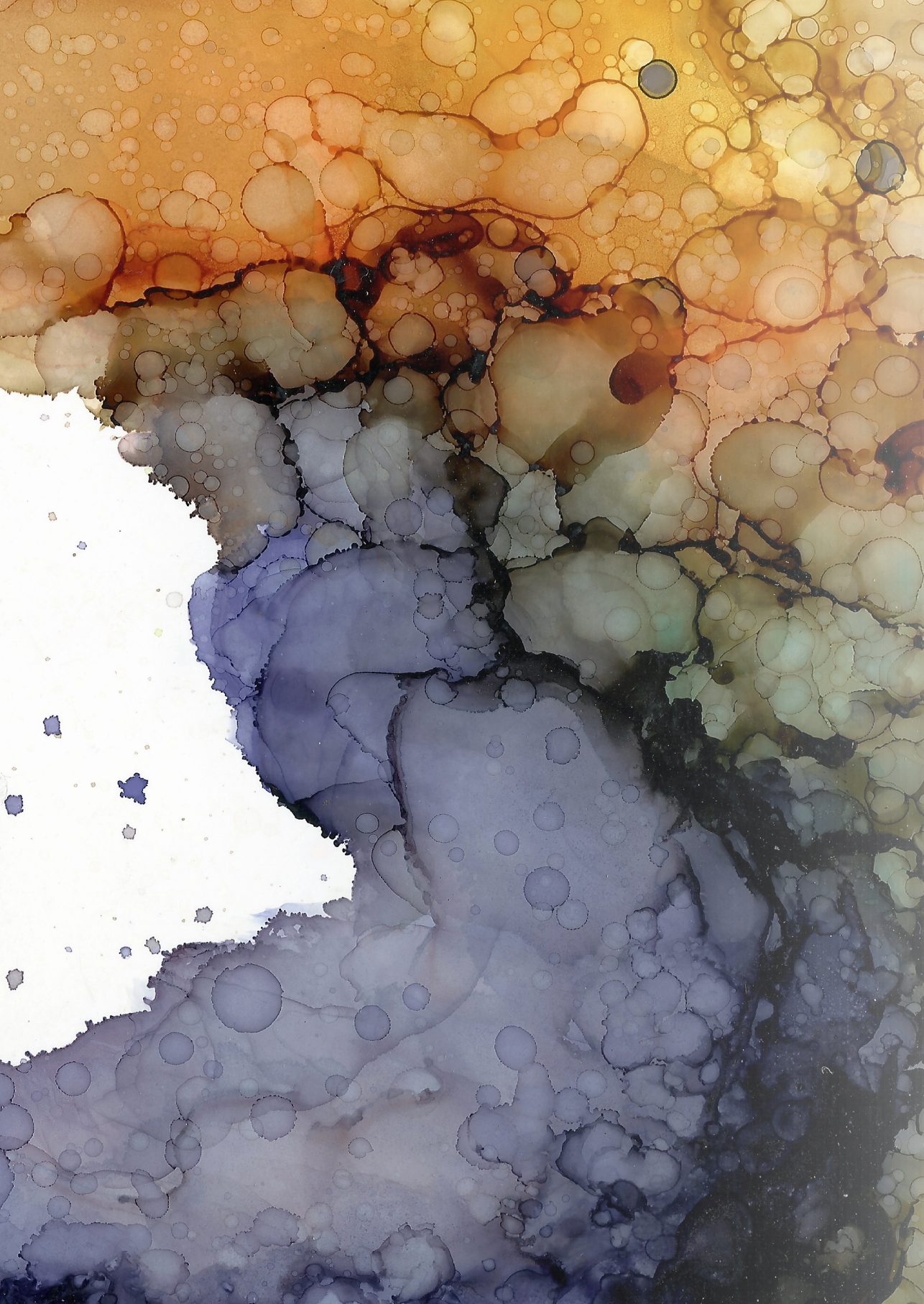

1

Introduction and thesis outline

INTRODUCTION

Treatment stratification in colorectal cancer

In the Netherlands, more than 14,000 people were diagnosed with colorectal cancer (CRC) in 2018, and over 5,000 patients died of this disease.[1] Worldwide, 1 in 10 cancer-related deaths are due to CRC.[2] The prognosis of patients with CRC largely depends on the progression of the disease at diagnosis. Disease progression is described by the Tumor – Node – Metastasis (TNM) classification, which combines the extent of invasion through the bowel wall, spread to locoregional lymph nodes and the presence of distant metastases to distinguish four stages of CRC. In stages I and II regional and distant metastases are absent; however invasion of the tumor through the bowel wall is more advanced in stage II. Stage III indicates the presence of lymph node metastases, and in stage IV disease has spread to distant organs.[3] These stages are strongly correlated with prognosis, with 5-year survival of 94% in patients with stage I CRC and only 12% in patients with stage IV CRC (Table 1).[1]

Table 1. Current prognosis for CRC.

TNM stage	**Incidence at presentation[1,*]**	**5-year recurrence risk[6]**	**5-year survival rate[1]**
Stage I: T1-2 N0 M0	19%	5%	94%
Stage II: T3-4 N0 M0	25%	12%	85%
Stage III: Any T N1-2 M0	31%	33%	72%
Stage IV: Any T, any N, M1	22%	-	12%

*Stage at presentation not registered in 3% of cases

Adjuvant chemotherapy is used to reduce the recurrence risk after primary cancer resection, with the aim of eliminating undetected (micrometastatic) disease. Because chemotherapy causes significant morbidity and even mortality[4], it is only offered to patients with high risk of recurrence. In general, recurrence risk increases with TNM stage (Table 1), and adjuvant chemotherapy is recommend for patients with stage III CRC and for a subgroup in stage II with additional risk factors (i.e. clinical presentation with intestinal occlusion or perforation, fewer than 12 lymph nodes sampled during resection, pT4, poorly differentiated tumors, and/or vascular or perineural invasion).[5]

Administration of adjuvant chemotherapy significantly lowers the recurrence risk. In a pooled analysis of patient cohorts and clinical trials, 5-year disease-free survival in stage III CRC improved from 49% in patients treated exclusively with surgery to 64% in patients treated with surgery and adjuvant chemotherapy.[7] These figures also indicate however, that

only half of the patients with stage III disease are at risk for developing metastases, meaning that there is substantial overtreatment. Moreover, a significant group of patients will still develop metastases despite the adjuvant therapy.[8] The diversity with respect to prognosis and therapeutic response illustrates that CRC is a highly heterogeneous disease, and that this heterogeneity is insufficiently captured in the current staging system. It further shows that current adjuvant treatment regimens are often ineffective. To increase survival rates, better risk stratification and alternative therapeutic strategies are needed.

Challenge

I. Identify early-stage CRC patients who are at risk for developing metastases
II. Stratify these at risk patients for appropriate adjuvant therapy

Transcriptome-based stratification

Numerous genetic and molecular characteristics of CRC have been proposed to improve prognostications and therapy allocation. In spite of the vast amount of research on genetic aberrations, only a single marker has been implemented for stratification of adjuvant therapy. Current guidelines advise assessment of mismatch repair status in stage II/III CRC, as microsatellite instable (MSI) tumors do not benefit from adjuvant chemotherapy with 5-fluorouracil.[5]

Several multigene expression assays have been developed that provide prognostic information in stage II and III CRC, including Oncotype DX colon cancer assay, Coloprint and ColDx.[9-11] Even though each of these tests has been clinically validated, and distinguishes groups with high and low risk of recurrence independent of other risk factors, they are not currently used for treatment stratification. The major limitation of these tests is that they do not provide leads on how to treat these 'high-risk' patients. The gene signatures do not reflect targetable signaling pathways, and have no predictive value in terms of chemotherapy benefit.[9]

The multigene assays were established in a biased fashion, by comparing gene expression profiles between patients with and without recurrence. The resulting gene sets provided little insight into the biology of CRC. Multiple research groups have undertaken unsupervised clustering approaches to determine the presence of molecular subtypes with distinct biological characteristics. These studies resulted in classifiers with three to six intrinsic molecular subtypes.[12-17] Their efforts were later combined by the CRC Subtyping Consortium, which has led to the discovery of four robust **Consensus Molecular Subtypes (CMSs)**.[18]

Stratification according to CMS could become a tool for guiding patient management, as it contributes to our understanding of disease and response heterogeneity in three ways:

1. Biological insights

The four subtypes show differences in activated signaling pathways, but also in terms of structural chromosomal abnormalities, epigenetics and mutational signatures. Furthermore, the subtypes are variably infiltrated with non-neoplastic cells. CMS1 tumors often show MSI, BRAF mutations, and profound infiltration with immune cells. CMS2 tumors express many genes classically implicated in CRC carcinogenesis and is therefore termed the 'canonical subtype'. CMS3 is characterized by prominent metabolic alterations and KRAS mutations are common. CMS4 cancers are rich in stromal cells, and epithelial-to-mesenchymal transition (EMT) genes, transforming growth factor (TGF)-β signaling, angiogenesis, and matrix remodeling pathways are upregulated (Figure 1).[18] CMS classification results in more homogeneous tumor subgroups and might lead to discovery of signaling pathways associated with aggressiveness and therapy response within each subtype. The CMS profiles provide leads for development of novel subtype-targeted therapies.[19]

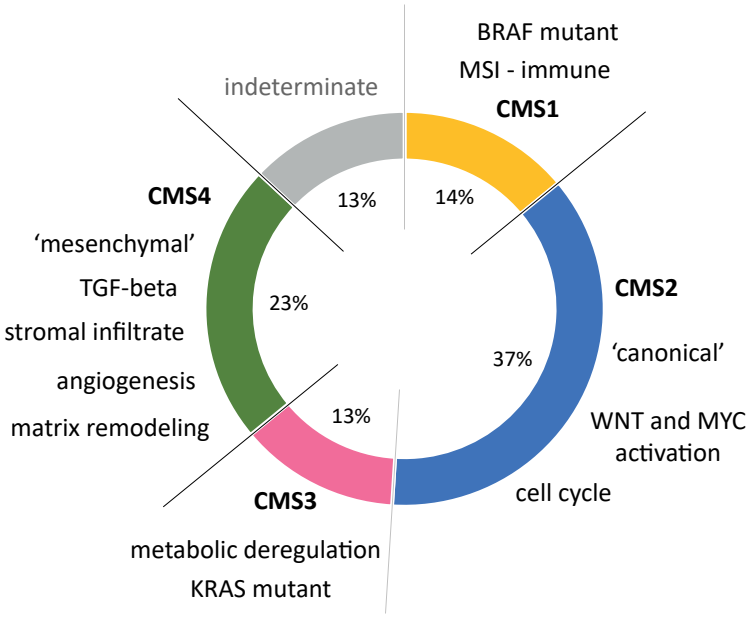

Figure 1. The Consensus Molecular Subtypes. Based on data from Guinney *et al.*, Nat Med. 2017.

2. Prognostic information

Although the classifier was not developed as a prognostic tool, the CMSs show significant differences in clinical outcomes of early-stage CRC, even in multivariable analysis correcting for clinicopathological markers, adjuvant chemotherapy, MSI, and KRAS and BRAF mutation status. Of the four subtypes, CMS1 was associated with the best disease-free survival after primary tumor resection. CMS4 has the worst outcome, with a twofold increased chance of relapse after curative surgery. In case of relapse however, CMS1 tumors have the worst prognosis.[18, 20, 21]

3. Prediction of therapeutic response

Multiple studies have linked the differences in underlying signaling pathways of CMSs with heterogeneous responses to anticancer therapies. Cell lines and xenografts from CMS4 tumors were resistant to oxaliplatin treatment, whereas CMS2 lines were sensitive.[22] Preclinical models of CMSs also showed differential response to targeted therapies.[19] These findings have been confirmed in clinical trials. Patients with stage III CMS4 tumors did not benefit from systemic adjuvant oxaliplatin treatment and metastatic CMS4 tumors were resistant to anti-EGFR therapy independent of RAS-mutation status.[21, 23] CMS2 and CMS3 tumors on the other hand appear more sensitive to chemo- and targeted therapy. Irinotecan-based therapies were effective only in mCRC with upregulated Wnt-pathway signaling (CMS2), bevacizumab increased progression-free survival in CMS2 and 3, and efficacy of adjuvant oxaliplatin was limited to the 'enterocyte' subtype from the CRCA classifier.[20, 21, 24] Finally, efficacy of immune checkpoint inhibitors seems limited to MSI tumors (CMS1).[25] Stratification of molecular subtypes in clinical trials would allow validation of subtype-specific biomarkers of response.

Tumor-stroma interactions in colorectal cancer

All cancers are composed of neoplastic cells mixed with a variety of non-neoplastic stromal cells, embedded in extracellular matrix (ECM). These stromal cells (immune cells, fibroblasts, endothelial cells, etc.) together with the ECM form the tumor microenvironment (TME). Interactions between cancer cells and the TME influence tumor behavior, progression and clinical outcome.

Cancer-associated fibroblasts (CAFs) are major constituents of desmoplastic stroma in CRC. High stromal content, the abundance of activated fibroblasts in tumor stroma and high expression of CAF gene signatures have each been associated with poor prognosis in CRC.[26-30] CAFs arise through activation of resident tissue fibroblasts and recruitment of mesenchymal stem cells via cancer-cell-derived TGF-β signalling.[31] CAFs in turn secrete a plethora of growth factors and cytokines that influence cancer cells and the TME, to stimulate proliferation, invasion, stemness and metastasis formation, as reviewed by

Koliaraki *et al.*[32] CAFs have also been implicated in chemotherapy-resistance, via induction of DNA repair and stemness.[33, 34]

Immune cell infiltrate also influences the behavior and prognosis of CRC. Interestingly, depending on the specific constitution of the infiltrate, this can either lead to anti-tumor immunity or pro-tumorigenic inflammation, as reviewed by Roeland *et al.*[35] The prognostic tool 'Immunoscore' is based on this notion, and shows that presence of cytotoxic lymphocytes is predictive of reduced recurrence risk in CRC.[36, 37]

The ECM forms a scaffold for cell adhesion and can bind growth factors, thereby influencing behavior of cancer cells. Numerous structural ECM molecules exist, including laminin, fibronectin and many types of collagens. The role of the ECM in cancer progression is reviewed in detail by Pickup *et al.*[38] The specific constitution, as well as the stiffness of the ECM can affect tumor cell survival, stemness and metastasis. Presence of collagen type I induces invasive behavior in three-dimensional CRC cell cultures, and collagen matrix stiffening can drive invasion and metastasis.[27, 39]

By studying microenvironmental gene signatures in light of CMS, it has become evident that the TME of CMS groups are clearly different. CMS1 and CMS4 are strongly infiltrated with stromal cells, whereas CMS2/3 mostly consist of neoplastic epithelial cells, with little immune cell infiltrate or desmoplasia.[18, 40-42] Both CMS1 and CMS4 highly express immune-related genes, but while CMS1 is enriched with cytotoxic T-cells, CMS4 tumors predominantly harbor pro-tumorigenic lymphocytes and monocytes.[40, 42] CMS4 tumors are further characterized by a high density of cancer-associated fibroblasts (CAFs). In fact, the CMS4 gene signature is largely dominated by CAF-expressed genes.[27, 29, 43] CMS4 is also enriched for pathways involved in cell adhesion and ECM remodeling.[18] Collagen type I is particularly highly expressed in mesenchymal-type CRC. Collagens are produced by CAFs and macrophages[44], linking the ECM composition to the presence of these stromal cell types in CMS4 CRC.

CMS4-targeted therapy

CMS4 primary CRC has the poorest prognosis of the four subtypes, and is resistant to currently used chemo- and targeted therapies. Thus, alternative treatment strategies are urgently needed for this subtype. Because of the extensive influence of the stromal compartment on the phenotype of CMS4, targeting tumor-stroma interactions could be an interesting therapeutic approach. Our research group has shown that the receptor tyrosine kinases (RTKs) Platelet-Derived Growth Factor Receptor (PDGFR) and c-KIT are upregulated in CMS4 CRC and contribute to the aggressive phenotype.[45, 46]

PDGFRs are mainly expressed on mesenchymal cell types, but can also be expressed by epithelial cells that have undergone epithelial-to-mesenchymal transition (EMT).[45, 47, 48] High PDGFR expression has been correlated with unfavorable prognosis in CRC and

various other cancers.[45, 48-51] PDGFR signaling stimulates cancer cell invasion and metastasis formation, and plays a role in (lymph)angiogenesis, by stimulating pericytes and inducing proliferation, migration and sprouting of (lymphatic) endothelial cells.[45, 52, 53]

In the normal colon, c-KIT is expressed by Paneth-like goblet cells that support intestinal stem cells.[54] In CRC, c-KIT/stem cell factor signaling is also involved in maintenance of cancer stem cells.[46, 55] c-KIT signaling further promotes EMT and appears highest in regions of hypoxia, linking hypoxia and stem-cell dynamics.[46, 56] Interestingly, mast cells also express c-KIT. Recently, their role in the TME is gaining attention. Mast cells are recruited by tumor cells through SCF signaling, release pro-angiogenic factors and stimulate tumor cell growth.[57, 58] High mast cell density was associated with poor survival, and linked to a pro-tumorigenic immune cell composition in CRC.[59] Mast cells are indeed highly present in CMS4 CRC.[42]

The expression of PDGFRs and c-KIT by both tumor cells and stromal cells, and their contribution to aggressive tumor behavior, render them attractive therapeutic targets. The receptors can be inhibited with a range of RTK-inhibitors, of which imatinib has the highest selectivity for these receptors. Imatinib treatment was effective in *in vitro* and *in vivo* models of CRC, by reducing invasiveness, metastatic potential and stem-like characteristics of mesenchymal-type colon cancer.[46, 55, 60, 61] The favorable safety profile of imatinib allows for translation of these preclinical results to a clinical trial with patients with mesenchymal-type CRC.

Surgical treatment of metastatic colorectal cancer

Metastatic spread to distant organs is most often the cause of death in CRC.[62] Approximately 20% of CRC patients present with metastases at initial diagnosis. In addition, >15% of patients without detectable metastases at diagnosis will develop these later on.[1, 6] CRC most often spreads to the liver, followed by the peritoneum and the lungs.[63, 64] Despite advances in surgical and chemotherapeutic treatment and the introduction of novel treatment modalities such as radiofrequency ablation and radioembolization, 5-year overall survival of patients with stage IV CRC has increased only marginally since the 1980s, from 4% to 12%.[65]

Surgical resection of metastatic lesions remains the only curative treatment option. Patients with isolated colorectal liver metastases (CRLM) (and those with limited extra-hepatic disease) may be candidates for hepatic surgery, which significantly improves their prognosis.[66] Induction chemotherapy can result in downsizing of metastases, allowing resection in up to 40% of patients with initially irresectable metastases.[67, 68] Techniques to increase the future remnant liver volume, such as portal vein embolization, as well as parenchymal-sparing surgery, have further widened the definition of resectability. However, even though resection might be technically feasible, extensive resection could cause

significant morbidity. Moreover, disease-free survival is limited in case of a high number of metastases.[69] Careful appraisal of the benefits of extended surgery, as well as the consequences for quality of life are essential for patients at this stage of disease.

Approximately 10% of patients with CRC develop peritoneal metastases (PMs).[70] In case of limited peritoneal disease, patients can be treated with cytoreductive surgery (CRS) and hyperthermic intraperitoneal chemotherapy (HIPEC). The goal of this combination strategy is to surgically remove all macroscopic PMs and to eliminate any residual microscopic disease by HIPEC. CRS-HIPEC significantly improves median overall survival of patients with PMs, but recurrence rates are high.[71, 72] The added value of HIPEC after CRS for CRC in currently under debate based on outcomes of the Prodige7 trial. This study failed to show survival benefit of CRS-HIPEC compared with CRS alone, and found a higher complication rate in patients treated with HIPEC.[73] Despite several limitations in study design and technical aspects[74, 75], these results suggest that the role of complete CRS is more important than that of HIPEC in achieving long-term survival. Moreover, two randomized phase III trials aiming at prevention or limitation of peritoneal spread failed to show benefit of HIPEC – the COLOPEC trial (adjuvant HIPEC in patients locally advanced (T4) CRC) and the PROPHYLOCHIP study (second-look surgery + HIPEC after systemic chemotherapy in patients at high risk of developing PM).[76, 77] Yet, the benefit of HIPEC after CRS has been demonstrated for ovarian cancer.[78] This implies that the HIPEC regimens used in CRC may be ineffective, but can be optimized.

There is currently no consensus on the choice of chemotherapy, the dose administered or the duration of perfusion.[79] Both mitomycin-C (MMC) and oxaliplatin are being used, and retrospective comparisons are hampered by the heterogeneous composition of published clinical cohorts.[80] To improve the efficacy of HIPEC and the outcome of PM-CRC, a better understanding of the biology of PMs and the impact of HIPEC are highly warranted.

THESIS OUTLINE

The aims of this thesis are:

1. To contribute to the clinical translation of the Consensus Molecular Subtypes classification by identifying patients with CMS4 CRC and evaluating molecular subtype heterogeneity;
2. To acquire further insights into the interactions between cancer cells and their microenvironment in CMS4, by testing novel tumor-stroma directed therapies in a pre-clinical model and in a clinical trial;
3. To study chemotherapy resistance in poor-prognosis CRC and to improve surgical and chemotherapeutic efficacy in metastatic CRC.

The translation of CMS to the clinic is hampered by the lack of a diagnostic assay that classifies patients into subtypes within a clinically relevant time window at reasonable costs on a per-patient basis. In **Chapter 2** we describe the development, testing and validation of a 4-gene RT-qPCR test that identifies CMS4 CRC. The test is used in a clinical study to select patients with CMS4 primary cancer for neo-adjuvant treatment with imatinib. Pre-clinical work showed that PDGFR and KIT inhibition reduces metastatic potential and stemness in CRC. The aim of this proof-of-concept trial (ImPACCT) is to investigate whether imatinib can reduce the aggressive phenotype of primary CMS4 colon cancer. The study protocol of the ImPACCT trial is presented in **Chapter 3**, together with preliminary data from CMS4 testing on endoscopic biopsies from the first 66 subjects included in the trial.

In **Chapter 4** we continue our search for therapies that target tumor-stroma interactions in CMS4 with an organoid model of mesenchymal-type CRC. To build on our previous finding that ECM rich in collagen type I induces mesenchymal gene expression and aggressive behavior, we unravel the signaling pathways involved in this interaction, and identify dasatinib as a potent anti-CMS4 drug.

In **Chapter 5** we study histopathological features and molecular subtypes in PMs from CRC, to help understand why patients with PM-CRC have such a dismal prognosis. We show that PMs are often stroma-rich and frequently classified as CMS4. We present a pre-clinical model of PM using organoid technology to study the efficacy of HIPEC in **Chapter 6**. We use the model as a platform to test novel combination strategies to increase HIPEC efficacy.

In **Chapters 7** we explore molecular classification of primary CRC and corresponding CRLM. We demonstrate that discordance in molecular subtyping between matched tumors is frequent. Neo-adjuvant chemotherapy affects gene expression in CRC cells and may contribute to this discordance.

Finally, in **Chapters 8 and 9**, we discuss surgical treatment of CRLM. To offer patients with CRLM a chance of cure, the margins of resectability are constantly sought and pushed forward. Advances in the oncological and surgical fields have made major liver resections technically possible, and liver resections are attempted even after long-term palliative chemotherapy. We evaluate the outcomes of major liver surgery and surgery after long-term chemotherapy, to contribute to improved patient selection for these high-risk procedures.

REFERENCES

1. Nederlandse Kankerregistratie (NKR) I. Cijfers over Kanker 2019 [Available from: https://www.cijfersoverkanker.nl/.
2. Bray F, Ferlay J, Soerjomataram I, et al. Global cancer statistics 2018: GLOBOCAN estimates of incidence and mortality worldwide for 36 cancers in 185 countries. *CA Cancer J Clin*. 2018;**68**(6):394-424.
3. American Joint Committee on Cancer. Colon and Rectum. In: Edge SB, Byrd SR, Compton CC, Fritz AG, Greene FL, Trotti A, editors. AJCC Cancer Staging Manual. 7th ed. New York: Springer-Verlag; 2010. p. 143-64.
4. Andre T, Boni C, Mounedji-Boudiaf L, et al. Oxaliplatin, fluorouracil, and leucovorin as adjuvant treatment for colon cancer. *N Engl J Med*. 2004;**350**(23):2343-51.
5. NCCN Guidelines Version 2.2019 Colon Cancer [Internet]. 2019. Available from: https://www.nccn.org/professionals/physician_gls/pdf/colon.pdf.
6. Osterman E, Glimelius B. Recurrence Risk After Up-to-Date Colon Cancer Staging, Surgery, and Pathology: Analysis of the Entire Swedish Population. *Dis Colon Rectum*. 2018;**61**(9):1016-25.
7. Bockelman C, Engelmann BE, Kaprio T, et al. Risk of recurrence in patients with colon cancer stage II and III: a systematic review and meta-analysis of recent literature. *Acta Oncol*. 2015;**54**(1):5-16.
8. Pahlman LA, Hohenberger WM, Matzel K, et al. Should the Benefit of Adjuvant Chemotherapy in Colon Cancer Be Re-Evaluated? *J Clin Oncol*. 2016;**34**(12):1297-9.
9. Yothers G, O'Connell MJ, Lee M, et al. Validation of the 12-gene colon cancer recurrence score in NSABP C-07 as a predictor of recurrence in patients with stage II and III colon cancer treated with fluorouracil and leucovorin (FU/LV) and FU/LV plus oxaliplatin. *J Clin Oncol*. 2013;**31**(36):4512-9.
10. Salazar R, Roepman P, Capella G, et al. Gene expression signature to improve prognosis prediction of stage II and III colorectal cancer. *J Clin Oncol*. 2011;**29**(1):17-24.
11. Kennedy RD, Bylesjo M, Kerr P, et al. Development and independent validation of a prognostic assay for stage II colon cancer using formalin-fixed paraffin-embedded tissue. *J Clin Oncol*. 2011;**29**(35):4620-6.
12. Schlicker A, Beran G, Chresta CM, et al. Subtypes of primary colorectal tumors correlate with response to targeted treatment in colorectal cell lines. *BMC Med Genomics*. 2012;**5**:66.
13. Marisa L, de Reynies A, Duval A, et al. Gene expression classification of colon cancer into molecular subtypes: characterization, validation, and prognostic value. *PLoS Med*. 2013;**10**(5):e1001453.
14. Sadanandam A, Lyssiotis CA, Homicsko K, et al. A colorectal cancer classification system that associates cellular phenotype and responses to therapy. *Nat Med*. 2013;**19**(5):619-25.
15. De Sousa EMF, Wang X, Jansen M, et al. Poor-prognosis colon cancer is defined by a molecularly distinct subtype and develops from serrated precursor lesions. *Nat Med*. 2013;**19**(5):614-8.
16. Budinska E, Popovici V, Tejpar S, et al. Gene expression patterns unveil a new level of molecular heterogeneity in colorectal cancer. *J Pathol*. 2013;**231**(1):63-76.
17. Roepman P, Schlicker A, Tabernero J, et al. Colorectal cancer intrinsic subtypes predict chemotherapy benefit, deficient mismatch repair and epithelial-to-mesenchymal transition. *Int J Cancer*. 2014;**134**(3):552-62.
18. Guinney J, Dienstmann R, Wang X, et al. The consensus molecular subtypes of colorectal cancer. *Nat Med*. 2015;**21**(11):1350-6.
19. Sveen A, Bruun J, Eide PW, et al. Colorectal Cancer Consensus Molecular Subtypes Translated to Preclinical Models Uncover Potentially Targetable Cancer Cell Dependencies. *Clin Cancer Res*. 2018;**24**(4):794-806.
20. Mooi JK, Wirapati P, Asher R, et al. The prognostic impact of consensus molecular subtypes (CMS) and its predictive effects for bevacizumab benefit in metastatic colorectal cancer: molecular analysis of the AGITG MAX clinical trial. *Ann Oncol*. 2018;**29**(11):2240-6.
21. Song N, Pogue-Geile KL, Gavin PG, et al. Clinical Outcome From Oxaliplatin Treatment in Stage II/III Colon Cancer According to Intrinsic Subtypes: Secondary Analysis of NSABP C-07/NRG Oncology Randomized Clinical Trial. *JAMA Oncol*. 2016;**2**(9):1162-9.
22. Linnekamp JF, Hooff SRV, Prasetyanti PR, et al. Consensus molecular subtypes of colorectal cancer are recapitulated in in vitro and in vivo models. *Cell Death Differ*. 2018.
23. Trinh A, Trumpi K, De Sousa EMF, et al. Practical and Robust Identification of Molecular Subtypes in Colorectal Cancer by Immunohistochemistry. *Clin Cancer Res*. 2017;**23**(2):387-98.
24. Del Rio M, Mollevi C, Bibeau F, et al. Molecular subtypes of metastatic colorectal cancer are associated with patient response to irinotecan-based therapies. *Eur J Cancer*. 2017;**76**:68-75.

25. Le DT, Uram JN, Wang H, et al. PD-1 Blockade in Tumors with Mismatch-Repair Deficiency. *N Engl J Med*. 2015;**372**(26):2509-20.
26. Huijbers A, Tollenaar RA, v Pelt GW, et al. The proportion of tumor-stroma as a strong prognosticator for stage II and III colon cancer patients: validation in the VICTOR trial. *Ann Oncol*. 2013;**24**(1):179-85.
27. Vellinga TT, den Uil S, Rinkes IH, et al. Collagen-rich stroma in aggressive colon tumors induces mesenchymal gene expression and tumor cell invasion. *Oncogene*. 2016;**35**(40):5263-71.
28. Tsujino T, Seshimo I, Yamamoto H, et al. Stromal myofibroblasts predict disease recurrence for colorectal cancer. *Clin Cancer Res*. 2007;**13**(7):2082-90.
29. Isella C, Terrasi A, Bellomo SE, et al. Stromal contribution to the colorectal cancer transcriptome. *Nat Genet*. 2015;**47**(4):312-9.
30. Berdiel-Acer M, Berenguer A, Sanz-Pamplona R, et al. A 5-gene classifier from the carcinoma-associated fibroblast transcriptomic profile and clinical outcome in colorectal cancer. *Oncotarget*. 2014;**5**(15):6437-52.
31. Calon A, Espinet E, Palomo-Ponce S, et al. Dependency of colorectal cancer on a TGF-beta-driven program in stromal cells for metastasis initiation. *Cancer Cell*. 2012;**22**(5):571-84.
32. Koliaraki V, Pallangyo CK, Greten FR, et al. Mesenchymal Cells in Colon Cancer. *Gastroenterology*. 2017;**152**(5):964-79.
33. Goncalves-Ribeiro S, Diaz-Maroto NG, Berdiel-Acer M, et al. Carcinoma-associated fibroblasts affect sensitivity to oxaliplatin and 5FU in colorectal cancer cells. *Oncotarget*. 2016;**7**(37):59766-80.
34. Lotti F, Jarrar AM, Pai RK, et al. Chemotherapy activates cancer-associated fibroblasts to maintain colorectal cancer-initiating cells by IL-17A. *J Exp Med*. 2013;**210**(13):2851-72.
35. Roelands J, Kuppen PJK, Vermeulen L, et al. Immunogenomic Classification of Colorectal Cancer and Therapeutic Implications. *Int J Mol Sci*. 2017;**18**(10).
36. Galon J, Costes A, Sanchez-Cabo F, et al. Type, density, and location of immune cells within human colorectal tumors predict clinical outcome. *Science*. 2006;**313**(5795):1960-4.
37. Pages F, Mlecnik B, Marliot F, et al. International validation of the consensus Immunoscore for the classification of colon cancer: a prognostic and accuracy study. *Lancet*. 2018;**391**(10135):2128-39.
38. Pickup MW, Mouw JK, Weaver VM. The extracellular matrix modulates the hallmarks of cancer. *EMBO Rep*. 2014;**15**(12):1243-53.
39. Baker AM, Bird D, Lang G, et al. Lysyl oxidase enzymatic function increases stiffness to drive colorectal cancer progression through FAK. *Oncogene*. 2013;**32**(14):1863-8.
40. Becht E, de Reynies A, Giraldo NA, et al. Immune and Stromal Classification of Colorectal Cancer Is Associated with Molecular Subtypes and Relevant for Precision Immunotherapy. *Clin Cancer Res*. 2016.
41. Lal N, White BS, Goussous G, et al. KRAS Mutation and Consensus Molecular Subtypes 2 and 3 Are Independently Associated with Reduced Immune Infiltration and Reactivity in Colorectal Cancer. *Clin Cancer Res*. 2018;**24**(1):224-33.
42. Trumpi K, Frenkel N, Peters T, et al. Macrophages induce "budding" in aggressive human colon cancer subtypes by protease-mediated disruption of tight junctions. *Oncotarget*. 2018;**9**(28):19490-507.
43. Calon A, Lonardo E, Berenguer-Llergo A, et al. Stromal gene expression defines poor-prognosis subtypes in colorectal cancer. *Nat Genet*. 2015;**47**(4):320-9.
44. Afik R, Zigmond E, Vugman M, et al. Tumor macrophages are pivotal constructors of tumor collagenous matrix. *J Exp Med*. 2016;**213**(11):2315-31.
45. Steller EJA, Raats DA, Koster J, et al. PDGFRB promotes liver metastasis formation of mesenchymal-like colorectal tumor cells. *Neoplasia*. 2013;**15**(2):204-17.
46. Fatrai S, van Schelven SJ, Ubink I, et al. Maintenance of Clonogenic KIT(+) Human Colon Tumor Cells Requires Secretion of Stem Cell Factor by Differentiated Tumor Cells. *Gastroenterology*. 2015;**149**(3):692-704.
47. Kitadai Y, Sasaki T, Kuwai T, et al. Expression of activated platelet-derived growth factor receptor in stromal cells of human colon carcinomas is associated with metastatic potential. *Int J Cancer*. 2006;**119**(11):2567-74.
48. Wehler TC, Frerichs K, Graf C, et al. PDGFRalpha/beta expression correlates with the metastatic behavior of human colorectal cancer: a possible rationale for a molecular targeting strategy. *Oncol Rep*. 2008;**19**(3):697-704.
49. Carvalho I, Milanezi F, Martins A, et al. Overexpression of platelet-derived growth factor receptor alpha in breast cancer is associated with tumour progression. *Breast Cancer Res*. 2005;**7**(5):R788-95.
50. Chu JS, Ge FJ, Zhang B, et al. Expression and prognostic value of VEGFR-2, PDGFR-beta, and c-Met in advanced hepatocellular carcinoma. *J Exp Clin Cancer Res*. 2013;**32**:16.

51. Henriksen R, Funa K, Wilander E, et al. Expression and prognostic significance of platelet-derived growth factor and its receptors in epithelial ovarian neoplasms. *Cancer Res*. 1993;**53**(19):4550-4.
52. Xue Y, Lim S, Yang Y, et al. PDGF-BB modulates hematopoiesis and tumor angiogenesis by inducing erythropoietin production in stromal cells. *Nat Med*. 2011;**18**(1):100-10.
53. Cao R, Bjorndahl MA, Religa P, et al. PDGF-BB induces intratumoral lymphangiogenesis and promotes lymphatic metastasis. *Cancer Cell*. 2004;**6**(4):333-45.
54. Rothenberg ME, Nusse Y, Kalisky T, et al. Identification of a cKit(+) colonic crypt base secretory cell that supports Lgr5(+) stem cells in mice. *Gastroenterology*. 2012;**142**(5):1195-205 e6.
55. Chen EC, Karl TA, Kalisky T, et al. KIT Signaling Promotes Growth of Colon Xenograft Tumors in Mice and Is Up-Regulated in a Subset of Human Colon Cancers. *Gastroenterology*. 2015;**149**(3):705-17 e2.
56. Schoning JP, Monteiro M, Gu W. Drug resistance and cancer stem cells: the shared but distinct roles of hypoxia-inducible factors HIF1alpha and HIF2alpha. *Clin Exp Pharmacol Physiol*. 2017;**44**(2):153-61.
57. Yu Y, Blokhuis B, Derks Y, et al. Human mast cells promote colon cancer growth via bidirectional crosstalk: studies in 2D and 3D coculture models. *Oncoimmunology*. 2018;**7**(11):e1504729.
58. Yu Y, Blokhuis BR, Garssen J, et al. A Transcriptomic Insight into the Impact of Colon Cancer Cells on Mast Cells. *Int J Mol Sci*. 2019;**20**(7).
59. Mao Y, Feng Q, Zheng P, et al. Low tumor infiltrating mast cell density confers prognostic benefit and reflects immunoactivation in colorectal cancer. *Int J Cancer*. 2018;**143**(9):2271-80.
60. Kitadai Y, Sasaki T, Kuwai T, et al. Targeting the expression of platelet-derived growth factor receptor by reactive stroma inhibits growth and metastasis of human colon carcinoma. *Am J Pathol*. 2006;**169**(6):2054-65.
61. Shinagawa K, Kitadai Y, Tanaka M, et al. Stroma-directed imatinib therapy impairs the tumor-promoting effect of bone marrow-derived mesenchymal stem cells in an orthotopic transplantation model of colon cancer. *Int J Cancer*. 2013;**132**(4):813-23.
62. Riihimaki M, Thomsen H, Sundquist K, et al. Colorectal cancer patients: what do they die of? *Frontline Gastroenterol*. 2012;**3**(3):143-9.
63. Riihimaki M, Hemminki A, Sundquist J, et al. Patterns of metastasis in colon and rectal cancer. *Sci Rep*. 2016;**6**:29765.
64. Knijn N, van Erning FN, Overbeek LI, et al. Limited effect of lymph node status on the metastatic pattern in colorectal cancer. *Oncotarget*. 2016;**7**(22):31699-707.
65. Brouwer NPM, Bos A, Lemmens V, et al. An overview of 25 years of incidence, treatment and outcome of colorectal cancer patients. *Int J Cancer*. 2018;**143**(11):2758-66.
66. Lemke J, Cammerer G, Ganser J, et al. Survival and Prognostic Factors of Colorectal Liver Metastases After Surgical and Nonsurgical Treatment. *Clin Colorectal Cancer*. 2016;**15**(4):e183-e92.
67. Lam VWT, Spiro C, Laurence JM, et al. A systematic review of clinical response and survival outcomes of downsizing systemic chemotherapy and rescue liver surgery in patients with initially unresectable colorectal liver metastases. *Ann Surg Oncol*. 2012;**19**(4):1292-301.
68. Tomasello G, Petrelli F, Ghidini M, et al. FOLFOXIRI Plus Bevacizumab as Conversion Therapy for Patients With Initially Unresectable Metastatic Colorectal Cancer: A Systematic Review and Pooled Analysis. *JAMA Oncol*. 2017;**3**(7):e170278.
69. Vigano L, Capussotti L, Lapointe R, et al. Early recurrence after liver resection for colorectal metastases: risk factors, prognosis, and treatment. A LiverMetSurvey-based study of 6,025 patients. *Ann Surg Oncol*. 2014;**21**(4):1276-86.
70. Segelman J, Granath F, Holm T, et al. Incidence, prevalence and risk factors for peritoneal carcinomatosis from colorectal cancer. *Br J Surg*. 2012;**99**(5):699-705.
71. Verwaal VJ, Bruin S, Boot H, et al. 8-Year Follow-Up of Randomized Trial: Cytoreduction and Hyperthermic Intraperitoneal Chemotherapy Versus Systemic Chemotherapy in Patients with Peritoneal Carcinomatosis of Colorectal Cancer. *Ann Surg Oncol*. 2008;**15**(9):2426-32.
72. van Eden WJ, Kok NFM, Woensdregt K, et al. Safety of intraperitoneal Mitomycin C versus intraperitoneal oxaliplatin in patients with peritoneal carcinomatosis of colorectal cancer undergoing cytoreductive surgery and HIPEC. *Eur J Surg Oncol*. 2018;**44**(2):220-7.
73. Quenet F, Elias D, Roca L, et al. A UNICANCER phase III trial of hyperthermic intra-peritoneal chemotherapy (HIPEC) for colorectal peritoneal carcinomatosis (PC): PRODIGE 7. *J Clin Oncol*. 2018;**36**(18_suppl):LBA3503-LBA.

74. Liberale G, Ameye L, Hendlisz A. PRODIGE 7 should be interpreted with caution. *Acta Chir Belg*. 2019;**119**(4):263-6.
75. Ceelen W. HIPEC with oxaliplatin for colorectal peritoneal metastasis: The end of the road? *Eur J Surg Oncol*. 2019;**45**(3):400-2.
76. Klaver CEL, Wisselink DD, Punt CJA, et al. Adjuvant hyperthermic intraperitoneal chemotherapy in patients with locally advanced colon cancer (COLOPEC): a multicentre, open-label, randomised trial. *Lancet Gastroenterol Hepatol*. 2019;**4**(10):761-70.
77. Goere D, Glehen O, Quenet F, et al. Results of a randomized phase 3 study evaluating the potential benefit of a second-look surgery plus HIPEC in patients at high risk of developing colorectal peritoneal metastases (PROPHYLOCHIP- NTC01226394). *J Clin Oncol*. 2018;**36**(15_suppl):3531.
78. van Driel WJ, Koole SN, Sikorska K, et al. Hyperthermic Intraperitoneal Chemotherapy in Ovarian Cancer. *N Engl J Med*. 2018;**378**(3):230-40.
79. Bushati M, Rovers KP, Sommariva A, et al. The current practice of cytoreductive surgery and HIPEC for colorectal peritoneal metastases: Results of a worldwide web-based survey of the Peritoneal Surface Oncology Group International (PSOGI). *Eur J Surg Oncol*. 2018;**44**(12):1942-8.
80. Wisselink DD, Braakhuis LLF, Gallo G, et al. Systematic review of published literature on oxaliplatin and mitomycin C as chemotherapeutic agents for hyperthermic intraperitoneal chemotherapy in patients with peritoneal metastases from colorectal cancer. *Crit Rev Oncol Hematol*. 2019;**142**:119-29.

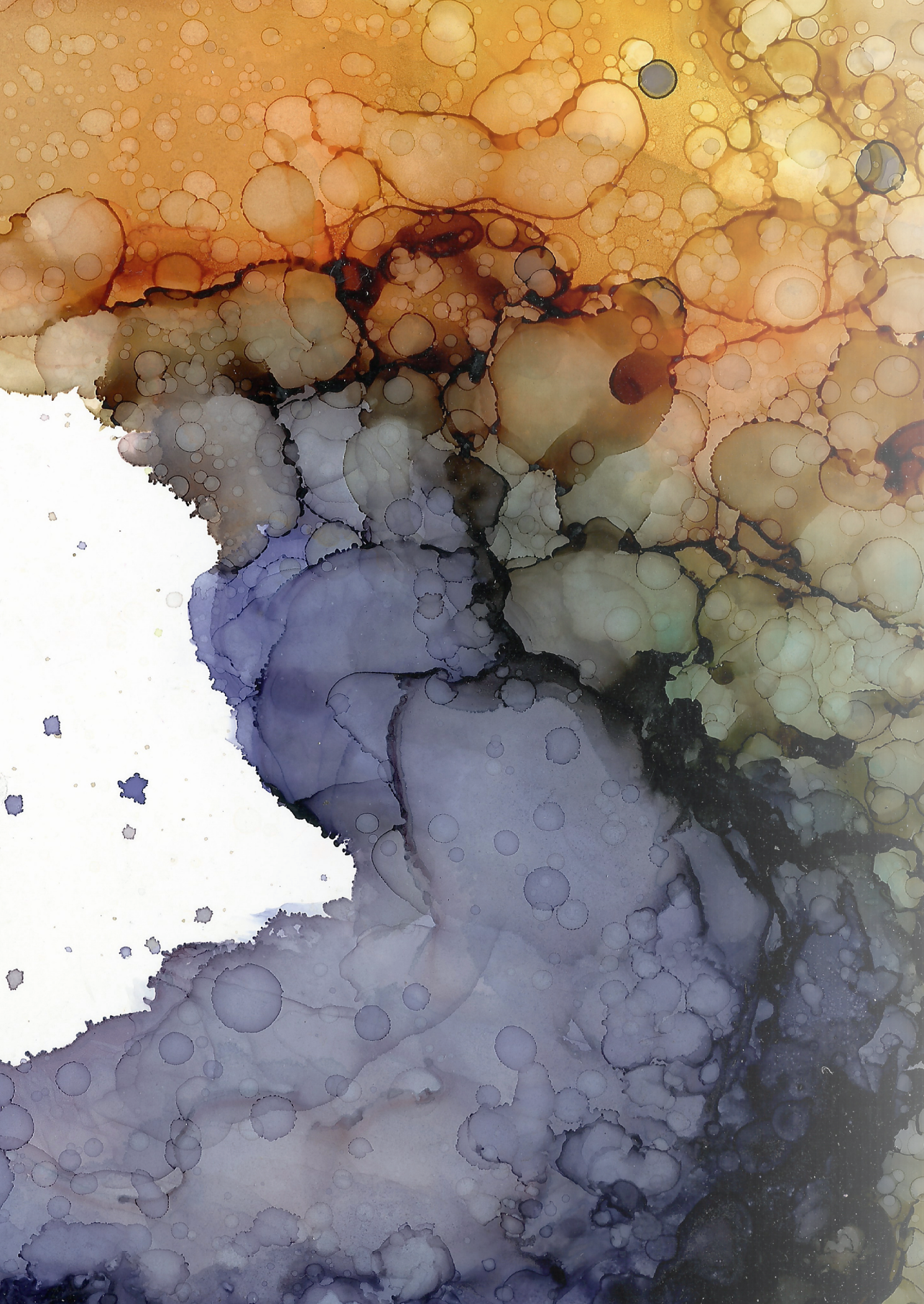

2

A novel diagnostic tool for selecting patients with mesenchymal-type colon cancer reveals intratumor subtype heterogeneity

Inge Ubink*, Sjoerd G. Elias*, Cathy B. Moelans, Miangela M. Laclé, Wilhelmina M.U. van Grevenstein, Paul J. van Diest, Inne H.M. Borel Rinkes and Onno Kranenburg

*Authors contributed equally to this work

Journal of the National Cancer Institute, 2017;109(8)

ABSTRACT

Background

Consensus molecular subtype 4 (CMS4) is a recently identified aggressive colon cancer subtype for which platelet-derived growth factor receptors (PDGFRs) and KIT are potential therapeutic targets. We aimed to develop a clinically applicable CMS4 reverse transcription polymerase chain reaction (RT-qPCR) test to select patients for PDGFR/KIT-targeted therapy.

Methods

We used logistic regression to develop a CMS4 prediction rule based on microarray expression values of PDGFRA, PDGFRB, PDGFC, and KIT (566 training and 1259 test samples, using the 273-gene random forest classifier as CMS4 reference standard). We next translated the prediction rule into a single-sample RT-qPCR test, which we independently validated in 29 fresh tumor samples. To study intratumor CMS4 heterogeneity, we used the RT-qPCR test to analyze five random regions of 20 colon tumors.

Results

The microarray-based prediction rule diagnosed CMS4-type tumors extremely well in both training and independent test samples (training: area under the curve [AUC] = 0.95, 95% confidence interval [CI] = 0.94 to 0.97; test: AUC = 0.95, 95% CI = 0.94 to 0.96), with excellent calibration and approximately 80% overall net benefit over a large threshold range. Translation into an RT-qPCR test did not affect discrimination (AUC = 0.97, 95% CI = 0.93 to 1.00, independent validation). RT-qPCR analysis of five random tumor regions revealed extensive intratumor CMS4 heterogeneity in nine out of 20 tumors. At least two regions likely have to be analyzed to identify patients that are predominantly CMS4 positive (>50% average CMS4 chance).

Conclusion

The CMS4 RT-qPCR test is a promising clinical tool for selecting individual patients for CMS4-subtype-targeted therapy.

INTRODUCTION

Mortality in colon cancer is almost invariably due to the development of distant metastases. New treatment strategies that prevent distant recurrence are therefore urgently needed. Clinicopathological features have limited ability to identify patients at high risk for relapse who might benefit from systemic therapy. The recently published consensus molecular subtype (CMS) classification of colorectal cancer distinguishes four molecular subtypes (CMS1-4) based on gene expression profiles, reflecting differences in the activity of specific signaling pathways.[1] This classification system can be used to develop subtype-directed targeted therapy and accompanying new methods of patient stratification.

CMS4 is associated with a clinically and statistically significantly worse disease-free and overall survival.[1] Novel diagnostic and treatment strategies for this subtype are therefore urgently needed. CMS4 tumors are characterized by high expression of genes reflecting epithelial-to-mesenchymal transition (EMT), transforming growth factor (TGF)-β signaling, and matrix remodeling and have a high stromal cell content.[1-3] TGF-β-activated cancer-associated fibroblasts can promote colon cancer metastasis in mouse models[4] and could likewise contribute to the early disease recurrence observed in patients with CMS4 tumors. In addition, we found that platelet-derived growth factor receptors (PDGFRs) and their ligands are highly co-expressed in CMS4 colon tumors. PDGFRs are tyrosine kinase receptors that are expressed on mesenchymal cell types and on epithelial tumor cells following EMT.[5] PDGFR expression correlates with tumor progression and an unfavorable prognosis in colon cancer and various other types of cancer.[6-9] Inhibition of PDGFR signaling limits colon cancer invasion and the formation of distant metastases.[10-12] Aggressive colon tumors also express KIT proto-oncogene receptor tyrosine kinase (KIT), the receptor for stem cell factor. KIT is structurally closely related to PDGFRs and its expression is mostly restricted to primitive stem-like cell types. KIT mutations and amplification contribute to the development of various types of cancer.[5, 13] In colon cancer, KIT signaling is required for maintenance of stem-like cancer cells and clone- and tumor-forming potential.[13, 14]

Targeted therapy of CMS4 tumors requires a diagnostic test for upfront patient selection. The original CMS classification is based on a 273-gene classifier.[1] The available methods for genome-wide RNA analysis (microarray, RNA sequencing) are relatively expensive, and their use as a single-sample predictor requires rapid routine access to a specialized facility and bioinformatics expertise. Hence, it has so far been difficult to advance RNA-based tumor classification to a routine clinical test. Reverse transcription quantitative polymerase chain reaction (RT-qPCR) tests, however, can be widely implemented in routine diagnostics.[15] In this study, we therefore set out to develop and validate an RT-qPCR test that discriminates CMS4 colon tumors from the other subtypes for individual patient selection.

Intratumor heterogeneity (ITH) with respect to molecular subtypes was not addressed in the consensus classification study.[1] Multiregion DNA sequencing of human colon cancers has revealed the existence of genetic ITH[16, 17], which is clinically relevant because distinct clones may have different capacities to metastasize and may display different responses to systemic therapy. To study the existence of molecular subtype ITH, we analyzed multiple regions of primary colon tumors with the newly developed RT-qPCR test. The results were used to design a strategy for the selection of patients with CMS4 colon tumors, which takes ITH into account.

METHODS

For a detailed explanation of all experimental procedures, patient series, and statistical analyses, we refer to the Supplementary Methods. We adhere to the TRIPOD[18] and MIQE[19] guidelines in reporting this study and used R version 3.1.3 for Mac (R Foundation for Statistical Computing, Vienna, Austria; https://www.R-project.org) for all analyses.

Patient Series

We used 11 distinct patient series for this manuscript. Nine provided only microarray gene expression data (Supplementary Table 1), one only RT-qPCR data (UMCU biobank) (Supplementary Table 2), and one both RT-qPCR as well as microarray gene expression data (Biopsies Of Surgical Specimens [BOSS] study) (Supplementary Table 3).

Development and Validation of a CMS4 Diagnostic Test

We devised a novel approach to generate a diagnostic RT-qPCR test that identifies CMS4 colon cancers (Supplementary Figure 1), which is briefly explained here. Raw microarray expression data were preprocessed and corrected for batch effects. The 273-gene random forest CMS classifier[1] was applied to each sample; 26.5% of the tumors were classified as CMS4 (Supplementary Figure 2, available online). Data set GSE39582 (n = 566, CMS4 = 136) was used as the training set to develop the test based on five candidate genes (PDGFRA, PDGFRB, PDGFB, PDGFC, and KIT). These genes were selected based on previous experimental data showing that PDGFR and KIT are overexpressed mesenchymal-type colon tumors and promote colon cancer progression, and for their potential predictive value for KIT/PDGFR-targeting therapeutics, including imatinib.[10, 11, 13, 14] Microarray expression values were transformed and normalized to approximate a normal Gaussian distribution (Supplementary Figure 3). The prediction rule was trained with a stepwise-backward binary logistic regression approach with internal validation. Genes that did not independently contribute to the model were excluded. The diagnostic test was validated

on the other microarray data sets (total n = 1259, CMS4 n = 347). RT-qPCR expression values from the UMCU Biobank cohort (n = 135) were used to establish the necessary transformation steps to yield a standard normal distribution for RT-qPCR data (Supplementary Figure 4). These transformation steps were incorporated in the microarray-based algorithm to derive the final RT-qPCR diagnostic test for CMS4. Finally, we evaluated the relation between the microarray-based and RT-qPCR-based test results for 29 BOSS samples that were queried by both gene expression platforms. These samples were fully independent of all diagnostic test development or cross-platform translation steps.

Intratumor Heterogeneity and Clinical Sampling Strategy

We obtained five biopsies from randomly selected nonadjacent areas from 20 fresh consecutively resected colon tumors (BOSS study). Each biopsy was analyzed with the CMS4 RT-qPCR test. The outcomes were mathematically pooled by correcting for the relative RNA yield. Tumors were considered CMS4 positive if the five-biopsy-weighed mean chance of CMS4 was 50% or greater. We performed an in silico simulation study with two-tiered bootstrap resampling runs. Sensitivity, specificity, positive predictive value, and negative predicted value were calculated for a one-, two-, three-, and four-biopsy approach, as well as the likelihood of being selected as CMS4 positive (weighed mean chance ≥ 50%).

Statistical Analyses

To assess discrimination of the CMS4 tests, we constructed receiver operating characteristic (ROC) curves and estimated the associated areas under the curves (AUCs). For calibration, we plotted the predicted probabilities against the observed probabilities, making use of a LOWESS smoother. For net benefit, we used decision curve analysis[20], extended to include the net benefit for nonselected patients as well as the overall net benefit[21]. At the threshold for CMS4 positivity (≥50% chance of CMS4), we calculated test accuracy measures (i.e. sensitivity, specificity, negative and positive predictive values, and percent agreement). Prognostic relevance was assessed by analyzing time to recurrence (TTR), disease-free survival (DFS), and overall survival (OS). Survival curves were compared using the log-rank test, and hazard ratios (HRs) were estimated by Cox regression. All statistical tests were two-sided, and a P value of less than .05 was considered statistically significant.

RESULTS

Development and Validation of a Microarray-Based Diagnostic Test for CMS4 Colon Cancer

We used the largest microarray data set—the CIT cohort[22]—to develop a diagnostic test for CMS4. Logistic regression analysis showed that PDGFB did not independently contribute to predicting CMS4 status and this gene was therefore excluded from the model. The final model thus consisted of PDGFRA, PDGFRB, PDGFC, and KIT; Table 1 shows corresponding regression coefficients and odds ratios. This test proved to be an excellent predictor of CMS4 in the training set, with an area under the receiver operating characteristic curve of 0.95 (95% confidence interval [CI] = 0.94 to 0.97) (Figure 1A). The diagnostic test was subsequently validated on the other eight microarray data sets, and its high discriminative performance was confirmed in each of the data sets, resulting in a combined AUC in the test sets of 0.95 (95% CI = 0.94 to 0.96) (Figure 1A). Furthermore, the test showed a near-perfect calibration of predicted vs actual CMS4 chance overall, across the full range of CMS4 chances, and when grouping patients below or above the 50% CMS4 chance threshold, both in the training and in the test data sets (Figure 1, B and C). At a threshold of 50% predicted CMS4 chance, 24.4% of patients in the validation data sets tested positive, with 82.7% positive predictive value (95% CI = 78.0 to 86.8), 73.2% sensitivity (95% CI = 68.2 to 77.8), 90.2% negative predictive value (95% CI = 88.2 to 92.0), and 94.2% specificity (95% CI = 92.5 to 95.6). Importantly, we found that the diagnostic performance of the four-gene test was independent of the stage of disease (Supplementary Figure 5).

In the subset of patients with data on recurrence (n = 830, median follow-up = 45 months, 189 events), those with a 50% or greater CMS4 chance had a statistically significantly worse time to recurrence compared with other patients (hazard ratio [HR] = 1.65, 95% CI = 1.22 to 2.22, P< .001). This result is completely in line with the results of the original CMS publication (1). Patients classified as CMS4 by the new four-gene test also had a statistically significantly poorer overall survival (n = 523, median follow-up = 52 months, 151 events, HR = 1.43, 95% CI = 1.03 to 2.00, P = .03) (Figure 1F).

Net benefit analysis is used to weigh the benefits and harms resulting from clinical decisions that are based on test results. As such, it provides insight into the clinical value of a novel test, in addition to its statistical performance.[23] A threshold for selecting patients at 50% or greater chance of CMS4 means that erroneously selecting a CMS4-negative patient is equally valued as erroneously not selecting a CMS4-positive patient. Decision curve analysis of the validation data sets showed that at this threshold the new four-gene test had an overall net benefit of 77 out of 100 (Figure 1D). This compares favorably with net benefit analyses of other diagnostic models that are currently being tested or implemented in the

Table 1. Chance of CMS4 in relation to the expression of four genes, based on the diagnostic test developed in the Marisa data set (n=566).*

Gene	Regression coefficient	OR (95%CI)	Wald P-value
$PDGFRA_{normalized}$, per SD	0.412	1.51 (1.00-2.28)	0.049
$PDGFRB_{normalized}$, per SD	1.753	5.77 (3.31-10.1)	<0.001
$PDGFC_{normalized}$, per SD	2.079	8.00 (4.32-14.8)	<0.001
$KIT_{normalized}$, per SD	0.548	1.73 (1.19-2.51)	0.004
Intercept	-2.901	--	--

* Results in this table are shown per SD increase in gene-expression level. All statistical tests were two-sided. CI=confidence interval; OR=odds ratio.

clinic.[24-26] We found that the overall net benefit of the four-gene test remains remarkably constant at approximately 80% over a wide range of thresholds (0.15–1.00). Similar net benefit results were obtained when applying the test to the training data set (Supplementary Figure 6).

Translation to a Four-Gene RT-qPCR Test for Identification of CMS4-Type Colon Tumors

To translate the microarray-based CMS4 test to a clinically applicable RT-qPCR test that can be used to select individual patients for therapy, we incorporated the transformation and normalization steps derived from RT-qPCR analysis of the UMCU Biobank cohort in the microarray-based algorithm. Using the same threshold of 50% or greater CMS4 chance, 23.0% (n = 31) of the tumors of the UMCU Biobank were identified as CMS4 based on RT-qPCR data. In line with the survival data in the microarray data sets, we found that patients with American Joint Committee on Cancer[27] stage I–III tumors identified as CMS4 by RT-qPCR (n = 104) had a poorer prognosis, with a 1.88 times higher risk (95% CI = 0.73 to 4.86, P = .18) of developing disease recurrence (median follow-up = 29 months, 21 recurrences) (Figure 2A) and a worse disease-free survival (median follow-up = 35 months, 50 events, HR = 1.86, 95% CI = 1.01 to 3.40, P = .04) (Figure 2B). Patients with tumors identified as CMS4 (stage I–IV, n = 131) also had a poorer overall survival (median follow-up = 32 months, 58 deaths, HR = 1.63, 95% CI = 0.91 to 2.90, P = .10) (Figure 2C).

The purpose of the newly developed test is to select patients with CMS4 colon tumors for subtype-targeted therapy. To assess the feasibility of subtype prediction, we performed the BOSS study Figure 3, A and B). Gene expression profiles from 29 biopsy samples allowed a direct comparison between the four-gene RT-qPCR test, the four-gene microarray test, and the original 273-gene random forest CMS classifier. Figure 3C shows that the predicted chance of CMS4 measured with RT-qPCR correlates very well with the chance derived from the four-gene microarray test (Pearson's R = 0.90, 95% CI = 0.79 to 0.95, $P < .001$).

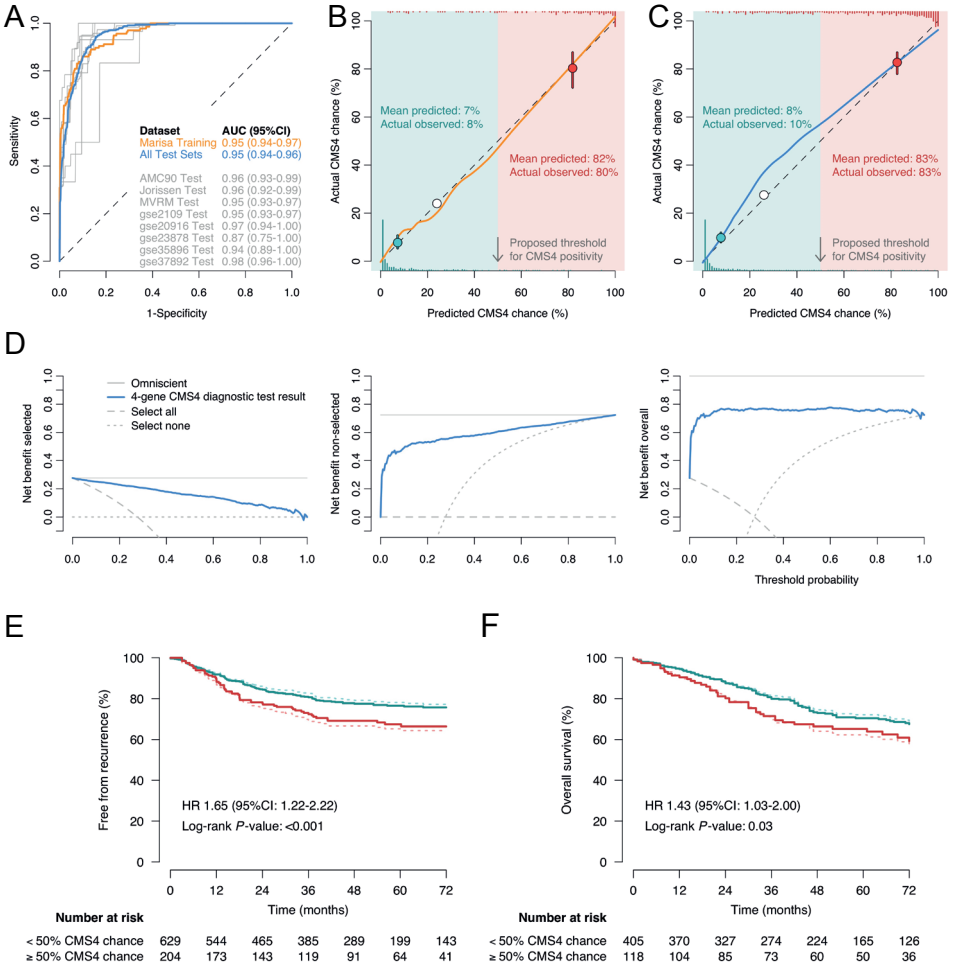

Figure 1. Performance of the 4-gene microarray test.
A) Receiver operating characteristic (ROC) curves to assess the discriminatory capacity of the four-gene microarray test. The reference standard is the applied 273-gene random forest CMS classifier. We estimated the area under the curve (AUC) within the training set (Marisa, orange line) and in the test sets (combined, blue line). **B and C)** Calibration curve analysis of predicted probability of CMS4 subtype vs actual probability in the training set (B; Marisa, n = 566) and the eight independent validation sets combined (C; n = 1259), after having corrected the diagnostic test for overoptimism by 1000-fold bootstrap resampling and uniform shrinkage (shrinkage factor 0.95). The solid black line shows the LOWESS smoothed relation between predicted and actual observed CMS4 chance. The Le Cessie-van Houwelingen goodness-of-fit test showed no statistically significant deviations between predicted and observed probabilities (training set P = .91; test sets combined P = .23). The histograms depict the distribution of predicted CMS4 chance in patients with (top and red) and without (bottom and green) actual CMS4 subtype according to the original random forest classifier. The three open circles show the mean predicted vs actual observed CMS4 chance in groups of patients: overall (white), within the subgroup below the 50% proposed threshold for CMS4 diagnostic test positivity (green), and within the subgroup above this threshold (red). The vertical bars accompanying the latter open circles show the 95% confidence intervals surrounding the actual observed CMS4 chance. **D)** Decision curve analysis, depicting the net benefit of the full range of thresholds for those selected (left), those not selected (middle), and the overall net benefit (right) based on all eight test data sets combined. At the ≥50% threshold, the test had an overall net benefit of 77 per ▶

▶ 100 patients tested, with a net benefit for those selected of 16 and for those not selected of 61. The maximum attainable net benefit per 100 patients tested is 27 for the selected, 73 for the nonselected, and 100 overall. **E and F)** Kaplan-Meier graphs depicting disease-free survival (DFS) (E) and overall survival (OS) (F) within Affymetrix data sets, according to CMS4 classification as predicted by our four-gene microarray test (solid lines) and by the original random forest classifier for comparison (dotted lines), both binned at a threshold for CMS4 probability of 50% (green < 50%, red ≥ 50%). Only patients with unequivocal 273-gene random classifier results were included to be able to directly compare our results with those reported by Guinney et al.[1] Hazard ratios (HRs) and associated 95% confidence intervals (CIs) are based on data set–stratified Cox proportional hazard models, and P values are based on data set–stratified log-rank tests. All statistical tests were two-sided. AUC = area under the curve; CI = confidence interval; HR = hazard ratio.

Furthermore, at a threshold of 50% or greater CMS4 chance, the four-gene RT-qPCR test identified seven of the nine biopsies that were assigned CMS4 status by applying the 273-gene CMS classifier (77.8% sensitivity). Of the 17 biopsies that were assigned a non-CMS4 status with the classifier, 16 were also CMS4-negative when analyzed with the RT-qPCR test (94.0% specificity) (Figure 3C). These results correspond with an excellent AUC of 0.97 (95% CI = 0.93 to 1.00) (Figure 3B inset).

Dealing With Intratumor CMS4 Subtype Heterogeneity by Sampling Multiple Tumor Regions

Multiregion analysis of tumors in the BOSS study demonstrated extensive ITH with respect to CMS4 status. CMS4 test results were homogeneously low (<50% CMS4 chance) in nine of 20 tumors; in two tumors, the test-results were consistently high (≥50% in 4 or 5 of the 5 biopsies). However, in the remaining nine tumors, results were highly variable (Figure 3B).

This poses a challenge for selecting patients for subtype-targeted therapy. During colonoscopy, it is practically not feasible to take more than five biopsies in addition to those that are obtained for standard diagnostics. However, analysis of fewer biopsies would be more easily implemented in a routine pathological setting. We therefore set out to determine an optimal strategy for patient selection for clinical trials, based on the smallest number of biopsies with acceptable test performance. As a starting point, we choose to use the weighed means of multiple biopsies, rather than the presence of a single positive region. Based on the weighed mean chance of five samples, we considered BOSS tumors #09, #10, and #12 to be CMS4 positive (Figure 3, B and D). Analysis of fewer biopsies leads to a gradual decline of the positive predictive value from 68.2% (four biopsies) to 45.0% (one biopsy) and the negative predictive value from 98.3% (four biopsies) to 93.6% (one biopsy). In general, the two- and three-biopsy strategies show relatively minor loss of sensitivity and specificity while the results are markedly worse for a one-biopsy strategy (Supplementary Table 4).

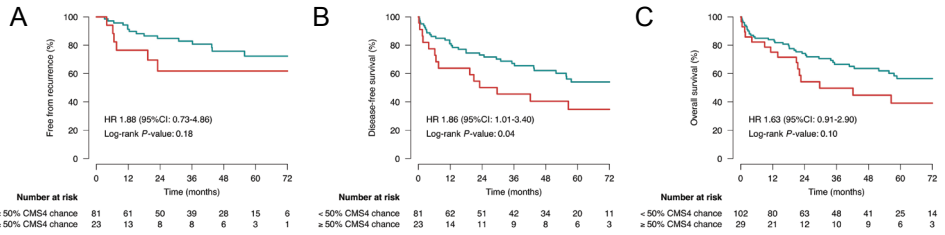

Figure 2. Prognosis of CMS4-type colon tumors identified by the four-gene reverse transcription polymerase chain reaction (RT-qPCR) test.
A–C) Kaplan-Meier graphs depicting recurrence-free survival (A), disease-free survival (DFS) (B), and overall survival (OS) (C) in UMCU Biobank set, according to CMS4 classification as predicted by our four-gene RT-qPCR test, binned at a threshold for CMS4 probability of 50% (green < 50%, red ≥ 50%). Disease-free survival is shown for patients without distant metastatic disease at presentation; overall survival is shown for all available patients. All statistical tests were two-sided. CI = confidence interval; HR = hazard ratio.

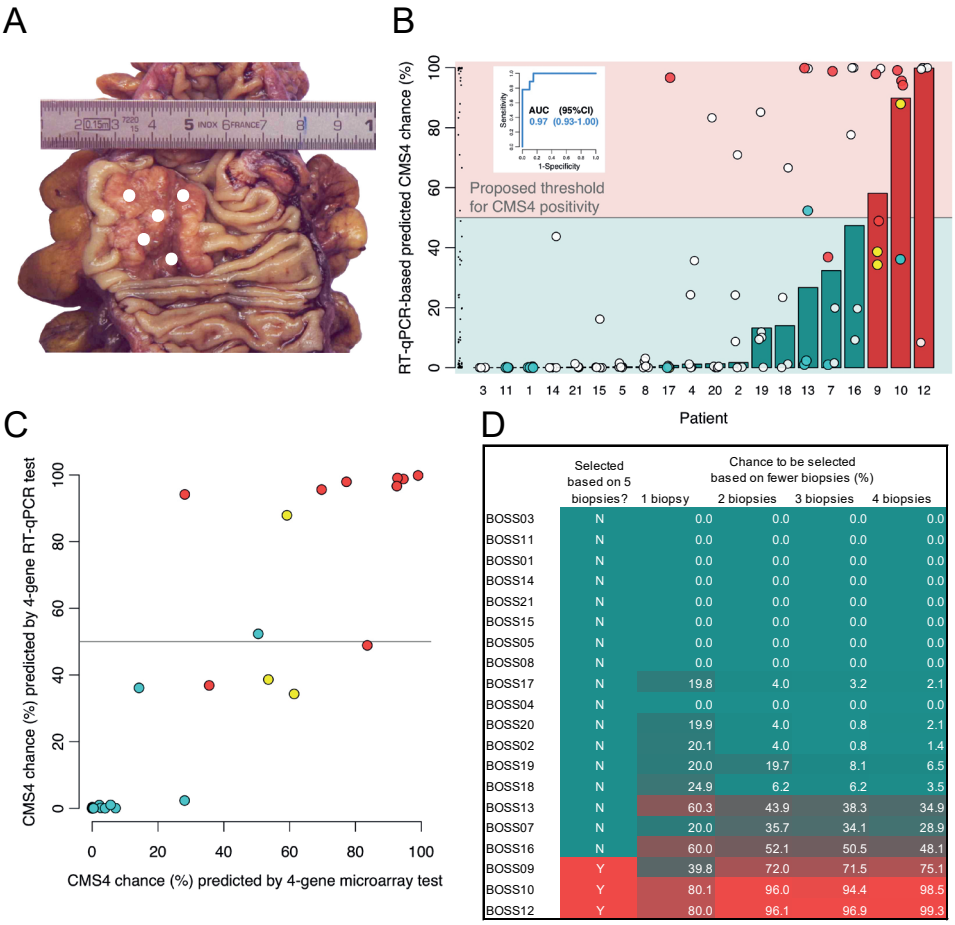

	Selected based on 5 biopsies?	Chance to be selected based on fewer biopsies (%)			
		1 biopsy	2 biopsies	3 biopsies	4 biopsies
BOSS03	N	0.0	0.0	0.0	0.0
BOSS11	N	0.0	0.0	0.0	0.0
BOSS01	N	0.0	0.0	0.0	0.0
BOSS14	N	0.0	0.0	0.0	0.0
BOSS21	N	0.0	0.0	0.0	0.0
BOSS15	N	0.0	0.0	0.0	0.0
BOSS05	N	0.0	0.0	0.0	0.0
BOSS08	N	0.0	0.0	0.0	0.0
BOSS17	N	19.8	4.0	3.2	2.1
BOSS04	N	0.0	0.0	0.0	0.0
BOSS20	N	19.9	4.0	0.8	2.1
BOSS02	N	20.1	4.0	0.8	1.4
BOSS19	N	20.0	19.7	8.1	6.5
BOSS18	N	24.9	6.2	6.2	3.5
BOSS13	N	60.3	43.9	38.3	34.9
BOSS07	N	20.0	35.7	34.1	28.9
BOSS16	N	60.0	52.1	50.5	48.1
BOSS09	Y	39.8	72.0	71.5	75.1
BOSS10	Y	80.1	96.0	94.4	98.5
BOSS12	Y	80.0	96.1	96.9	99.3

▶ **Figure 3.** Analysis of intratumor heterogeneity with regard to molecular subtypes by validation and clinical application of the four-gene RT-qPCR test.
A and B) Intratumor heterogeneity (ITH) in Biopsies Of Surgical Specimens study (BOSS) samples. Five random biopsy samples were obtained from fresh colon cancer resection specimens (n = 20) (A). Each biopsy was analyzed separately with the new reverse transcription polymerase chain reaction (RT-qPCR) test (B). The y-axis shows the predicted chance of CMS4 as measured with the RT-qPCR test. The cloud of black dots next to the y-axis shows the distribution of individual biopsy test results. Each large dot in the plot also represents the test outcome of an individual biopsy sample; a white dot means that the biopsy was only analyzed with the four-gene RT-qPCR test, colored dots were also tested with microarray; red dots were classified as CMS4 by the random forest classifier, green dots were classified as another subtype, and yellow dots were indeterminate samples. The bars represent the weighed mean chance of having the CMS4 subtype determined by mathematical pooling of the five RT-qPCR test results (see Supplementary Methods for details). Red bars indicate that the weighed mean chance was ≥50%; green bars indicate a weighed mean chance below the threshold. The inlay shows the receiver operating characteristic (ROC) curve of the four-gene RT-qPCR test, with the random forest CMS4 classifier as reference standard, based on the 29 biopsies that were both analyzed by RT-qPCR and Affymetrix microarray. **C)** Validation of RT-qPCR test scatter plot shows the four-gene microarray test results vs four-gene RT-qPCR test results (n = 29). Linear regression slope of 1.02 (95% confidence interval [CI] = 0.82 to 1.13); intercept at 0.02 (95% CI = -0.08 to 0.11). The agreement between the two four-gene tests at the 50% threshold was 86% (kappa = 0.70; 95% CI = 0.42 to 0.97). The biopsies were also classified with the random forest CMS classification (red = CMS4, green = other subtype, yellow = indeterminate). **D)** Influence of the number of biopsies analyzed on individual patient CMS4 classification and patient selection for targeted therapy, as compared with obtaining five biopsies per patient (data from the BOSS study, 20 patients contributing 99 biopsies). RT-qPCR = reverse transcription quantitative polymerase chain reaction.

DISCUSSION

In this report, we describe the development of a test that identifies CMS4 (mesenchymal-type) colon tumors based on RT-qPCR analysis of the expression of only four genes. Crucial to the clinical applicability of the assay is its external and cross-platform validation (from microarray to RT-qPCR), with excellent preservation of discriminatory ability. In contrast to gene expression arrays or RNA sequence analysis, RT-qPCR tests can be readily and widely implemented in molecular diagnostic laboratories, also in nonacademic centers. Translation of the test to formalin-fixed paraffin-embedded (FFPE) material would further increase the applicability of the test in multicenter follow-up studies. This will require an independent normalization procedure and a thorough assessment of the effect of the FFPE procedure on the sensitivity and specificity of the test.

Traditionally, diagnostic tests based on gene expression are developed using an unbiased approach, to identify genes that are predictive of prognosis or therapy response. Several genetic tools that predict recurrence risk for colorectal cancer patients have been developed in this fashion, including the 12-gene OncotypeDX recurrence score (Genomic Health), the 13-gene ColoGuideEx prognostic predictor, and the 18-gene ColoPrint assay.[28-30] Although these tests can identify patients with low and high risk for recurrence, they do not provide insight into biological differences and do not select patients for a specific type of therapy. The consensus molecular subtype classification couples activation of specific biological pathways to the different subtypes.[1] This enables development of patient selection

tools using a biased approach by selection of subtype-specific gene products that can be targeted therapeutically. The RT-qPCR test developed in this study includes PDGFRs and KIT, two key targets of a series of anticancer drugs, including imatinib and dasatinib. It is conceivable that small gene sets reflecting other CMS4-enriched pathways (e.g., complement, TGF-β) could also be developed as patient selection tools. Furthermore, by using a similar approach to the one presented here, it should be possible to develop novel diagnostic tools for the other CMSs.

We envision that the new test will be further developed as a prognostic as well as a predictive tool. Prospective studies are required to demonstrate whether the test has added value in identifying the approximately 30% of stage II or III colon cancer patients that will develop recurrence. In addition, adjuvant chemotherapy is estimated to prevent distant recurrence in only approximately 15% of the treated patients.[31] The test could be used to select patients with CMS4 tumors who might benefit from alternative adjuvant therapies. Novel CMS4-directed therapy is particularly warranted as a recent study has shown that these tumors fail to respond to oxaliplatin.[32] Imatinib has revolutionized the treatment of (mesenchymal) gastrointestinal stromal tumors (GISTs), prolonging median survival in advanced disease from 10 to 20 months to over 50 months.[33] Based on our preclinical prior work[10, 13] and that of others[11, 12, 14, 34], we propose that drugs cotargeting PDGFR and KIT, such as imatinib, could have therapeutic potential in the treatment of CMS4 colon cancer and that such patients can now be identified with the new test.

Next-generation sequencing has been used to demonstrate genomic ITH in many solid tumor types, including colon cancer[16, 17], but this issue has not been addressed in any of the gene expression–based classification studies in colon cancer.[1] Cellular gene expression is determined by a complex interplay of (epi)genetic factors and signals from the microenvironment.[16, 35-37] We have previously shown that KIT is highly expressed in regions of hypoxia.[13] In addition, tumor biopsies consist not only of cancer cells, but also contain non-neoplastic cells that have a major impact on the gene expression profiles of unsegregated samples. By applying the novel diagnostic test, we demonstrated considerable intratumor heterogeneity with respect to CMS4 status. Future studies should address the relationship between subtype ITH and genetic ITH in colorectal tumors.

In the original CMS study, tumors that were classified as non-CMS4, based on single-area analysis, still had a considerable chance of developing distant metastases.[1] A major question is whether such metastases originated from CMS4 regions that were missed in the single-area analyses or whether metastases can also originate from non-CMS4 regions. Studies in which multiple tumor regions are prospectively collected and analyzed in relation to disease progression are required to shed light on this issue.

Based on our study of ITH, we propose to select patients for CMS4-targeted therapy by analyzing two or more biopsies from separate tumor regions and assessing the weighed

mean CMS4 chance. Although analysis of two biopsies clearly does not capture subtype ITH as well as analysis of five biopsies would, this strategy resulted in only minor loss of discriminative test performance and has a higher chance of being implemented in routine diagnostics. We recently initiated a proof-of-concept trial that evaluates the effects of imatinib therapy on the aggressive biology of CMS4 tumors in the preoperative window period (ImPACCT trial; ClinicalTrials.gov NCT02685046). For this trial, patients are preselected based on the weighed mean RT-qPCR test results from three endoscopic biopsies. However, if CMS4 driver pathways are indeed universally implicated in colon cancer metastasis, regardless of the percentage of CMS4 tissue in the primary tumor (subtype ITH), the number of biopsies that needs to be analyzed should be increased or the threshold for patient selection should be lowered. Importantly, lowering the threshold will not affect the total net benefit of the test, but will shift the benefit toward the treated patient group. The results from the ImPACCT trial and future clinical studies in which the effects of targeted therapy on CMS4 tumors are documented will allow an optimized application of the new test as a diagnostic tool.

This study was limited to the design of a diagnostic tool for the identification of CMS4 tumors only. The developed test works well on fresh-frozen tumor tissue but was not evaluated on FFPE tissue, which may further increase its applicability. Finally, the sample size of the study investigating subtype ITH was relatively small but sufficiently large to refute the hypothesis that such ITH does not exist. A larger prospective study is now required to determine the frequency and extent of subtype ITH in relation to prognosis and treatment response.

In conclusion, we have developed a four-gene RT-qPCR diagnostic tool that can be used to select individual patients with CMS4-type colon tumors for targeted treatment. By analyzing multiple tumor areas with the new test, we have demonstrated the existence of extensive intratumor subtype heterogeneity and present a practical approach to dealing with this extra level of complexity in the context of patient selection.

REFERENCES

1. Guinney J, Dienstmann R, Wang X, et al. The consensus molecular subtypes of colorectal cancer. *Nat Med*. 2015;**21**(11):1350-6.
2. Calon A, Lonardo E, Berenguer-Llergo A, et al. Stromal gene expression defines poor-prognosis subtypes in colorectal cancer. *Nat Genet*. 2015;**47**(4):320-9.
3. Isella C, Terrasi A, Bellomo SE, et al. Stromal contribution to the colorectal cancer transcriptome. *Nat Genet*. 2015;**47**(4):312-9.
4. Calon A, Espinet E, Palomo-Ponce S, et al. Dependency of colorectal cancer on a TGF-beta-driven program in stromal cells for metastasis initiation. *Cancer Cell*. 2012;**22**(5):571-84.
5. Heldin CH, Lennartsson J. Structural and functional properties of platelet-derived growth factor and stem cell factor receptors. *Cold Spring Harb Perspect Biol*. 2013;**5**(8):a009100.
6. Jechlinger M, Sommer A, Moriggl R, et al. Autocrine PDGFR signaling promotes mammary cancer metastasis. *J Clin Invest*. 2006;**116**(6):1561-70.
7. Chu JS, Ge FJ, Zhang B, et al. Expression and prognostic value of VEGFR-2, PDGFR-beta, and c-Met in advanced hepatocellular carcinoma. *J Exp Clin Cancer Res*. 2013;**32**:16.
8. Sulzbacher I, Birner P, Traxler M, et al. Expression of platelet-derived growth factor-alpha alpha receptor is associated with tumor progression in clear cell renal cell carcinoma. *Am J Clin Pathol*. 2003;**120**(1):107-12.
9. Henriksen R, Funa K, Wilander E, et al. Expression and prognostic significance of platelet-derived growth factor and its receptors in epithelial ovarian neoplasms. *Cancer Res*. 1993;**53**(19):4550-4.
10. Steller EJA, Raats DA, Koster J, et al. PDGFRB promotes liver metastasis formation of mesenchymal-like colorectal tumor cells. *Neoplasia*. 2013;**15**(2):204-17.
11. Kitadai Y, Sasaki T, Kuwai T, et al. Targeting the expression of platelet-derived growth factor receptor by reactive stroma inhibits growth and metastasis of human colon carcinoma. *Am J Pathol*. 2006;**169**(6):2054-65.
12. Shinagawa K, Kitadai Y, Tanaka M, et al. Stroma-directed imatinib therapy impairs the tumor-promoting effect of bone marrow-derived mesenchymal stem cells in an orthotopic transplantation model of colon cancer. *Int J Cancer*. 2013;**132**(4):813-23.
13. Fatrai S, van Schelven SJ, Ubink I, et al. Maintenance of Clonogenic KIT(+) Human Colon Tumor Cells Requires Secretion of Stem Cell Factor by Differentiated Tumor Cells. *Gastroenterology*. 2015;**149**(3):692-704.
14. Chen EC, Karl TA, Kalisky T, et al. KIT Signaling Promotes Growth of Colon Xenograft Tumors in Mice and Is Up-Regulated in a Subset of Human Colon Cancers. *Gastroenterology*. 2015;**149**(3):705-17 e2.
15. Lohmann S, Herold A, Bergauer T, et al. Gene expression analysis in biomarker research and early drug development using function tested reverse transcription quantitative real-time PCR assays. *Methods*. 2013;**59**(1):10-9.
16. Sottoriva A, Kang H, Ma Z, et al. A Big Bang model of human colorectal tumor growth. *Nat Genet*. 2015;**47**(3):209-16.
17. Kogita A, Yoshioka Y, Sakai K, et al. Inter- and intra-tumor profiling of multi-regional colon cancer and metastasis. *Biochem Biophys Res Commun*. 2015;**458**(1):52-6.
18. Collins GS, Reitsma JB, Altman DG, et al. Transparent Reporting of a multivariable prediction model for Individual Prognosis or Diagnosis (TRIPOD): the TRIPOD statement. *Ann Intern Med*. 2015;**162**(1):55-63.
19. Bustin SA, Benes V, Garson JA, et al. The MIQE guidelines: minimum information for publication of quantitative real-time PCR experiments. *Clin Chem*. 2009;**55**(4):611-22.
20. Vickers AJ, Elkin EB. Decision curve analysis: a novel method for evaluating prediction models. *Med Decis Making*. 2006;**26**(6):565-74.
21. Rousson V, Zumbrunn T. Decision curve analysis revisited: overall net benefit, relationships to ROC curve analysis, and application to case-control studies. *BMC Med Inform Decis Mak*. 2011;**11**:45.
22. Marisa L, de Reynies A, Duval A, et al. Gene expression classification of colon cancer into molecular subtypes: characterization, validation, and prognostic value. *PLoS Med*. 2013;**10**(5):e1001453.
23. Vickers AJ, Van Calster B, Steyerberg EW. Net benefit approaches to the evaluation of prediction models, molecular markers, and diagnostic tests. *BMJ*. 2016;**352**:i6.
24. Braun K, Sjoberg DD, Vickers AJ, et al. A Four-kallikrein Panel Predicts High-grade Cancer on Biopsy: Independent Validation in a Community Cohort. *Eur Urol*. 2016;**69**(3):505-11.

25. Huang YQ, Liang CH, He L, et al. Development and Validation of a Radiomics Nomogram for Preoperative Prediction of Lymph Node Metastasis in Colorectal Cancer. *J Clin Oncol*. 2016.
26. Moons KG, de Groot JA, Linnet K, et al. Quantifying the added value of a diagnostic test or marker. *Clin Chem*. 2012;**58**(10):1408-17.
27. American Joint Committee on Cancer. Colon and Rectum. In: Edge SB, Byrd SR, Compton CC, Fritz AG, Greene FL, Trotti A, editors. AJCC Cancer Staging Manual. 7th ed. New York: Springer-Verlag; 2010. p. 143-64.
28. Yothers G, O'Connell MJ, Lee M, et al. Validation of the 12-gene colon cancer recurrence score in NSABP C-07 as a predictor of recurrence in patients with stage II and III colon cancer treated with fluorouracil and leucovorin (FU/LV) and FU/LV plus oxaliplatin. *J Clin Oncol*. 2013;**31**(36):4512-9.
29. Agesen TH, Sveen A, Merok MA, et al. ColoGuideEx: a robust gene classifier specific for stage II colorectal cancer prognosis. *Gut*. 2012;**61**(11):1560-7.
30. Maak M, Simon I, Nitsche U, et al. Independent validation of a prognostic genomic signature (ColoPrint) for patients with stage II colon cancer. *Ann Surg*. 2013;**257**(6):1053-8.
31. Bockelman C, Engelmann BE, Kaprio T, et al. Risk of recurrence in patients with colon cancer stage II and III: a systematic review and meta-analysis of recent literature. *Acta Oncol*. 2015;**54**(1):5-16.
32. Song N, Pogue-Geile KL, Gavin PG, et al. Clinical Outcome From Oxaliplatin Treatment in Stage II/III Colon Cancer According to Intrinsic Subtypes: Secondary Analysis of NSABP C-07/NRG Oncology Randomized Clinical Trial. *JAMA Oncol*. 2016;**2**(9):1162-9.
33. Blanke CD, Rankin C, Demetri GD, et al. Phase III randomized, intergroup trial assessing imatinib mesylate at two dose levels in patients with unresectable or metastatic gastrointestinal stromal tumors expressing the kit receptor tyrosine kinase: S0033. *J Clin Oncol*. 2008;**26**(4):626-32.
34. Bellone G, Ferrero D, Carbone A, et al. Inhibition of cell survival and invasive potential of colorectal carcinoma cells by the tyrosine kinase inhibitor STI571. *Cancer Biol Ther*. 2004;**3**(4):385-92.
35. Kim TM, Jung SH, An CH, et al. Subclonal Genomic Architectures of Primary and Metastatic Colorectal Cancer Based on Intratumoral Genetic Heterogeneity. *Clin Cancer Res*. 2015.
36. Pisco AO, Huang S. Non-genetic cancer cell plasticity and therapy-induced stemness in tumour relapse: 'What does not kill me strengthens me'. *Br J Cancer*. 2015;**112**(11):1725-32.
37. Abelson S, Shamai Y, Berger L, et al. Niche-dependent gene expression profile of intratumoral heterogeneous ovarian cancer stem cell populations. *PLoS One*. 2013;**8**(12):e83651.

SUPPLEMENTARY METHODS

Patient series

We used eleven distinct patient series for this manuscript. Nine were publically available microarray datasets (GSE39582, GSE33113, GSE17537, GSE14333, GSE13294, GSE20916, GSE2109, GSE23878, GSE35896, GSE37892) comprising a total of 1,825 unique samples (see **Supplementary Table 1** for details).

As a training set for the RT-qPCR test rule we established a cohort of tumors collected at the University Medical Center Utrecht. Fresh-frozen primary tumor tissue samples from colon cancer patients who underwent surgery between 2004 and 2014 were retrospectively collected. Neoadjuvantly treated tumors were excluded, as well as primary rectal cancers and tumors staged T1 (American Joint Committee on Cancer tumor node metastasis (TNM) staging system[1]). Clinical and pathological data were extracted from medical records and pathology reports and delivered pseudo-anonymously by a trusted third party. Collection, storage and use of tissue and patient data were performed in agreement with the 'Code for Proper Secondary Use of Human Tissue in The Netherlands' (available at http://www.federa.org/codes-conduct). The study protocol was approved by the UMCU Biobank's ethical committee (protocol ID #14-255). Tissue samples of 148 tumors from 143 patients were available. Of the 148 samples, 135 (91%) fulfilled RNA quality requirements (see **Supplementary Table 2** for patient and tumor characteristics). This sample size was deemed sufficient to characterize the distribution of our genes of interest when assessed by RT-qPCR (i.e. a sample of 135 provides 95% confidence that the observed standard deviation is within 12% of the true standard deviation, and the observed mean is within 5% of the true mean (based on simulated data with 10,000 times random sampling, provided that the samples are normally distributed, and considering a fairly large relative standard deviation of 0.3)). Accurate estimation of this distribution was a prerequisite for translating our microarray developed CMS4-test to the RT-qPCR platform (see below).

For validation of the RT-qPCR test and assessment of intratumor heterogeneity, we collected 20 colon cancer resection specimens from routine surgery. Characteristics of resection specimens included in the BOSS study can be found in **Supplementary Table 3**. Immediately after resection, the specimen was transferred to the Pathology department. Under supervision of an experienced pathologist, five biopsy samples from randomly selected non-adjacent tumor areas were obtained with different endoscopic biopsy forceps to prevent cross-contamination. Endoscopic forceps were used to simulate the clinical diagnostic setting. The samples were snap-frozen in liquid nitrogen and stored at -80°C. This study was given the acronym BOSS (Biopsies Of Surgical Specimens); the protocol was also approved by the UMCU Biobank's ethical committee (protocol ID #14-256). The sample size provides 96% power to detect a prevalence of heterogeneity of 15% or more

(where heterogeneity is defined as CMS4-status agreement of all five biopsies per patient). If none of the 20 patients would show intratumor heterogeneity, this would exclude a clinically relevant prevalence of CMS4-heterogeneity within patients and would lead to the adoption of a one-biopsy strategy.

RNA isolation and RT-qPCR analysis

Frozen tissue samples from the UMCU Biobank were cut in 20 µm-thick cryosections with a cryostat. Five sections were immediately immersed in 350 µL RLT buffer (RNeasy Mini Kit, Qiagen, Stockholm, Sweden) + 1% β-mercaptoethanol. Frozen BOSS biopsy samples were immersed in RLT buffer + 1% β-mercaptoethanol and disrupted and homogenized using a rotator-stator device. Total RNA was isolated according to the manufacturer's instructions. On-column DNase digestion was performed. Membrane-bound RNA was eluted from the column in 30 µL RNase-free water and stored at -80°C. The RNA concentration was measured using NanoDrop 2000 (Thermo Scientific). The RNA integrity was assessed with the Agilent RNA 6000 Nano Kit on an Agilent 2100 Bioanalyzer; only samples with an RNA integrity number (RIN) >7 were subjected to further analysis.

cDNA was prepared from 500ng RNA using the High Capacity RNA-to-cDNA kit (Applied Biosciences). The reverse transcription (RT) product was diluted five times prior to the quantitative real-time polymerase chain reaction (qPCR). 2ul of the diluted RT-product was added to 10ul TaqMan Universal Master Mix, 1ul TaqMan assay (Life Technologies; *PDGFRA*: Hs00998018_m1, *PDGFRB*: Hs01019589_m1, *PDGFC*: Hs01044219_m1, *KIT*: Hs00174029_m1, *GAPDH*: Hs02758991_g1) and 7ul H_2O to a final reaction volume of 20ul. TaqMan RT-qPCR was performed with Viia™ 7 system (Applied Biosystems). The reaction started with 10 minutes at 95°C, followed by 40 cycles of 10 seconds at 95°C + 60 seconds at 60°C. Duplicate wells were run for each assay, the mean Ct was used in subsequent analyses. Relative gene expression was quantified with the ΔCt method, using *GAPDH* as a reference gene. RNA isolated from the Hs729 rhabdomyosarcoma cell line [Hs729T] (ATCC® HTB-153™) was used as external calibrator to correct for potential inter-run variation.

We mathematically pooled the five separate BOSS samples per patient to derive a weighed mean chance of CMS4, so that the relative contribution of each of the five biopsies to the final test score is determined by the RNA concentration of that sample. For each gene we calculated the mean gene expression of five biopsies according to the function: mean $\Delta Ct = -\log_2((2\text{^-}\Delta Ct_1\text{*}[RNA]_1)/sum[RNA]_{1\text{-}5} + (2\text{^-}\Delta Ct_2\text{*}[RNA]_2)/sum[RNA]_{1\text{-}5} + (2\text{^-}\Delta Ct_3\text{*}[RNA]_3)/sum[RNA]_{1\text{-}5} + (2\text{^-}\Delta Ct_4\text{*}[RNA]_4)/sum[RNA]_{1\text{-}5} + (2\text{^-}\Delta Ct_5\text{*}[RNA]_5)/sum[RNA]_{1\text{-}5})$. The mean ΔCt values are then entered into the 4-gene RT-qPCR prediction to yield the weighed mean chance of CMS4.

Microarray gene expression data processing and CMS classification

The Raw Affymetrix U133plus2 CEL files of the selected patient samples from the nine included publicly available gene expression datasets were retrieved from the Gene Expression Omnibus (**Supplementary Table 1**), and supplemented with CEL files from our BOSS study. We preprocessed all microarray gene expression data using frozen robust multiarray analysis (fRMA)[2] (R package *frma* version 1.16.0) with rma background correction, quantile normalization, and random effect summarization. Following this, we used ComBat[3] (without covariates) to adjust for batch effects on the fully aggregated microarray dataset (ComBat, R package *sva version 3.10.0*). We obtained batch identifiers for the CIT dataset from the authors and used scan dates in combination with hospital of origin as a proxy for batch in the other datasets (binning samples with unique scan dates per hospital or per dataset if needed).

We then CMS-classified each sample as described by Guinney *et al.*[4] For this, we first selected the probe set with the highest median absolute deviation for each gene, then log2-transformed and scaled all data to a standard normal distribution, and applied the 273-gene random forest CMS classifier (available at Github, https://github.com/Sage-Bionetworks/crcsc; applied with predict.randomForest, R package *randomForest* version 4.6-10), obtaining for each sample the predicted probability of belonging to the CMS1, 2, 3 or 4 subtype. As the random forest classifier was originally trained on part of the same samples present in our aggregated dataset, and as the available randomForest object included information on true consensus clustering-based CMS-labels of the random forest training samples that also included GSM IDs for many, we were able to compare the results of applying the random forest classifier to our data following our preprocessing steps, and with the random forest classifier performance on the original data. This resulted in a sensitivity of 0.976 and a specificity of 0.939 for true CMS4 status in our data (n=537), compared to the originally reported 0.917 sensitivity and 0.966 specificity of the random forest classifier (for Affymetrix/RNAseq data).

Development of a microarray-based CMS4 diagnostic test using PDGFRA, PDGFRB, PDGFB, PDGFC, and KIT expression

All following steps involving the microarray-based CMS4 diagnostic test development were performed exclusively within the Marisa training dataset (n=566). We first selected the probe set with the highest overall fRMA-processed and ComBat-corrected expression level for each candidate CMS4 predictor gene (i.e. 203131_at for *PDGFRA*, 202273_at for *PDGFRB*, 216061_x_at for *PDGFB*, 218718_at for *PDGFC*, and 205051_s_at for *KIT*). To allow robust cross-platform translation of our diagnostic test, we then transformed the expression values for each gene to approximate a standard normal Gaussian distribution (with mean 0, SD 1, skewness 0, and Pearson's kurtosis 3). For this, we first natural log

transformed expression values if inspection of histograms showed a right-skewed distribution, subsequently used a Box-Cox power transformation[5] to approximate a Gaussian distribution (boxcox, R package *MASS* version 7.3-40), and then scaled the data to a standard normal distribution. This resulted in the following necessary transformation steps (i.e. for the fRMA-processed/ComBat-corrected gene expression values): $PDGFRA_{normalized} = (PDGFRA_{expression}^{3.082} - 801) / 225$; $PDGFRB_{normalized} = (PDGFRB_{expression}^{0.201} - 1.502) / 0.0237$; $PDGFB_{normalized} = (- (\ln(PDGFB_{expression})^{-4.269}) + 0.0692) / 0.00556$; $PDGFC_{normalized} = (PDGFC_{expression}^{1.234} - 13.211) / 1.962$; $KIT_{normalized} = (- (\ln(KIT_{expression})^{-0.445}) + 0.749) / 0.0210$ (**Supplementary Fig. 3**).

We used these normalized gene-expression data to build a binary logistic regression model to predict CMS4 status as the diagnostic outcome. The CMS4 status was derived from the 273-gene random forest classifier with subjects considered to be CMS4 positive if the random forest posterior CMS4 probability was ≥0.5 (n=136); all others were considered to be CMS4 negative (n=430). With an approximately 27:1 event per variable ratio (i.e. CMS4 positive patients per candidate predictor gene), the Marisa dataset was deemed large enough for robust logistic regression modeling[6]. This left 1259 samples from public repositories for external validation of our developed test. Visual inspection of restricted cubic spline functions (5 knots) showed no important deviations from log-linearity for each of the five predictor genes with CMS4 status, and likelihood ratio tests for non-linearity in a full multivariable model with each predictor modeled as a spline were not significant for any predictor; each predictor was thus subsequently modeled linearly. We used a stepwise-backward modeling approach to select individual genes for the final diagnostic test, as based on the Akaike Information Criterion. Using this approach, only *PDGFB* was removed from the model (at a *P*-value of 0.68), and the final model thus consisted of *PDGFRA*, *PDGFRB*, *PDGFC* and *KIT*.

To correct this model for potential overoptimism (i.e. yielding too extreme predictions in new patients), we used a 1,000-fold bootstrap resampling internal validation procedure including predictor selection (*PDGFRA* was selected in 75% of bootstraps, *PDGFRB* in 100%, *PDGFB* in 20%, *PDGFC* in 100%, and *KIT* in 97%). By testing the resulting logistic regression model from each bootstrap sample on the full Marisa dataset we obtained a shrinkage factor of 0.953 (i.e. the slope of the bootstrap-derived linear predictor when fitted to the Marisa data, averaged over all bootstrap runs). Each regression coefficient of the "apparent" model (as specified and fitted in the full Marisa dataset) was then multiplied by this shrinkage factor, resulting in an "optimism-corrected" model after updating the model's intercept. This intercept updating is necessary to ensure that the average predicted CMS4 probability as derived with the shrunken regression coefficients match the actual observed average random-forest based CMS4 status in the Marisa dataset.

The CMS4 probability for new patients can then be calculated using the formula 1/

(1+exp(-linear predictor)), where the linear predictor is defined as the logistic regression equation of the "optimism-corrected" model: β_0 + $PDGFRA_{normalized\ expression}$*$\beta_{PDGFRA}$ + $PDGFRB_{normalized\ expression}$*$\beta_{PDGFRB}$ + $PDGFC_{normalized\ expression}$*$\beta_{PDGFC}$ + $KIT_{normalized\ expression}$*$\beta_{KIT}$. ($\beta_0$ denotes the updated intercept, and the other βs denote the shrunken logistic regression coefficients for each predictor). We changed none of the coefficients nor the intercept of the resulting CMS4 diagnostic test in subsequent performance evaluation and validation steps.

Evaluation of diagnostic test performance

To assess the performance of the developed CMS4 diagnostic test, we applied the test to all individual samples available for analysis, resulting in a predicted probability of CMS4 for each. For the microarray-based data, we used the Marisa-derived transformation steps (see above) for each predictor gene for all samples, following which we applied the diagnostic test without optimism correction (the "apparent" model) to the Marisa samples, and the optimism-corrected diagnostic test to the other samples. We compared the predicted CMS4 probabilities with the 273-gene random forest classifier-derived CMS4 status both continuously as well as using a threshold for the test results. For this report, this threshold was set at ≥50% chance of CMS4, as this is in line with the random forest derived CMS4 status (considered positive at a posterior CMS4 probability of ≥0.5), and as this threshold represents an equal weighing of harms and benefits to misidentified true CMS4 positive and negative patients (false positives and negatives) and correctly identified CMS4 positive and negative patients (true positives and negatives). In other words, a missed CMS4 patient is as bad as a false positive test result at this threshold. This makes sense, as the purpose of our diagnostic test is to select patients for PDGF/KIT targeted therapy for which we currently do not know the harms and benefits in this patient population.

First, we evaluated the test-derived predicted probabilities continuously to assess discrimination, calibration, and net benefit. For discrimination, we constructed receiver operating characteristic (ROC) curves and estimated the associated area under the curve (AUC), within the microarray development and test data (the latter combined and for each test dataset separately), and for the BOSS samples as based on the RT-qPCR results. An AUC of 0.5 means that the test discriminates as well between true CMS4 positive and negative patients as a test that merely assigns the average CMS4 probability to each patient (worthless), and an AUC of 1.0 means that the test discrimination is perfect.

For calibration, we plotted the predicted probabilities against the observed probabilities within the microarray development and aggregated test data making use of a LOWESS smoother. A test with perfect calibration will show a straight diagonal line, implying perfect agreement between predicted and observed CMS4 chance. To test for deviations between predicted and observed probabilities we used the le Cessie-van Houwelingen goodness-of-fit test[7]. Besides evaluating calibration continuously, we also compared the average predicted

CMS4 probability with the observed CMS4 frequency considering all patients, and within patients above and below the test positivity threshold.

For net benefit, we used decision curve analysis[8], extended to include the net benefit for non-selected patients as well as the overall net benefit[9]. The net benefit for those selected is calculated by subtracting from the number of true positives, the number of false positives multiplied by a weight that is based on the threshold for test positivity, and dividing the result by the number of patients tested (i.e. TP/n – (FP)/n*(p/(1-p)); TP=true positives, FP=false positives, p=threshold, n=total patients). For a threshold of 20% the weight is 0.20/(1-0.20)=0.25, and for a threshold of 80% the weight is 0.80/(1-0.20)=4. In the first example, false positives are considered 0.25 times as important as false negatives; in the second example, false positives are considered 4 times as important as false negatives. Just as with ROC curves, this net benefit can be estimated from the data for all possible thresholds, leading to a decision curve. The net benefit for patients who are not selected is calculated similarly by subtracting the number of false negatives from the number of true negatives, and the overall net benefit is then the sum of the net benefit for selected and unselected patients. A net benefit for those selected of 15 per 100 would mean that the test performs equivalently at that threshold to a test that would identify 15 true positives per 100 patients tested without identifying any false positives. The net benefit for those selected can thus never exceed the prevalence of the condition that the test aims to diagnose. Vice versa, the net benefit for those that are not selected can never exceed one minus the prevalence, and the overall net benefit cannot exceed 100%. The net benefit can also reach negative values, implying more harm than good. Here, we restricted the net benefit analyses to the microarray-based aggregated test data, and specifically report the numeric results at a threshold of 50% (implying equal weighing of false positives as false negatives).

At this 50% CMS4 probability threshold, we also calculated test accuracy measures (i.e. sensitivity, specificity, negative and positive predictive values, and percent agreement), within the microarray development and aggregated test datasets. As we developed our CMS4 diagnostic test in a patient cohort that included AJCC stage I though IV disease, and as the clinical relevance of our diagnostic test may likely depend on the stage of the disease, we also evaluated these test accuracy measures and the AUC within AJCC stage subgroups, both in the microarray development and aggregated test datasets for which stage was available.

Application of the diagnostic test to patient samples

As the gene-expression data that were used to derive the test were first transformed to a standard normal Gaussian distribution, the resulting regression equation underlying the diagnostic test can potentially be used with any gene-expression platform for which the necessary transformation steps are known to derive such a distribution. To allow translation

to the RT-qPCR platform, we first used dCt expression values of the 135 UMCU Biobank samples to establish the necessary transformation steps to yield a standard normal Gaussian distribution, resulting in: $PDGFRA_{normalized} = -(\ln(PDGFRA_{expression})^{0.227} - 1.167) / 0.0196$; $PDGFRB_{normalized} = -(\ln(PDGFRB_{expression})^{1.540} - 2.468) / 0.331$; $PDGFC_{normalized} = -(\ln(PDGFC_{expression})^{2.814} - 8.885) / 1.387$; $KIT_{normalized} = -(KIT_{expression}^{0.707} - 5.123) / 0.466$ (**Supplementary Fig. 6**). Following these transformation steps we applied the optimism-corrected diagnostic test to all RT-qPCR queried samples.

Evaluation of the microarray- to RT-qPCR-platform translation

We selected 30 BOSS samples with high RIN values, and various of RT-qPCR-based predicted chances of CMS4 from 7 different resection specimens for full Affymetrix gene expression profiling. This allowed us to compare the RT-qPCR test with the 4-gene microarray test and the original random forest-based CMS classifier. Affymetrix microarray analysis, fragmentation of RNA, labeling, hybridization to Human Genome U133 Plus 2.0 microarrays and scanning were performed following the manufacturer's protocol (Affymetrix). One sample did not meet library preparation quality criteria and was excluded from the analyses. These samples were fully independent of all diagnostic test development or cross-platform translation steps. We plotted the 4-gene RT-qPCR-test against the 4-gene microarray-based test results and estimated the Pearson's correlation coefficient (r), and the corresponding r^2 as a measure of explained variation. Furthermore, we fitted a linear regression line (with the RT-qPCR results as dependent and the microarray results as independent variable) to assess any bias (i.e. deviations of the intercept from 0 and of the slope from 1). We also evaluated the percent agreement and kappa between the RT-qPCR- and microarray-based test results when classifying samples to be CMS4 positive at a predicted probability threshold of ≥0.5.

Prognostic relevance of diagnostic test result

Time-to-recurrence (TTR), disease-free survival (DFS) and the overall survival (OS) were compared between patients who tested positive on our test and those who tested negative. TTR was measured from the date of surgery to the date of recurrence; the observations were censored at the date of death without recurrence. DFS was measured from the date of surgery to the date of recurrence or death from any cause. OS was measured from the date of surgery to the date of death. For DFS, we restricted the analyses to patients without metastases at presentation. For OS, data was analyzed across all stages. Survival curves were compared using the log-rank test (stratified for patient series for the microarray-based analyses). Hazard ratios (HRs) were estimated by Cox regression. The proportionality of the hazard assumption was not violated in any of the models according to inspection of Schoenfeld residual plots.

Intratumor heterogeneity (ITH) and clinical sampling strategy

In the Biopsies Of Surigical Specimens (BOSS) study 5 biopsies were obtained from random regions of 20 freshly resected colon tumors, as described above. All biopsies were analyzed separately with the 4-gene RT-qPCR test to identify CMS4-positive areas. Since we observed considerable ITH, we set out to estimate the amount of biopsies needed for correct identification of CMS4 positive patients. BOSS patients 9, 10, and 12 were considered as true CMS4 positive patients because their five-biopsy weighed mean chance of CMS4 was higher than 50%, and all other tumors were considered truly CMS4 negative (i.e., the five-biopsy results served as the reference standard). We next performed an *in silico* simulation study with 100,000 two-tiered bootstrap resampling runs (at patient (n=20) and biopsy level (varying between one and four) for each 100k bootstrap run)). Within each bootstrap, we calculated the weighed mean chance for each patient, based on the sampled biopsies for that patient for that bootstrap and then classified each patient in CMS4 positive or negative based on the proposed 50% chance threshold. Sensitivity, specificity, positive predictive value and negative predicted value were calculated for a 1-,2-,3-, and 4-biopsy approach. In approximately 4% of the bootstraps, none of the BOSS 9, 10, or 12 patients were sampled, and these bootstraps did not contribute to the sensitivity estimates. Likewise, in approximately 1% of bootstraps, none of the patients were deemed CMS4 test positive, and these bootstraps did not contribute to the positive predictive value estimates. We also calculated for each patient the likelihood of being selected as CMS4 positive (weighed mean chance more than 50%) based on 1,2,3 or 4 random biopsies.

REFERENCES

1. American Joint Committee on Cancer. Colon and Rectum. In: Edge SB, Byrd SR, Compton CC, Fritz AG, Greene FL, Trotti A, editors. AJCC Cancer Staging Manual. 7th ed. New York: Springer-Verlag; 2010. p. 143-64.
2. McCall MN, Bolstad BM, Irizarry RA. Frozen robust multiarray analysis (fRMA). *Biostatistics*. 2010;**11**(2):242-53.
3. Johnson WE, Li C, Rabinovic A. Adjusting batch effects in microarray expression data using empirical Bayes methods. *Biostatistics*. 2007;**8**(1):118-27.
4. Guinney J, Dienstmann R, Wang X, et al. The consensus molecular subtypes of colorectal cancer. *Nat Med*. 2015;**21**(11):1350-6.
5. Box GEP, Cox DR. An Analysis of Transformations. *Journal of the Royal Statistical Society Series B-Statistical Methodology*. 1964;**26**(2):211-52.
6. Peduzzi P, Concato J, Kemper E, et al. A simulation study of the number of events per variable in logistic regression analysis. *J Clin Epidemiol*. 1996;**49**(12):1373-9.
7. le Cessie S, van Houwelingen JC. A Goodness-of-Fit Test for Binary Regression Models, Based on Smoothing Methods. *Biometrics*. 1991;**47**(4):1267-82.
8. Vickers AJ, Elkin EB. Decision curve analysis: a novel method for evaluating prediction models. *Med Decis Making*. 2006;**26**(6):565-74.
9. Rousson V, Zumbrunn T. Decision curve analysis revisited: overall net benefit, relationships to ROC curve analysis, and application to case-control studies. *BMC Med Inform Decis Mak*. 2011;**11**:45.

SUPPLEMENTARY FIGURES AND TABLES

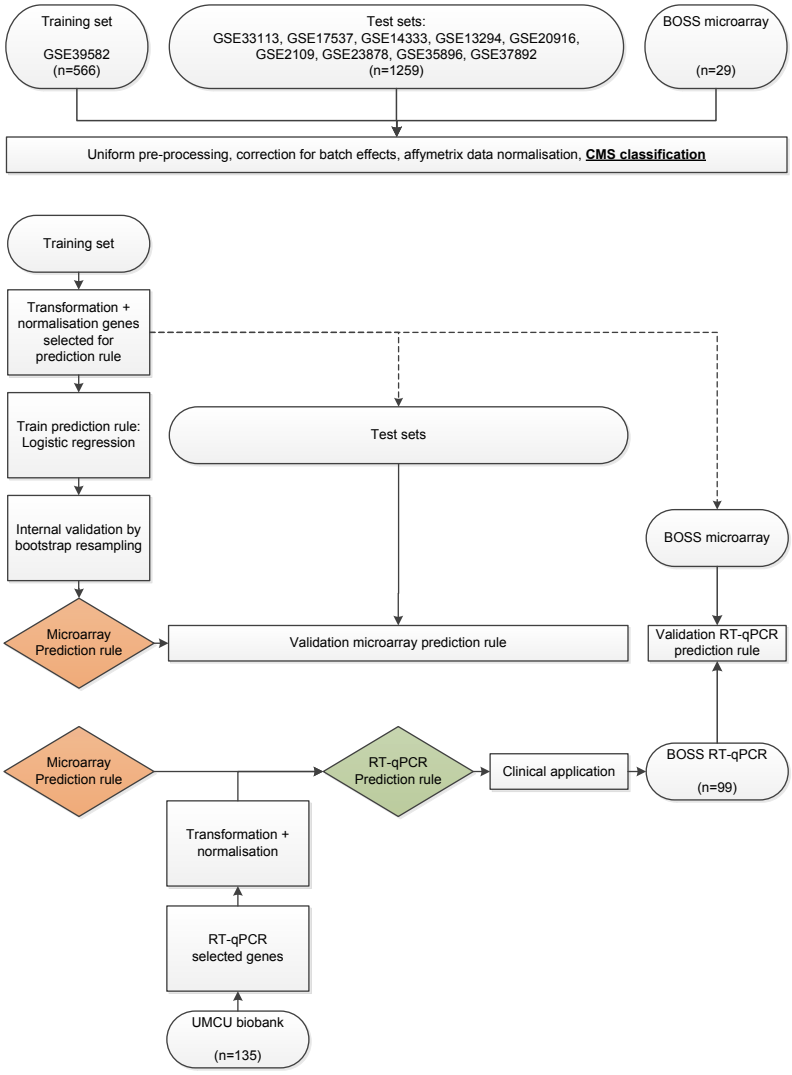

Supplementary Figure 1. Workflow for development of a RT-qPCR test that identifies CMS4-type colon tumors. First, separate microarray training and test sets were created for derivation of a prediction rule by pre-processing and normalizing the datasets simultaneously and by classifying all tumors according to the CMS classification. Second, the dataset GSE39582, was used to train a prediction rule with logistic regression analysis. This rule was subsequently tested on the other datasets. Third, to be able to apply the rule on RT-qPCR data we determined the range of gene expression of the four selected genes by RT-qPCR in 135 colon tumor samples from the UMCU Biobank. These results were used to optimize the prediction rule for RT-qPCR-based analysis of gene expression. Fourth, combined microarray and RT-qPCR analysis of 29 colon cancer biopsy samples (5 random biopsies from 7 different colon tumors, BOSS study) allowed us to assess the performance of the final prediction rule and to assess intratumor heterogeneity with respect to the CMS4 subtype.

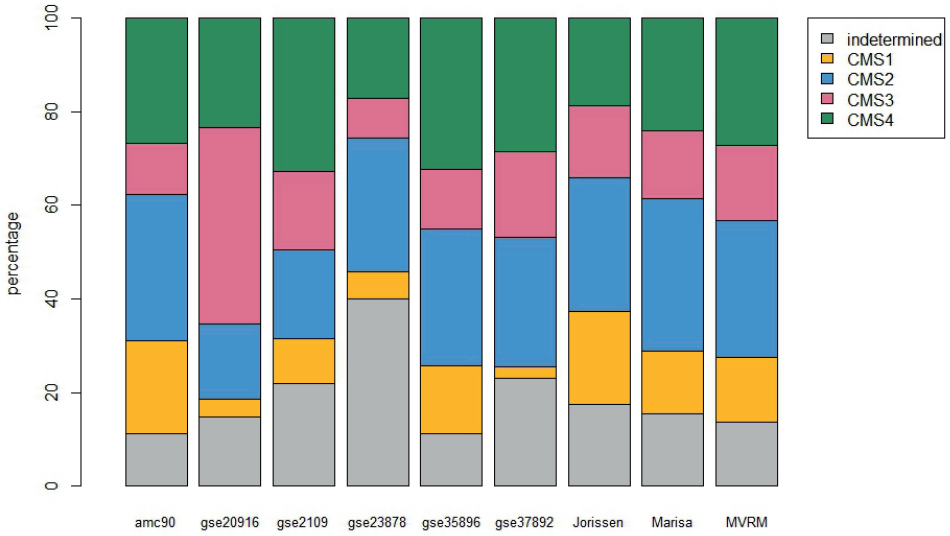

Supplementary Figure 2. Distribution of CMS classification per dataset, derived by application of the 273-gene random forest CMS classifier.

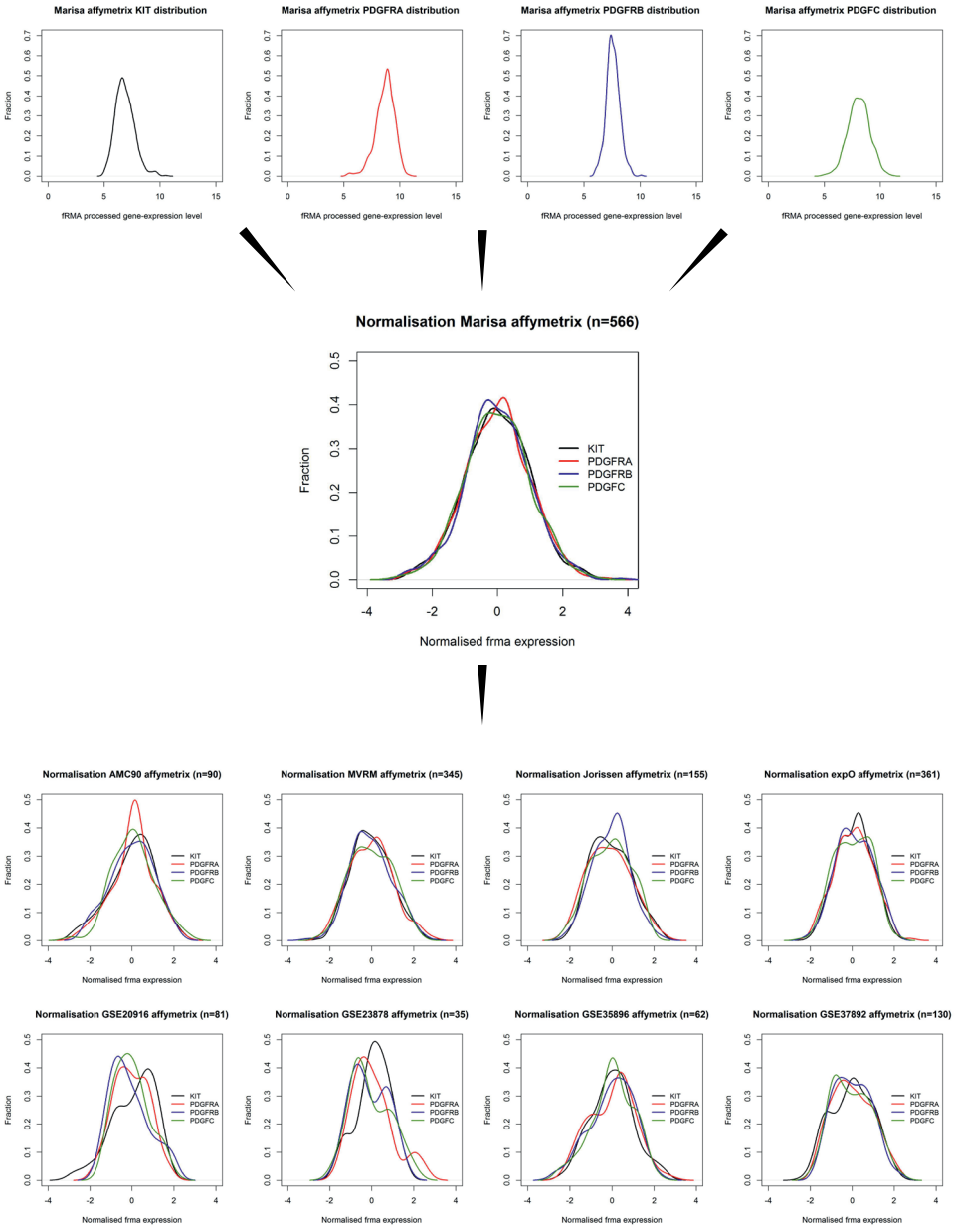

Supplementary Figure 3. Transformation and normalization of Affymetrix gene expression data.
To allow robust cross-platform translation of our diagnostic test, we transformed the expression values in the CIT (GSE39582) dataset for each gene to approximate a standard normal Gaussian distribution (with mean 0, SD 1, skewness 0, and Pearson's kurtosis 3). The other datasets were transformed and normalized using the values derived from the CIT dataset.

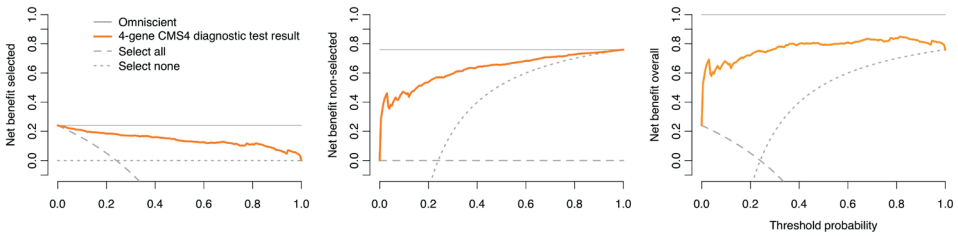

Supplementary Figure 4. Decision curve analysis, depicting the net benefit of the full range of thresholds for those selected (left), those not selected (middle) and the overall net benefit (right) based on the training data set.

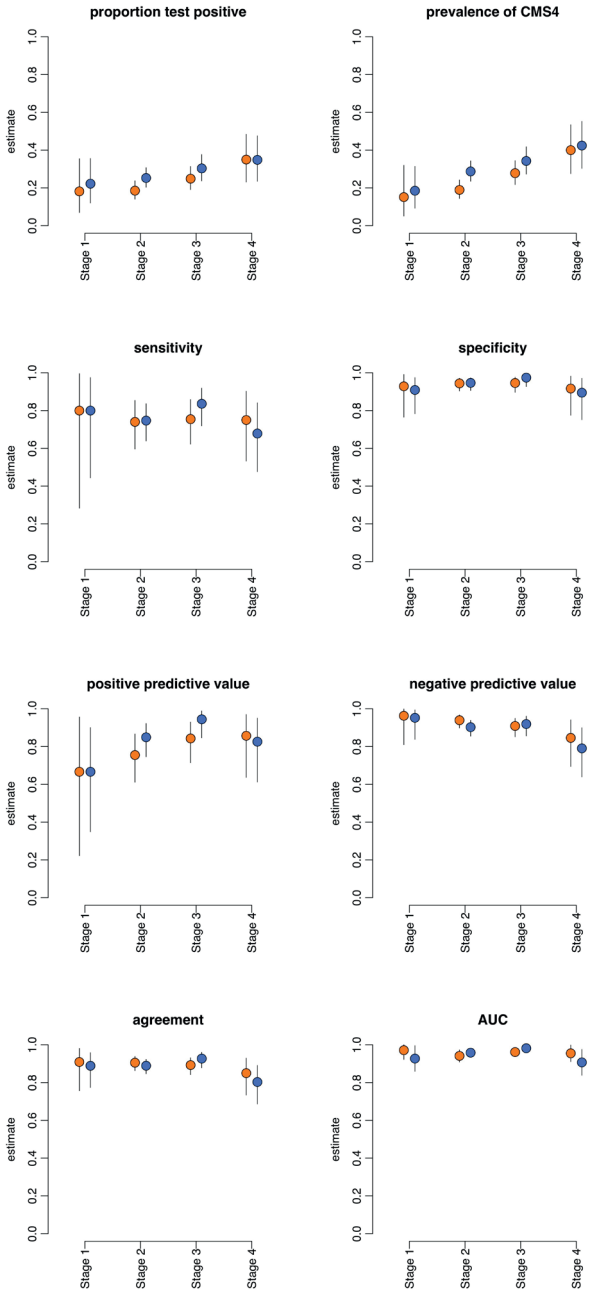

Supplementary Figure 5. Accuracy measures of 4-gene microarray test per AJCC stage in development set (Marisa (n=566), orange) and aggregated test datasets for which stage was reported ((n=587), blue). Prevalence CMS4 per stage is based on the original random forest CMS classifier, all other graphs show accuracy measures of the 4-gene test.

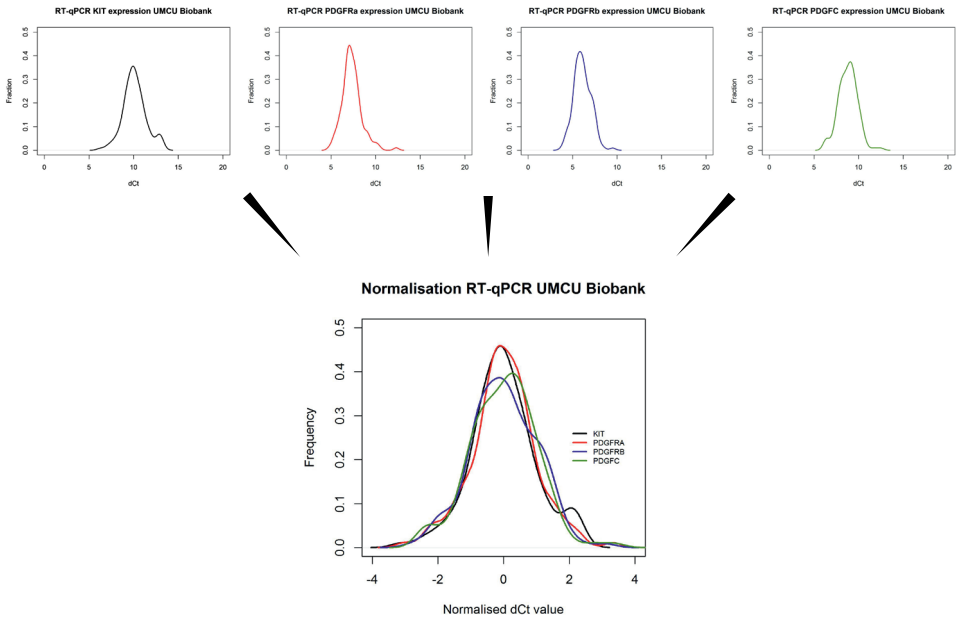

Supplementary Figure 6. Transformation and normalization of RT-qPCR gene expression data from UMCU Biobank.
RT-qPCR expression values were transformed to a standard normal Gaussian distribution. These transformation and normalization steps are required to calculate, for an individual patient, the chance of CMS4 subtype based on RT-qPCR gene expression data.

Supplementary Table 1. Characteristics of Affymetrix datasets used for derivation and validation of the micro-array based prediction rule.

Dataset/GEO accession number	CIT GSE39582	AMC-AJCCII-90 GSE33113	MVRM GSE17537 GSE14333	Jorissen GSE13294	GSE20916	expO GSE2109	GSE23878	GSE35896	GSE37892
Characteristics									
Number of samples	566	90	345	155	81	361	35	62	130
Age in years, median [range]	68 [22-97]	74 [34-95]	66 [23-94]	NR	63 [38-83]	65 [35-95]	NR	NR	68 [22-97]
Gender male, n (%)	310 (54.8)	42 (46.6)	190 (55.1)	NR	43 (53.1)	186 (51.5)	23 (65.7)	30 (48.4)	69 (53.1
Tumor location	colon	colon	colon + rectum 87vs 13%‡	NR	colon + rectum 81 vs. 19%	colon + rectum 93 vs 7%	NR	NR	colon
AJCC TNM / Duke stage, n (%)				NR	NR	**	NR	NR	
0	4 (0.7)	0	0	-	-	3 (1.0)	-	-	0
I/A	33 (5.8)	0	48 (13.9)	-	-	50 (15.9)	-	-	0
II/B	264 (46.6)	90 (100)	109 (31.6)	-	-	111 (35.2)	-	-	73 (56.2)
III/C	205 (36.2)	0	110 (31.9)	-	-	102 (32.4)	-	-	57 (43.8)
IV/D	60 (10.6)	0	78 (22.6)	-	-	49 (15.6)	-	-	0
Adjuvant chemotherapy		*NR*		*NR*	*NR*	*NR*	*NR*	*NR*	*NR*
TNM stage II, n (%)	56 (21.2)	-	22 (23.4)§	-	-	-	-	-	-
TNM stage III, n (%)	147 (71.7)	-	63 (69.2)‖	-	-	-	-	-	-
Overall survival		*NR*		*NR*	*NR*	*NR*	*NR*	*NR*	*NR*
No. of events(%)	191 (33.7)*	-	20 (36.3)¶	-	-	-	-	-	-
Follow-up (months), median [range]	51 [0-201]	-	50 [0-111]	-	-	-	-	-	-
Disease-free survival				*NR*	*NR*	*NR*	*NR*	*NR*	
No. of events (%)	177(31.2)†	18 (20.0)	69 (24.5)#	-	-	-	-	-	37 (28.5)
Follow-up (months), median [range]	43 [0-201]	39 [1-118]	40 [0-143]	-	-	-	-	-	43 [1-103]

ACJJ TNM=American Joint Committee on Cancer Tumor-Nodes-Metastasis staging; NR= not reported. * Reported for 562 cases. † Reported for 557 cases, ‡reported for 289 cases. § Reported for 94 cases. || Reported for 91 cases. ¶ Reported for 55 cases. # Reported for 281 cases. ** Reported for 315 cases

Supplementary Table 2. Characteristics of 135 tumor samples derived from 131 patients, from the UMCU Biobank that were used for normalization of the RT-qPCR test.

Characteristic	**No. (%)**
Patient characteristics (*n=131*)	
Age in years, median [range]	69 [27-88]
Gender male	71 (54.2)
TNM stage	
I	3 (2.3)
II	57 (43.5)
III	44 (33.6)
IV	27 (20.6)
Nodal status	
N0	68 (51.9)
N1	35 (26.7)
N2,	28 (21.4)
<10 LN examined	15 (11.4)
Adjuvant chemotherapy	
TNM stage II	2 (3.5)
TNM stage III	21 (47.7)
Tumor characteristics *(n=135)*	
Tumor location	
Caecum	31 (23.0)
Ascending colon/hepatic flexure,	34 (25.2)
Transverse colon,	17 (12.6)
Descending colon/splenic flexure	11 (8.1)
Sigmoid	42 (31.1)
Tumor diameter in cm, median [range]	5.0 [2.0-17.0]
pT-status	
T2	16 (11.9)
T3	90 (66.7)
T4	29 (21.5)
Histological type	
Adenocarcinoma	93 (68.9)
Mucinous adenocarcinoma	34 (25.2)
Other	8 (5.9)
Differentiation grade	
Well	5 (3.7)
Moderate	95 (70.4)
Poor	30 (22.2)
Undifferentiated	1 (0.7)
Not reported	4 (3.0)
Lymph, Vascular invasion	
Present	46 (34.1)
Absent	60 (44.4)
Not reported	6 (4.4)

Supplementary Table 3. Characteristics of resection specimens included in the BOSS study.

Sample	Location tumor	TNM	Stage
BOSS01	Sigmoid	T3N0M1	IV
BOSS02	Caecum	T4N1M1	III
BOSS03	Sigmoid	T3N0M0	II
BOSS04	Sigmoid	T3N2M1	IV
BOSS05	Sigmoid	T2N0M0	I
BOSS07	Sigmoid	T3N0M0	II
BOSS08	Colon ascendens	T2N0M0	I
BOSS09	Colon ascendens	T3N1M1	IV
BOSS10	Hepatic flexure	T3N0M0	II
BOSS11	Colon ascendens	T2N0M0	I
BOSS12	Sigmoid	T4N2M1	IV
BOSS13	Caecum	T4N0M0	II
BOSS14	Caecum	T4N0M0	II
BOSS15	Sigmoid	T2N0M0	I
BOSS16	Caecum	T4N1M1	IV
BOSS17	Colon ascendens	T4N1M0	III
BOSS18	Sigmoid	T4N2M1	IV
BOSS19	Sigmoid	T3N0M0	II
BOSS20	Caecum	T3N0M0	II
BOSS21	Sigmoid	T4N2M0	III

Supplementary Table 4. Influence of the number of biopsies analyzed on CMS4 classification on group-level.

Measure	No. of biopsies			
	1	2	3	4
CMS4-test positive patients, %	22.2	21.7	20.2	20.0
Positive predictive value, %	45.0	60.9	64.9	68.2
Negative predictive value, %	93.6	97.7	97.7	98.3
Sensitivity, %	66.6	88.1	87.6	91.0
Specificity, %	85.6	90.0	91.6	92.5

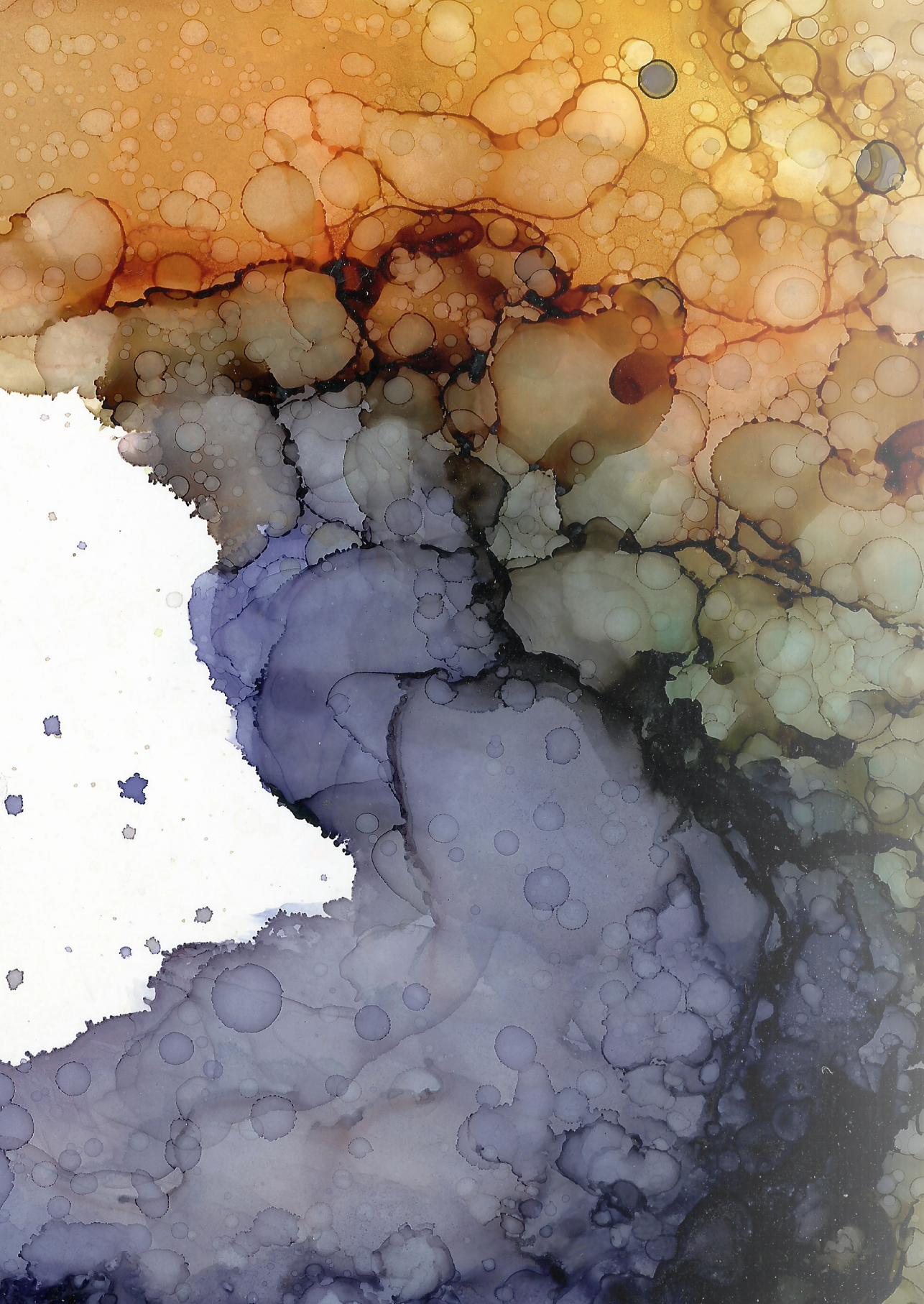

3

Imatinib treatment of poor prognosis mesenchymal-type primary colon cancer: a proof-of-concept study in the preoperative window period (ImPACCT)

ImPACCT study protocol

Inge Ubink, Haiko J. Bloemendal, Sjoerd G. Elias, Menno A. Brink, Matthijs P. Schwartz, Yvon C.W. Holierhoek, Paul M. Verheijen, Anneroos W. Boerman, Ron H.J. Mathijssen, Wendy W.J. de Leng, Roel A. de Weger, Wilhelmina M.U. van Grevenstein, Miriam Koopman, Martijn P. Lolkema, Onno Kranenburg and Inne H.M. Borel Rinkes

BMC Cancer, 2017;17(1):282-9

Preliminary data and discussion

Inge Ubink, Niek A. Peters, Alexander Constantinides, Joyce van Kuik, Menno A. Brink, Leon M.G. Moons, Haiko J. Bloemendal, Sjoerd G. Elias, Onno Kranenburg and Inne H.M. Borel Rinkes

IMPACCT STUDY PROTOCOL

ABSTRACT

Background

The identification of four Consensus Molecular Subtypes (CMS1-4) of colorectal cancer forms a new paradigm for the design and evaluation of subtype-directed therapeutic strategies. The most aggressive subtype - CMS4 - has the highest chance of disease recurrence. Novel adjuvant therapies for patients with CMS4 tumors are therefore urgently needed. CMS4 tumors are characterized by expression of mesenchymal and stem-like genes. Previous pre-clinical work has shown that targeting Platelet-Derived Growth Factor Receptors (PDGFRs) and the related KIT receptor with imatinib is potentially effective against mesenchymal-type colon cancer. In the present study we aim to provide proof for the concept that imatinib can reduce the aggressive phenotype of primary CMS4 colon cancer.

Methods

Tumor biopsies from patients with newly diagnosed stage I-III colon cancer will be analyzed with a novel RT-qPCR test to pre-select patients with CMS4 tumors. Selected patients (n=27) will receive treatment with imatinib (400mg per day) starting two weeks prior to planned tumor resection. To assess treatment-induced changes in the aggressive CMS4 phenotype, RNA sequencing will be performed on pre- and post-treatment tissue samples.

Discussion

The development of effective adjuvant therapy for primary colon cancer is hindered by multiple factors. First, new drugs that may have value in the prevention of (early) distant recurrence are almost always first tested in patients with heavily pre-treated metastatic disease. Second, measuring on-target drug effects and biological consequences in tumor tissue is not commonly a part of the study design. Third, due to the lack of patient selection tools, clinical trials in the adjuvant setting require large patient populations. Finally, the evaluation of recurrence-prevention requires a long-term follow-up. In the ImPACCT trial these issues are addressed by including newly diagnosed pre-selected patients with CMS4 tumors prior to primary tumor resection, rather than non-selected patients with late-stage disease. By making use of the pre-operative window period, the biological effect of imatinib treatment on CMS4 tumors can be rapidly assessed. Delivering proof-of-concept for drug action in early stage disease should form the basis for the design of future trials with subtype-targeted therapies in colon cancer patients.

Trial registration: ClinicalTrials.gov: NCT02685046. Registration date: February 9, 2016.

BACKGROUND

Mortality from colon cancer is almost invariably due to the development of distant metastases. In current practice, pathological (TNM stage) and clinical characteristics (age, co-morbidity) mainly determine the choice of adjuvant chemotherapy. However, these features have limited value in predicting which patients are at risk of developing metastases. In clinical trials, the five-year recurrence rate in stage III colon cancer patients is approximately 50% without adjuvant chemotherapy. With adjuvant treatment this is reduced to ~35%, implying that such treatment is only effective in a subgroup of patients.[1] Consequently, the majority of patients are currently being under- or over-treated. It is therefore important to be able to identify patients who are at high risk of recurrence and to develop more effective therapies to prevent relapse. Relapse-prevention trials in the adjuvant setting are challenging however, due to the long follow-up periods and the large numbers of patients that are required for sufficient statistical power. Prior evidence of drug activity and the availability of a companion diagnostic tool for patient selection could greatly facilitate the design and increase the quality of such studies.

Novel adjuvant therapies should be based on an understanding of the pathways that drive metastasis formation. Recent studies on molecular classification of colon cancer have provided insight into these pathways. Several research groups have independently developed classification systems for primary colon cancer based on gene expression profiles.[2-8] Cross-cohort analysis of the results has led to the identification of four consensus molecular subtypes (CMS1-4). Of these, CMS4 (~25% of colon cancers) is associated with a significantly worse disease-free and overall survival.[9] Novel treatment strategies for this subtype are thus particularly needed.

The pro-metastatic pathways that are upregulated in CMS4 provide opportunities for subtype-targeted therapy. CMS4 tumors are characterized by high expression of stem cell and mesenchymal genes, and a high stromal content.[9] We have previously shown that Platelet-Derived Growth Factor Receptors (PDGFRs) and KIT are highly expressed in mesenchymal-type colon tumors and that their expression strongly correlates with disease-free survival. Moreover, *in vitro* and *in vivo* inhibition of PDGFR and KIT tyrosine kinase signaling reduced invasiveness, metastatic potential and stem-like characteristics of mesenchymal-type colon cancer.[10-12] Based on these findings we hypothesize that patients with poor-prognosis mesenchymal-type colon cancers could benefit from treatment with imatinib, a tyrosine kinase inhibitor with high selectivity for PDGFR and KIT.

To test this hypothesis in a proof-of-concept study, we designed the ImPACCT trial (*Im*atinib as *P*re-operative *A*nti-*C*olon *C*ancer *T*argeted therapy). In ImPACCT, patients with CMS4 colon cancer are identified with a recently developed 4-gene RT-qPCR test that measures *PDGFRA, PDGFRB, PDGFC* and *KIT* expression levels in diagnostic tumor

biopsies.[13] Pre-selected patients with CMS4 tumors are then treated with imatinib during the pre-operative window period (the time between initial cancer diagnosis and surgery). This allows comparison of pre-treatment diagnostic tumor biopsies with biopsies obtained from the resection specimen after treatment. The primary objective is to assess whether imatinib treatment reduces the aggressive phenotype of CMS4 tumors in colon cancer patients. ImPACCT may not only form the basis for future adjuvant studies with imatinib, but could also serve as a blueprint for other proof-of-concept studies with subtype-targeted therapies.

Figure 1. Study flow chart.

METHODS

Study design

The ImPACCT trial is an open-label, multi-center proof-of-concept study. The primary endpoint of this trial is the effect of imatinib treatment on tumor biology, which is a pharmacodynamic endpoint, and as such this trial could be deemed a phase II/translational trial. A study flow chart is depicted in Figure 1.

Objectives

The primary objective of this trial is to investigate the effects of treatment on pro-metastatic pathways in aggressive primary CMS4 tumors. RNA sequencing will be performed on pre- and post-treatment tissue samples to document imatinib-induced genome-wide gene expression changes.

Secondary objectives include: to assess the extent of inhibition of PDGFR- and KIT after imatinib treatment; to relate intra-tumoral imatinib pharmacokinetics (PK) to systemic imatinib concentrations; to relate the level of inhibition of PDGFR/KIT signaling and the extent of changes in gene expression to the systemic and intra-tumoral PK of imatinib and its active metabolite CGP74588; to assess changes in tumor markers during treatment by measuring the concentrations of plasma-CEA and circulating tumor DNA (ctDNA) and to study the effects of imatinib on organoid-forming potential. Finally, the effect of short-term exposure to imatinib immediately followed by bowel surgery on the complication rate will be monitored.

Study population

All patients who are scheduled for a diagnostic colonoscopy on account of clinical suspicion of colon carcinoma will be approached for permission to obtain extra biopsies for this study in case a tumor is found in the colon. These biopsies are pre-screened with the new RT-qPCR test that predicts the chance of a tumor being CMS4, based on the combined expression of imatinib targets *PDGFRA, PDGFRB, PDGFC* and *KIT*. If the predicted chance of CMS4 in the biopsies is 50% or higher, patients will be approached for imatinib therapy. The study population that undergoes treatment with imatinib will thus consist of treatment-naïve newly diagnosed colon cancer patients with a tumor with a high probability of having the CMS4 phenotype. In- and exclusion criteria for enrolment in the second part of the trial (imatinib therapy) are listed in Table 1.

Table 1. In- and exclusion criteria for treatment with imatinib.

Inclusion criteria	Exclusion criteria
- Male or female aged ≥18 years; - Histologically proven adenocarcinoma of the colon; - Completed cancer staging with CT-abdomen and CT-thorax/X-thorax according to hospital's standard of care; - Confirmed eligibility for surgery with curative intent as deemed by the hospital's multidisciplinary board review; - Test positive for CMS4 subtype; - ≥4 properly stored pre-treatment biopsies for gene expression analysis/ELISA; - WHO performance status 0 or 1; - Adequate hematology status and organ function (defined as: normal creatinine clearance (≥60 ml/min (MDRD)), ALAT within 2.5x upper limit of normal (ULN), PT-INR < 1.5, leukocytes > 1,5*10^9/L, Hb > 6.0 mmol/L, platelets > 100*10^9/L); - Willingness and ability to comply with scheduled visits, treatment plans and laboratory tests; - Provision of written informed consent.	- The presence of synchronous distant metastases; - Current hospital standard of care dictates that subject should undergo any neoadjuvant therapy; - Concurrent participation in another clinical trial using any medicinal product, or participation in such a trial in the period of three months prior to the current trial; - Women who are pregnant, plan to become pregnant or are lactating during the study or for up to 30 days after the last dose of imatinib; - Known HIV or Hepatitis B/C infection; - Known symptomatic congestive heart failure; - Co-morbidity requiring concomitant treatment with drugs that act as strong inducers of CYP3A4 or with drugs with a narrow therapeutic range influenced by imatinib.

Study procedures

Patients preselected with the RT-qPCR test will be screened by a medical oncologist for inclusion in the second part of this study. Included patients will receive treatment with imatinib starting two weeks prior to planned tumor resection. Imatinib will be administered orally at a daily dosage of 400 milligram for two weeks, with the last dose given within 12 hours before surgery. Patients are requested to register drug intake and any adverse events in a patient diary. Before the start of imatinib therapy and at the end of the treatment period, blood samples will be obtained to measure ctDNA and plasma-CEA. Plasma imatinib trough levels will be determined on the day of surgery. Immediately following tumor resection, biopsies will be taken from the surgical specimen (post-treatment biopsies). Gene and protein expression of the pre-treatment biopsies (from colonoscopy) and post-treatments biopsies will be compared to assess the effects of imatinib therapy on PDGFR- and KIT-signaling and on the mesenchymal gene expression profile. After surgery, patients will be monitored according to standard of care. Any postoperative adverse events up until 14 days after discontinuation of study medication (end of study) will be documented.

Sample size calculation

This study is designed as a proof-of-concept study with multiple outcomes of interest. We expect the effect size of imatinib treatment on the various parameters to be very high, since we specifically select patients who express high levels of the drug targets. However, we are

aware of possible factors that may reduce the observed effect size. This includes intratumor heterogeneity in target expression – causing potential misclassification – and variation in drug distribution throughout the tumor and between patients. Therefore, we anticipate a medium to high Cohen effect size for the primary endpoint (i.e. Cohen's effect size of 0.65). To demonstrate such an effect, we need to include 27 (evaluable) patients, based on a two-sided paired-samples t-test with a significance level α of 0.05 and power 1-β of 90%. We specifically chose this high power in order not to dismiss effects that are potentially relevant for further development of imatinib therapy in colorectal cancer patients. Given that approximately 25% of colon cancers are CMS4, at least 4*27=108 eligible patients with newly diagnosed colon cancer will need to be prescreened with the RT-qPCR test. Since <10% of the patients undergoing colonoscopy are diagnosed with colon cancer, at least 1.100 patients will have to be approached for prescreening informed consent.

Statistical analyses

Imatinib-induced changes in the expression of specific gene signatures associated with CMS4 will be assessed by RNA-sequencing analysis. The signatures will be obtained from published literature and our own data. In addition, imatinib-induced gene expression changes will be analyzed in a non-biased way by gene ontology and gene enrichment analyses. Using the appropriate statistical tests depending on distribution of the data (paired samples t-test in case of normal distribution or Wilcoxon signed-rank test if the distribution remains non-normal even after transformation) we will test whether there is a significant change in gene signature expression. Phosphorylation of PDGFRα/β and KIT will be quantitatively assessed as a fraction of the total amount of PDGFRα/β and KIT present in a sample. Post-treatment imatinib-induced inhibition of PDGFR phosphorylation will be compared relative to the pre-treatment sample (i.e. the patient's internal control) using the appropriate statistical tests. Correlations between plasma trough levels and intratumoral concentration of imatinib, and between the extent of PDGFR and KIT inhibition and systemic/intratumoral imatinib concentrations will be evaluated using Pearson correlation coefficient. The Wilcoxon matched pairs signed rank test will be used to compare serial ctDNA and CEA levels. Organoid-forming potential of the tumors after imatinib therapy will be compared with the general success rate of organoid-establishment from colon cancers, using a Fisher exact test. In case of missing data, samples will be excluded pair-wise.

DISCUSSION

Targeted anti-cancer therapies that seem promising in pre-clinical and early-phase clinical trials often fail to show benefit in phase III randomized controlled trials. Up to sixty percent of phase III trials have negative outcomes.[14, 15] This high failure rate underscores the need for optimization of trial design, including better patient selection. Since the successful addition of oxaliplatin to the adjuvant chemotherapy regimen in 2004[16], no further advances have been made in the outcome of patients with stage II/III colon cancer. The lack of recent positive adjuvant chemotherapy trials is partly due to the fact that hardly any new drugs are actually tested in the adjuvant setting. Novel treatments are generally first tested in patients with metastatic disease who have no regular treatment options left, and who have often received multiple lines of systemic treatment. Therapies aimed at preventing the development or outgrowth of metastases are probably most effective at early disease stages, but their clinical development may be terminated due to lack of efficacy in late-stage disease.[17] Moreover, new (combination) treatments that are effective in metastatic disease do not necessarily have value in the adjuvant setting, as exemplified by trials PETACC-03 (5-FU/LV plus irinotecan)[18], NSABP C-08 (FOLFOX6 plus bevacizumab)[19] and N0147 (FOLFIRI plus cetuximab)[20]. To address this problem, design and approval of clinical trials in which promising drugs are tested in treatment-naïve patients with early-stage disease, rather than in late-stage patients who progressed under standard treatment, is needed.

Prospective stratification and/or inclusion based on predictive molecular biomarkers will presumably improve trial results by enrichment for responsive patients.[21] However, microsatellite instability is currently the only molecular marker that is being used in the clinical decision process for adjuvant chemotherapy in colon cancer.[22] The four recently identified CMSs in colon cancer show marked differences in the activity of various biological pathways, which could provide the basis for subtype-specific targeted therapy.[9] CMS4 (the mesenchymal/stem-like/stroma-rich subtype) has the poorest prognosis and, importantly, this subtype seems associated with a lack of benefit from oxaliplatin treatment.[23] These findings call for clinical trials with novel therapies specifically targeting CMS4 tumors. In ImPACCT we aim to deliver proof-of-concept that PDGFR/KIT inhibition with imatinib reduces the aggressive phenotype of newly diagnosed primary CMS4 colon tumors. Delivering proof-of-concept for drug activity in early stages of drug development is pivotal to prevent unfounded trial phase transition.[14, 15]

ImPACCT is conducted with treatment-naïve patients during the pre-operative window period, which allows us to obtain high quality tissue material before and after imatinib therapy without additional interventions: pre-treatment samples will be obtained during diagnostic colonoscopy and post-treatment biopsies are collected from the resection specimen; both procedures are part of standard of care. By comparison of pre- and

posttreatment tissue samples, the effects of imatinib on CMS4 tumors can be evaluated at a cellular level. The treatment period of 14 days is within the normal time frame from diagnosis to surgery (the pre-operative window). We expect that two weeks of treatment will be sufficient to induce changes in gene expression: given that steady state plasma concentrations will be attained within four days (the plasma half-life of imatinib is 18 hours [24]), patients will be exposed to the full dose for ten days. The chosen daily dose of 400mg is the standard dose for chronic myeloid leukemia, gastrointestinal stromal tumors (GIST) and myelodysplastic syndrome.

Experimental therapy during the pre-operative window period could potentially lead to an increase in postoperative complications. However, based on two phase II trials that evaluated the use of neoadjuvant imatinib therapy for otherwise irresectable or metastatic GIST, we believe it is safe to administer the last dose of imatinib within 12 hours before surgery. In these trials imatinib was administered for several months and stopped one day prior to surgery. Both studies concluded that this approach was feasible, and the reported postoperative complications were acceptable and not out of the ordinary considering the extensive abdominal surgery.[25, 26]

Instead of assessing a clinical endpoint (e.g. disease-free survival), this proof-of-concept trial investigates a surrogate endpoint (gene expression changes) to demonstrate a 'biological' treatment effect. This endpoint requires a relatively limited sample size and can be determined after only two weeks of therapy, which limits the burden placed on participants. If treatment effects are indeed demonstrated, knowledge of the size of the effect on tumor biology can be used to drive the design of a larger randomized phase II trial.

The design of the ImPACCT trial presented here allows rapid evaluation of the mechanism of action of a targeted therapy in a subtype-stratified patient population by analysis of paired pre- and post-treatment biopsies, without interfering with or delaying standard-of-care, by making use of the pre-operative window period. This design can serve as a blueprint for subtype-directed proof-of-concept trials in colon cancer, with the ultimate goal of designing effective adjuvant therapy that eradicates occult metastases.

PRELIMINARY DATA AND DISCUSSION

Between August 2016 and May 2018, endoscopic biopsies were collected from 67 lesions in 66 patients. Based on clinical histopathology, two cancers were classified as non-adenocarcinoma malignancies and excluded from further analysis. Three lesions were benign adenomas. Diagnostic biopsies from ten tumors failed to yield a preoperative diagnosis of CRC, but adenocarcinoma was confirmed after surgery in all of these cases.

Biopsies were snap-frozen in individual sterile cryotubes. Three of the five biopsies were processed for CMS4 testing. Only if the yield and/or quality of two or more samples was too low (i.e. concentration lower than 20ng/ul or RNA Integrity Number (RIN) below 5), the remaining biopsies were used as well. RT-qPCR testing was performed as described previously.[13] A total of 201 biopsies from 62 adenocarcinomas and 3 adenomas were analyzed. Median RNA yield per biopsy was 7.5µg (interquartile range (IQR) 3.8-12.6µg) and median RIN of the samples with sufficient RNA was 8.2 (IQR 7.4-9.0). The large majority of samples (178/201; 89%) met the quality control criteria and were suitable for CMS4 testing with RT-qPCR. All nine adenoma samples tested negative for CMS4, consistent with a previous study on CMS in adenomas.[27] Of the 169 tested adenocarcinoma biopsies, 53 (31%) were CMS4-positive.

Intratumor heterogeneity with regard to CMS (CMS-ITH) was taken into account by determining the weighed mean CMS4 chance of 2-3 biopsies per tumor.[13] At least two good quality samples were available from every tumor, allowing CMS4 classification for each included patient. Of the 62 adenocarcinomas, 24 (39%) were classified as CMS4-positive. Interestingly, nine out of the ten tumors that could not be classified as CRC based on diagnostic biopsies tested CMS4-negative.

Of the 24 CMS4-positive tumors, 14 (58%) had one or more CMS4 negative regions, while 16% of the CMS4-negative tumors had a CMS4-positive region (Figure 2A). This shows that there is extensive CMS-ITH in primary CRC. Conflicting subtype assignment has been linked to differences in stromal content between the tumor core and the invasive margin.[28] However, the biopsies in this study were all obtained from the mucosal surface of the cancer. Thus, spatial variation in CMS4 status is not restricted to tumor core-front differences, but also exists at the mucosal surface. An important consequence of this finding is that CMS classification on single-region biopsies could lead to incorrect subtype assignment and inappropriate patient stratification in studies with CMS-targeted therapy.

Clinicopathological features of the cohort are shown in Table 2. CMS4-positivity was associated with poor prognostic factors. There was a trend towards enrichment of CMS4 in higher TNM stages (Figure 2B) and spread to local lymph nodes and (lymph)angio-invasion was present in 63% and 57% of CMS4+ tumors, compared with 48% and 45% of CMS4- tumors respectively. Due to small numbers, these findings were not statistically significant.

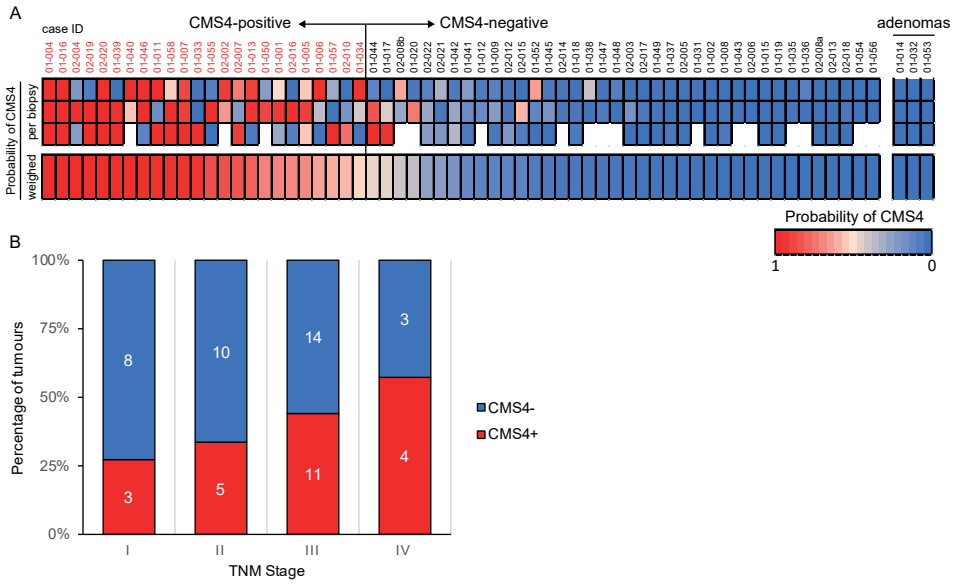

Figure 2.
A:Heatmap depicting CMS4 test results per biopsy (top rows) and the weighed mean of the combined biopsy results per patient (bottom row). The test generates a predicted probability of CMS4 ranging from 0 to 1.Tumors with a probability higher than 0.5 are classified as CMS4-positive (red). The three cases on the far right are adenomas. B: Distribution of CMS-positive (red) and -negative (blue) tumors across the four TNM-stages.

The ImPACCT trial was terminated prematurely due to slow patient enrollment. The major rate limiting factor was patient inclusion for pretreatment biopsies. Patient informed consent was required prior to colonoscopy to obtain additional fresh-frozen biopsies. In daily clinical practice, it turned out to be impossible to inform every patient undergoing colonoscopy about the study. Furthermore, given that CRC is diagnosed in only ~5% of patients who undergo colonoscopy because of clinical symptoms of CRC or a positive occult fecal blood test[29, 30], most people asked for informed consent are burdened with this question unnecessarily. This was an additional hurdle for some gastroenterologists to request for informed consent.

Patient inclusion in the second part of the trial was hampered by two additional obstacles (Figure 3). First, of the 24 patients with CMS4 CRC, 13 (55%) did not meet the inclusion criteria for imatinib treatment. Four patients had metastatic disease and one patient was in poor clinical condition. We had anticipated these reasons for subject exclusion, but two other reasons for exclusion were more common than expected: in four patients there was no 'pre-operative window' because the tumor was causing bowel obstruction, and another four patients required neoadjuvant (chemo)radiotherapy. Second, more than half of the 11

Table 2. Clinicopathological characteristics of the 62 CRC.

Characteristic		Not CMS4	CMS4	*P-value*
TNM stage, *N* (%)[a]				*0.563*
Stage I	11 (19)	8	3	
Stage II	15 (26)	10	5	
Stage III	25 (43)	14	11	
Stage IV	7 (12)	3	4	
Tumor size (cm), median [range][b]	4.6 [1.0-10.3]	5 [3.8-6.3]	4 [2.8-5.1]	*0.474*
Histological subtype, *N* (%)[b]				*0.197*
Adenocarcinoma	42 (76)	22	20	
Mucinous adenocarcinoma	10 (18)	8	2	
Signet-cell carcinoma	2 (4)	2	0	
Medullary carcinoma	1 (2)	1	0	
Differentiation grade, *N* (%)[c]				*0.767*
Well-moderate	50 (94)	29	21	
Undifferentiated	3 (6)	2	1	
Mismatch repair status, *N* (%)[d]				*0.068*
Microsatellite-stable (MSS)	34 (72)	17	17	
Microsatellite-instable (MSI)	13 (28)	11	3	
Lymphatic or angio-invasion, *N* (%)[e]				*0.329*
No invasion	27 (50)	18	9	
Invasion	27 (50)	15	12	

[a] data available from 58/62 cases. [b] data available from 55/62 cases. [c] data available from 53/62 cases. [d] data available from 47/62 cases. [e] data available from 54/62 cases.

eligible patients refused to participate in the drug trial. This rather low willingness to participate was also noticed in breast cancer window-of-opportunity trials.[31] As a consequence, the relatively small sample size required for our endpoint (n=27) was counterbalanced by difficulties in subject enrolment.

Declarations

Ethics approval and consent to participate

The study has been approved by the medical ethical committee of the University Medical Center Utrecht, the Netherlands (15/527) and the Central Committee on Research Involving Human Subjects (NL50620.041.15). The trial was performed in accordance with the protocol and the Medical Research Involving Human Subjects Act (WMO). The medicinal part of the trial was conducted in agreement with the International Conference on Harmonization Good Clinical Practice (ICH GCP) guidelines and the World Medical

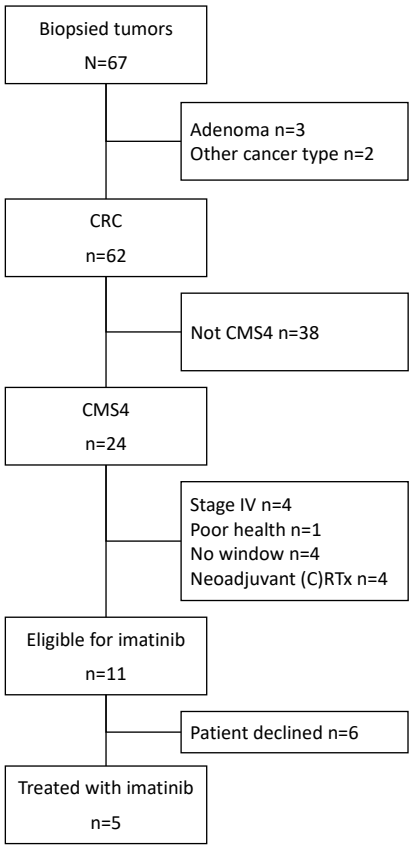

Figure 3. Patient enrollment in the ImPACCT trial.

Association (WMA) declaration of Helsinki (version 2013). Written informed consent was obtained from all study participants.

Sponsor

This was an investigator-driven trial, sponsored by the University Medical Center Utrecht. The sponsor had no involvement in the study design, in writing of this manuscript or in the decision to submit the paper for publication.

Funding

This study was supported by grants from the Dutch Cancer Society (UU2014-6617) and ZonMw (95104001). The funders had no involvement in the study design, in writing of this manuscript or in the decision to submit the paper for publication.

Acknowledgements
We wish to acknowledge Joyce van Kuik and Shivanand Richardson for implementing and performing the RT-qPCR test at the Laboratory of Molecular Pathology, UMC Utrecht.

REFERENCES

1. Bockelman C, Engelmann BE, Kaprio T, et al. Risk of recurrence in patients with colon cancer stage II and III: a systematic review and meta-analysis of recent literature. *Acta Oncol*. 2015;**54**(1):5-16.
2. Marisa L, de Reynies A, Duval A, et al. Gene expression classification of colon cancer into molecular subtypes: characterization, validation, and prognostic value. *PLoS Med*. 2013;**10**(5):e1001453.
3. Roepman P, Schlicker A, Tabernero J, et al. Colorectal cancer intrinsic subtypes predict chemotherapy benefit, deficient mismatch repair and epithelial-to-mesenchymal transition. *Int J Cancer*. 2014;**134**(3):552-62.
4. Schlicker A, Beran G, Chresta CM, et al. Subtypes of primary colorectal tumors correlate with response to targeted treatment in colorectal cell lines. *BMC Med Genomics*. 2012;**5**:66.
5. Budinska E, Popovici V, Tejpar S, et al. Gene expression patterns unveil a new level of molecular heterogeneity in colorectal cancer. *J Pathol*. 2013;**231**(1):63-76.
6. De Sousa EMF, Wang X, Jansen M, et al. Poor-prognosis colon cancer is defined by a molecularly distinct subtype and develops from serrated precursor lesions. *Nat Med*. 2013;**19**(5):614-8.
7. Sadanandam A, Lyssiotis CA, Homicsko K, et al. A colorectal cancer classification system that associates cellular phenotype and responses to therapy. *Nat Med*. 2013;**19**(5):619-25.
8. Cancer Genome Atlas Network. Comprehensive molecular characterization of human colon and rectal cancer. *Nature*. 2012;**487**(7407):330-7.
9. Guinney J, Dienstmann R, Wang X, et al. The consensus molecular subtypes of colorectal cancer. *Nat Med*. 2015;**21**(11):1350-6.
10. Steller EJA, Raats DA, Koster J, et al. PDGFRB promotes liver metastasis formation of mesenchymal-like colorectal tumor cells. *Neoplasia*. 2013;**15**(2):204-17.
11. Fatrai S, van Schelven SJ, Ubink I, et al. Maintenance of Clonogenic KIT(+) Human Colon Tumor Cells Requires Secretion of Stem Cell Factor by Differentiated Tumor Cells. *Gastroenterology*. 2015;**149**(3):692-704.
12. Kitadai Y, Sasaki T, Kuwai T, et al. Targeting the expression of platelet-derived growth factor receptor by reactive stroma inhibits growth and metastasis of human colon carcinoma. *Am J Pathol*. 2006;**169**(6):2054-65.
13. Ubink I, Elias SG, Moelans CB, et al. A Novel Diagnostic Tool for Selecting Patients With Mesenchymal-Type Colon Cancer Reveals Intratumor Subtype Heterogeneity. *J Natl Cancer Inst*. 2017;**109**(8).
14. Kola I, Landis J. Can the pharmaceutical industry reduce attrition rates? *Nat Rev Drug Discov*. 2004;**3**(8):711-5.
15. Seruga B, Ocana A, Amir E, et al. Failures in Phase III: Causes and Consequences. *Clin Cancer Res*. 2015;**21**(20):4552-60.
16. Andre T, Boni C, Mounedji-Boudiaf L, et al. Oxaliplatin, fluorouracil, and leucovorin as adjuvant treatment for colon cancer. *N Engl J Med*. 2004;**350**(23):2343-51.
17. Weber GF. Why does cancer therapy lack effective anti-metastasis drugs? *Cancer Lett*. 2013;**328**(2):207-11.
18. Van Cutsem E, Labianca R, Bodoky G, et al. Randomized phase III trial comparing biweekly infusional fluorouracil/leucovorin alone or with irinotecan in the adjuvant treatment of stage III colon cancer: PETACC-3. *J Clin Oncol*. 2009;**27**(19):3117-25.
19. Allegra CJ, Yothers G, O'Connell MJ, et al. Phase III trial assessing bevacizumab in stages II and III carcinoma of the colon: results of NSABP protocol C-08. *J Clin Oncol*. 2011;**29**(1):11-6.
20. Huang J, Nair SG, Mahoney MR, et al. Comparison of FOLFIRI with or without cetuximab in patients with resected stage III colon cancer; NCCTG (Alliance) intergroup trial N0147. *Clin Colorectal Cancer*. 2014;**13**(2):100-9.
21. Hayashi K, Masuda S, Kimura H. Impact of biomarker usage on oncology drug development. *J Clin Pharm Ther*. 2013;**38**(1):62-7.
22. Sargent DJ, Marsoni S, Monges G, et al. Defective mismatch repair as a predictive marker for lack of efficacy of fluorouracil-based adjuvant therapy in colon cancer. *J Clin Oncol*. 2010;**28**(20):3219-26.
23. Song N, Pogue-Geile KL, Gavin PG, et al. Clinical Outcome From Oxaliplatin Treatment in Stage II/III Colon Cancer According to Intrinsic Subtypes: Secondary Analysis of NSABP C-07/NRG Oncology Randomized Clinical Trial. *JAMA Oncol*. 2016;**2**(9):1162-9.
24. Gotta V, Buclin T, Csajka C, et al. Systematic review of population pharmacokinetic analyses of imatinib and relationships with treatment outcomes. *Ther Drug Monit*. 2013;**35**(2):150-67.

25. Doyon C, Sideris L, Leblanc G, et al. Prolonged Therapy with Imatinib Mesylate before Surgery for Advanced Gastrointestinal Stromal Tumor Results of a Phase II Trial. *Int J Surg Oncol*. 2012;**2012**:761576.
26. Eisenberg BL, Harris J, Blanke CD, et al. Phase II trial of neoadjuvant/adjuvant imatinib mesylate (IM) for advanced primary and metastatic/recurrent operable gastrointestinal stromal tumor (GIST): early results of RTOG 0132/ACRIN 6665. *J Surg Oncol*. 2009;**99**(1):42-7.
27. Komor MA, Bosch LJ, Bounova G, et al. Consensus molecular subtype classification of colorectal adenomas. *J Pathol*. 2018;**246**(3):266-76.
28. Alderdice M, Richman SD, Gollins S, et al. Prospective patient stratification into robust cancer-cell intrinsic subtypes from colorectal cancer biopsies. *J Pathol*. 2018;**245**(1):19-28.
29. Saratzis A, Winter-Beatty J, El-Sayed C, et al. Colorectal cancer screening characteristics of patients presenting with symptoms of colorectal cancer and effect on clinical outcomes. *Ann R Coll Surg Engl*. 2015;**97**(5):369-74.
30. Rockey DC, Koch J, Cello JP, et al. Relative frequency of upper gastrointestinal and colonic lesions in patients with positive fecal occult-blood tests. *N Engl J Med*. 1998;**339**(3):153-9.
31. Wisinski KB, Faerber A, Wagner S, et al. Predictors of willingness to participate in window-of-opportunity breast trials. *Clin Med Res*. 2013;**11**(3):107-12.

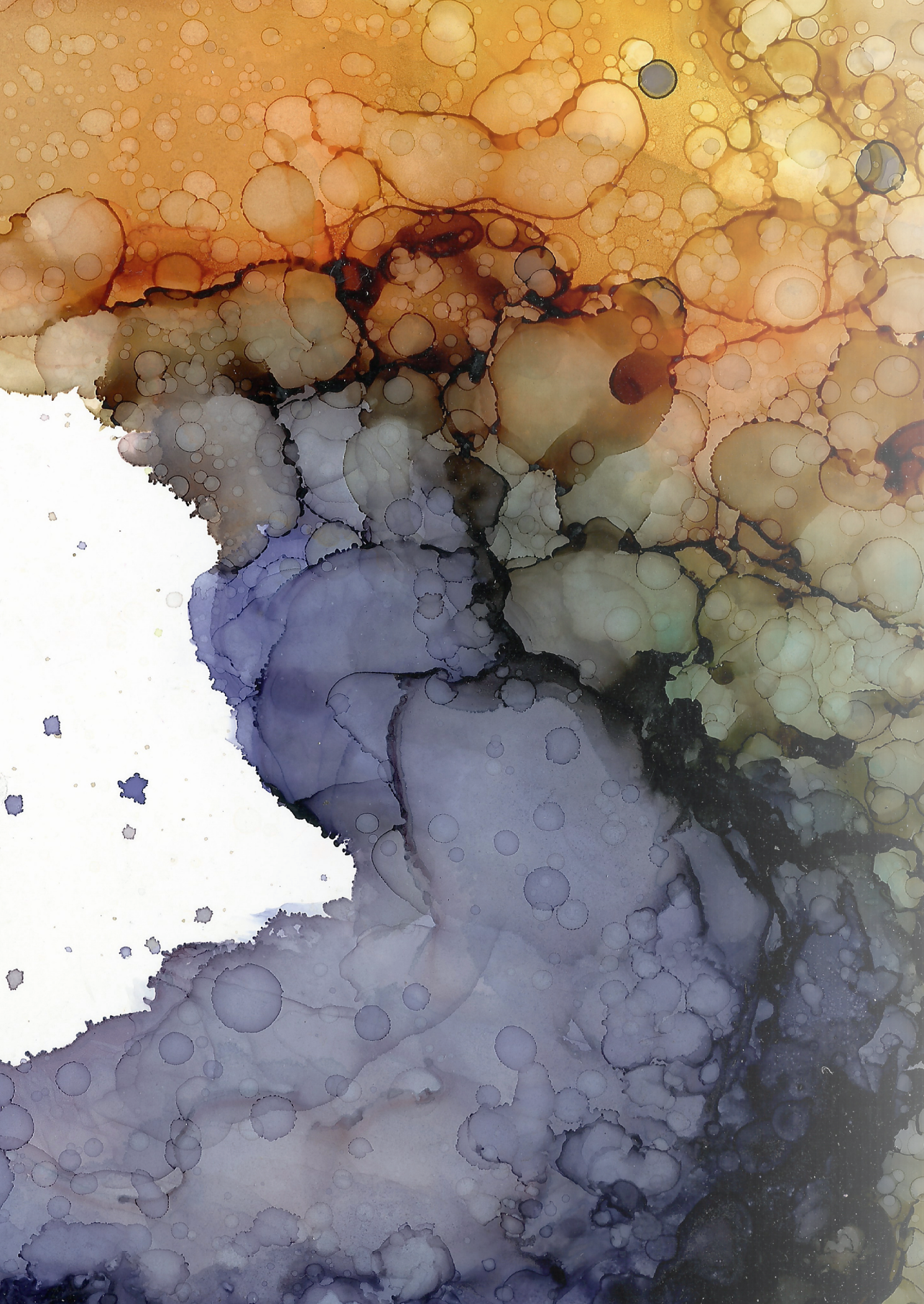

4

Dasatinib inhibits fibroblast-led invasion and regenerative capacity of colorectal cancer organoids in collagen type I

Thomas T. Vellinga*, Cornelia Veelken*, Inge Ubink*, Kirsten K.J. Verheij, Danielle A. Raats, Niek A. Peters, Susanne J. van Schelven, André Verheem, Peter Friedl, Inne H.M. Borel Rinkes and Onno Kranenburg

*Authors contributed equally to this work.

Manuscript in preparation

ABSTRACT

Colorectal cancers (CRC) can be classified into four consensus molecular subtypes (CMS1-4). Patients with CMS4 CRC have the highest chance of developing metastases and have the poorest prognosis. CMS4 tumors are characterized by a high stromal content and an extracellular matrix dominated by collagen type I. Here we show that collagen-I induces a CMS4-like gene expression program in human CRC organoids. We identify dasatinib as a candidate CMS4-targeting drug based on its affinity for tyrosine kinases highly expressed in CMS4. We show that dasatinib has a strong and long-lasting inhibitory effect on the regenerative potential of CRC organoids. Furthermore, it limits and reverses sheet migration of three-dimensional CRC organoid cultures between two layers of fibrillar collagen. In a co-culture system, fibroblasts directly interact with CRC organoids, and induce formation of invasive multicellular strands and detachment of cancer cell clusters from the organoids. Dasatinib treatment reduces the number of fibroblasts, disrupts heterotypic tumor cell-fibroblast interactions and induces apoptosis and regression in established invasion zones. By targeting tyrosine kinases that are expressed on both tumor cells and cancer-associated fibroblasts, dasatinib could interfere with the invasive phenotype of colorectal cancer in desmoplastic stroma. We therefore propose that dasatinib may have clinical utility in the treatment of stroma-rich CRC.

INTRODUCTION

The development of distant metastases is the most important determinant of survival in patients with colorectal cancer (CRC) and most other types of cancer. Despite improvements in surgical procedures, chemotherapy, and local radiation techniques, prognosis of patients with metastatic CRC remains poor, with five-year overall survival of only 15%.[1] To improve the outcome for patients with CRC, prevention of dissemination and outgrowth of metastases is crucial. Current adjuvant chemotherapy regimens reduce the risk of distant recurrence after primary CRC surgery in patients with stage III disease from 50% to 35%, which means that only 15% of these patients benefit from adjuvant treatment.[2] Thus, there is an urgent need for novel treatment strategies that eliminate residual disease or prevent its outgrowth.

The Consensus Molecular Classification system distinguishes four molecular subtypes of colorectal cancer (CMS1-4), based on recurrent patterns of gene expression. CMS4 is frequently referred to as the 'mesenchymal subtype', and is characterized by a high stromal content and expression of gene signatures reflecting epithelial-to-mesenchymal transition and a more stem-like phenotype. CMS4 tumors have the highest propensity to form metastases.[3-5] The processes of invasion and metastases in CRC are incompletely understood. Increasing evidence suggests that the tumor microenvironment plays an active role in tumor progression. High stromal content is associated with poor prognosis in CRC, and the constitution of the stroma further predicts outcome.[4-7] CMS4 cancers are particularly rich in desmoplastic stroma.[8] We have previously shown that collagen type I dominates the extracellular matrix (ECM) of CMS4 CRC, and that interaction with collagen-I induces mesenchymal gene expression and collective tumor cell invasion in human colorectal cancer organoids.[9]

To search for potentially effective CMS4-targeting drugs, we explored the effects of collagen-I on CRC organoids and identified signaling intermediates potentially associated with CRC invasion. We selected existing FDA-approved tyrosine kinase inhibitors based on their affinity for kinases that are highly expressed in CMS4, and further investigated the c-Src inhibitor dasatinib as a potentially effective inhibitor of CMS4 biology. Dasatinib strongly suppressed migration of organoids on a collagen-I matrix, and three-dimensional fibroblast-led invasion in collagen-I. It thereby impairs both the onset and progression of invasion and the detachment of cell clusters. Our results suggest that dasatinib could have clinical utility in the treatment of stroma-rich mesenchymal-type CRC.

MATERIALS AND METHODS

Cell culture

The patient-derived CRC organoids p8t, p9t, p19ta, p19tb, p9t, and p26t were established as part of a living biobank of CRC[10], and were kindly provided by the HUB foundation (hub4organoids.eu). The patient-derived CRC organoids HUB-02-B2-028 (TOR8), HUB-02-B2-031 (TOR9) and HUB-02-B2-040 (TOR10) were established at the Hubrecht Institute, within biobanking protocol HUB-Cancer TcBio#12-093 that was approved by the medical ethical committee of the University Medical Center Utrecht. Organoids were cultured in Matrigel (Corning, 356231) with basal medium 2+ containing advanced-DMEM/F12 (Life Technologies, 12634028), supplemented with penicillin (100 U/ml) and streptomycin (100 µg/ml; PAA), Hepes (10 mM, Lonza, BE17-737E)), Glutamax (400 µM, Life Technologies, 35050038), B27 (0.2X, Life Technologies, 17504044), N-Acetyl-L-cysteine (1mM, Sigma-Aldrich, A9165-5G), Noggin (10%), A83-01 (500 nM, Biovision, 1725-1) and SB202190 (10 µM, Sigma-Aldrich, S7067) at 37°C and 5% CO_2. For gene expression analysis, luminex, colony-formation and matrix invasion assays, Matrigel was replaced by 1.5 mg/ml collagen-I (10 mg/ml collagen-I (Ibidi, Martinsried, Germany) mixed with BM2+, pH buffered with NaOH).

Human lung fibroblasts MRC5 were maintained in cell culture containing Dulbecco's modified Eagle medium (DMEM; Gibco/Thermo Fisher Scientific), supplemented with 10% fetal calf serum (FCS; Sigma Aldrich), penicillin (100 U/ml) and streptomycin (100 µg/ml), L-glutamine (2 mM; Gibco/Thermo Fisher Scientific), and sodium pyruvate (1 mM; Gibco/Thermo Fisher Scientific) at 37°C and 5% CO_2.

Collagen matrix sheet migration assay

To stimulate collagen-I sheet migration, a bottom layer of 2 mg/ml collagen-I dissolved in phosphate-buffered saline was created and allowed to polymerize at room temperature for one hour. Droplets of collagen (5-10ul) with organoids were placed on top of this layer and also allowed to polymerize at room temperature for one hour, creating an interface between collagen layers, after which BM2+ medium with dasatinib (100nM; Sellenckchem, S1021) or DMSO (0.002%) was added and cells were placed in an incubator at 37°C. Micrographs were taken with the EVOS inverted microscope. To study whether dasatinib could also reverse the observed sheet migration phenotype, dasatinib treatment was initiated at day five, after migration sheets had formed on the matrix interface.

Luminex assay

Organoids were dissociated into single cells. Half of the cells were cultured in basement medium extract (Cultrex® Pathclear Reduced Growth Factor BME type 2, #3533-001-02) and the other half were cultured in collagen-I as described for the collagen matrix invasion

assay. After three days medium was removed from the cells and immediately frozen down to -80°C. Medium was refreshed and again removed and frozen down four days later (seven days after first seeding the cells). CXCL1 and CXCL8 concentrations were measured using an in-house developed and validated (ISO9001 certified) multiplex immunoassay based on Luminex technology (xMAP, Luminex Austin TX USA). The assay was performed as described.[11] In short, samples were incubated with antibody-conjugated MagPlex microspheres for one hour at room temperature with continuous shaking, followed by one hour incubation with biotinylated antibodies, and 10 minute incubation with phycoerythrin-conjugated streptavidin diluted in high performance ELISA buffer (HPE, Sanquin the Netherlands). Acquisition was performed with the Biorad FlexMAP3D (Biorad laboratories, Hercules USA) in combination with xPONENT software version 4.2 (Luminex). Data was analyzed by 5-parametric curve fitting using Bio-Plex Manager software, version 6.1.1 (Biorad).

Western Blot

Organoids were cultured in Matrigel for three days, collected with dispase and replated in collagen-I (Ibidi, 1.5 mg/ml). After one day, organoids were treated with 100 nM dasatinib (or 0.002% DMSO in control) for indicated time periods. Organoids were extracted from collagen with collagenase and lysed in laemmli lysis buffer (2.5% SDS, 20% glycerol, 120 mM Tris pH 6.8). Equal amounts of protein were run on SDS-PAA gels and were analyzed by western blot (Trans-Blot Turbo, Bio-Rad, Hercules, CA, USA). The following primary antibodies were used: Src (CS2109, Cell Signaling Technology, Danvers, MA, USA), phospho-Src Y-416 (CS2101, Cell Signaling), phospho-Src Y-418 (ab4816, Abcam, Cambridge, UK) and β-Actin (AC-15, #NB600-501, Novus Biologicals, Littleton, CO, USA).

Colony formation assay (CFA)

Organoids were dissociated into single cells with TrypLE™ Express (Thermo Fisher Scientific). Cell viability was assessed with trypan blue staining, and 500 or 1000 viable single cells were plated in 100ul collagen-I. Dasatinib (Sellenckchem, S1021) was diluted in dimethylsulfoxide (DMSO) to a stock concentration of 50 μM, and further diluted in BM2+ medium. Plated cells were treated with 100nM dasatinib or 0.002% DMSO, starting 2 days after plating the cells, during 14 days. Medium was refreshed twice per week. Colonies were counted with light microscopy (EVOS, Thermo Fisher Scientific). The experiments were performed in triplicate, and repeated three times for each cell line. For secondary CFA, the colonies from the first CFA were dissociated into single cells. Viability was assessed with trypan blue; 500 viable cells were plated in collagen-I. Cells from colonies treated with dasatinib were divided in two groups: one group received no further treatment; the second group was again treated with 100nM dasatinib. The secondary CFA was performed in triplicate.

Co-culture invasion assay

Organoids were cultured in Matrigel until they reached a size of 0.75-5.0 mm^3. Matrigel was dissolved with ice cold PBS and organoids were transferred to a 15 ml falcon tube, followed by three washing steps with 10ml ice cold PBS and centrifugation in between (5 min, 111 g, 4°C). Organoids were resuspended and kept on ice in BM2+ medium until embedding in collagen. MRC5 fibroblasts cells from 2D culture (80% confluency) were detached using Trypsin /EDTA (0.075%/2 mM, Thermo Fisher Scientific) in PBS followed by addition of medium containing 10% FCS. Cells were spun down, resuspended in BM2+ and counted. Acidic collagen-I stock solution (5 mg/ml; Corning, REF 3542495) was mixed with 10x PBS, Milli-Q, and 1N NaOH to a final concentration of 5mg/ml at pH 7.4. 100-150 organoids and 4000 MRC5 fibroblasts were mixed with the collagen and plated as drops (80 µl) in a 24-well plate and maintained at 37°C for 30 min until polymerization. For long-term culture, BM2+ medium, supplemented with 2.5% FCS to induce fibroblast elongation and maintain cell vitality, was added. Medium was refreshed at day 3 and every second consecutive day with the addition of dasatinib (100 nM) or DMSO (0.002%). At day 3, 7 and 12 after embedding, samples were fixed (4% PBS-buffered paraformaldehyde; 30 min at 21 °C), washed with excess PBS (5x5 min) and stained for microscopy.

Immunofluorescence

For epifluorescence microscopy of CRC invasion in 3D, samples were stained with DAPI and AlexaFluor548-phalloidin (18h at 4°C) and washed with PBS (5x5 min). Samples for confocal microscopy of 3D invasion were incubated in blocking buffer (PBS/10% normal goat serum/0.1% BSA/0.1% Triton X-100; Sigma) for 2 h at 20°C, followed by incubation with rabbit monoclonal anti-vimentin (MA5-14564; Thermo Fisher Scientific) and mouse monoclonal anti-p120 antibody (BD610133, BD Biosciences) in blocking buffer overnight (4 °C on a shaking platform), washing with PBS (5x5 min) and incubation with secondary pre-absorbed goat anti-rabbit or anti-mouse IgG coupled to AlexaFluor -488 or 647 (Invitrogen/Thermo Fisher Scientific), DAPI and AlexaFluor568-phalloidin in blocking buffer (18h at 4°C). After washing in PBS (5x5 min), samples were placed in a 3D glass chamber filled with PBS and analyzed by bright-field and confocal microscopy. For confocal imaging of sheet migration, samples were incubated with 1% w/v bovine serum albumin, 1% v/v DMSO and 0.2% v/v Triton X-100 in PBS (PBD02T) (4h at 20°C) followed by incubation with AlexaFluor488-phalloidin and DAPI in blocking buffer (18h, 4°C) followed 5x5 min washing in PBD02T.

Imaging of 3D organoid co-cultures

Growth and invasion from overviews of multiple organoids were visualized with bright-field and epifluorescence microscopy (Leica DMI6000B, 5x/0.12 air objective, 1392x1040

pixels, 20 µm inter slice distance, 400-1000 µm z-size, tile scan of 20-30 images). Images were composed from multiple fields and automatically stitched. Maximum intensity projections (standard deviation) were generated using ImageJ/Fiji (version 1.51) from 3D image stacks. Confocal microscopy (Zeiss LSM880 scanner; 40x/1.0 NA water-immersion objective) was performed with sequential single-channel scanning (5 µm inter-slice distance).

For bright-field time-lapse microscopy, organoids and fibroblasts were embedded in collagen-I as described above and recorded starting on day 2 for 30 hours (Okolab 2.0, 37 °C , 5% CO_2, 10x objective).

Image analysis

Images were analyzed with ImageJ/Fiji (version 1.51). To analyze sheet migration between collagen-I-layers, the surface area of the migratory sheet of the largest organoid in a collagen droplet was measured by subtracting the surface area of the main organoid structure from the total surface area of the organoid structure including the migratory sheet.

3D collagen invasion was quantified as the number of invasive organoids and the percentage of invasive strands with detached clusters. The frequency of interaction between CRC cells and fibroblasts were manually counted using the phalloidin signal along the cell-cell interface. Apoptosis in invasion zones was detected as nuclear fragmentation from the DAPI signal. Fibroblasts were recognized by DAPI signal as elongated single nuclei. Unless stated otherwise, data represent three independent collagen cultures from one batch of organoids, including a total of 300-450 organoids. For the analysis of co-cultures (number of organoids, percentage of invasive strands with detached clusters or apoptotic tip, number of fibroblasts) at day 12, 6-8 replicates from two independent experiments representing 600-1,200 organoids were used. Graphs were created with GraphPad Prism version 7.02.

Bioinformatical analyses and statistics

Total RNA was isolated from tumor organoids according to manufacturer's protocol (RNeasy Mini Kit, Qiagen, Hilden, Germany). Affymetrix microarray analyses were performed by the Department of Oncogenomics, Amsterdam Medical Center. Fragmentation of RNA, labeling, hybridization to Human Genome U133 Plus 2.0 microarrays and scanning were performed following the manufacturer's protocol (Affymetrix, Thermo Fisher Scientific). All bioinformatics analyses were performed using R2: Genomics Analysis and Visualization Platform (r2.amc.nl). To visualize expression of particular gene sets in distinct sample subgroups the option 'relate two tracks' was used. Condensation of gene set expression into single values per tumor/sample was performed with the 'View Gene Set' option and by storing the obtained values as a track for subsequent analyses. Dot plots visualizing the comparative expression of gene sets were created using

the 'relate two tracks option'. Pearson correlation (r) values and accompanying p-values were obtained by selecting the xy plot option. The generation of tumor subgroups on the basis of differential expression of gene sets was performed using the k-means option (10x100 draws). Survival differences between groups were visualized in Kaplan Meier curves and p values were generated with the log rank test. Correction for multiple testing was done with the Bonferroni method. Overlap between gene sets was identified with the web-based GeneVenn tool (http://genevenn.sourceforge.net/). Data from invasion assays were analyzed with Mann-Whitney test, ANOVA, or multiple t-test, as appropriate. P-values below 0.05 were considered statistically significant.

RESULTS

Interaction with type I collagen induces gene expression associated with CMS4 in human colorectal cancer organoids.

Three different human CRC organoid lines (p8t, p9t, and p26t) were grown in either Matrigel or collagen type I for seven days. Matrigel mainly consists of laminin, collagen type IV and entactin, similar to the basement membrane of a healthy colon, whereas collagen type I more closely resembles the interstitial ECM surrounding invading tumor cells that have breached the basement membrane.[12] We used microarray gene expression profiling to identify differences in gene expression between organoids cultured in reconstituted type I collagen and in Matrigel (Figure 1a, Supplementary Table 1). We selected the 250 genes that were most significantly up- or downregulated in collagen-I, and analyzed the expression of these genes in a composite cohort of colorectal tumors (n=3232) that were used to develop the CMS classification.[3] Expression of the set of 250 upregulated genes (COL250-UP) was significantly correlated with expression of signature genes that identify the mesenchymal subtype CMS4, and inversely correlated with expression of signature genes identifying the canonical epithelial subtype CMS2 (Figure 1b). We next used the gene sets to cluster the CMS-3232 cohort into three groups (low, intermediate, or high expression of COL250-UP) by k-means clustering (Supplementary Figure 1a).

Figure 1. Collagen-I-induced gene expression changes. ▶
(a) Heatmap showing the 601 genes that were differentially expressed (ANOVA p<0.01) between cultures in matrigel and collagen-I. Colour codes: group – red = collagen-I, green = matrigel; organoid ID – blue = organoid p9t, green = organoid p8t, blue = organoid p26t. (b) Scatterplot showing the expression of CMS4 signature genes related to expression of COL250-UP genes in tumors from the CMS-3232 cohort. Inset: Pearson correlation (r-value) of CMS1-4 signature gene sets with the COL250-UP gene set. (c) Distribution of 3232 CMS classified tumors amongst the COL250-UP clusters. (d) STRING network analysis of protein activation upon culturing in collagen-I showing c-Src at the center of the protein network (red circle). (e) Volcano plot of ANOVA p-value versus fold change of gene expression from organoids cultured in collagen-I or in Matrigel. CXCL8 and CXCL1 are highlighted.

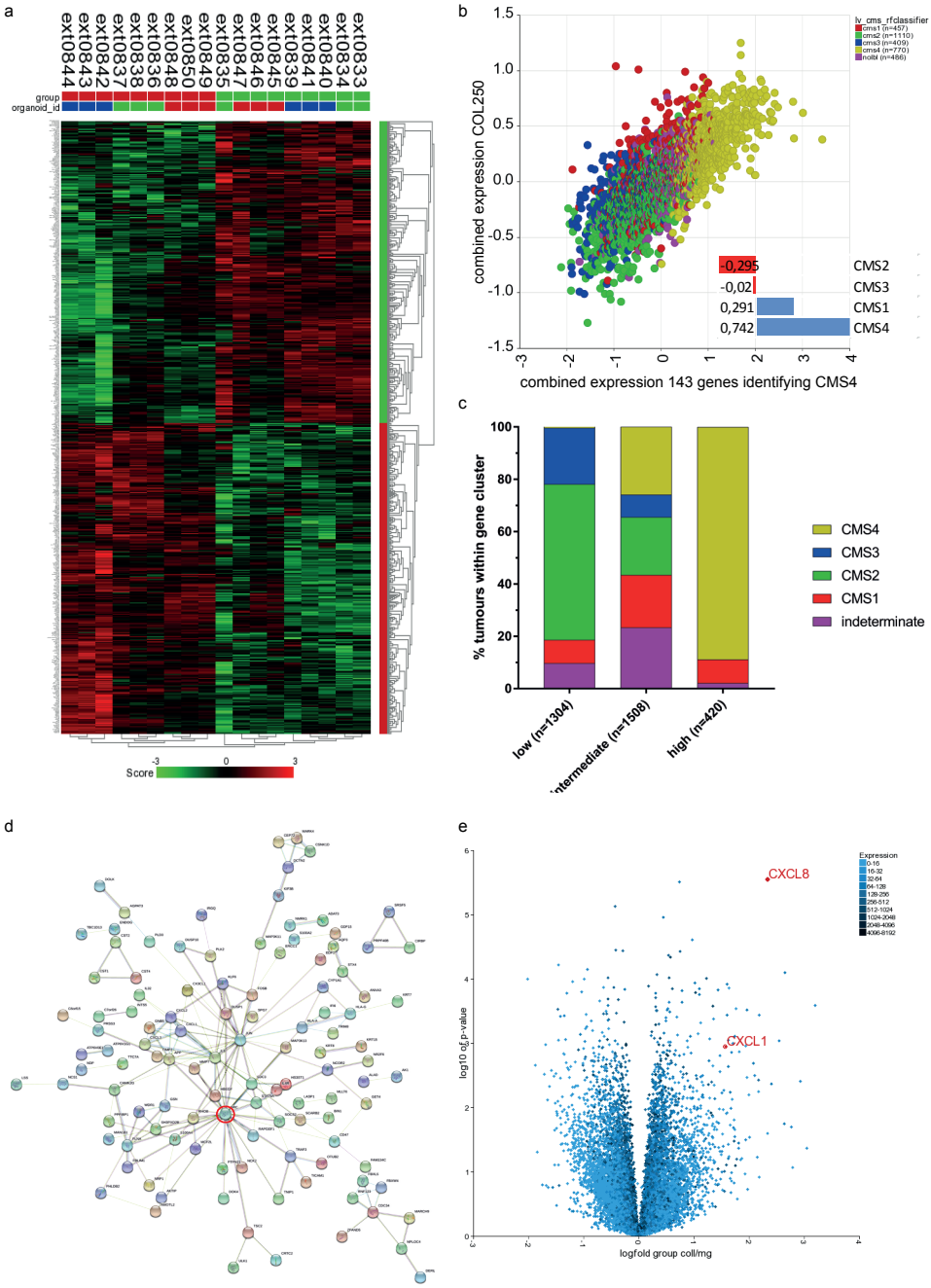
a
ext0844
ext0843
ext0842
ext0837
ext0838
ext0836
ext0848
ext0850
ext0849
ext0835
ext0847
ext0846
ext0845
ext0839
ext0841
ext0840
ext0834
ext0833
group
organoid_id
Score
b
combined expression COL250
combined expression 143 genes identifying CMS4
lv_cms_rfclassifier
cms1 (n=457)
cms2 (n=1110)
cms3 (n=409)
cms4 (n=770)
mixed (n=486)
-0,295
-0,02
0,291
0,742
CMS2
CMS3
CMS1
CMS4
c
% tumours within gene cluster
low (n=1304)
intermediate (n=1508)
high (n=420)
CMS4
CMS3
CMS2
CMS1
indeterminate
d
e
CXCL8
CXCL1
log10 p-value
logfold group coll/mg
Expression

Table 1. Kd values and selectivity for CMS4- associated TKs of eight FDA-approved drugs

	# targets		selectivity score	Kd for CMS4-associated tyrosine kinases																		
	all	<300	σ (3 uM)	KIT	PDGFRA	PDGFRB	FLT1	DDR2	KDR	AXL	TIE1	FGR	FYN	HCK	BTK	EPHA3	EPHA7	FER	FES	FGFR1	ITK	JAK1	JAK3
Foretinib	18	17	0.440	2.5	4.5	0.96	3.8	3.6	12	0.093	0.79	40	88	15	76	1	2.5	37	110	690	69		
Dasatinib	13	9	0.267	0.81	0.47	0.63	5000	3.2	2900			0.5	0.79	0.35	1.4	0.093				3700			640
Vandetanib	15	6	0.236	260	230	88	260	320	820	250	1500	270	360	360	1700	2000	2400			560			
Pazopanib	14	6	0.215	2.8	4.9	2	14	98	14		700	1600	2700	5700				2700	1400	990			6900
Sorafenib	15	7	0.168	28	62	37	31	6.6	59	4500	68	7800	8400	8500		1900	5300			2800			7300
Cediranib	15	8	0.163	0.38	0.41	0.32	0.74	48	1.1	490	290	1100	1200	590	4300	3700	620			53			
Nilotinib	9	5	0.124	29	180	73		33			1000	320	1600	390		110							
Imatinib	6	4	0.057	13	31	14		15				2400	3100										

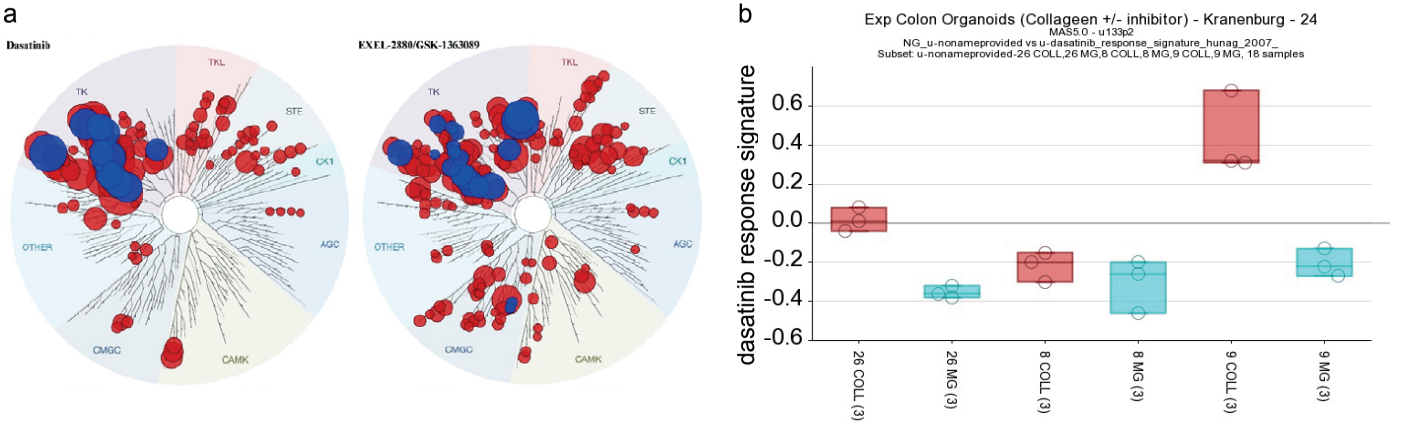

Figure 2. Identification of dasatinib as a potential anti-CMS4 drug.
(a) Activity spectra of dasatinib and foretinib (EXEL-2880) mapped on the human kinome. The size of each red spot reflects the dissociation constant of each drug for specific kinases. Larger spots indicate lower Kd and more efficient inhibition. Kinases from the 22TK panel are highlighted in blue. Images generated using TREEspot™ Software Tool and reprinted with permission from KINOMEscan®, a division of DiscoveRx Corporation, © DISCOVERX CORPORATION 2010. (b) Expression of gene signature of genes positively correlated with dasatinib response18 in organoids p26t, p8t and p9t in collagen-I and matrigel matrix.

The COL250-UP-high group consisted almost exclusively of tumors that had previously been classified as CMS4 (Figure 1c). A subset of CMS1 tumors also clustered in the COL250-UP-high group, while nearly all CMS2 and CMS3 tumors were assigned to the low or intermediate groups. High expression of the COL250-UP gene set was associated with shorter disease-free and overall survival (Supplementary Figure 1b,c). Vice versa, expression of the COL250-DOWN gene set was highest in epithelial subtypes (CMS1-3) and lowest in the mesenchymal subtype CMS4 (Supplementary Figure 1d) .Furthermore, high expression of the COL250-DOWN gene set was associated with a marked better relapse-free and overall survival (Supplementary Figure 1e,f,g). These data indicate that switching the extracellular matrix from Matrigel to collagen type I induces a CMS4-like phenotype in human colorectal organoids.

To gain insight into the mechanisms that drive collagen-I-induced gene expression changes in organoids, we searched for functional protein association networks by using STRING (string-db.org). This analysis revealed that collagen-I-induced genes form a network around the non-receptor tyrosine kinase c-Src (Figure 1d). c-Src activates multiple signal transduction pathways involved in proliferation, survival, angiogenesis and migration/invasion of cancer cells.[13] c-Src activation results in increased expression of interleukin-8 (IL-8, CXCL8).[14] Indeed, IL-8 was the most significantly upregulated gene (p=2.84E-6) in collagen-I compared with Matrigel culture (Figure 1e). The structurally related chemokine CXCL1 (GRO1-alpha) was also upregulated in collagen-I (p= 1.12E-3). To validate these findings, we measured the production of these chemokines by three independent CRC organoid lines in BME and collagen-I with a luminex assay. After three days, the CXCL8 concentration in medium from organoid TOR9 was 3.5 times higher in collagen-I culture, compared with BME culture, and after seven days it was 11 times higher (Supplementary Table 2). No change in CXCL8 production was observed in the other organoid cultures. CXCL1 concentrations were elevated in medium from all three tested organoids (TOR8, TOR9 and TOR10). After three days, concentrations were 9 times, 13 times and 3 times higher respectively in collagen-I compared with BME cultures. After seven days, TOR9 even produced 96 times more CXCL1 in collagen-I than in BME. Thus, the collagen-I induced upregulation of gene expression corresponds with increased production of the chemokines CXCL1 and CXCL8 in collagen-I compared with BME.

Dasatinib as a candidate CMS4-targeting drug

To search for potential therapeutic targets in CMS4 CRC we focused on the human kinome. We identified fifty-five kinases that are positively correlated with the CMS4 signature genes in two independent colon cancer cohorts (GSE39582[15] n=566, and TCGA[16] n=276; single gene p-values <e-6; Supplementary Table 2). Twenty-two of these were tyrosine kinases (TK), to which we refer as the 22TK panel. TKs are attractive therapeutic targets and a large

number of approved TK inhibitors (TKIs) are available for the treatment of cancer and other diseases. We made use of a dataset reporting on the quantitative dissociation constants (*K*d) of drug-target interactions for 72 distinct kinase inhibitors[17]. Two kinases from the 22TK panel (ROR1, ROR2) were missing in the dataset and could not be analyzed. The *K*ds of each of the 72 kinase inhibitors for the remaining 20 TKs are shown in Supplementary Table 3. The most potent inhibitor was foretinib, which binds 18 of the 20 queried CMS4 TKs with a *K*d lower than 300 nM. The twenty-five most efficient 22TK inhibitors contained eight FDA-approved anti-cancer drugs, which are not currently indicated for the treatment of colon cancer: foretinib, dasatinib, cediranib, sorafenib, pazopanib, vandetanib, nilotinib, and imatinib (Table 1). When plotting the inhibition profiles of these eight drugs onto the human kinome, we found excellent overlap between the targets of foretinib and dasatinib and the CMS4 22TK panel (Figure 2a). Dasatinib is a potent inhibitor of c-Src and the expression of a gene signature predicting sensitivity to dasatinib[18] was significantly upregulated by embedding organoids in collagen-I (Figure 2b). Based on this overlap, and the superior selectivity score of dasatinib compared with foretinib (0.27 versus 0.44, respectively (Table 1, Figure 2a)), we selected dasatinib for further studies.

Dasatinib reduces clone formation and inhibits sheet migration of CRC organoids

First, we assessed whether dasatinib could inhibit its classical target Src in colorectal cancer organoids. Organoid culture in collagen activated c-Src by phosphorylation at tyrosine residue 416/418. Dasatinib treatment (100nM, concentration based on[19]) resulted in rapid, complete and lasting inhibition of autophosphorylation in two independent organoid lines (Figure 3a). We next performed CFA to test the effect of dasatinib on regenerative capacity of organoids grown in collagen-I, and found a consistent reduction of colony formation by ~50% in three different organoid lines (Figure 3b). After re-plating the resulting colonies in a second CFA, we found that the regenerative capacity of p9t cells was impaired even in the absence of continued drug exposure, whereas p26t and p19tb regained regenerative capacity after withdrawal of dasatinib. All three cell lines showed continued diminished colony forming potential in the presence of dasatinib (Figure 3b).

We recently showed that collagen-I induces emigration of cell sheets from human CRC organoids along the interface of two collagen-I matrix layers.[9] Sheet migration between collagen layers could be prevented by dasatinib treatment, as shown in Figure 3c. The migratory phenotype could also be reversed by treatment with dasatinib. After dasatinib treatment, we observed a marked reorganization at the invasive front, leading to the formation of a sharply demarcated epithelial barrier (Figure 3d). This treatment effect may be clinically relevant, as in patients, local cancer cell invasion will have occurred before initiation of dasatinib therapy.

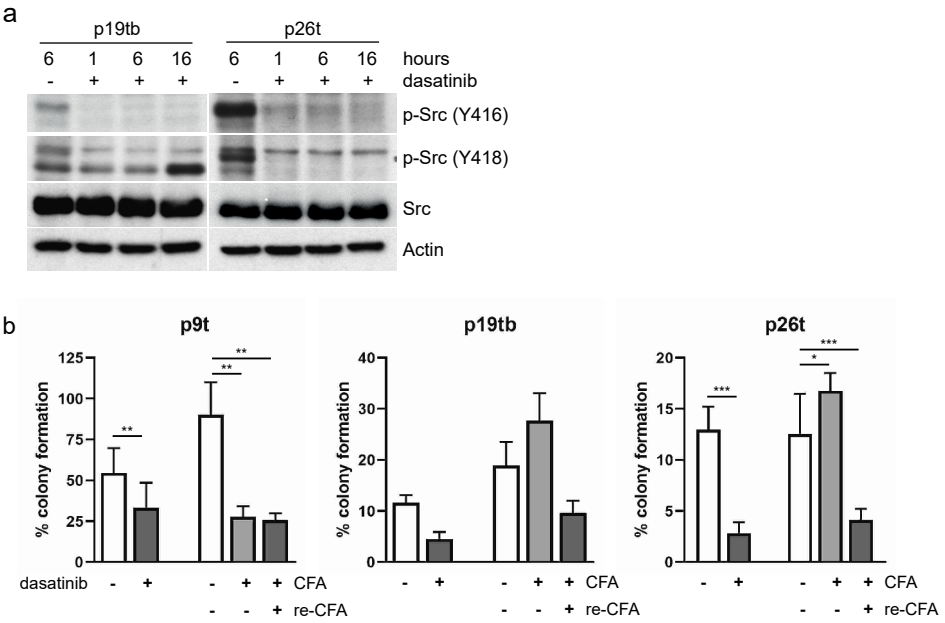

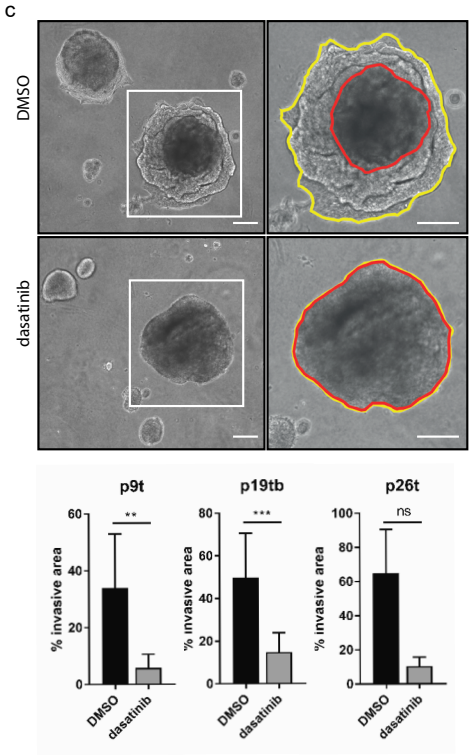

Figure 3. Effects of dasatinib on colony formation in collagen-I and organoid migration along a collagen-I interface.
(a) Western blot analysis of Src autophosphorylation in collagen-I. 3-day old organoids were plated in collagen-I. After 1 day, cells were treated with 0.002% DMSO for 6 hours or 100nM dasatinib for 1,6 or 16 hours. (b) CFA with three different organoid lines treated with 100nM dasatinib, and secondary CFA after pre-treatment with dasatinib in the first CFA, with and without continued TKI treatment. Bars represent mean plus standard deviation (SD) of combined results from repeated experiments performed in triplicate. *p<0.05, **p<0.01, ***p<0.001 (Mann Whitney test for primary CFA and one-way ANOVA, multiple comparisons test for secondary CFA). (c) Dasatinib inhibits migration of 3D organoids along the collagen-I matrix interface. Representative images of the sheet-like migrating organoid p19tb are shown (top = DMSO-treated, bottom = dasatinib-treated). The yellow line delineates the total surface area of the organoid, the red line surrounds the non-invasive organoid structure, scale bar = 200 µm. The percentage of invasive area relative to the total surface area of the organoid is quantified in the graphs (p9t: n=5-6 organoids per condition, p19tb: n=9-10 organoids per condition, p26t: n=3 organoids per condition), bars represent mean plus standard deviation (SD), **p=0.0043, ***p=0.0003, ns=not significant (Mann Whitney test). ▶

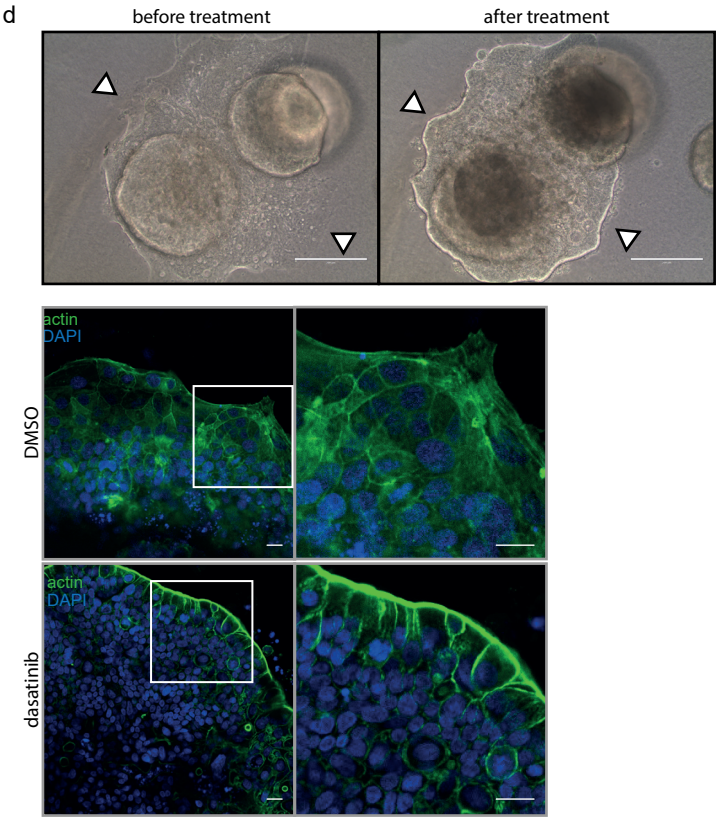

▶ (d) Dasatinib reverses collagen-I sheet migration. Left panel: micrographs showing migration of organoid p9t after five days in collagen-I culture (top), upon which treatment was started; dasatinib treatment (100 nM) resulted in reorganization of the migration front (white arrow heads) after five days (bottom), scale bar = 200 µm. Right panel: confocal microscopy images showing differences in actin organization at the migration front of DMSO-treated organoids (top) compared with dasatinib-treated organoids (bottom), scale bar = 20 µm.

Dasatinib inhibits fibroblast-led three-dimensional invasion in collagen-I

The ECM of CMS4 tumors is rich in dense stroma and cancer-associated fibroblasts.[4, 5] Collective invasion of tumor cells through the ECM requires track clearance by leader cells.[20] Fibroblasts can function as leader cells, guiding the directional invasion of tumor cell strands in a range of cancer types.[21] To study the role of fibroblasts in directing colorectal cancer cell invasion in collagen-I, we co-cultured p19ta organoids with MRC5 lung fibroblasts, which are considered to be activated fibroblasts[22]. Organoids embedded in three-dimensional (3D) fibrillar collagen without fibroblasts showed continued growth but little invasion (mono-culture, Figure 4a). In co-culture with fibroblasts however, 17% of the organoids formed multicellular strand-like invasion zones (Figure 4a-c). Fibroblasts

approached and physically connected to tumor organoids prior to onset of invasion (movies 1-4, available upon request), consistent with reports on fibroblast-led collective tumor cell invasion[23]. After twelve days of co-culture, the tips of the invasive strands were either connected to fibroblasts (50%) or lacked physical connections to fibroblasts (50%, Supplementary Figure 2a). Heterotypic interactions between fibroblasts and invasive cells emigrating from the CRC organoids contained high levels of F-actin and p120 catenin (Figure 4b), indicating cadherin-based cell-cell junctions between fibroblasts and tumor cells, as described[21].

We next studied the effect of dasatinib on fibroblast-led 3D invasion. Treatment was started three days after establishment of the co-cultures, when invasion was initiated (Supplementary Figure 2b). Treatment with dasatinib reduced the number of fibroblasts with 44% from day 3 to day 12 while fibroblasts continued to proliferate in control culture (Figure 4d). CRC organoid invasion was reduced by 50% (Figure 4c) and 20% of the remaining invasive strands were connected to fibroblasts by day 12 (Figure 4e). In untreated co-cultures, release of 'budding' tumor cell clusters from invasive strands was observed in 23% of all invasive strands, and this rate was reduced by half with dasatinib treatment (Figure 4f, g). Dasatinib further increased apoptotic events in the tips of the invasive strands, most prominently in strands lacking contact with fibroblasts (Figure 4h, i; 31% vs. 15% apoptosis, compared to DMSO). These data show that fibroblasts induce CRC invasion in 3D organoid culture. Interaction between fibroblasts and organoids trigger collective CRC cell invasion and budding, and both phenomena can be inhibited by dasatinib.

DISCUSSION

In the present study we found that collagen-I, which is particularly abundant in CMS4 cancers[9], instigates an invasive, CMS4-like phenotype in patient-derived CRC organoids. This is in line with our previous data showing that the epithelial tumor cells in CMS4 cancers express a distinct set of mesenchymal genes.[9] Organoid culture in collagen-I resulted in a pronounced upregulation of chemokines CXCL1 and CXCL8. Both chemokines have recently been implicated in CRC progression and high expression correlates with poor prognosis.[24-26] CXCL1 and CXCL8 can recruit neutrophils that have pro-tumorigenic properties, and CXCL1 production by primary CRC can direct cells at distant sites to create premetastatic niches.[25, 27]

We found c-Src at the center of the protein network that was upregulated upon exposure to collagen-I. Src activation has been linked to collagen matrix stiffening, invasion and metastasis formation in various cancers, including breast, lung and colorectal cancer.[28-31]

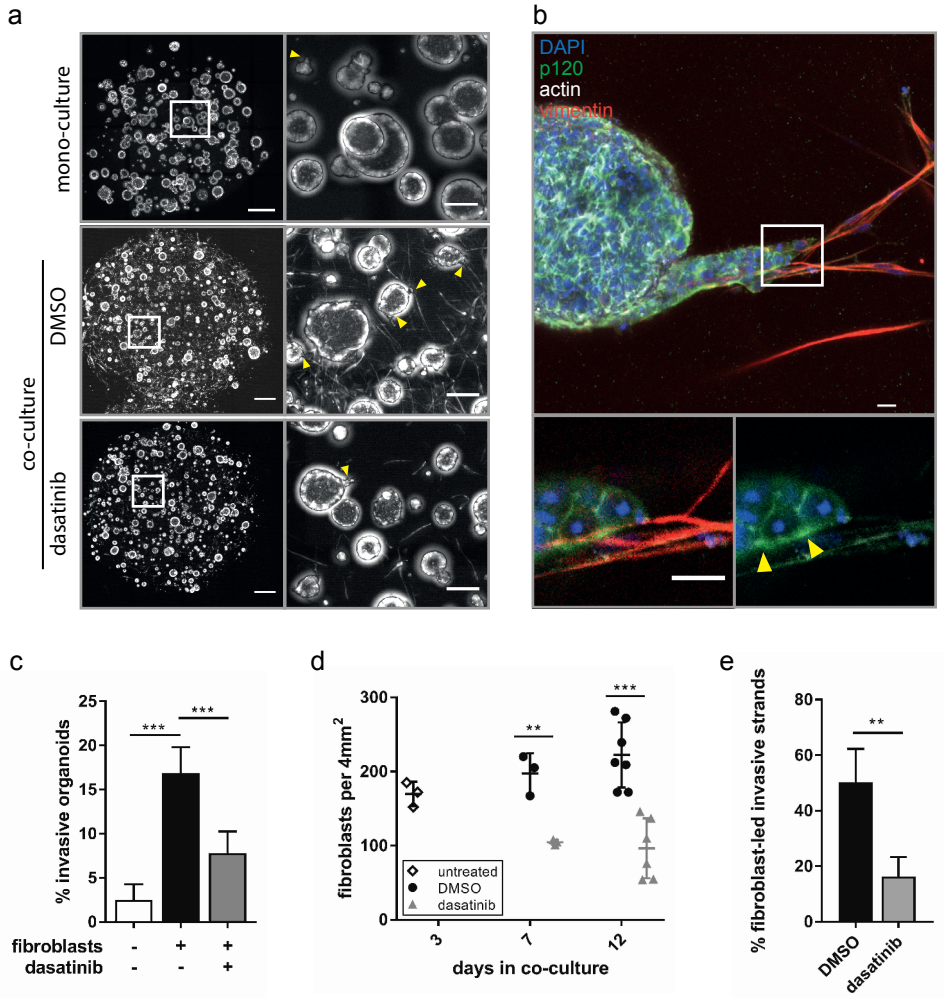

Figure 4. Dasatinib inhibits fibroblast-induced invasion in three-dimensional collagen-I matrix.
(a) Left: overview images of collagen-I matrices with p19ta mono-culture (top) and co-cultures of p19ta organoids with MRC5 fibroblasts without dasatinib treatment (middle) and with dasatinib treatment (bottom) after 12 days. Fluorescence shows F-actin (phalloidin) signal, scale bar = 200 µm. Right: magnifications showing invasive strands emerging from the organoids (yellow arrow heads), scale bar = 1000 µm. (b) Confocal microscopy image showing interaction (intense p120 staining, yellow arrow heads) between an invasive organoid strand and a fibroblast. Scale bars = 20 µm. (c) Quantification of fibroblast-induced invasion at day 12, bars represent mean plus standard deviation (SD) based on combined results from two repeated experiments with 3-4 gels per condition, ***p<0.0001 (one-way ANOVA, multiple comparisons test). (d) Dasatinib reduces the total number of fibroblasts in the co-culture over time. Co-culture gels were fixed and analyzed at three time points: at day 3 (before start of dasatinib/DMSO treatment), and at day 7 and day 12. **p=0.004, ***p=0.0002 (Multiple t-test, Statistical significance determined using the Holm-Sidak method, with alpha = 0.05). (e) Dasatinib reduces the percentage of fibroblast-associated invasive strands in co-culture. Bars represent mean plus standard deviation (SD) based on two repeated experiments with 3-4 gels per condition measured at day 12, **p=0.0012 (Mann Whitney test). (f) Confocal microscopy image showing budding of a tumor cell cluster from the invasive strand, guided by a fibroblast, scale bars = 20 µm. (g) Dasatinib decreases the number of invasive strands that show viable budding cells in co-culture. Bars represent mean plus standard deviation (SD) based on two repeated

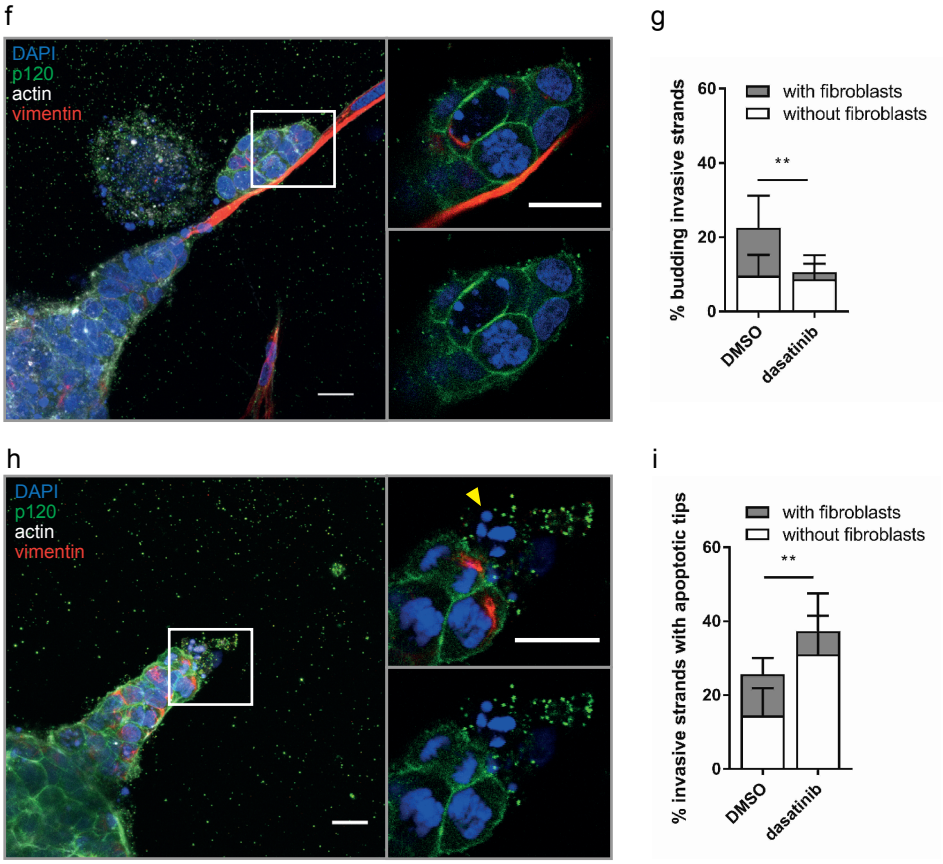

experiments with 3-4 gels per condition measured at day 12. The reduction in budding events with fibroblasts was significant (**p=0.0093, two-way ANOVA with multiple comparisons). (h) Confocal microscopy image showing apoptotic nuclei (yellow arrow head) at the tip of an invasive strand, scale bars = 20 µm. (i) Dasatinib increases the percentage of invasive strands with apoptotic tips. Bars represent mean plus standard deviation (SD) based on two repeated experiments with 3-4 gels per condition measured at day 12. The increase in apoptosis in strands without fibroblasts was significant (** p=0.0081, two-way ANOVA with multiple comparisons).

The TKI dasatinib is a potent inhibitor of c-Src, and also targets other kinases that are highly expressed in CMS4 CRC. We found that dasatinib inhibited – and even reversed – the invasive behavior of CRC organoids in collagen-I by restoring epithelial integrity at the tumor-matrix interface. Dasatinib also interfered with regenerative capacity of cancer organoids after dissociation.

Dasatinib was originally developed as an inhibitor of BCR-ABL and c-Src, but the spectrum of its high-affinity targets includes many pro-metastatic tyrosine kinases. To what extent inhibition of the various targets contributes to the observed treatment effects in our models is difficult to discern and most likely context-dependent, since many of its targets have proven pro-metastatic activity. In the context of CMS4 CRC – with collagen-I dominating the ECM – it is interesting to note that dasatinib is a potent inhibitor of the collagen-receptor DDR2. Elevated DDR2 expression in gastric cancer cells has been associated with increased peritoneal dissemination, and either knockdown of DDR2 or treatment with dasatinib reduced peritoneal metastasis formation in vivo.[32] Similarly, in head and neck squamous cell carcinoma, DDR2 overexpression was found to stimulate migration and invasion, which could be inhibited by dasatinib.[33] The specific role of DDR2 and other members of the CMS4 22TK panel in colon cancer progression require further investigation.

We developed a co-culture system with organoids and fibroblasts in collagen type I, to study the interactions between organoids and a CMS4-like tumor microenvironment. The presence of fibroblasts induced invasion of CRC organoids in a 3D collagen matrix, whereas hardly any invasion occurred in 3D mono-culture. Some of the invasive tumor cell strands were connected to fibroblasts, while others lacked fibroblast contact. This suggests multiple potential mechanisms by which fibroblasts induce CRC invasion, including transient contact with tip cells to lead CRC invasion[21], formation of collagen tracks to enable autonomous CRC invasion[34], and/or paracrine signaling through cytokine or growth factor release to induce ECM remodeling and invasion of CRC cells[35]. The induction of sheet migration between collagen layers in the absence of fibroblasts indicates that migration and invasion of CRC organoids depends on space and/or collagen alignment.

Treatment with dasatinib reduced the number of fibroblasts in the co-culture, reduced the number of invasive strands, and caused apoptosis of tumor cells located at the tips of the invasive strands. Based on these results we propose that stromal fibroblasts lead CRC invasion and promote survival of invading tumor cell strands and clusters. By targeting tyrosine kinases that are expressed on fibroblasts and/or on tumor cells, dasatinib abrogates the invasive phenotype of colorectal cancer organoids in desmoplastic stroma. These results are in line with previous studies documenting anti-invasive and anti-metastatic effects of dasatinib in preclinical models of various cancer types [19, 36-38]

This study shows how new insights into the biology of CRC subtypes can guide the design of targeted therapies. Collectively, the results suggest a model in which collagen-rich ECM and stromal fibroblasts promote mesenchymal gene expression and invasion of tumor cells, and that targeting these interactions could be an effective therapy for CMS4 CRC.

REFERENCES

1. Hackl C, Neumann P, Gerken M, et al. Treatment of colorectal liver metastases in Germany: a ten-year population-based analysis of 5772 cases of primary colorectal adenocarcinoma. *BMC Cancer*. 2014;**14**(1):810.
2. Bockelman C, Engelmann BE, Kaprio T, et al. Risk of recurrence in patients with colon cancer stage II and III: a systematic review and meta-analysis of recent literature. *Acta Oncol*. 2015;**54**(1):5-16.
3. Guinney J, Dienstmann R, Wang X, et al. The consensus molecular subtypes of colorectal cancer. *Nat Med*. 2015;**21**(11):1350-6.
4. Calon A, Lonardo E, Berenguer-Llergo A, et al. Stromal gene expression defines poor-prognosis subtypes in colorectal cancer. *Nat Genet*. 2015;**47**(4):320-9.
5. Isella C, Terrasi A, Bellomo SE, et al. Stromal contribution to the colorectal cancer transcriptome. *Nat Genet*. 2015;**47**(4):312-9.
6. Huijbers A, Tollenaar RA, v Pelt GW, et al. The proportion of tumor-stroma as a strong prognosticator for stage II and III colon cancer patients: validation in the VICTOR trial. *Ann Oncol*. 2013;**24**(1):179-85.
7. Ueno H, Kanemitsu Y, Sekine S, et al. Desmoplastic Pattern at the Tumor Front Defines Poor-prognosis Subtypes of Colorectal Cancer. *Am J Surg Pathol*. 2017;**41**(11):1506-12.
8. Calon A, Espinet E, Palomo-Ponce S, et al. Dependency of colorectal cancer on a TGF-beta-driven program in stromal cells for metastasis initiation. *Cancer Cell*. 2012;**22**(5):571-84.
9. Vellinga TT, den Uil S, Rinkes IH, et al. Collagen-rich stroma in aggressive colon tumors induces mesenchymal gene expression and tumor cell invasion. *Oncogene*. 2016;**35**(40):5263-71.
10. van de Wetering M, Francies HE, Francis JM, et al. Prospective derivation of a living organoid biobank of colorectal cancer patients. *Cell*. 2015;**161**(4):933-45.
11. de Jager W, te Velthuis H, Prakken BJ, et al. Simultaneous detection of 15 human cytokines in a single sample of stimulated peripheral blood mononuclear cells. *Clin Diagn Lab Immunol*. 2003;**10**(1):133-9.
12. Crotti S, Piccoli M, Rizzolio F, et al. Extracellular Matrix and Colorectal Cancer: How Surrounding Microenvironment Affects Cancer Cell Behavior? *J Cell Physiol*. 2017;**232**(5):967-75.
13. Wheeler DL, Iida M, Dunn EF. The role of Src in solid tumors. *Oncologist*. 2009;**14**(7):667-78.
14. Trevino JG, Summy JM, Gray MJ, et al. Expression and activity of SRC regulate interleukin-8 expression in pancreatic adenocarcinoma cells: implications for angiogenesis. *Cancer Res*. 2005;**65**(16):7214-22.
15. Marisa L, de Reynies A, Duval A, et al. Gene expression classification of colon cancer into molecular subtypes: characterization, validation, and prognostic value. *PLoS Med*. 2013;**10**(5):e1001453.
16. Cancer Genome Atlas Network. Comprehensive molecular characterization of human colon and rectal cancer. *Nature*. 2012;**487**(7407):330-7.
17. Davis MI, Hunt JP, Herrgard S, et al. Comprehensive analysis of kinase inhibitor selectivity. *Nat Biotechnol*. 2011;**29**(11):1046-51.
18. Huang F, Reeves K, Han X, et al. Identification of candidate molecular markers predicting sensitivity in solid tumors to dasatinib: rationale for patient selection. *Cancer Res*. 2007;**67**(5):2226-38.
19. Morton JP, Karim SA, Graham K, et al. Dasatinib inhibits the development of metastases in a mouse model of pancreatic ductal adenocarcinoma. *Gastroenterology*. 2010;**139**(1):292-303.
20. Haeger A, Krause M, Wolf K, et al. Cell jamming: collective invasion of mesenchymal tumor cells imposed by tissue confinement. *Biochim Biophys Acta*. 2014;**1840**(8):2386-95.
21. Labernadie A, Kato T, Brugues A, et al. A mechanically active heterotypic E-cadherin/N-cadherin adhesion enables fibroblasts to drive cancer cell invasion. *Nat Cell Biol*. 2017;**19**(3):224-37.
22. Shimizu M, Takakuwa Y, Nitta S. Study of stimulation-secretion coupling in a flow culture system: periodic secretion of hepatocyte growth factor by interleukin-1 alpha-stimulated human embryonic lung fibroblasts. *Biochim Biophys Acta*. 1995;**1244**(2-3):357-62.
23. Gaggioli C, Hooper S, Hidalgo-Carcedo C, et al. Fibroblast-led collective invasion of carcinoma cells with differing roles for RhoGTPases in leading and following cells. *Nat Cell Biol*. 2007;**9**(12):1392-400.
24. Zhuo C, Wu X, Li J, et al. Chemokine (C-X-C motif) ligand 1 is associated with tumor progression and poor prognosis in patients with colorectal cancer. *Biosci Rep*. 2018;**38**(4).
25. Ogawa R, Yamamoto T, Hirai H, et al. Loss of SMAD4 Promotes Colorectal Cancer Progression by Recruiting Tumor-Associated Neutrophils via the CXCL1/8-CXCR2 Axis. *Clin Cancer Res*. 2019;**25**(9):2887-99.

26. Fisher RC, Bellamkonda K, Alex Molina L, et al. Disrupting Inflammation-Associated CXCL8-CXCR1 Signaling Inhibits Tumorigenicity Initiated by Sporadic- and Colitis-Colon Cancer Stem Cells. *Neoplasia*. 2019;**21**(3):269-81.
27. Wang D, Sun H, Wei J, et al. CXCL1 Is Critical for Premetastatic Niche Formation and Metastasis in Colorectal Cancer. *Cancer Res*. 2017;**77**(13):3655-65.
28. Baker AM, Cox TR, Bird D, et al. The role of lysyl oxidase in SRC-dependent proliferation and metastasis of colorectal cancer. *J Natl Cancer Inst*. 2011;**103**(5):407-24.
29. Baker AM, Bird D, Lang G, et al. Lysyl oxidase enzymatic function increases stiffness to drive colorectal cancer progression through FAK. *Oncogene*. 2013;**32**(14):1863-8.
30. Peng DH, Ungewiss C, Tong P, et al. ZEB1 induces LOXL2-mediated collagen stabilization and deposition in the extracellular matrix to drive lung cancer invasion and metastasis. *Oncogene*. 2017;**36**(14):1925-38.
31. Payne SL, Fogelgren B, Hess AR, et al. Lysyl oxidase regulates breast cancer cell migration and adhesion through a hydrogen peroxide-mediated mechanism. *Cancer Res*. 2005;**65**(24):11429-36.
32. Kurashige J, Hasegawa T, Niida A, et al. Integrated Molecular Profiling of Human Gastric Cancer Identifies DDR2 as a Potential Regulator of Peritoneal Dissemination. *Sci Rep*. 2016;**6**:22371.
33. von Massenhausen A, Sanders C, Bragelmann J, et al. Targeting DDR2 in head and neck squamous cell carcinoma with dasatinib. *Int J Cancer*. 2016;**139**(10):2359-69.
34. Drifka CR, Loeffler AG, Esquibel CR, et al. Human pancreatic stellate cells modulate 3D collagen alignment to promote the migration of pancreatic ductal adenocarcinoma cells. *Biomed Microdevices*. 2016;**18**(6):105.
35. Cao H, Eppinga RD, Razidlo GL, et al. Stromal fibroblasts facilitate cancer cell invasion by a novel invadopodia-independent matrix degradation process. *Oncogene*. 2016;**35**(9):1099-110.
36. Erami Z, Herrmann D, Warren SC, et al. Intravital FRAP Imaging using an E-cadherin-GFP Mouse Reveals Disease- and Drug-Dependent Dynamic Regulation of Cell-Cell Junctions in Live Tissue. *Cell Rep*. 2016;**14**(1):152-67.
37. Serrels A, Macpherson IR, Evans TR, et al. Identification of potential biomarkers for measuring inhibition of Src kinase activity in colon cancer cells following treatment with dasatinib. *Mol Cancer Ther*. 2006;**5**(12):3014-22.
38. Park SI, Zhang J, Phillips KA, et al. Targeting SRC family kinases inhibits growth and lymph node metastases of prostate cancer in an orthotopic nude mouse model. *Cancer Res*. 2008;**68**(9):3323-33.

SUPPLEMENTARY FIGURES AND TABLES

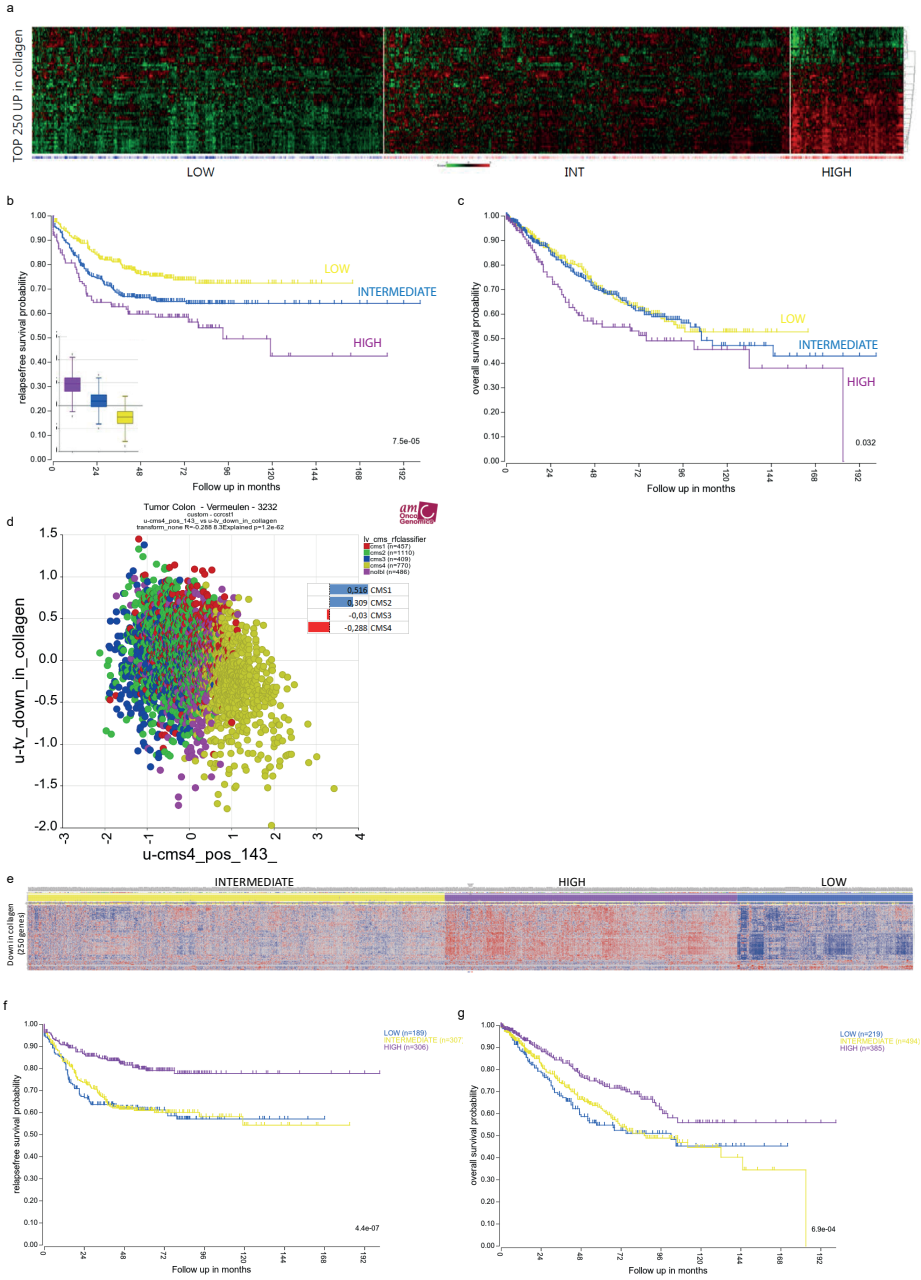

Supplementary Figure 1.
(a) Heatmap showing the expression of the 250 genes upregulated by collagen-I (COL250-UP) in the three ▶

▶ clusters derived from k-means clustering. (b) Kaplan Meier curve of relapse-free survival based on clusters of COL250-UP. (c) Kaplan Meier curve of overall survival based on clusters of COL250-UP. (d) Scatterplot showing the expression of CMS4 signature genes related to expression of COL250-DOWN genes in the CMS-3232 cohort. Inset: Pearson correlation (r-value) of CMS1-4 signature gene sets with the COL250-DOWN gene set. (e) Heatmap showing the expression of the 250 most significantly downregulated genes in collagen-I (COL250-DOWN) in the three clusters derived from k-means clustering. (f) Kaplan Meier curve of relapse-free survival based on clusters of COL250-DOWN. (g) Kaplan Meier curve of overall survival based on clusters of COL250-DOWN.

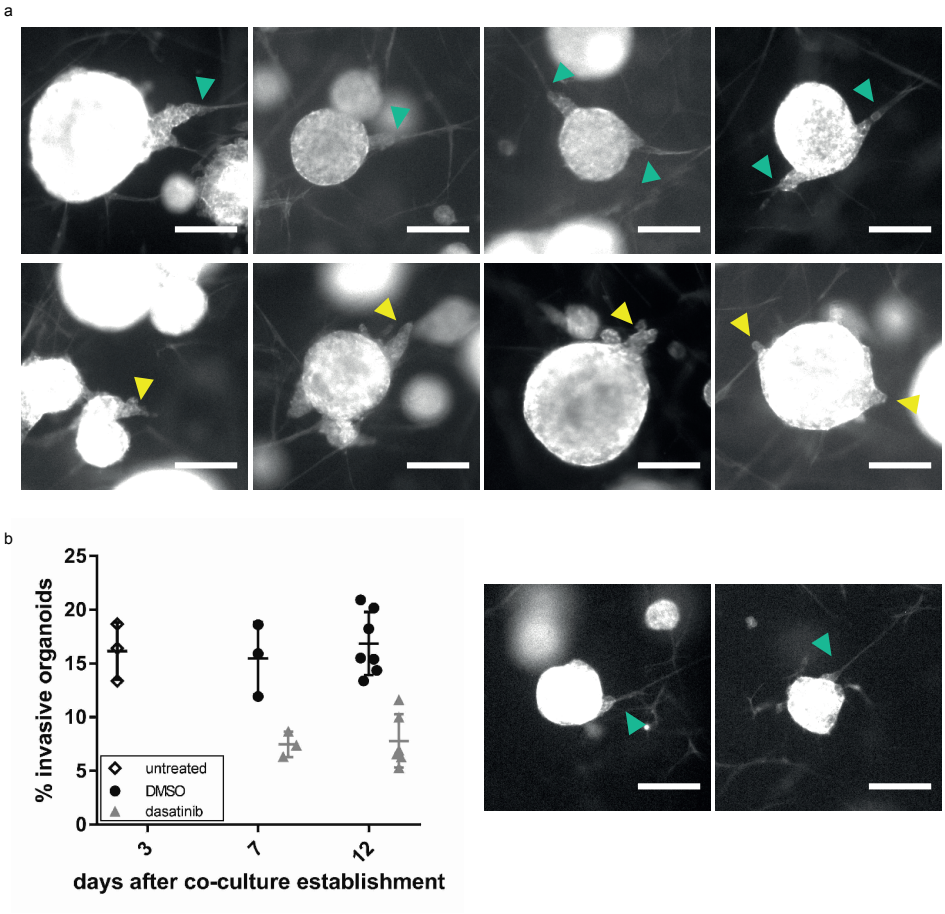

Supplementary Figure 2.
(a) Invasion of organoids p19ta in 3D collagen-I induced by fibroblasts; both guided by fibroblasts (green arrows, top row) and unguided (yellow arrows, bottom row) after 12 days. Fluorescence shows F-actin signal. (b) Fibroblast-led invasive strand formation over time. Co-cultures were fixed and analysed at three time points: at day 3 (before start of dasatinib treatment), day 7 and day 12. Images on the right show examples of fibroblast-led invasive strand formation at day 3, scale bar = 150 µm.

Supplementary Table 1. List of the 601 genes that are significantly differently expressed (up- and downregulated genes) in organoids cultured in collagen-I compared with organoids cultured in matrigel.

#Program: R2: Genomics analysis and visualization platform
#Website: http://r2.amc.nl
#Developer: Jan Koster (jankoster@amc.uva.nl)
#Support: r2-support@amc.uva.nl
#Date: 2018-04-25 (10:11:18)
#Dataset: ps_okran_organoidmgcol18_u133p2
#Data transformation: transform_2log
#Dataset: ps_okran_organoidmgcol18_u133p2
#Data transformation: transform_2log
#Comparison: groups
#Group: group -> coll
#Group: group -> mg
#Test: anova
#Output: anova 0.01 no
#Minimal presentcalls: 1

UPREGULATED IN COLLAGEN VS MATRIGEL

#H:probeset	HUGO	R-value	p-value
202859_x_at	CXCL8	-0.869	2.84E-06
229372_at	GOLT1A	-0.868	3.08E-06
223983_s_at	C19orf12	-0.843	1.10E-05
236616_at	PSD4	-0.826	2.44E-05
223132_s_at	TRIM8	-0.816	3.67E-05
1555833_a_at	IRGQ	-0.812	4.28E-05
213857_s_at	CD47	-0.81	4.61E-05
204259_at	MMP7	-0.795	8.00E-05
224784_at	MLLT6	-0.794	8.43E-05
209004_s_at	FBXL5	-0.79	9.50E-05
200696_s_at	GSN	-0.789	9.83E-05
205466_s_at	HS3ST1	-0.785	0.000115468
201939_at	PLK2	-0.784	0.000118891
223084_s_at	CCNDBP1	-0.781	0.000130223
230218_at	HIC1	-0.779	0.000138247
201578_at	PODXL	-0.779	0.000140082
218853_s_at	MOSPD1	-0.778	0.000142591
206224_at	CST1	-0.777	0.000147848
204519_s_at	PLLP	-0.776	0.000151132
209369_at	ANXA3	-0.775	0.000160338
218004_at	BSDC1	-0.774	0.000164137
228303_at	GALNT6	-0.772	0.000174701
200932_s_at	DCTN2	-0.768	0.000196136
222570_at	NCS1	-0.764	0.000226663
210589_s_at	GBAP1	-0.763	0.000228789
239430_at	IGFL1	-0.76	0.000255199
211530_x_at	HLA-G	-0.759	0.000260529
212052_s_at	TBC1D9B	-0.758	0.000268149
217943_s_at	MAP7D1	-0.756	0.000286905
232602_at	WFDC3	-0.756	0.000287172
225688_s_at	PHLDB2	-0.754	0.000299414
212711_at	CAMSAP1	-0.754	0.0003002
201863_at	FAM32A	-0.753	0.00030815
227981_at	CYB561D1	-0.753	0.000309248
35147_at	MCF2L	-0.752	0.000323347
209016_s_at	KRT7	-0.748	0.000359592
201041_s_at	DUSP1	-0.748	0.000359631

DOWNREGULATED IN COLLAGEN VS MATRIGEL

#H:probeset	HUGO	R-value	p-value
225326_at	RBM27	0.852	7.35E-06
204020_at	PURA	0.817	3.56E-05
230078_at	RAPGEF6	0.816	3.67E-05
207787_at	KRT33B	0.803	6.02E-05
217100_s_at	UBXN7	0.798	7.12E-05
212919_at	DCP2	0.79	9.56E-05
224554_at	GHSR	0.789	9.91E-05
229896_at	LOC101926943	0.789	0.000100092
34471_at	MYH8	0.786	0.000109901
211337_s_at	TUBGCP4	0.78	0.000133421
1558790_s_at	ZNF252P-AS1	0.78	0.000135598
226277_at	COL4A3BP	0.778	0.000144845
1557945_at	TCTE3	0.775	0.000157186
215224_at	SNORA21	0.773	0.00016686
202956_at	ARFGEF1	0.767	0.000204809
226025_at	ANKRD28	0.766	0.000209529
232558_at	LAMC3	0.765	0.000217886
206550_s_at	NUP155	0.759	0.000258956
226085_at	CBX5	0.755	0.00029599
1567686_at	CECR9	0.752	0.000317113
209814_at	ZNF330	0.75	0.000339248
219544_at	BORA	0.749	0.00034562
213074_at	PHIP	0.749	0.000350204
229770_at	GLT1D1	0.748	0.000355975
235060_at	LOC100190986	0.746	0.00037322
236841_at	LOC100134445	0.745	0.000383596
211953_s_at	IPO5	0.741	0.000428753
231825_x_at	ATF7IP	0.74	0.000440683
229870_at	LOC644656	0.74	0.000442297
221568_s_at	LIN7C	0.739	0.000464936
233852_at	POLH	0.732	0.000555402
236981_at	C17orf99	0.73	0.000585603
1553479_at	TMEM145	0.73	0.000589307
213496_at	PLPPR4	0.727	0.000626296
1562738_a_at	USP3-AS1	0.724	0.000683354
226663_at	ANKRD10-IT1	0.722	0.00071833
207712_at	BAGE	0.718	0.000785114

Supplementary Table 1. Continued

UPREGULATED IN COLLAGEN VS MATRIGEL			
#H:probeset	**HUGO**	**R-value**	**p-value**
823_at	CX3CL1	-0.745	0.00039262
212359_s_at	ZSWIM8	-0.744	0.000397095
203373_at	SOCS2	-0.743	0.000412706
204000_at	GNB5	-0.74	0.000442225
1553180_at	ADAMTS19	-0.737	0.000479996
218333_at	DERL2	-0.736	0.000497206
209059_s_at	EDF1	-0.734	0.000518323
217819_at	GOLGA7	-0.726	0.000653909
55093_at	CHPF2	-0.723	0.000694069
215005_at	NECAB2	-0.722	0.000711025
242521_at	CARD8-AS1	-0.721	0.000735793
203720_s_at	ERCC1	-0.72	0.000762511
204268_at	S100A2	-0.719	0.000772173
206994_at	CST4	-0.719	0.000777453
226190_at	MAP3K13	-0.716	0.000825176
200096_s_at	ATP6V0E1	-0.716	0.000828161
1553102_a_at	CCDC69	-0.715	0.000845687
203828_s_at	IL32	-0.713	0.00089047
202452_at	ZER1	-0.712	0.00090973
233537_at	KRTAP3-1	-0.712	0.000914648
224186_s_at	RNF123	-0.711	0.000947034
1555912_at	ST7-AS1	-0.71	0.000952615
219952_s_at	MCOLN1	-0.71	0.000955269
206022_at	NDP	-0.709	0.000994242
217983_s_at	RNASET2	-0.707	0.001037971
217795_s_at	TMEM43	-0.706	0.001066547
205020_s_at	ARL4A	-0.705	0.001080073
202768_at	FOSB	-0.704	0.001099236
204470_at	CXCL1	-0.703	0.001124964
227949_at	PHACTR3	-0.703	0.001139924
223184_s_at	AGPAT3	-0.698	0.001290855
227903_x_at	TPGS1	-0.697	0.001297453
205402_x_at	PRSS2	-0.696	0.001324867
224981_at	TMEM219	-0.696	0.001335457
244557_at	LINC00610	-0.695	0.001356619
225738_at	RAPGEF1	-0.695	0.001370782
208555_x_at	CST2	-0.695	0.001376184
204202_at	IQCE	-0.694	0.001394116
202898_at	SDC3	-0.694	0.001397128
200810_s_at	CIRBP	-0.691	0.001481226
201464_x_at	JUN	-0.691	0.001484299
212968_at	RFNG	-0.691	0.001493408
225597_at	SLC45A4	-0.69	0.001523394
212697_at	FAM134C	-0.69	0.00153299
206058_at	SLC6A12	-0.69	0.001541713
218928_s_at	SLC37A1	-0.689	0.001549132
213932_x_at	HLA-A	-0.689	0.001560811
208968_s_at	CIAPIN1	-0.685	0.001724549
224727_at	EMC10	-0.684	0.001734732
208737_at	ATP6V1G1	-0.682	0.00184222

DOWNREGULATED IN COLLAGEN VS MATRIGEL			
#H:probeset	**HUGO**	**R-value**	**p-value**
238449_at	SMG1P5	0.715	0.000862676
208694_at	PRKDC	0.714	0.00086952
229972_at	LOC101926963	0.714	0.000881766
210892_s_at	GTF2I	0.713	0.000903237
218781_at	SMC6	0.712	0.000916203
204394_at	SLC43A1	0.712	0.000925648
205832_at	CPA4	0.708	0.001022162
200726_at	PPP1CC	0.707	0.001028846
214509_at	HIST1H3I	0.707	0.001037539
226690_at	ADCYAP1R1	0.706	0.001049826
208775_at	XPO1	0.706	0.001070172
214785_at	VPS13A	0.703	0.001128976
226977_at	IGIP	0.703	0.001147514
215024_at	CCZ1B	0.702	0.00117226
230165_at	SGO2	0.702	0.001176125
212402_at	ZC3H13	0.701	0.001184375
1562674_at	LOC101929325	0.701	0.001193723
219918_s_at	ASPM	0.699	0.001256715
1564653_s_at	LEKR1	0.695	0.001356441
222529_at	SLC25A37	0.694	0.001398564
219067_s_at	NSMCE4A	0.694	0.001413384
206691_s_at	PDIA2	0.693	0.001442717
216199_s_at	MAP3K4	0.692	0.001465436
220411_x_at	PODNL1	0.692	0.001466086
230090_at	GDNF	0.692	0.001476557
218659_at	ASXL2	0.69	0.001512993
1556911_at	ALMS1-IT1	0.689	0.00157882
208494_at	SLC6A7	0.688	0.001584613
226431_at	FAM117B	0.688	0.001591239
201567_s_at	GOLGA4	0.688	0.001603047
228323_at	CASC5	0.688	0.001615668
203564_at	FANCG	0.687	0.001649213
206525_at	GABRR1	0.687	0.001650287
211454_x_at	FKSG49	0.686	0.001687939
212213_x_at	OPA1	0.685	0.001696719
211767_at	GINS4	0.684	0.001751531
229442_at	C18orf54	0.683	0.001776892
221426_s_at	OR3A3	0.682	0.00181183
212022_s_at	MKI67	0.681	0.001845846
1554019_s_at	CEP57L1	0.681	0.001846074
225777_at	SAPCD2	0.681	0.001846779
204822_at	TTK	0.681	0.001857771
216870_x_at	DLEU2	0.681	0.001872268
203182_s_at	SRPK2	0.68	0.001883623
203764_at	DLGAP5	0.68	0.001885802
1556597_a_at	LOC284513	0.68	0.00190465
203318_s_at	ZNF148	0.679	0.001947526
206989_s_at	SCAF11	0.679	0.001964003
207429_at	SLC22A2	0.678	0.001965721
230924_at	TTLL6	0.678	0.001989434

Supplementary Table 1. Continued

UPREGULATED IN COLLAGEN VS MATRIGEL			
#H:probeset	**HUGO**	**R-value**	**p-value**
225629_s_at	ZBTB4	-0.681	0.001845808
204237_at	GULP1	-0.681	0.00185734
91816_f_at	MEX3D	-0.677	0.002015353
205749_at	CYP1A1	-0.677	0.002044048
226307_at	CRTC2	-0.676	0.00208053
214733_s_at	YIPF1	-0.676	0.002087886
202587_s_at	AK1	-0.675	0.002111071
231823_s_at	SH3PXD2B	-0.675	0.002114292
208774_at	CSNK1D	-0.675	0.002136369
225848_at	ZNF746	-0.674	0.002155789
1569925_at	DNAH17-AS1	-0.673	0.002222494
204824_at	ENDOG	-0.671	0.002287051
222449_at	PMEPA1	-0.671	0.00229408
202207_at	ARL4C	-0.67	0.002327583
202104_s_at	SPG7	-0.67	0.002349169
204481_at	BRPF1	-0.67	0.002357261
203002_at	AMOTL2	-0.668	0.002429617
225177_at	RAB11FIP1	-0.668	0.002436951
228458_at	C6orf226	-0.667	0.002513877
53968_at	INTS5	-0.666	0.002545304
242841_at	LOC100505570	-0.666	0.002564708
226966_at	PRPF40B	-0.663	0.002725275
226405_s_at	ARRDC1	-0.662	0.002746639
203826_s_at	PITPNM1	-0.662	0.002746889
204125_at	NDUFAF1	-0.662	0.002754268
207760_s_at	NCOR2	-0.662	0.002768131
218436_at	SIL1	-0.661	0.002795056
218562_s_at	TMEM57	-0.658	0.002965178
228291_s_at	KIZ	-0.658	0.00296714
200859_x_at	FLNA	-0.658	0.002992567
224808_s_at	GET4	-0.658	0.003005036
224893_at	ATL3	-0.658	0.003012094
223090_x_at	VEZT	-0.658	0.003016141
1568617_a_at	CAMSAP3	-0.656	0.003092916
229582_at	INO80C	-0.656	0.003095492
226380_at	PTPN21	-0.656	0.003112019
200609_s_at	WDR1	-0.656	0.003115877
231849_at	KRT80	-0.656	0.003128888
203821_at	HBEGF	-0.655	0.003170927
218130_at	C17orf62	-0.655	0.003188339
209774_x_at	CXCL2	-0.655	0.003192038
226298_at	RUNDC1	-0.654	0.003249617
204734_at	KRT15	-0.653	0.003303418
227170_at	ZNF316	-0.653	0.003331317
225258_at	FBLIM1	-0.652	0.003344455
218601_at	URGCP	-0.652	0.003371992
220249_at	HYAL4	-0.652	0.003372
1556588_at	ST20-AS1	-0.652	0.003393246
201050_at	PLD3	-0.651	0.003411879
224923_at	TTC7A	-0.651	0.00343168

DOWNREGULATED IN COLLAGEN VS MATRIGEL			
#H:probeset	**HUGO**	**R-value**	**p-value**
1559964_at	LOC401261	0.677	0.00204109
203095_at	MTIF2	0.676	0.00207302
228565_at	KIAA1804	0.675	0.002099265
202705_at	CCNB2	0.675	0.002129058
1562637_at	SAMD12	0.674	0.002182494
206789_s_at	POU2F1	0.673	0.002200413
222958_s_at	DEPDC1	0.673	0.002200433
225176_at	LNPEP	0.673	0.002220119
226589_at	TMEM192	0.673	0.002227195
210821_x_at	CENPA	0.672	0.00226815
228783_at	BVES	0.671	0.002293006
213168_at	SP3	0.671	0.002295292
1561400_at	LINC01180	0.671	0.002297999
214715_x_at	ZNF160	0.671	0.002304957
1563753_at	BPI	0.671	0.002321632
203376_at	CDC40	0.67	0.002336505
209408_at	KIF2C	0.67	0.002356273
205370_x_at	DBT	0.67	0.002361507
1565620_at	AGAP4	0.669	0.002377478
226508_at	PHC3	0.669	0.002377911
1552862_at	RUSC1-AS1	0.669	0.002381214
242201_at	PMS2P5	0.668	0.002440901
224743_at	IMPAD1	0.668	0.002458831
1564385_at	LOC219688	0.666	0.002560178
219540_at	ZNF267	0.665	0.002611774
241731_x_at	ZNF440	0.665	0.002618196
1562424_at	LOC285889	0.665	0.002620865
209642_at	BUB1	0.664	0.002639567
224160_s_at	ACAD9	0.664	0.002668618
219990_at	E2F8	0.664	0.002670174
211040_x_at	GTSE1	0.662	0.002761822
205526_s_at	KATNA1	0.661	0.002806365
210053_at	TAF5	0.661	0.002811939
202468_s_at	CTNNAL1	0.66	0.002857062
207009_at	PHOX2B	0.659	0.002938762
212534_at	ZNF24	0.659	0.002953169
224273_at	C3orf20	0.657	0.00303221
209572_s_at	EED	0.657	0.003072611
227586_at	TMEM170A	0.656	0.003097005
229353_s_at	NUCKS1	0.656	0.003099632
218750_at	TAF1D	0.654	0.003215925
1559050_at	HCG27	0.654	0.003219957
1558310_s_at	LOC100132356	0.654	0.003224443
206721_at	CCDC181	0.653	0.003307278
230942_at	CMTM5	0.653	0.003308504
225040_s_at	RPE	0.652	0.003363804
221209_s_at	OTOR	0.652	0.003371037
209680_s_at	KIFC1	0.651	0.003418517
244422_at	LOC101928370	0.651	0.003439511
210686_x_at	SLC25A16	0.651	0.003464673

Supplementary Table 1. Continued

UPREGULATED IN COLLAGEN VS MATRIGEL			
#H:probeset	**HUGO**	**R-value**	**p-value**
65884_at	MAN1B1	-0.651	0.003454254
218834_s_at	TMEM132A	-0.65	0.003503183
225671_at	SPNS2	-0.65	0.003530713
223250_at	KLHL7	-0.649	0.003533238
222549_at	CLDN1	-0.649	0.003539367
210201_x_at	BIN1	-0.648	0.003651207
231579_s_at	TIMP2	-0.647	0.003693007
228839_s_at	LINC00863	-0.646	0.003745417
214953_s_at	APP	-0.646	0.003767115
221563_at	DUSP10	-0.646	0.003769084
1553968_a_at	ADAT3	-0.645	0.003852828
227265_at	FGL2	-0.645	0.003858445
203180_at	ALDH1A3	-0.644	0.003955368
226454_at	MARCH9	-0.643	0.003963435
213185_at	KIAA0556	-0.643	0.003990415
39248_at	AQP3	-0.643	0.004019592
223431_at	BLOC1S4	-0.642	0.004036932
215735_s_at	TSC2	-0.642	0.004039186
226698_at	FCHSD1	-0.642	0.004054631
203735_x_at	PPFIBP1	-0.642	0.004067051
203315_at	NCK2	-0.642	0.004080121
221571_at	TRAF3	-0.642	0.004095249
200618_at	LASP1	-0.641	0.004112076
212784_at	CIC	-0.641	0.004135397
204415_at	IFI6	-0.64	0.004240818
39891_at	ZNF710	-0.639	0.004289601
203186_s_at	S100A4	-0.638	0.004350625
232259_s_at	ZBTB11-AS1	-0.638	0.004420254
1563327_a_at	LINC01545	-0.637	0.004430304
204611_s_at	PPP2R5B	-0.636	0.004542526
221519_at	FBXW4	-0.635	0.004598434
212443_at	NBEAL2	-0.635	0.00462283
204488_at	DOLK	-0.635	0.004623647
1561330_at	DSG4	-0.634	0.004710858
219147_s_at	NMRK1	-0.634	0.00473984
221577_x_at	GDF15	-0.634	0.00475823
222392_x_at	PERP	-0.633	0.004778049
209262_s_at	NR2F6	-0.633	0.004784774
213324_at	SRC	-0.633	0.004793621
229909_at	B4GALNT3	-0.632	0.004867306
225621_at	ALG2	-0.632	0.004886742
44696_at	TBC1D13	-0.632	0.004937975
217796_s_at	NPLOC4	-0.631	0.004958978
204075_s_at	CEP104	-0.631	0.004984015
203652_at	MAP3K11	-0.631	0.004985975
204495_s_at	C15orf39	-0.63	0.005072142
221337_s_at	ADAM29	-0.629	0.00514545
202910_s_at	ADGRE5	-0.629	0.005195349
204275_at	CAPN15	-0.629	0.005209391
202122_s_at	PLIN3	-0.628	0.005216727

DOWNREGULATED IN COLLAGEN VS MATRIGEL			
#H:probeset	**HUGO**	**R-value**	**p-value**
232207_at	GUSBP4	0.65	0.003472241
212673_at	METAP1	0.65	0.003477873
220796_x_at	SLC35E1	0.65	0.003529289
200842_s_at	EPRS	0.649	0.003552549
221786_at	C6orf120	0.649	0.003569059
217549_at	NCKAP1L	0.649	0.003590963
220887_at	CCDC177	0.648	0.003615262
202870_s_at	CDC20	0.648	0.003657373
228562_at	ZBTB10	0.648	0.003666379
213387_at	ATAD2B	0.647	0.003674675
1560821_at	ARHGAP22	0.647	0.003680388
218422_s_at	RBM26	0.647	0.003701917
238639_x_at	LOC102724312	0.647	0.00370508
215470_at	GTF2H2B	0.647	0.003739277
210820_x_at	COQ7	0.646	0.003803567
1558755_x_at	ZNF763	0.645	0.003823706
218542_at	CEP55	0.645	0.003839389
221096_s_at	TMCO6	0.645	0.003869179
219588_s_at	NCAPG2	0.644	0.00394442
227545_at	BARD1	0.643	0.003961332
224944_at	TMPO	0.643	0.00399026
205879_x_at	RET	0.643	0.004011089
204529_s_at	TOX	0.639	0.004312345
219927_at	FCF1	0.639	0.004325794
204162_at	NDC80	0.639	0.004329814
201795_at	LBR	0.639	0.004330803
213628_at	CLCC1	0.639	0.004337777
224721_at	WDR75	0.638	0.004389553
1556194_a_at	HSPA4L	0.636	0.004534967
206292_s_at	SULT2A1	0.636	0.00453751
205134_s_at	NUFIP1	0.636	0.00456846
226925_at	PXYLP1	0.636	0.004573322
1558128_at	LOC730202	0.635	0.004606894
218428_s_at	REV1	0.635	0.004625842
217250_s_at	CHD5	0.635	0.004654756
218755_at	KIF20A	0.634	0.004694605
220331_at	CYP46A1	0.634	0.004734708
239506_s_at	LINC00608	0.634	0.004740312
1566480_x_at	MEIOC	0.633	0.004833821
228252_at	PIF1	0.633	0.004835578
221520_s_at	CDCA8	0.631	0.004942614
206945_at	LCT	0.631	0.004975418
242608_x_at	FAM161B	0.631	0.004987883
220807_at	HBQ1	0.63	0.005065461
243785_at	LOC100272217	0.63	0.005104884
1558844_at	LOC100506127	0.629	0.005171651
205356_at	USP13	0.629	0.005188691
1553244_at	FANCB	0.629	0.005189095
202223_at	STT3A	0.629	0.005197613
207828_s_at	CENPF	0.628	0.005228585

Supplementary Table 1. Continued

UPREGULATED IN COLLAGEN VS MATRIGEL			
#H:probeset	**HUGO**	**R-value**	**p-value**
212757_s_at	CAMK2G	-0.628	0.005274278
221100_at	C6orf15	-0.627	0.005390521
202027_at	TMEM184B	-0.626	0.005438045
206304_at	MYBPH	-0.626	0.005480635
224983_at	SCARB2	-0.625	0.00554865
1557731_at	LOC400620	-0.625	0.005590706
209183_s_at	C10orf10	-0.624	0.005680927
212298_at	NRP1	-0.623	0.005698525
225212_at	SLC25A25	-0.623	0.005718315
209691_s_at	DOK4	-0.622	0.005832725
212540_at	CDC34	-0.622	0.005835161
64942_at	GPR153	-0.622	0.005866256
202245_at	LSS	-0.621	0.005921781
205234_at	SLC16A4	-0.621	0.005947225
214965_at	SPATA2L	-0.621	0.005998517
239648_at	DCUN1D3	-0.62	0.006022725
203010_at	STAT5A	-0.62	0.006022894
209333_at	ULK1	-0.62	0.006055126
225205_at	KIF3B	-0.62	0.006077895
207196_s_at	TNIP1	-0.619	0.006134052
47083_at	C7orf26	-0.619	0.006137972
203530_s_at	STX4	-0.619	0.006178578
204981_at	SLC22A18	-0.618	0.006226853
218999_at	TMEM140	-0.618	0.006242079
227862_at	TRNP1	-0.618	0.00626663
55065_at	MARK4	-0.618	0.006277387
210275_s_at	ZFAND5	-0.618	0.006305478
209008_x_at	KRT8	-0.617	0.006367572
219928_s_at	CABYR	-0.616	0.006471996
239763_at	PRDM11	-0.616	0.00651008
222105_s_at	NKIRAS2	-0.615	0.006614238
204715_at	PANX1	-0.614	0.0066693
218231_at	NAGK	-0.614	0.006681402
226738_at	WDR81	-0.614	0.006701641
219369_s_at	OTUB2	-0.614	0.006742227
238039_at	SCAMP1-AS1	-0.614	0.006757376
203233_at	IL4R	-0.613	0.006796796
1569144_a_at	CYSRT1	-0.612	0.006934213
56821_at	SLC38A7	-0.612	0.006952841
213191_at	TICAM1	-0.612	0.006971646
212099_at	RHOB	-0.611	0.007018795
1560734_at	OR4N4	-0.611	0.007019996
225912_at	TP53INP1	-0.611	0.007028149
231328_s_at	RASGRP4	-0.611	0.007048079
203256_at	CDH3	-0.611	0.007052984
1556489_at	TMEM247	-0.611	0.007080598
236984_at	C4orf26	-0.611	0.007101171
218373_at	AKTIP	-0.611	0.007107883
231905_at	C20orf96	-0.609	0.007255649
212277_at	MTMR4	-0.609	0.007277019

DOWNREGULATED IN COLLAGEN VS MATRIGEL			
#H:probeset	**HUGO**	**R-value**	**p-value**
204170_s_at	CKS2	0.628	0.005262729
232266_x_at	CDK13	0.627	0.005329985
224781_s_at	RBM17	0.627	0.005343863
210125_s_at	BANF1	0.627	0.005354378
228894_at	NR6A1	0.626	0.005446782
239691_at	C12orf77	0.626	0.005455618
206158_s_at	CNBP	0.626	0.005477377
218152_at	HMG20A	0.626	0.00548366
226181_at	TUBE1	0.623	0.005706203
202589_at	TYMS	0.623	0.005773089
1560141_at	LOC100133039	0.622	0.005811112
223590_at	ZNF700	0.622	0.005828671
242578_x_at	SLC22A3	0.622	0.005888176
227628_at	GPX8	0.621	0.00597529
204825_at	MELK	0.621	0.005991832
206365_at	XCL1	0.62	0.006097579
1555940_a_at	PRKCA-AS1	0.62	0.006102029
228927_at	ZNF397	0.619	0.006148928
214264_s_at	EFCAB11	0.619	0.006162541
1570124_at	SLC29A4	0.619	0.006178066
218905_at	INTS8	0.618	0.006261523
233815_at	NAALAD2	0.618	0.006282981
225056_at	SIPA1L2	0.618	0.00629942
204835_at	POLA1	0.618	0.006303254
226962_at	ZBTB41	0.617	0.00632955
202240_at	PLK1	0.617	0.006335523
222224_at	NACA2	0.617	0.006364076
223734_at	MGARP	0.617	0.00639455
229097_at	DIAPH3	0.617	0.006411982
233775_x_at	LOC100289333	0.616	0.006436594
1558942_at	ZNF765	0.616	0.00653931
242173_at	PLD5	0.615	0.006564097
201637_s_at	FXR1	0.615	0.006568088
233971_at	FAM166A	0.614	0.006685643
213248_at	LOC730101	0.614	0.006721858
238602_at	DIS3L2	0.614	0.0067276
205167_s_at	CDC25C	0.614	0.006733257
238237_at	LOC100130964	0.614	0.006768873
213271_s_at	DOPEY1	0.613	0.006810953
201092_at	RBBP7	0.613	0.006848858
219769_at	INCENP	0.613	0.00688682
1562895_at	LOC101927502	0.612	0.006899694
225617_at	ODF2	0.611	0.007091217
206007_at	PRG4	0.61	0.007132053
201519_at	TOMM70	0.61	0.007154686
240814_at	MGC39584	0.61	0.007155721
206047_at	GNB3	0.61	0.007207003
234165_at	PTGDR	0.609	0.007258866
209444_at	RAP1GDS1	0.609	0.007290786
1560832_at	LINC01029	0.609	0.007295009

Supplementary Table 1. Continued

UPREGULATED IN COLLAGEN VS MATRIGEL			
#H:probeset	**HUGO**	**R-value**	**p-value**
207850_at	CXCL3	-0.609	0.007295968
212266_s_at	SRSF5	-0.609	0.007297488
1555832_s_at	KLF6	-0.609	0.007311442
236430_at	TMED6	-0.609	0.007324267
218487_at	ALAD	-0.609	0.007330009
227334_at	USP54	-0.609	0.007337788
230780_at	LINC00886	-0.609	0.007348149
221864_at	ORAI3	-0.608	0.007395596
212845_at	SAMD4A	-0.608	0.00742914
1559880_at	LZTS1-AS1	-0.608	0.007437357
208420_x_at	SUPT6H	-0.608	0.007444509
204952_at	LYPD3	-0.608	0.007462514
218569_s_at	KBTBD4	-0.607	0.007533331
213127_s_at	MED8	-0.607	0.007617926
224962_at	C9orf69	-0.606	0.007662713
202732_at	PKIG	-0.606	0.007665385
202012_s_at	EXT2	-0.606	0.00771185
213485_s_at	ABCC10	-0.606	0.007725818
208818_s_at	COMT	-0.605	0.007818733
218363_at	EXD2	-0.604	0.00792625
211843_x_at	CYP3A7-CYP3A51P	-0.604	0.007965802
201703_s_at	PPP1R10	-0.603	0.008031603
210042_s_at	CTSZ	-0.603	0.008072052
218260_at	DDA1	-0.603	0.008079631
218996_at	TFPT	-0.603	0.008089358
225524_at	ANTXR2	-0.603	0.008109669
220056_at	IL22RA1	-0.602	0.008145106
213512_at	C14orf79	-0.602	0.008239059
201460_at	MAPKAPK2	-0.602	0.008249302
213361_at	TDRD7	-0.602	0.008259499
212400_at	FAM102A	-0.601	0.00827574
217716_s_at	SEC61A1	-0.601	0.008287879
48106_at	SLC48A1	-0.601	0.008405074
38069_at	CLCN7	-0.6	0.008452404
221510_s_at	GLS	-0.6	0.008470399
204647_at	HOMER3	-0.6	0.008512761
224919_at	MRPS6	-0.599	0.008554428
210264_at	GPR35	-0.599	0.00855686
231806_s_at	STK36	-0.598	0.008790212
209332_s_at	MAX	-0.597	0.008909534
203118_at	PCSK7	-0.596	0.009053733
223023_at	BET1L	-0.596	0.009054295
210946_at	PLPP1	-0.596	0.009085772
203935_at	ACVR1	-0.596	0.009099157
228315_at	ZMAT3	-0.596	0.009102672
226264_at	SUSD1	-0.596	0.009111537
223141_at	UCK1	-0.595	0.009123445
235033_at	NPEPL1	-0.595	0.00918096
205490_x_at	GJB3	-0.595	0.009222139

DOWNREGULATED IN COLLAGEN VS MATRIGEL			
#H:probeset	**HUGO**	**R-value**	**p-value**
220572_at	LOC100506282	0.608	0.007383116
229538_s_at	IQGAP3	0.608	0.00739048
240239_at	ZNF566	0.608	0.007433802
211721_s_at	ZNF551	0.608	0.007449195
214710_s_at	CCNB1	0.608	0.007453283
202174_s_at	PCM1	0.607	0.007513467
240685_at	LINC01095	0.607	0.007545181
1561990_at	LOC157931	0.607	0.007547816
1566968_at	SPRY4-IT1	0.607	0.007548867
223716_s_at	ZRANB2	0.607	0.007601785
204492_at	ARHGAP11A	0.606	0.007652354
219497_s_at	BCL11A	0.606	0.007669969
210052_s_at	TPX2	0.606	0.007688593
231603_at	RNASE11	0.605	0.007790683
229420_at	SNORD4A	0.604	0.00794753
211987_at	TOP2B	0.604	0.007948172
212964_at	HIC2	0.604	0.007953052
208564_at	KCNA2	0.604	0.007978405
237475_x_at	CCDC152	0.603	0.008024505
36553_at	ASMTL	0.603	0.008067982
204639_at	ADA	0.603	0.008072102
218478_s_at	ZCCHC8	0.603	0.00811505
239355_at	GMCL1	0.601	0.008335338
201413_at	HSD17B4	0.601	0.008337952
223463_at	RAB23	0.601	0.00838289
219494_at	RAD54B	0.6	0.008470447
231872_at	LRRCC1	0.6	0.008505383
1563638_at	TVP23A	0.6	0.008510863
201699_at	PSMC6	0.6	0.008548708
1561691_at	LINC00326	0.599	0.008576005
203253_s_at	PPIP5K2	0.599	0.008600448
228571_at	RBAK	0.599	0.008629277
235698_at	ZFP90	0.598	0.008699119
230941_at	LINC01125	0.598	0.008748363
223035_s_at	FARSB	0.598	0.008794669
235387_at	GSTCD	0.597	0.008960411
210300_at	REM1	0.596	0.008982007
204228_at	PPIH	0.596	0.009007675
1564050_at	LOC100131347	0.596	0.009098789
209759_s_at	ECI1	0.596	0.009107332
237325_at	DRICH1	0.595	0.009129134
204987_at	ITIH2	0.595	0.009174291
1553934_at	LINC00305	0.595	0.00923873
233516_s_at	SPAG17	0.594	0.009316125
242301_at	CBLN2	0.594	0.009353009
242195_x_at	NUMBL	0.594	0.009375046
203375_s_at	TPP2	0.593	0.00947681
202396_at	TCERG1	0.593	0.009513854
1556460_a_at	ARHGAP22-IT1	0.592	0.009606635

Supplementary Table 1. Continued

UPREGULATED IN COLLAGEN VS MATRIGEL			
#H:probeset	**HUGO**	**R-value**	**p-value**
203964_at	NMI	-0.595	0.009239939
217903_at	STRN4	-0.595	0.009260264
225874_at	UBALD1	-0.594	0.009311976
204153_s_at	MFNG	-0.594	0.009323473
221504_s_at	ATP6V1H	-0.594	0.009326899
212312_at	BCL2L1	-0.594	0.009346792
203266_s_at	MAP2K4	-0.594	0.009389351
40255_at	DDX28	-0.594	0.009392451
235900_at	SPNS3	-0.593	0.009512945
219052_at	HPS6	-0.593	0.009520209
218464_s_at	FAM222B	-0.593	0.009522524
227882_at	FKRP	-0.593	0.009553572
210538_s_at	BIRC3	-0.592	0.009620232
203238_s_at	NOTCH3	-0.592	0.009669441
236269_at	ZNF628	-0.591	0.009747215
202767_at	ACP2	-0.591	0.009750778
208926_at	NEU1	-0.591	0.00975126
215807_s_at	PLXNB1	-0.59	0.009924647
200919_at	PHC2	-0.59	0.009930317

DOWNREGULATED IN COLLAGEN VS MATRIGEL			
#H:probeset	**HUGO**	**R-value**	**p-value**
228959_at	PDK3	0.592	0.009706732
215690_x_at	GPAA1	0.592	0.009707486
242360_at	LDB2	0.591	0.009722689
203621_at	NDUFB5	0.591	0.009744777
203062_s_at	MDC1	0.591	0.009753498
240185_at	LOC100147773	0.591	0.009757682
242966_x_at	RFX2	0.591	0.009771802
235217_at	LINC01004	0.591	0.009783213
226327_at	ZNF507	0.591	0.00986252
213097_s_at	DNAJC2	0.59	0.009945061

Supplementary Table 2. Luminex assay results.
Concentration of CXCL1 and CXCL8 in the medium from organoid lines TOR8, TOR9 and TOR10 after three and seven days of culturing in either BME or collagen-I matrix.

	GRO-1 alpha (CXCL1), pg/ml			
	day 3		**day 7**	
	BME	collagen-I	BME	collagen-I
TOR8	202.68	1812.27	295.28	3991.08
TOR9	453.97	5968.55	586.62	56495.49
TOR10	81.91	267.06	321.83	1168.83

	IL-8 (CXCL8), pg/ml			
	day 3		**day 7**	
	BME	collagen-I	BME	collagen-I
TOR8	229.45	194.04	229.86	230.26
TOR9	287.45	1013.89	288.42	3222.79
TOR10	211.19	198.17	286.16	386.88

Supplementary Table 3. Kinases correlated with CMS4 signature genes.
List of kinases whose expression is associated with CMS4 gene expression in two independent datasets (GSE39582 15 n=566, and TCGA16 n=276); Venn diagram showing overlap between the results from the two datasets; list of 55 kinases that are associated with CMS4 in both datasets; list of 22 tyrosine kinases from the list of 55.

CIT566	R
DDR2	0.929
AXL	0.86
AKT3	0.835
PDGFRB	0.823
FGFR1	0.816
PKD2	0.808
NUAK1	0.804
LATS2	0.745
TIE1	0.737
EPHA3	0.659
MAP3K3	0.656
ILK	0.63
FYN	0.595
HCK	0.594
PDGFRA	0.584
ROR2	0.567
LRRK2	0.558
KDR	0.534
TGFBR1	0.526
FGR	0.517
FLT1	0.496
BMPR2	0.485
JAK3	0.477
BTK	0.453
SNRK	0.436
ROR1	0.434
PIM1	0.403
FES	0.401
OSR1	0.384
DAPK1	0.382
PLK2	0.361
SPEG	0.351
ULK2	0.347
TRIO	0.347
IRAK3	0.34
HIPK3	0.336
ITK	0.333
TTBK2	0.322
AAK1	0.316
NEK7	0.312
FER	0.312
DYRK3	0.306
MAP3K8	0.302
MAPKAPK2	0.294
KIT	0.288
TGFBR2	0.284

TCGA286	R
PDGFRB	0.941
DDR2	0.932
AKT3	0.919
AXL	0.897
PKD2	0.877
TIE1	0.873
FGFR1	0.867
NUAK1	0.831
FLT4	0.827
EPHA3	0.791
MAP3K3	0.79
PDGFRA	0.757
FGR	0.744
ROR2	0.741
KDR	0.728
LRRK2	0.724
HCK	0.721
BTK	0.716
FES	0.716
LATS2	0.715
CAMK1G	0.71
FLT1	0.705
SPEG	0.653
TGFBR1	0.636
BMPR1B	0.63
BMPR2	0.626
WNK3	0.624
CDKL5	0.608
ROR1	0.605
ILK	0.604
IRAK3	0.602
SNRK	0.602
TTBK2	0.602
PAK3	0.581
JAK3	0.578
BRSK1	0.569
FYN	0.569
CAMK2A	0.567
HIPK3	0.551
DYRK3	0.532
ALK	0.527
MAST4	0.519
FLT3	0.512
EPHA5	0.511
CAMK4	0.508
ITK	0.5

CIT566	R
EPHA7	0.282
ZAK	0.279
NEK9	0.274
PLK3	0.272
MARK4	0.264
PKN1	0.256
BMPR1B	0.255
PINK1	0.25
MAST4	0.244
ULK1	0.242
ROCK1	0.236
NEK1	0.231
RNASEL	0.224
JAK1	0.22
MAP3K6	0.218
PKD1	0.216

TCGA286	R
EPHB6	0.491
NEK1	0.484
TRIO	0.475
BMX	0.473
EPHA7	0.452
ROCK1	0.451
EPHA6	0.447
GCK	0.447
KIT	0.44
PHKG1	0.432
PKD1	0.427
LATS1	0.42
TGFBR2	0.414
HIPK4	0.412
OSR1	0.404
MUSK	0.402
FER	0.399
MAP3K2	0.399
NEK7	0.398
RET	0.387
DAPK1	0.386
JAK1	0.381
PIM1	0.375
IGF1R	0.371
DAPK3	0.369
NEK9	0.367
BLK	0.363
ATM	0.361
AAK1	0.356
WNK1	0.355
NRBP1	0.35
ULK1	0.349
PLK2	0.348
ZAP70	0.348
EPHA4	0.334
PIM2	0.325
MAP3K1	0.313
MYO3A	0.311
TAF1L	0.308
ULK2	0.305
MARK4	0.304
PIK3R4	0.301
MAP3K8	0.3

CIT566	TCGA286
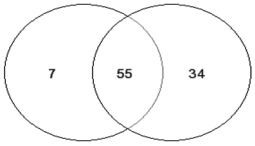	
overlap (55 kinases)	**overlap (22 tyrosine kinases)**
AAK1	**AXL**
AKT3	**BTK**
AXL	**DDR2**
BMPR1B	**EPHA3**
BMPR2	**EPHA7**
BTK	**FER**
DAPK1	**FES**
DDR2	**FGFR1**
DYRK3	**FGR**
EPHA3	**FLT1**
EPHA7	**FYN**
FER	**HCK**
FES	**ITK**
FGFR1	**JAK1**
FGR	**JAK3**
FLT1	**KDR**
FYN	**KIT**
HCK	**PDGFRA**
HIPK3	**PDGFRB**
ILK	**ROR1**
IRAK3	**ROR2**
ITK	**TIE1**
JAK1	
JAK3	
KDR	
KIT	
LATS2	
LRRK2	

CIT566	TCGA286
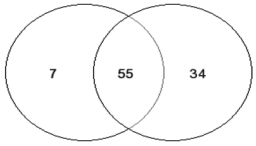	
overlap (55 kinases)	**overlap (22 tyrosine kinases)**
MAP3K3	
MAP3K8	
MARK4	
MAST4	
NEK1	
NEK7	
NEK9	
NUAK1	
OSR1	
PDGFRA	
PDGFRB	
PIM1	
PKD1	
PKD2	
PLK2	
ROCK1	
ROR1	
ROR2	
SNRK	
SPEG	
TGFBR1	
TGFBR2	
TIE1	
TRIO	
TTBK2	
ULK1	
ULK2	

Supplementary Table 4. Affinity of 72 kinase inhibitors for 20 kinases from the 22TK panel, based on results from Huang et al.[18]

	# targets		selectivity score	*K*d for CMS4-associated tyrosine kinases								
	all	<300	σ (3 uM)	KIT	PDGFRA	PDGFRB	FLT1	DDR2	KDR	AXL	TIE1	FGR
Foretinib	18	17	0.440	2.5	4.5	0.96	3.8	3.6	12	0.093	0.79	40
AST-487	19	12	0.492	5.4	27	8.1	86	11	200	570	0.29	190
PD-173955	17	11	0.345	1.8	5.6	1.4	23	12	690		1200	2.4
JNJ-28312141	19	11	0.389	3.6	27	28	53	100	460	5.3		220
Dasatinib	13	9	0.267	0.81	0.47	0.63	5000	3.2	2900			0.5
Cediranib	15	8	0.163	0.38	0.41	0.32	0.74	48	1.1	490	290	1100
SKI-606	15	8	0.425	420	5100	200		140		52	2900	6.3
Ki-20227	11	7	0.135	0.69	0.49	0.29	130	88	18	140		1800
ABT-869	10	7	0.184	2	4.2	1.9	7.5	3800	8.1	340	110	
CHIR-258/TKI-258	14	7	0.360	7.5	54	3.8	69	8600	68	3800	4000	190
Sorafenib	15	7	0.168	28	62	37	31	6.6	59	4500	68	7800
AG-013736	12	6	0.197	3.2	0.51	0.57	5.8	5300	5.9	420	97	1800
Pazopanib	14	6	0.215	2.8	4.9	2	14	98	14		700	1600
BMS-540215	9	6	0.086	36	11	50	10		5		1100	
Vandetanib	15	6	0.236	260	230	88	260	320	820	250	1500	270
AC220	9	5	0.075	4.8	11	7.7	41	1100	87		3200	
AB-1010	8	5	0.062	8.1	25	8.4		26				640
AMG-706	10	5	0.078	3.7	10	9.1	12		26			6900
PTK-787	5	5	0.031	5.1	96	25	9.6		62			
Nilotinib	9	5	0.124	29	180	73		33			1000	320
PP-242	15	5	0.435	360	220	78	1200	6100	1200	1200		160
VX-680/MK-0457	19	5	0.347	240	1600	310	100	230	2000	210	270	790
MLN-518	6	4	0.057	2.7	2.4	4.5	3100	120		6300		
Imatinib	6	4	0.057	13	31	14		15				2400
AZD-1152HQPA	10	4	0.114	17	38	41	110	6600	500	390	350	
PLX-4720	11	4	0.140	180	190	200	1900	4100	2100			62
Crizotinib	13	4	0.321				2300			7.8	110	670
PKC-412	14	3	0.430	220	380	110	450		3200	620	1400	730
CHIR-265/RAF-265	11	3	0.117	200	1100	240	800	960	1300		150	
BIRB-796	10	3	0.137	170	1200	1100	410	33	3900		8.3	
CP-690550	3	2	0.062									
GSK-1838705A	4	2	0.137							300		
HKI-272	8	2	0.181							190	390	1900
INCB18424	3	2	0.257									
PHA-665752	8	1	0.303	3200	2000	1900		7600		110	1200	1900
MLN-8054	11	1	0.098				1000			440	1600	220
Erlotinib	12	0	0.181	1700	1800	1400	4400		5700	4000	850	1100
LY-317615	4	0	0.132			3300				3300		
CI-1033	13	0	0.161	7800	5200	7500	7500			5700	2200	2800
VX-745	4	0	0.023		8800	8400						1300
Gefitinib	4	0	0.111							1800		2600
Flavopiridol	4	0	0.262		5900					3500		
BIBF-1120 (derivative)	19		0.518	5.7	16	15	63	42	2.9	12	2200	300
TG-101348	20		0.539	130	2700	45	4300	950	5200	160	700	82
SU-14813	19		0.542	0.68	1.1	0.29	4.7	9900	2.3	84	5700	390
Sunitinib	20		0.596	0.37	0.79	0.075	1.8	2900	1.5	9	3900	270

***K*d for CMS4-associated tyrosine kinases**											
FYN	HCK	BTK	EPHA3	EPHA7	FER	FES	FGFR1	ITK	JAK1	JAK3	
88	15	76	1	2.5	37	110	690	69			
50	880		80	1100	590	360	620	990	74	260	
4.9	3.3	220	7.6		3500	680	62		330	510	
340	3700	77	1600	6700	120	1100	3500	490	200	18	
0.79	0.35	1.4	0.093				3700			640	
1200	590	4300	3700	620			53				
11	3.4	4.8	5.8		360	330		1700		1200	
7100	440	7400									
			3500	110							
440	3300						150	530		410	
8400	8500		1900	5300			2800			7300	
							380	1200		3100	
2700	5700				2700	1400	990			6900	
	2700			1700			99				
360	360	1700	2000	2400			560				
			6500	3700							
140	690		2500								
2800	8600						6200		5200		
1600	390		110								
300	190	3200	390				570		300	86	
530	6200	4400	1500		4200	7400	550	350	5900	630	
3100											
	3900	1200									
2300	2700					3600	5300				
1300		7800	700	470	270	450		2000	330	200	
2100	720				1200		1600		670	12	
2100	1200				8600		4700				
			880	860			4300				
1100									1.6	0.16	
					9.3	52				4700	
6400	490	160			510	590				2000	
			6100						3.4	2	
										470	
1300	1500	4200	2100	1000	4400		2400				
	1800		2400	1400						700	
							4000			1700	
5300	4200	1600	2100					5600		630	
2100											
	4400		5500								
			3300							1600	
630	5300	310	8600		73	1200	92	210	2500	8.2	**unspecific (σ>0.5)**
38	2100	850	7100	6500	1100	530	280	490	18	74	
2600	2200	4000	2300	1500	34		1900	190	5900	580	
520	880	2100	2100	2400	1100	960	520	13	6000	1200	

Supplementary Table 4. Continued

	# targets		selectivity score	*Kd* for CMS4-associated tyrosine kinases								
	all	<300	σ (3 uM)	KIT	PDGFRA	PDGFRB	FLT1	DDR2	KDR	AXL	TIE1	FGR
R406	20		0.609	6.8	60	3.3	16	43	40	82	76	33
KW-2449	20		0.658	53	130	30	73	2100	120	180	300	440
TAE-684	20		0.671	110	840	150	550	4100	940	12	15	120
CEP-701	20		0.803	150	350	29	120	400	220	35	680	52
Staurosporine	20		0.878	19	10	1.8	150	42	220	6.8	65	17
GSK-461364A	2		0.101			2900					1400	
BIBW-2992	2		0.075							5300		
CI-1040	1		0.008			3100						
GSK-690693	1		0.145			3900						
SB-203580	1		0.093					5000				
BI-2536	1		0.143									
BMS-387032/ SNS-032	1		0.161				9900					
LY-333531	1		0.197									
A-674563	1		0.277									
AZD-6244/ARRY-886	0		0.005									
GW-2580	0		0.010									
SGX-523	0		0.010									
Lapatinib	0		0.016									
MLN-120B	0		0.021									
GDC-0879	0		0.042									
BMS-345541	0		0.044									
PI-103	0		0.057									
GDC-0941	0		0.080									
AT-7519	0		0.093									
R547	0		0.119									
TG-100-115	0		0.132									

Supplementary Table 4. Continued

***Kd* for CMS4-associated tyrosine kinases**											
FYN	HCK	BTK	EPHA3	EPHA7	FER	FES	FGFR1	ITK	JAK1	JAK3	
28	150	190	360	39	130	200	44	400	21	36	**unspecific (σ>0.5)**
660	4300	1000	810	390	1100	750	370	240	1200	39	
1400	410	23	4000	200	1.4	4.8	47	34	410	17	
84	270	66	160	260	28	370	310	290	8.8	2.3	
33	20	210	27	630	24	23	90	19	6.1	12	
	2200										**ineffective (<3 targets and all IC50 > 1000)**
						1900					
										1200	
										1500	

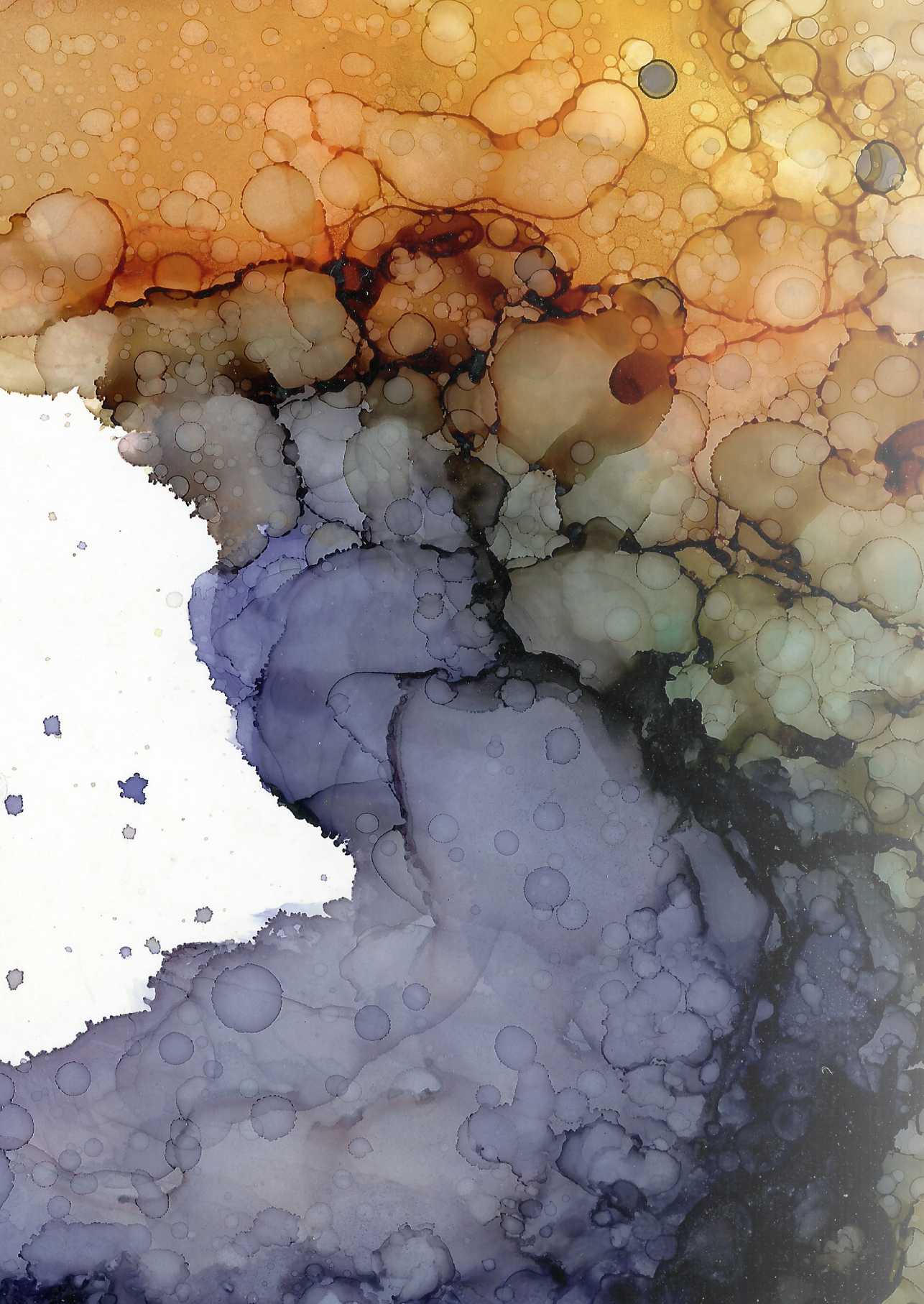

5

Histopathological and molecular classification of colorectal cancer and corresponding peritoneal metastases

Inge Ubink, Wijntje J. van Eden, Petur Snaebjornsson, Niels F. M. Kok, Joyce van Kuik, Wilhelmina M. U. van Grevenstein, Miangela M. Laclé, Joyce Sanders, Remond J. A. Fijneman, Sjoerd G. Elias, Inne H. M. Borel Rinkes, Arend G. J. Aalbers and Onno Kranenburg

British Journal of Surgery, 2018;105(2):e204-e211

ABSTRACT

Background

Patients with colorectal peritoneal carcinomatosis have a very poor prognosis. The recently developed consensus molecular subtype (CMS) classification of primary colorectal cancer categorizes tumors into four robust subtypes, which could guide subtype-targeted therapy. CMS4, also known as the mesenchymal subtype, has the greatest propensity to form distant metastases. CMS4 status and histopathological features of colorectal peritoneal carcinomatosis were investigated in this study.

Methods

Fresh-frozen tissue samples from primary colorectal cancer and paired peritoneal metastases from patients who underwent cytoreductive surgery combined with hyperthermic intraperitoneal chemotherapy were collected. Histopathological features were analysed, and a reverse transcriptase–quantitative PCR test was used to assess CMS4 status of all collected lesions.

Results

Colorectal peritoneal carcinomatosis was associated with adverse histopathological characteristics, including a high percentage of stroma in both primary tumors and metastases, and poor differentiation grade and high-grade tumor budding in primary tumors. Furthermore, CMS4 was significantly enriched in primary tumors with peritoneal metastases, compared with unselected stage I–IV tumors (60 per cent (12 of 20) *versus* 23 per cent; $P = 0.002$). The majority of peritoneal metastases (75 per cent, 21 of 28) were also classified as CMS4. Considerable intrapatient subtype heterogeneity was observed. Notably, 15 of 16 patients with paired tumors had at least one CMS4-positive tumor location.

Conclusion

Significant enrichment for CMS4 was observed in colorectal peritoneal carcinomatosis.

INTRODUCTION

The peritoneum is a common site of metastatic spread in patients with colorectal cancer. Approximately 5 per cent of all patients with colorectal cancer present with colorectal peritoneal carcinomatosis (CRPC) at first diagnosis, and another 5 per cent develop metachronous CRPC.[1] Patients with CRPC have a poor prognosis, with a median survival of only 6 months if left untreated.[2] Currently, cytoreductive surgery combined with hyperthermic intraperitoneal chemotherapy (CRS-HIPEC) is the only potentially curative treatment option, which may improve median overall survival to more than 30 months in selected patients.[3] Unfortunately, in spite of complete cytoreduction, more than half of the patients experience recurrent disease within 2 years.[3]

In addition to classical histopathological features, colorectal cancer can be stratified into four consensus molecular subtypes (CMS1-4), based on gene expression profiling. These subtypes have distinct biological characteristics and prognostic significance.[4] CMS4 has been associated with worse disease-free and overall survival than the other subtypes. CMS4 is characterized by high expression of genes reflecting epithelial-to-mesenchymal transition, transforming growth factor (TGF) β signaling and matrix remodeling.[4] CMS4 tumors often show a profound desmoplastic reaction with high stromal cell content.[5]

Several studies have suggested that the differences in underlying signaling pathways of CMSs account for heterogeneous responses to anticancer therapies. Irinotecan-based therapies appeared effective only in metastatic colorectal cancer with upregulated Wnt pathway signaling (CMS2).[6] Metastatic colorectal cancer of CMS4 seemed resistant to antiepidermal growth factor receptor therapy independent of *RAS*-mutation status.[7, 8] Patients with stage III CMS4 tumors did not benefit from systemic adjuvant oxaliplatin treatment.[9] which could be relevant in the context of CRPC since oxaliplatin is a commonly used intraperitoneal chemotherapeutic agent in HIPEC.[10]

Patients are currently selected for CRS-HIPEC based on clinical, rather than biological features.[11] The aim of this study was to investigate whether CRPC is enriched for stroma-rich and/or CMS4 variants of CRC. A better understanding of signaling pathways that drive CRPC would allow patient selection and repurposing of (targeted) therapies, which are required to further improve outcome for patients with CRPC. Molecular and histopathological classification of CRPC, as reported here, is a first step towards reaching this goal.

METHODS

Patients

This study was performed at The Netherlands Cancer Institute (NCI), Amsterdam and University Medical Centre Utrecht (UMCU), two tertiary oncological referral centers in the Netherlands. Patients who underwent CRS-HIPEC for CRPC, and from whom fresh-frozen tissue from both the primary tumor and one or more peritoneal metastases were sampled were eligible for the study. Patients were included if at least one of these samples met the quality criteria for reverse transcriptase–quantitative PCR (RT-qPCR) analysis. Clinical data were extracted from prospectively maintained CRS-HIPEC databases at both centers. The extent of CRPC was estimated by the Dutch 7 Region Count.[12] The study protocol was approved by the ethical committees of the Biobanks at NCI and UMCU (project codes CFMPB491 and 17-163, respectively). Collection, storage and use of patient derived tissue and data were performed either under informed consent, or in compliance with the Code for Proper Secondary Use of Human Tissue in The Netherlands.

Histopathology

All hematoxylin and eosin-stained slides derived from the primary tumors and corresponding peritoneal metastases were reassessed. TNM staging was done according to the UICC 5th edition.[13] Tumor type and differentiation were assessed according to the WHO Classification of Tumors of the Digestive System.[14] Primary tumors were classified as right-sided if they were located in the caecum, ascending or transverse colon; tumors in the descending colon, sigmoid and rectum were considered left-sided. Features evaluated without additional staining on hematoxylin and eosin-stained slides of both the primary tumors and peritoneal metastasis were: venous and lymphatic invasion (using conventional methodology, and included intra- and extramural invasion), amount of mucin (as a percentage of tumor area), number of signet ring cells (as a percentage of tumor cells), tumor border configuration[15], tumor budding[16], stroma-carcinoma percentage[17], and inflammatory score[18]. Microsatellite status was determined using immunohistochemistry for mismatch repair proteins. *KRAS* and *BRAF* mutational status were determined with Ion Torrent™ (PGM Cancer Hotspot panel v2Plus; Thermo Fisher Scientific; Waltham, Massachutes, USA) or MassARRAY Dx colon panel (Agena Bioscience, San Diego, California, USA).

RNA isolation and CMS4 RT-qPCR analysis

Tumor cell percentage of fresh-frozen tissue was evaluated (JS and MML); only samples that contained at least 10 per cent tumor cells were processed for RNA isolation. Frozen tissue samples were cut in 20-30 µm-thick cryosections with a cryostat and immersed in

RLT buffer (RNeasy® Mini Kit, Qiagen, Stockholm, Sweden) plus 1 per cent β-mercaptoethanol. RNA isolation, including on-column DNase digestion, was performed according to the manufacturer's instructions. RNA concentration was measured using a NanoDrop™ 2000 instrument (Thermo Fisher Scientific, Waltham, Massachusetts, USA). RNA integrity was assessed using an Agilent RNA 6000 Nano Kit and an Agilent 2100 Bioanalyzer® (Agilent Technologies, Santa Clara, California, USA); only samples with an RNA integrity number (RIN) over 6 were subjected to further analysis. The CMS4 RT-qPCR test was performed as described previously.[19] The test is based on the expression of four genes (*PDGFRA, PDGFRB, PDGFC* and *KIT*), and results in a CMS4 probability ranging from 0 to 1, with 0.5 as cut-off point for CMS4 positivity.

Statistical analysis

Fisher's exact test was used to characterize the relationship between categorical variables. Correlations between continuous variables were tested using linear regression analysis. Disease-free survival and overall survival rates from the date of CRS-HIPEC were determined by the Kaplan-Meier method. Estimates are reported with 95 per cent confidence intervals. All statistical tests were two-sided with a threshold for statistical significance of 5 per cent. SPSS® for Windows® version 21.0 (IBM, Armonk, New York, USA) was used for statistical analyses. Graphs were created with GraphPad Prism® version 7 (GraphPad Software, San Diego, California, USA).

RESULTS

Clinicopathological classification of CRPC

Twenty-four patients met the inclusion criteria. Baseline characteristics are shown in Table 1, and details on the CRS-HIPEC procedure and oncological outcomes in Supplementary Table 1. The majority of patients had synchronous CRPC, mostly without evidence of systemic metastases. Primary tumors were equally distributed between the left and right colon. Nearly all patients had regional lymph nodes metastases.

To further characterize the CRPC cohort, histopathological features of both primary tumors and metastases were examined (Table 2). Primary tumors frequently showed venous invasion, infiltrating growth at the invasive margin, and high-grade tumor budding. Furthermore, none of the included CRPC samples scored a high inflammatory score (Supplementary Table 2). Both primary tumors and peritoneal metastases often had a high stroma percentage, and there was a significant correlation between stroma percentage in paired primary tumors and metastases (Figure 1).

Table 1. Baseline characteristics.

	No. of patients*
Age (years)†	63 (39–72)
Sex ratio (M : F)	12 : 12
Primary tumor location	
Right colon‡	14
Left colon	10
pT category	
pT3	2
pT4a	18
pT4b	4
pN category	
pN0	1
pN1	11
pN2	12
Metastases	
Metachronous	2
Synchronous	22
Primary tumor histological subtype	
Adenocarcinoma	14
Mucinous adenocarcinoma	8
Signet ring cell carcinoma	2
Primary tumor differentiation grade	
Good/moderate	14
Poor	10
Site of metastatic disease	
PC only	20
PC + systemic	4
MMR status	
MMR proficient	21
MMR deficient	3
***KRAS* mutation status**	
Wild type	14
Mutant	10
***BRAF* mutation status**	
Wild type	18
Mutant	6

*Unless indicated otherwise; †values are median (range). ‡Includes two poorly differentiated appendiceal carcinomas. PC, peritoneal carcinomatosis; MMR, mismatch repair.

CMS4 assessment of primary tumors and peritoneal metastases

Of 59 identified fresh-frozen samples, 48 met the quality requirements for CMS4 RT-qPCR analysis (more than 10 per cent tumor cells and RIN over 6). Twenty primary cancers were analyzed with the diagnostic RT-qPCR test for CMS4, of which twelve were classified as CMS4 (60 (95 per cent confidence interval (CI) 39 to 78) per cent). In the original CMS publication[4], 23 per cent of non-selected primary stage I-IV tumors were classified as CMS4. Thus, CRPC is significantly enriched for CMS4 (P=0.002). Primary tumors in the present CRPC cohort were even more frequently CMS4 than the stage IV tumors in the original CMS publication, although not statistically significantly (60 per cent *versus* 40 per cent, P=0.096). Adenocarcinomas more often appeared CMS4 positive than primary tumors with mucinous histology (8 of 12 versus 2 of 6 respectively), but this was not statistically significant in this small cohort (P=0.181). The two primary signet cell carcinomas were both classified

Table 2. Histopathological characteristics.

	Primary tumors (*n* = 24)	**Peritoneal metastases** (*n* = 35)
Venous invasion		
No	14	34
Yes	10	1
Lymphatic invasion		
No	15	32
Yes	9	3
Tumor border configuration		
Pushing	4	17
Infiltrating	20	18
Stroma (% of surface area)		
≤ 50	5	21
> 50	19	14
Tumor budding score		
Bd1	4	18
Bd2	6	5
Bd3	14	12
Mucin (% of surface area)		
0	12	20
1–50	7	6
51–100	5	9
Signet ring cell (% of tumor cells)		
0	19	28
1–50	3	5
51–100	2	2
Inflammatory score		
0–2	18	31
3–6	6	4
7–12	0	0

as CMS4. CMS4 positivity was associated with poor tumor differentiation and higher inflammatory scores in the primary tumors (P=0.005 and P=0.042 respectively, Figure 2a,b)

The majority of peritoneal metastases (21 of 28; 75 (95 per cent CI 57 to 87) per cent) were also classified as CMS4. This is significantly higher than the incidence of mesenchymal-type liver metastases in two previously published studies (34 of 72 (47 per cent)[8], *P*=0.004 and 60 of 129 (47 per cent)[20], *P*=0.007). Figure 2c shows the CMS4 test results of all metastases, grouped by intraperitoneal location. In this small dataset, no clear relation between metastasis location and probability of being CMS4 was observed. For both primary tumors and metastatic lesions, the probability of CMS4 was not correlated with the stroma percentage (Supplementary Figure 1).

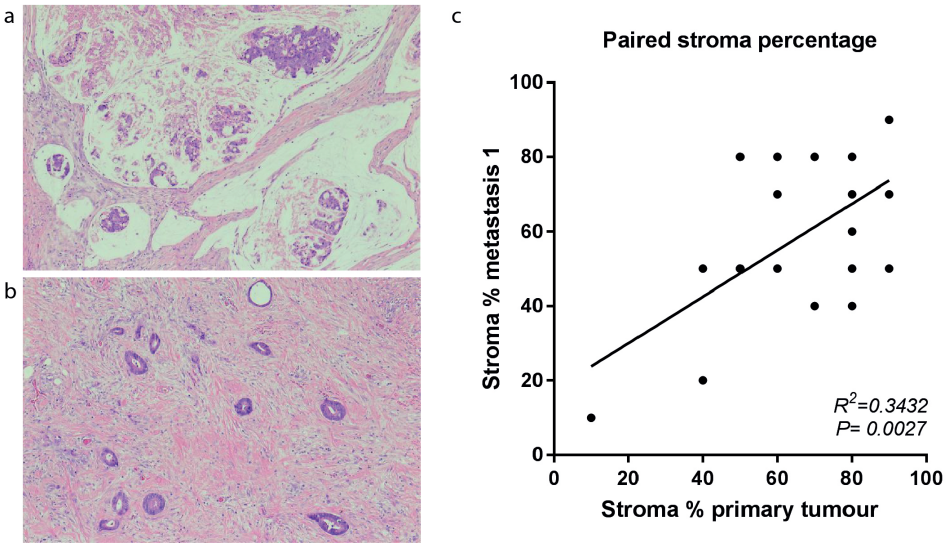

Figure 1. Stroma score in primary tumours and peritoneal metastases. (a,b) Representative micrographs of peritoneal metastases with a low stroma score (a, scored as 10 per cent) and a high stroma score (b, scored as 90 per cent) (haematoxylin and eosin stain, original magnification × 10). (c) Correlation between stroma score of primary tumours and corresponding peritoneal metastases (R^2 = 0.343, P = 0.003).

Intrapatient subtype heterogeneity

Good-quality paired samples from primary tumors and corresponding metastases were available from 16 patients. Remarkably, all patients, except for patient #21, had at least one CMS4-positive lesion (Figure 3). In eight patients, the CMS4 classification differed between the primary tumor and the metastases, indicating considerable intrapatient heterogeneity with respect to tumor CMS4 status. Notably, intrapatient heterogeneity was observed in all three patients who had more than one metastasis available for CMS4 testing.

DISCUSSION

In this study, histopathological features and CMS4 status were assessed in a cohort of patients who underwent CRS-HIPEC for CRPC. CMS4-postivity was observed in 60 per cent of primary tumors in the cohort (12 of 20), which is significantly higher than the reported incidence of CMS4 in unselected stage I-IV CRC[4]. CMS4 colorectal cancer has a higher propensity for relapse and distant metastases, and a worse overall survival.[4] Furthermore, the majority of primary tumors in this CRPC cohort (79 per cent, 19 of 24) were found to have a high stroma percentage. The carcinoma-stroma ratio has been

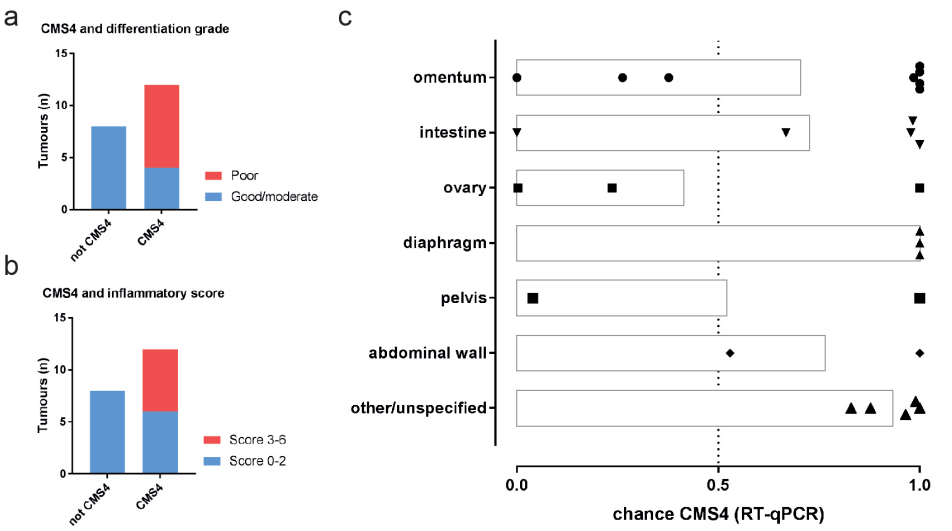

Figure 2. Consensus molecular subtype (CMS) 4 status in relation to histopathological features.
CMS4 in relation to (a) differentiation grade (P = 0.005, Fisher exact test), (b) inflammation (P = 0.142, Fisher exact test) and (c) the site of peritoneal metastases. In (c) RT–qPCR results for all 28 metastatic lesions are grouped according to site of metastasis; bars represent the mean probability of being CMS4 (0.5 or more classified as CMS4).

identified as an individual predictor for survival in CRC, with a high stroma score (over 50 per cent) related to poor prognosis.[17] In an analysis of 701 stage II-III cancers, 71 per cent of tumors were scored as stroma-low (50 per cent or less stroma)[17], which contrasts strongly with this CRPC cohort of predominantly stroma-high tumors.

Although CMS4 is characterized by high stromal content[4, 5], such a correlation was not found in the CRPC cohort studied here. There are several possible explanations. Although stroma percentage provides an estimate of the quantity of stroma within a tumor, it does not provide information on the abundance and types of cells within the stroma. Functional differences in cancer stroma may be more important determinants of aggressive tumor behavior than simply the percentage of tumor stroma.[21] The mesenchymal subtype is not solely determined by the stromal component, but tumor cell-intrinsic gene expression also contributes to the mesenchymal phenotype of the poor prognosis CRC subtype.[22, 23] Extensive infiltration with cancer-associated fibroblasts (CAFs) and tumor cell-intrinsic mesenchymal gene expression may be two distinct means of acquiring aggressive cancer behavior.

The primary tumors in this CRPC cohort frequently had histological features that have previously been associated with poor prognosis, including poor differentiation grade, mucinous histology, venous invasion, high-grade tumor budding, infiltrating tumor border

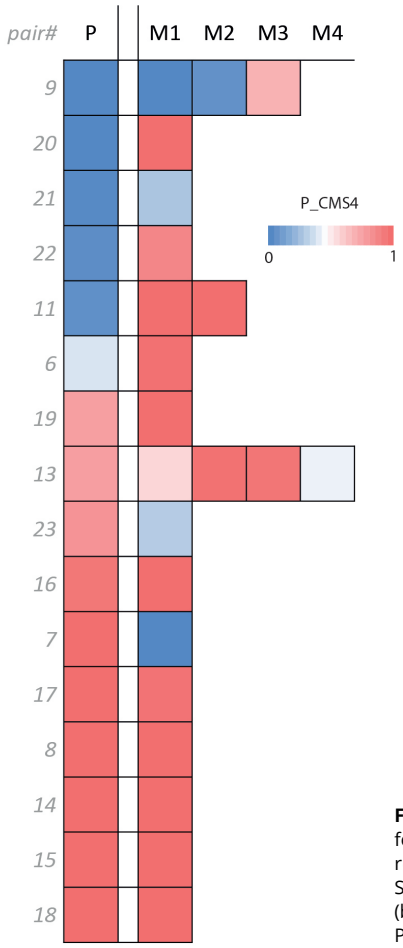

Figure 3. Intrapatient heterogeneity in CMS4 RT-qPCR test results for paired primary tumours and peritoneal metastases. The test results in a predicted probability of CMS4 ranging from 0 to 1. Samples with a probability below 0.5 are classified as not CMS4 (blue), and those with a probability of 0.5 or greater as CMS4 (red). P, primary; M1–4, metastatic lesions 1–4

configuration, and low inflammatory score [15, 16, 18, 24] Furthermore, one-quarter of the tumors had a *BRAF* mutation, which is higher than the reported incidence of *BRAF* mutations in metastatic CRC in literature (~10%[25]). Indeed, *BRAF* mutations have been associated with higher rates of peritoneal dissemination[25] and with a poor prognosis[26] in colorectal cancer.

Three-quarters of the peritoneal metastases analyzed in this study were also classified as CMS4. CMS4 is characterized by TGF-β signalling[4, 5], and TGF-β can stimulate transdifferentiation of peritoneal fibroblasts and mesothelial cells into activated myofibroblasts[27]. The interaction between tumor cells and fibroblasts is thought to be important in the establishment of peritoneal metastases.[28-30] The dependence of peritoneal metastases on TGF-β signaling could explain the enrichment of CMS4 that was observed in this cohort. Since no association was observed between the stroma percentage and probability of CMS4 in the peritoneal metastases,

further research into the type of reactive stroma in CMS4 and non-CMS4 metastases in relation to TGF-β pathway activation is needed.

Heterogeneity in CMS4 status between primary tumors and metastatic lesions was frequently observed. Considerable intratumor heterogeneity with respect to CMS4 status when analyzing multiple regions within a primary tumor was recently reported by this group.[19] Subtype heterogeneity between primary tumors and peritoneal metastases could thus be a consequence of intratumor heterogeneity. Alternatively, molecular classification of metastases could be influenced by the specific intra-abdominal location of the metastases, as gene expression in tumor cells is influenced by the tumor microenvironment.[22] Although the small cohort studied here provides insufficient data to draw firm conclusions, both CMS4-positive and -negative lesions were found at most metastatic sites, which does not support this hypothesis.

Currently, patients with CRPC are treated based on clinicopathological features, regardless of genetic alterations or molecular subtyping. CMS4 has been associated with a poorer response to anticancer drugs[4, 7, 9], although these findings need prospective validation. The observation that nearly all patients had at least one CMS4 positive tumor lesion could thus have clinical implications. Mitomycin C and oxaliplatin are the most frequently used chemotherapeutic agents in HIPEC. Retrospective comparisons between these two drugs are contradictory; one study favors MMC[10], while another shows clear benefit of oxaliplatin[31]. When given as adjuvant therapy in stage III CRC, oxaliplatin did not benefit patients with CMS4 cancers.[9] Given the enrichment of CMS4 in CRPC, and its potential resistance to oxaliplatin, prospective studies are required to study the benefit of oxaliplatin in the HIPEC procedure, in relation to CMS4 status.

This study is limited by the small sample size, and the findings deserve validation in a larger cohort. Since fresh-frozen samples were not routinely collected, no consecutive series of CRPC was available. The interest in paired samples of both primary tumors and peritoneal metastases resulted in predominant inclusion of synchronous CRPC, as primary cancer surgery in patients with metachronous CRPC was usually performed at another hospital. These factors may have resulted in considerable selection bias. This small series is insufficient to determine the relation between molecular subtype and outcome following HIPEC. Despite these limitations, the findings are an incentive to further explore molecular classification of CRPC. Combined with clinical and histological parameters, molecular classification could advance personalized treatment of peritoneal metastases.

Acknowledgements

The authors would like to acknowledge the NKI-AVL Core Facility Molecular Pathology & Biobanking for supplying NKI-AVL Biobank material. I.U. is supported by a grant from the Dutch Cancer Society (UU2014-6617).

REFERENCES

1. Segelman J, Granath F, Holm T, et al. Incidence, prevalence and risk factors for peritoneal carcinomatosis from colorectal cancer. *Br J Surg*. 2012;**99**(5):699-705.
2. Razenberg LG, Lemmens VE, Verwaal VJ, et al. Challenging the dogma of colorectal peritoneal metastases as an untreatable condition: Results of a population-based study. *Eur J Cancer*. 2016;**65**:113-20.
3. Kuijpers AM, Mirck B, Aalbers AG, et al. Cytoreduction and HIPEC in the Netherlands: nationwide long-term outcome following the Dutch protocol. *Ann Surg Oncol*. 2013;**20**(13):4224-30.
4. Guinney J, Dienstmann R, Wang X, et al. The consensus molecular subtypes of colorectal cancer. *Nat Med*. 2015;**21**(11):1350-6.
5. Calon A, Lonardo E, Berenguer-Llergo A, et al. Stromal gene expression defines poor-prognosis subtypes in colorectal cancer. *Nat Genet*. 2015;**47**(4):320-9.
6. Del Rio M, Mollevi C, Bibeau F, et al. Molecular subtypes of metastatic colorectal cancer are associated with patient response to irinotecan-based therapies. *Eur J Cancer*. 2017;**76**:68-75.
7. Trinh A, Trumpi K, De Sousa EMF, et al. Practical and Robust Identification of Molecular Subtypes in Colorectal Cancer by Immunohistochemistry. *Clinical cancer research : an official journal of the American Association for Cancer Research*. 2016.
8. De Sousa EMF, Wang X, Jansen M, et al. Poor-prognosis colon cancer is defined by a molecularly distinct subtype and develops from serrated precursor lesions. *Nat Med*. 2013;**19**(5):614-8.
9. Song N, Pogue-Geile KL, Gavin PG, et al. Clinical Outcome From Oxaliplatin Treatment in Stage II/III Colon Cancer According to Intrinsic Subtypes: Secondary Analysis of NSABP C-07/NRG Oncology Randomized Clinical Trial. *JAMA Oncol*. 2016;**2**(9):1162-9.
10. Prada-Villaverde A, Esquivel J, Lowy AM, et al. The American Society of Peritoneal Surface Malignancies evaluation of HIPEC with Mitomycin C versus Oxaliplatin in 539 patients with colon cancer undergoing a complete cytoreductive surgery. *J Surg Oncol*. 2014;**110**(7):779-85.
11. Simkens GA, Rovers KP, Nienhuijs SW, et al. Patient selection for cytoreductive surgery and HIPEC for the treatment of peritoneal metastases from colorectal cancer. *Cancer Manag Res*. 2017;**9**:259-66.
12. Verwaal VJ, van Ruth S, de Bree E, et al. Randomized trial of cytoreduction and hyperthermic intraperitoneal chemotherapy versus systemic chemotherapy and palliative surgery in patients with peritoneal carcinomatosis of colorectal cancer. *Journal of clinical oncology : official journal of the American Society of Clinical Oncology*. 2003;**21**(20):3737-43.
13. AJCC Cancer Staging Manual. 5th ed. Philidelphia: J.B. Lippincott; 1997.
14. WHO Classification of Tumours of the Digestive System. Lyon: International Agency for Research on Cancer (IARC); 2010.
15. Compton C, Fenoglio-Preiser CM, Pettigrew N, et al. American Joint Committee on Cancer Prognostic Factors Consensus Conference: Colorectal Working Group. *Cancer*. 2000;**88**(7):1739-57.
16. Lugli A, Kirsch R, Ajioka Y, et al. Recommendations for reporting tumor budding in colorectal cancer based on the International Tumor Budding Consensus Conference (ITBCC) 2016. *Mod Pathol*. 2017.
17. Huijbers A, Tollenaar RA, v Pelt GW, et al. The proportion of tumor-stroma as a strong prognosticator for stage II and III colon cancer patients: validation in the VICTOR trial. *Ann Oncol*. 2013;**24**(1):179-85.
18. Ogino S, Nosho K, Irahara N, et al. Lymphocytic reaction to colorectal cancer is associated with longer survival, independent of lymph node count, microsatellite instability, and CpG island methylator phenotype. *Clin Cancer Res*. 2009;**15**(20):6412-20.
19. Ubink I, Elias SG, Moelans CB, et al. A Novel Diagnostic Tool for Selecting Patients With Mesenchymal-Type Colon Cancer Reveals Intratumor Subtype Heterogeneity. *J Natl Cancer Inst*. 2017;**109**(8).
20. Trumpi K, Ubink I, Trinh A, et al. Neoadjuvant chemotherapy affects molecular classification of colorectal tumors. *Oncogenesis*. 2017;**6**(7):e357.
21. Berdiel-Acer M, Sanz-Pamplona R, Calon A, et al. Differences between CAFs and their paired NCF from adjacent colonic mucosa reveal functional heterogeneity of CAFs, providing prognostic information. *Mol Oncol*. 2014;**8**(7):1290-305.
22. Vellinga TT, den Uil S, Rinkes IH, et al. Collagen-rich stroma in aggressive colon tumors induces mesenchymal gene expression and tumor cell invasion. *Oncogene*. 2016;**35**(40):5263-71.
23. Isella C, Brundu F, Bellomo SE, et al. Selective analysis of cancer-cell intrinsic transcriptional traits defines novel clinically relevant subtypes of colorectal cancer. *Nat Commun*. 2017;**8**:15107.

24. Massalou D, Benizri E, Chevallier A, et al. Peritoneal carcinomatosis of colorectal cancer: novel clinical and molecular outcomes. *Am J Surg*. 2017;**213**(2):377-87.
25. Franko J, Shi Q, Meyers JP, et al. Prognosis of patients with peritoneal metastatic colorectal cancer given systemic therapy: an analysis of individual patient data from prospective randomised trials from the Analysis and Research in Cancers of the Digestive System (ARCAD) database. *Lancet Oncol*. 2016;**17**(12):1709-19.
26. Richman SD, Seymour MT, Chambers P, et al. KRAS and BRAF mutations in advanced colorectal cancer are associated with poor prognosis but do not preclude benefit from oxaliplatin or irinotecan: results from the MRC FOCUS trial. *J Clin Oncol*. 2009;**27**(35):5931-7.
27. Yao Q, Qu X, Yang Q, et al. CLIC4 mediates TGF-beta1-induced fibroblast-to-myofibroblast transdifferentiation in ovarian cancer. *Oncol Rep*. 2009;**22**(3):541-8.
28. Kojima M, Higuchi Y, Yokota M, et al. Human subperitoneal fibroblast and cancer cell interaction creates microenvironment that enhances tumor progression and metastasis. *PLoS One*. 2014;**9**(2):e88018.
29. Cai J, Tang H, Xu L, et al. Fibroblasts in omentum activated by tumor cells promote ovarian cancer growth, adhesion and invasiveness. *Carcinogenesis*. 2012;**33**(1):20-9.
30. Kenny HA, Krausz T, Yamada SD, et al. Use of a novel 3D culture model to elucidate the role of mesothelial cells, fibroblasts and extra-cellular matrices on adhesion and invasion of ovarian cancer cells to the omentum. *Int J Cancer*. 2007;**121**(7):1463-72.
31. Leung V, Huo YR, Liauw W, et al. Oxaliplatin versus Mitomycin C for HIPEC in colorectal cancer peritoneal carcinomatosis. *Eur J Surg Oncol*. 2017;**43**(1):144-9.

SUPPLEMENTARY FIGURES AND TABLES

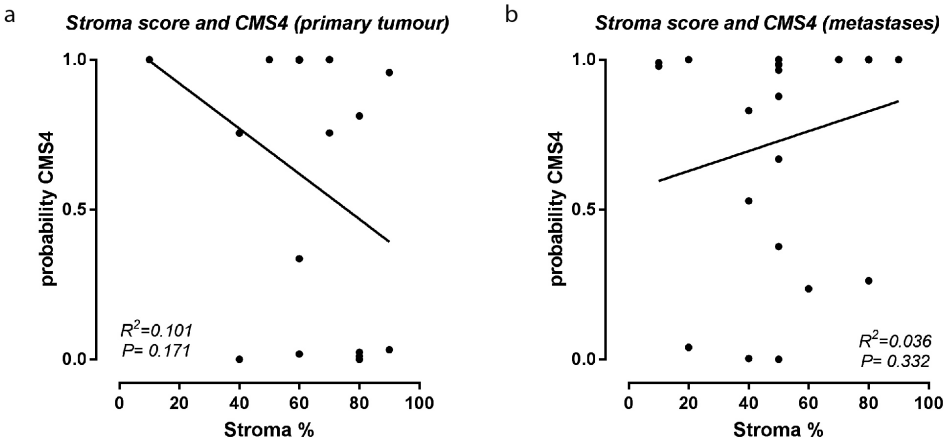

Supplementary Figure 1. Correlation between CMS4 probability and stroma percentage in individual lesions. (a) primary tumors (b) peritoneal metastases.

Supplementary Table 1. Peri-operative characteristics.

ASA classification	
ASA 1, n (%)	10 (42)
ASA 2, n (%)	14 (58)
Co-morbidity	
No, n (%)	13 (54)
Yes, n (%)	11 (46)
Region count, median [range][a]	5 [2-7]
Completeness of surgery	
R1, n (%)	20 (83)
R2a/b, n (%)	2 (8)
Open-close, n (%)	1 (4)
Not reported, n (%)	1 (4)
HIPEC	
Mitomycin-C, n (%)	14 (58)
Oxaliplatin, n (%)	9 (38)
Not performed, n (%)	1 (4)
Systemic chemotherapy	
No chemotherapy, n (%)	5 (21)
Neoadjuvant chemotherapy, n (%)	4 (17)
Peri-operative chemotherapy, n (%)	2 (8)
Adjuvant chemotherapy, n (%)	13 (54)

Supplementary Table 1. Continued

Disease-free survival (mo), median [95% CI]	9.4 [5.6-13.3]
Recurrence location[b]	
Local (PC), n (%)	9 (47)
Systemic, n (%)	2 (11)
Local + systemic, n (%)	8 (42)
Treatment recurrence[b]	
No treatment, n (%)	6 (32)
Chemotherapy, n (%)	10 (53)
CRS-HIPEC, n (%)	1 (5)
Resection, n (%)	1 (5)
Radiotherapy, n (%)	1 (5)
Overall survival (mo), median [95% CI]	21.2 [12.8-29.6]

Supplementary Table 2. Individual components of the inflammatory score.

	Primary tumours (n = 24)	**Peritoneal metastases (n = 35)**
Intra-epithelial lymphocytes		
Absent, n (%)	23 (96)	32 (91)
Mild, n (%)	0 (0)	3 (9)
Moderate, n (%)	1 (4)	0 (0)
Prominent, n (%)	0 (0)	0 (0)
Periglandular lymphocytes		
Absent, n (%)	8 (33)	14 (40)
Mild, n (%)	14 (58)	18 (51)
Moderate, n (%)	2 (8)	3 (9)
Prominent, n (%)	0 (0)	0 (0)
Tumor border lymphocytic infiltrate		
Absent, n (%)	15 (63)	25 (71)
Mild, n (%)	9 (38)	9 (26)
Moderate, n (%)	0 (0)	1 (3)
Prominent, n (%)	0 (0)	0 (0)
Tertiary lymphoid structures		
Absent, n (%)	17 (71)	31 (89)
Mild, n (%)	6 (25)	4 (11)
Moderate, n (%)	1 (4)	0 (0)
Prominent, n (%)	0 (0)	0 (0)

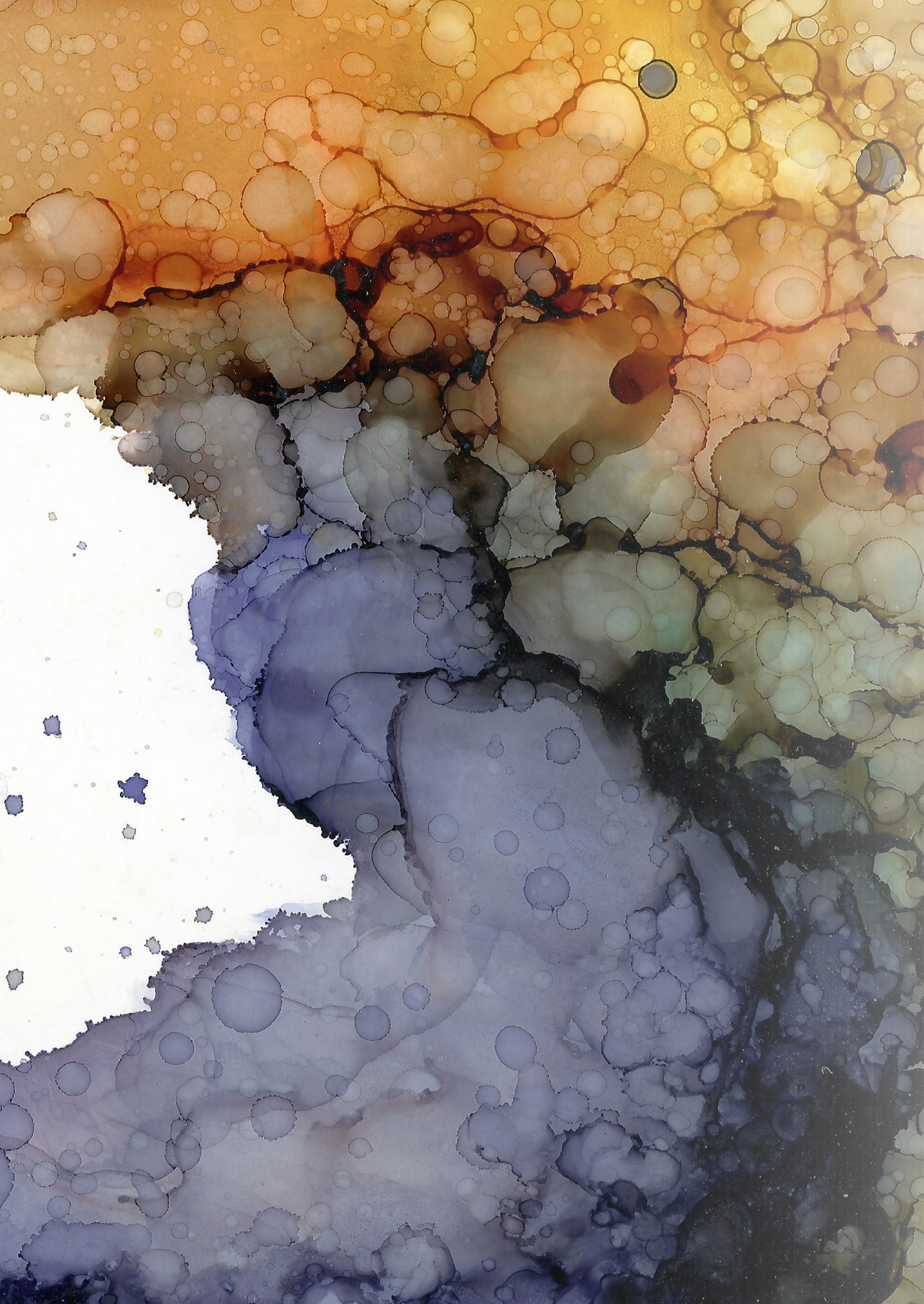

6

Organoids from colorectal peritoneal metastases as a platform for improving hyperthermic intraperitoneal chemotherapy

Inge Ubink, Ana C.F. Bolhaqueiro, Sjoerd G. Elias, Daniëlle A.E. Raats, Alexander Constantinides, Niek A. Peters, Emma C.E. Wassenaar, Ignace H.J.T. de Hingh, Koen P. Rovers, Wilhelmina M.U. van Grevenstein, Miangela M. Laclé, Geert J.P.L. Kops, Inne H.M. Borel Rinkes and Onno Kranenburg

British Journal of Surgery 2019;106(10):1404-1414

ABSTRACT

Background

Patients with peritoneal metastases from colorectal cancer have a poor prognosis. If the intraperitoneal tumor load is limited, patients may be eligible for cytoreductive surgery followed by hyperthermic intraperitoneal chemotherapy (HIPEC). This treatment has improved overall survival, but recurrence rates are high. The aim of this study was to create a preclinical platform for the development of more effective intraperitoneal chemotherapy strategies.

Methods

Using organoid technology, five tumor cultures were generated from malignant ascites and resected peritoneal metastases These were used in an in vitro HIPEC model to assess sensitivity to mitomycin C (MMC) and oxaliplatin, the drugs used most commonly in HIPEC. The model was also used to test a rational combination treatment involving MMC and inhibitors of the checkpoint kinase ATR.

Results

MMC was more effective in eliminating peritoneal metastasis-derived organoids than oxaliplatin at clinically relevant concentrations. However, the drug concentrations required to eliminate 50 per cent of the tumor cells (IC50) were higher than the median clinical dose in two of five organoid lines for MMC, and all five lines for oxaliplatin, indicating a general resistance to monotherapy. ATR inhibition increased the sensitivity of all peritoneal metastasis-derived organoids to MMC, as the IC50 decreased 2.6–12.4-fold to well below concentrations commonly attained in clinical practice. Live-cell imaging and flow cytometric analysis showed that ATR inhibition did not release cells from MMC-induced cell cycle arrest, but caused increased replication stress and accelerated cell death.

Conclusion: Peritoneal metastasis-derived organoids can be used to evaluate existing HIPEC regimens on an individual-patient level and for development of more effective treatment strategies.

INTRODUCTION

Peritoneal metastases (PMs) develop in approximately 10 per cent of patients with colorectal cancer.[1] These patients generally have a very poor prognosis, with a median survival of only 6–9 months without treatment.[2] For selected patients with limited PMs and treatable extraperitoneal disease, cytoreductive surgery (CRS) combined with hyperthermic intraperitoneal chemotherapy (HIPEC) is a potentially curative localized treatment option.[3] The goal is to remove all macroscopic PMs surgically, while eliminating any residual microscopic disease by HIPEC. CRS–HIPEC has significantly improved median overall survival of patients with PMs from colorectal cancer to 36 months.[4-7]

Retrospective comparisons between oxaliplatin and mitomycin C (MMC), the two drugs most commonly used in HIPEC for PMs from colorectal cancer, generated contradictory results.[7-10] As a consequence, there is currently no consensus on the choice of chemotherapy, the dose administered or the duration of perfusion.[3] Regardless of the chemotherapy drug used in HIPEC, recurrence rates after CRS–HIPEC are high and more than half of patients experience disease recurrence within 2 years.[7, 11, 12] The added value of HIPEC after CRS has recently been questioned in light of results from the Prodige 7 RCT[12], which showed that adding oxaliplatin-based HIPEC to CRS provided no survival benefit. However, clinical proof that HIPEC after CRS can effectively target minimal residual disease in the peritoneum has been provided by a large phase III study in ovarian cancer.[13] Rather than omitting HIPEC from the treatment of PMs from colorectal cancer, efforts should be made to improve the efficacy of intraperitoneal chemotherapy.

Simply increasing the HIPEC dose is not feasible, as a higher perfusate concentration leads to a higher plasma concentration, which has been associated with increased toxicity.[14] A rational combination treatment of MMC with inhibition of ataxia telangiectasia and Rad3-related protein kinase (ATR) could enhance HIPEC efficacy. ATR inhibitors are currently being tested in a number of clinical trials, either alone or in combination with chemotherapy.[15] MMC causes cytotoxicity mainly through formation of interstrand crosslinks.[16] This type of DNA damage activates ATR, which induces cell cycle arrest to allow DNA repair. Inhibition of ATR after exposure to MMC could lead to fatal collapse of replication forks and increased cell death.[17]

To evaluate current HIPEC agents and novel combination therapies, a representative *in vitro* model of colorectal PM is required. Tumor-derived organoids are ideally suited for this purpose, as they retain the genetic and phenotypic characteristics of the original cancers, and can accurately predict clinical therapeutic response *in vitro*.[18-20] The aim of this project was to create an organoid-based preclinical model of PM from colorectal cancer to study current HIPEC regimens and to test novel combination strategies that augment the efficacy of HIPEC.

METHODS

A detailed description of the methodology is provided as Supplementary materials and methods.

Tissue collection and organoid culture

Tissue samples from PMs were collected during cytoreductive surgery or diagnostic laparoscopy within biobanking protocol HUB-Cancer TcBio#12-09, which was approved by the medical ethics committee of the University Medical Centre Utrecht. Ascites was collected within the context of the CRC-PIPAC trial (NCT03246321) at the Catherina Hospital, Eindhoven. Before treatment with electrostatically precipitated pressurized intraperitoneal aerosol chemotherapy, 40 ml ascites was aspirated using a gastronasal tube and a syringe through one of the laparoscopic trocar openings.

Chemotherapy regimens and drug concentrations

Before undertaking drug screens on the PM-derived organoids, the concentrations of MMC and oxaliplatin that are commonly attained in the peritoneal cavity during HIPEC procedures were investigated. Data from 40 HIPEC procedures for PMs from colorectal cancer or pseudomyxoma peritonei carried out at the University Medical Centre Utrecht between January 2016 and July 2018 were collected. Perfusion volume, body surface area (BSA) and chemotherapy dose were extracted from intraoperative recordings of the perfusion pump system Performer HT® (RanD, Medolla, Italy). At University Medical Centre Utrecht, chemotherapy dose is determined by BSA, at 35 mg/m^2 for MMC and 460 mg/m^2 for oxaliplatin. The concentration of intraperitoneal chemotherapy further depends on the volume used for dialysis. During HIPEC, MMC is added to the total perfusion fluid in three separate doses. First, 50 per cent of the total dose is added, followed by 25 per cent after 30 and 60 min. This compensates for systemic uptake of MMC and results in a relatively stable perfusate concentration.[21] As a result, the maximum concentration reached in the perfusate is roughly equal to the starting concentration (50 per cent of the total dose divided by the total perfusate volume).

Subsequent drug screens were performed across a wide range of concentrations including the calculated clinical concentrations. MMC (S8146; Selleckchem, Munich, Germany) was dissolved in dimethylsulphoxide (DMSO) to a stock concentration of 60 mmol/l, and was further diluted in basal culture medium without niche factors to a concentration range of 0.4–300 μmol/l. Oxaliplatin (5 mg/ml solution; Fresenius Kabi, Bad Homburg, Germany) was diluted in 0.45 per cent sodium chloride/2.5 per cent glucose solution to preserve solubility in a physiological carrier solution[22], to a concentration range of 8.6 μmol/l to 6.29 mmol/l.

In an effort to improve MMC-based HIPEC, combination treatment of MMC with VE-821, an inhibitor of ATR, was assessed. The clinical derivative of VE-821 (VX-970) was also assessed for enhancement of response to MMC, to evaluate whether this rational combination strategy could be translated to the clinical setting. VE-821 (Sigma Aldrich, Saint Louis, Missouri, USA) and VX-970 (VE-822; Selleckchem) were dissolved in DMSO at a stock concentration of 10 mmol/l, and added to basal growth medium at the concentrations indicated.

Hyperthermic intraperitoneal chemotherapy *in vitro*

The clinical presentation of microscopic tumor cell deposits attached to the peritoneum was simulated by allowing multicellular organoids to adhere to a bottom layer of basement membrane extract (BME). As such, organoids were in direct contact with the chemotherapy solution, similar to micrometastases during HIPEC. Bottom layers of 40 µl BME were dispensed in a 96-well plate (Costar® 3904; Corning, New York, USA) by use of a Multidrop™ Combi Reagent Dispenser with a small tubing cassette (ThermoFisher Scientific, Waltham, Massachusetts, USA). Approximately 3000 2-day-old organoids suspended in 100 µl basal culture medium were dispensed on top of the BME. Two days after plating, medium was aspirated, and the organoids were incubated with 100 µl preheated chemotherapy at a range of concentrations for 30 min (oxaliplatin) or 90 min (MMC) at 42°C, in line with current standard clinical treatment protocols[10]. ATR inhibitors VE-821 and VX-970 were added during the 72 h after HIPEC. As a measure of cell viability, ATP levels were assessed using a CellTiterGlo® 2.0 kit (Promega, Fitchburg, Wisconsin, USA) on a Spectramax M5e reader (Molecular Devices, San Jose, California, USA). Viability was normalized to the mean of three control wells per batch, which were treated with 0.5 per cent DMSO in MMC and glucose/sodium chloride solution in oxaliplatin experiments, and included the respective inhibitors in the drug combination experiments. Viability assays were performed in triplicate and repeated multiple times on different days, yielding a total of 1422 data points from 61 separate experiments.

Live-cell imaging

TOR14 organoids expressing mNeon-tagged histone 2B were incubated with either basal culture medium, 1 µmol/l VE821, 0.5 µmol/l MMC, or 0.5 µmol MMC + 1 µmol VE821 for 90 min at 42°C. The chemotherapy agent was washed away, medium was replaced and 1 µmol/l VE-821 was added to the appropriate wells. The plate was mounted on an inverted confocal microscope (Nikon TiE-based CSU-W1 Spinning Disk; Nikon Minato, Tokyo, Japan) equipped with a culture chamber at 37°C and 5 per cent carbon dioxide. Organoids were imaged every 15 min over 72 h to follow cell fate after treatment.

RESULTS

Organoids derived from colorectal peritoneal metastases

A panel of five patient-derived PM organoid lines was established for this study; four were generated from solid lesions and the fifth from malignant ascites (Figure 1; Supplementary Table 1). The five organoid lines showed divergent morphologies *in vitro*, with either predominant tubular formation (TOR10MII, TOR22 and p02-1), a papillary growth pattern with some tubular formation (TOR14) or a solid growth pattern (TOR17) (Figure 2a). These growth patterns are common in colorectal adenocarcinoma histology. Organoid morphology closely resembled the histology of the original metastases. The orthotopic xenograft of TOR10 showed the same histological features as the original carcinoma, with evident mucin lakes comprising more than 50 per cent of the tumor mass, classifying them as mucinous carcinomas. The organoid TOR10MII also produced extracellular mucin, as confirmed by a positive periodic acid Schiff stain (data not shown). Comparison of hotspot mutations between the original tumors and the organoids showed that 13 of 14 mutations found in the tumors were also identified in the matched organoid (Figure 2b). Thus, the PM-derived organoid lines faithfully recapitulated the histological and genetic characteristics of the cancers from which they were derived.

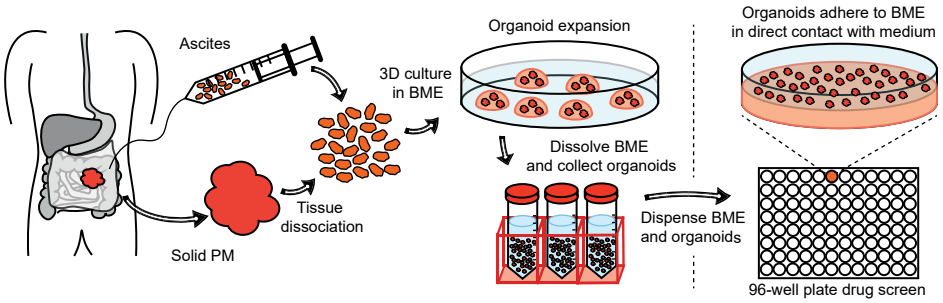

Figure 1. Organoid generation and testing.
Organoids were generated directly from malignant ascites or from solid lesions by first digesting the tissue enzymatically. Three-dimensional (3D) tumor organoids were grown out by culturing single cells in 3D basement membrane extract (BME) immersed in basal culture medium. For the in vitro HIPEC experiments, organoids were plated on top of a layer of BME, rather than inside the matrix, to maximize drug exposure and simulate the clinical features of microscopic peritoneal metastases (PMs).

In vivo models system for hyperthermic intraperitoneal chemotherapy *in vitro*

Before performing drug screens on the organoid panel, the concentrations of intraperitoneal chemotherapy drugs in 40 consecutive HIPEC procedures were evaluated. Both BSA and perfusate volumes varied widely between patients (Table 1). Importantly, BSA was a poor

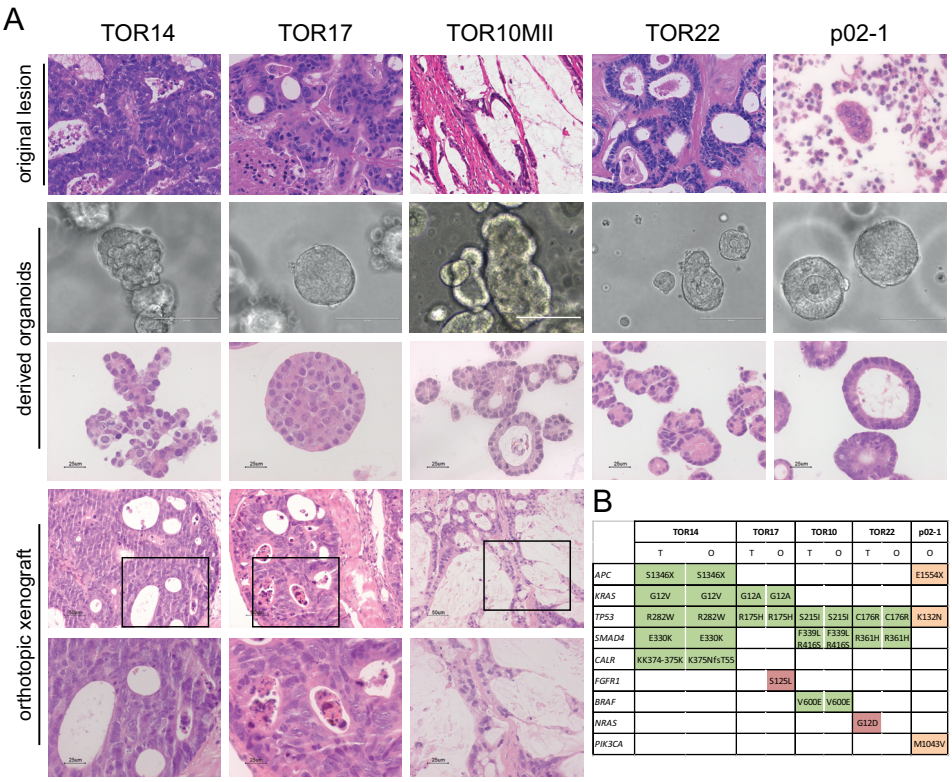

	TOR14		TOR17		TOR10		TOR22		p02-1
	T	O	T	O	T	O	T	O	O
APC	S1346X	S1346X							E1554X
KRAS	G12V	G12V	G12A	G12A					
TP53	R282W	R282W	R175H	R175H	S215I	S215I	C176R	C176R	K132N
SMAD4	E330K	E330K			F339L R416S	F339L R416S	R361H	R361H	
CALR	KK374-375K	K375NfsT55							
FGFR1				S125L					
BRAF					V600E	V600E			
NRAS							G12D		
PIK3CA									M1043V

Figure 2. Morphological and molecular comparison of organoids of peritoneal metastases with parent tumors from which they were derived.
(a) Histological or cytological (p02-1) comparison of parent tumors (haematoxylin and eosin stain; TOR14, TOR17, TOR22 and p02-1: original magnification × 40; TOR10: original magnification × 20) with matched organoids (bright field, scale bar 100 µm; haematoxylin and eosin stain, scale bar 25 µm) and orthotopic xenografts in mouse caecum (haematoxylin and eosin stain, original magnification × 10 and × 40). (b) Comparison of hotspot mutations in original tumors (T) and matched organoids (O). The tumor cell content of solid peritoneal lesions of p02-1 was too low (less than 5 per cent) to call mutations reliably.

predictor of abdominal volume in both men and women (Figure 3a), which led to variable perfusate concentrations. The calculated median starting concentration was 13.6 (range 9.7–19.8) µmol/l for MMC (Figure 3b) and 306 (215–439) µmol/l for oxaliplatin.

The viability of organoids in response to a range of drug concentrations, including the calculated clinical concentrations, was then assessed. The experimental set-up of the *in vitro* drug screen is shown in Figure 1. Dose–response curves to MMC and oxaliplatin for each organoid showed that drug sensitivity varied considerably between individual patient-derived organoids (Figure 3c,d). The concentration required to eliminate 50 per cent of the tumor cells (IC50) for MMC ranged from 3.3 to 22.2 µmol/l; TOR14 was most sensitive to

MMC and p02-1 least sensitive. The IC50 for oxaliplatin ranged from 297 to 692 μmol/l, with TOR10MII as the most sensitive organoid line (Table 2). The assay proved robust and reproducible, with limited variation in IC50 values in repeated experiments over several months (Figure 3e,f). The dose–response curves also showed that the doses of MMC and oxaliplatin achieved clinically were insufficient to eliminate all cancer cells completely in these organoid lines. This highlights the need for improving the efficacy of HIPEC treatment.

Table 1. Perfusion data for patients undergoing hyperthermic chemotherapy.

	No. of patients*
Sex ratio (M : F)	18 : 22
Body surface area (m^2)†	1.84 (1.55–2.36)
Patient volume (ml)†	6055 (3000–9300)
Total perfusate volume (ml)†	7060 (4800–11 018)

*Unless indicated otherwise; †values are median (range).

Table 2. Half-maximal inhibitory concentration for mitomycin C and oxaliplatin by organoid line.

Organoid line	**IC50 (μmol/l)**	
	Mitomycin C	**Oxaliplatin**
TOR 14	3.3 (2.3 – 4.6)	368 (326 - 414)
TOR17	12.9 (15.5 – 30.9)	692 (375 - 1277)
TOR22	7.4 (4.4 – 12.5)	364 (243 - 544)
TOR10MII	5.6 (4.7 – 6.6)	297 (253 - 348)
P02-1	22.2 (10·8 – 45.5)	549 (449 - 672)

Estimated half-maximal inhibitory concentrations (IC50) were pooled over all batches using a non-linear mixed-effect model. Values in parentheses are 95 per cent confidence intervals.

ATR inhibition increases the efficacy of mitomycin C

Given the recent finding that oxaliplatin-based HIPEC is not effective in a clinical setting[12] and that MMC appeared more effective at clinical concentrations than oxaliplatin in the PM-organoid model, further improvement of MMC HIPEC was considered more promising, and combination treatment with ATR inhibition was assessed. The ATR inhibitor VE-821 showed limited toxicity as monotherapy (Supplementary Figure 1), but greatly sensitized all PM organoids to MMC, as shown by statistically significant reductions of 2.6–12.4-fold in IC50 values (Figure 4a; Supplementary Table 2). Importantly, for each organoid line, the IC50 values for MMC in the combination treatment were below the concentrations of MMC attained clinically.

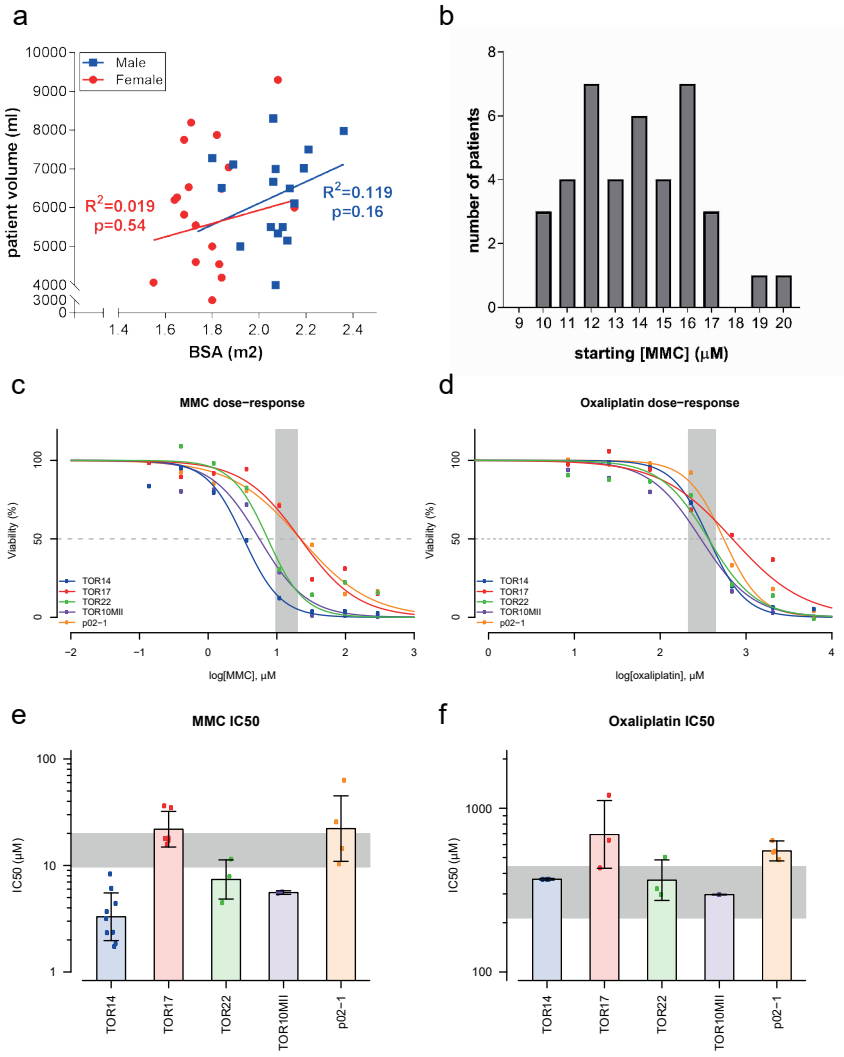

Figure 3. Organoids as an in vitro model to study the efficacy of hyperthermic intraperitoneal chemotherapy regimens.
(a) Scatter plot of body surface area (BSA) versus intra-abdominal perfusion volume, which together determine the concentration of HIPEC drug in the clinic (men: R^2= 0·019, P = 0·540; women: R^2 = 0·119, P = 0·161). (b) Frequency distribution histogram of calculated starting concentrations of mitomycin C (MMC) in 40 HIPEC procedures. (c,d) Dose–response curves illustrating the variation in sensitivity to MMC (c) and oxaliplatin (d) on the individual patient-derived organoids. The shaded areas represent the clinically relevant concentration ranges determined in the clinical cohort. The dashed line crosses the individual curves at the concentration required to eliminate 50 per cent of the tumor cells (IC50). (e,f) Estimated between-batch variation (variation between separate in vitro HIPEC experiments) for MMC (e) and oxaliplatin (f). Bars represent the estimated IC50 values pooled over all batches using a non-linear mixed-effect model as determined in c and d; error bars show estimated standard deviation in IC50 values between batches, and symbols indicate estimated per-batch IC50 values (both based on random batch effects included in the model). The shaded areas represent the clinically relevant concentration ranges determined in the clinical cohort.

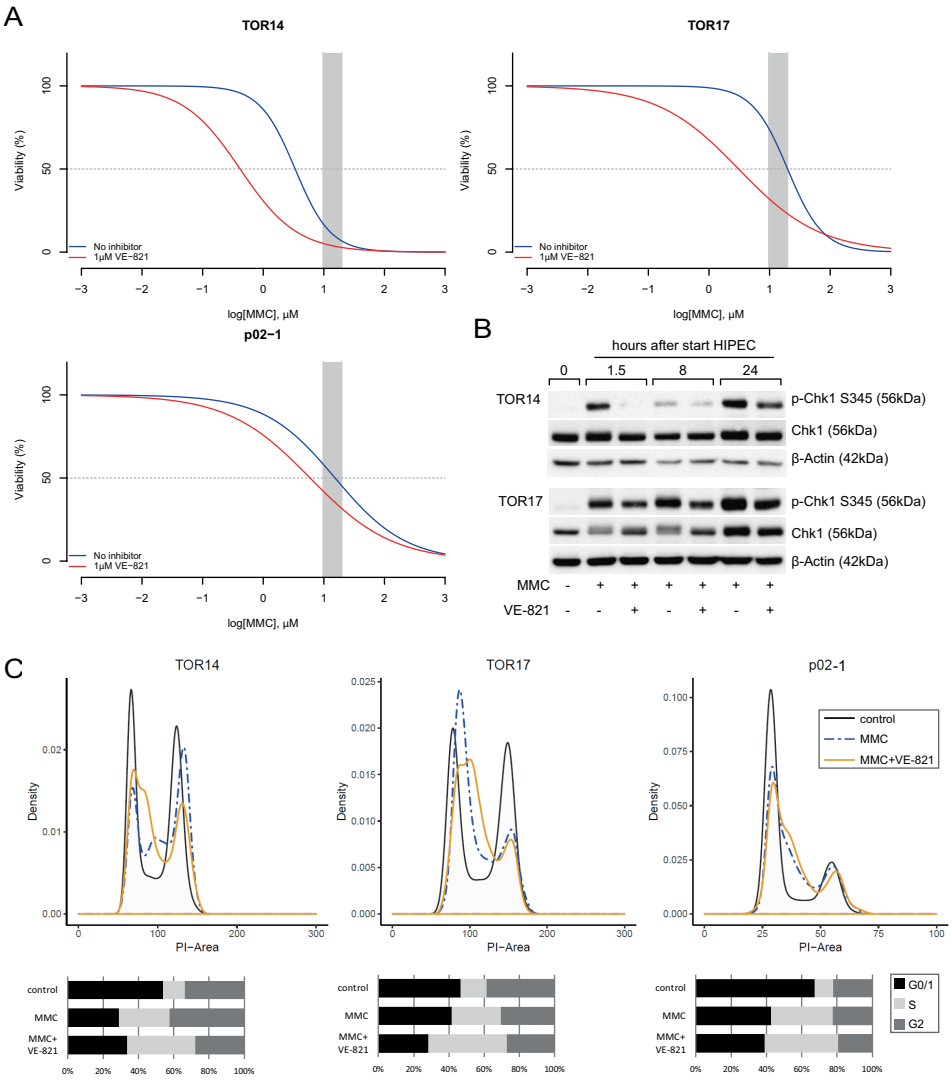

Figure 4. Effects of mitomycin C and ATR inhibition on organoid viability and cell cycle distribution.
(a) Dose–response curves comparing mitomycin C (MMC) monotherapy and the combination of MMC and ATR inhibitor VE-821 in the individual organoids. The shaded area represents the clinically relevant concentration ranges determined in the clinical cohort. The dashed line crosses the individual curves at the concentration required to eliminate 50 per cent of the tumor cells. (b) Western blot analysis of checkpoint kinase 1 (Chk1) phosphorylation over time, following 90 min of treatment with hyperthermic MMC or a combination of MMC and VE-821; p-Chk1 S345, Chk1 phosphorylated on serine 345. (c) Cell cycle profiles of the different organoids 24 h after treatment (90 min at 42°C) with either no drugs (control), MMC (TOR14, 3 µmol/l; TOR17, 20 µmol/l; p02-1, 24 µmol/l), or MMC followed by 24 h of treatment with 1 µmol/l VE-821. The DNA content of individual cells was measured by propidium iodide (PI) intensity.(d) Quantification of cell cycle distribution. Data for TOR22 and TOR10MII are shown in Supplementary Figure 2.

To understand the mechanism of action of the combination therapy, the effects of the drugs on cell cycle distribution and cell fate were characterized. MMC treatment at IC50 concentrations induced rapid phosphorylation of the ATR substrate Checkpoint kinase 1 (Chk1) (Figure 4b) and led to cell cycle arrest in the S phase (Figure 4c). Chk1 phosphorylation was reduced by combining MMC with VE-821 (Figure 4b). However, rather than inducing a shift from S phase towards G2/M phase, co-treatment with VE-821 and MMC induced a more pronounced S-phase arrest than MMC alone (Figure 4c). Live-cell imaging of TOR14 over 72 h after MMC treatment confirmed that combination treatment did not increase the fraction of death in mitosis compared with monotherapy with MMC (Videos 1–4, available online). In both conditions, most cell death occurred during a period of interphase (Figure 5a,b). Cell death appeared to occur earlier in cells co-treated with MMC and ATR inhibitors than in cultures treated with MMC alone (Supplementary Figures 3 and 4).

Flow cytometric analysis showed that MMC induced a profound increase in replication protein A (RPA) foci. RPA binds to single-strand DNA at sites of DNA damage, and the increased presence of RPA foci is indicative of replication stress.[23, 24] Combined treatment with MMC and VE-821 slightly increased the number of RPA foci per cell as reflected by the mean fluorescence of RPA70, and induced a pronounced increase in RPA phosphorylation (RPA32, phosphorylated on either serine 4 or 8) (Figure 5c). Replication stress can lead to massive chromosome breakage and subsequent cell death.[23]

To evaluate whether this combination strategy could be translated to the clinical setting, VX-970, the clinical derivative of VE-821, was tested in combination with MMC. VX-970 also inhibited Chk1 phosphorylation induced by MMC in a dose-dependent fashion (Figure 5d), and dramatically lowered the IC50 value of MMC (Figure 5e; Supplementary Table 2), similar to VE-821. This suggests that MMC plus ATR inhibition is a feasible combination strategy in HIPEC for PM from colorectal cancer.

DISCUSSION

Retrospective comparisons between MMC and oxaliplatin as intraperitoneal chemotherapy agents in HIPEC for PM from colorectal cancer are contradictory.[7-10] This may be due to heterogeneous patient populations, variation in selection criteria for CRS–HIPEC and differences in the application of perioperative systemic chemotherapy. Furthermore, the intraperitoneal drug concentration during HIPEC varies widely as a consequence of BSA-based chemotherapeutic dose. This study has shown that BSA correlates poorly with intraperitoneal volume, and perfusate volume influences the concentration to which peritoneal micrometastases are exposed. Finally, even though there may not be a clear

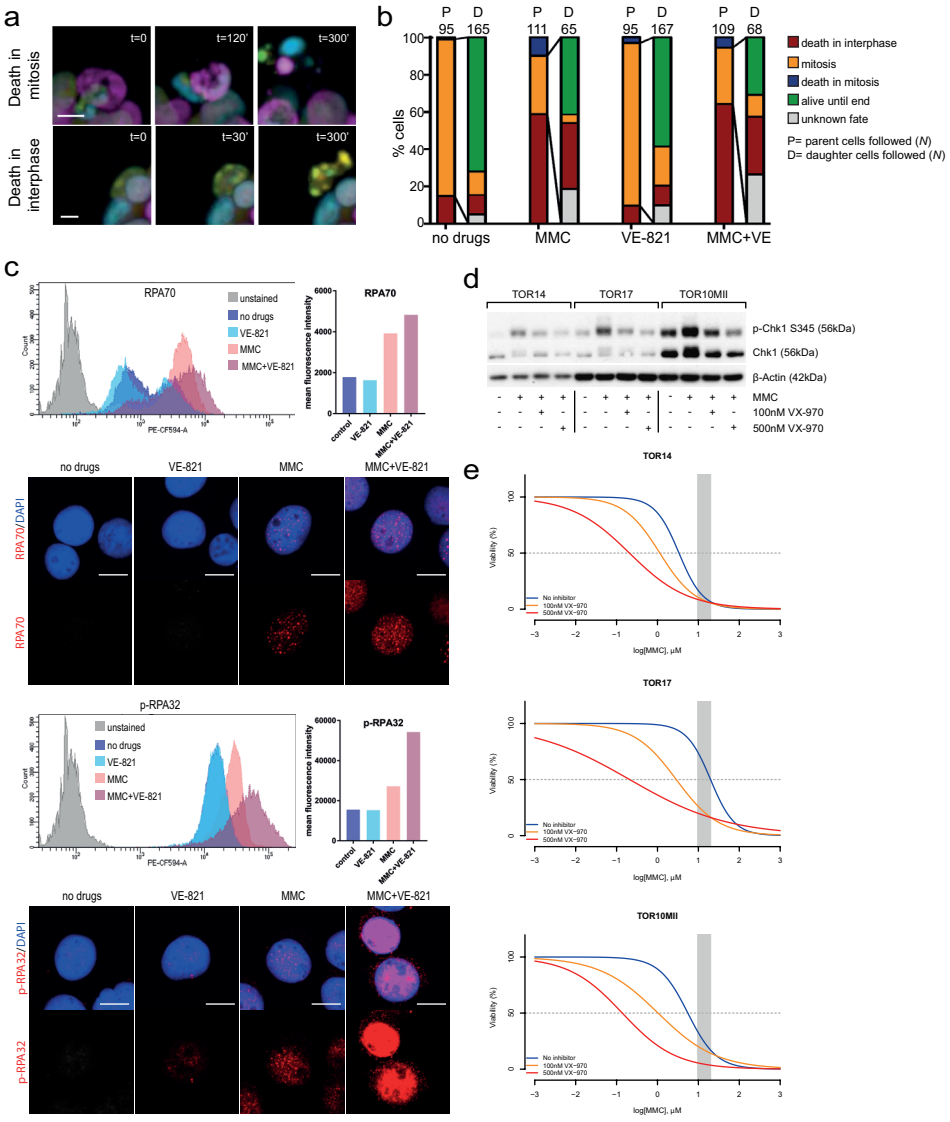

Figure 5. Effects of mitomycin C and ATR inhibition on cell fate and replication stress.
(a) Examples of cell death events observed during live-cell imaging. Upper panel shows cell death in mitosis (cell death is preceded by mitotic chromosome condensation) and lower panel death in interphase (no chromosomal condensation observed before the formation of apoptotic bodies) (scale bar 10 µm). (b) Quantification of TOR14 cell fates observed during 72 h of live-cell imaging after treatment with either no drugs, 0.5 µmol/l mitomycin C (MMC) for 90 min, 1 µmol/l VE-821 for 72 h, or 0.5 µmol/l MMC for 90 min + 1 µmol/l VE-821 for 72 h. If a parent cell (P) underwent mitosis, the fates of the resulting daughter cells (D) were also followed. (c) Analysis of replication protein A (RPA) foci in response to MMC or the combination treatment of MMC + VE-821 in TOR14. Flow cytometry profiles for the different conditions are shown in the frequency distribution plots, and the mean intensities of the RPA or phosphorylated RPA (p-RPA) signal per cell are plotted separately. PE-CF594-A, fluorescence area. Maximum projection confocal images of cells from the same experiment illustrate the increased number of RPA or p-RPA foci in the combination treatment. The red ▶

▶ signal represents the RPA or p-RPA, and the blue signal shows 4',6-diamidino-2-phenylindole staining (scale bar 10 μm). (d) Western blot analysis of checkpoint kinase 1 (Chk1) phosphorylation after 90 min of treatment with hyperthermic MMC or the combination of MMC and VX-970 (100 and 500 nmol/l); p-Chk1 S345, Chk1 phosphorylated on serine 345. (e) Dose–response curves comparing MMC monotherapy and the combination of MMC and VX-970 (100 and 500 nmol/l) in the individual organoids. The shaded area represents the clinically relevant concentration ranges determined in the clinical cohort. The dashed line crosses the individual curves at the concentration required to eliminate 50 per cent of the tumor cells.

superiority of either chemotherapy agent at group level, one drug might perform better than the other in individual patients, depending on the tumor biology of the metastases.

In the present study, organoid technology was used to develop a model system for evaluating the efficacy of HIPEC. Considerable differences in sensitivity to MMC and oxaliplatin were observed between patient-derived organoid lines. Moreover, hyperthermic chemotherapy at commonly attained clinical doses had only a minor effect on the viability of several organoid lines. This indicates that current HIPEC regimens are insufficient to eradicate residual microscopic disease at least in a subgroup of patients with colorectal PMs, and this is consistent with the high recurrence rates observed after CRS–HIPEC and the negative result from the Prodige 7 trial.[7, 11, 12]

In an effort to improve MMC efficacy, combined treatment with MMC and inhibitors of the replication checkpoint kinase ATR was assessed in this study. The addition of ATR inhibitors to MMC was effective in eliminating microscopic metastases at clinical doses of MMC in all PM-derived organoids tested. These findings are in line with a model in which ATR inhibition causes unrestrained replication origin firing despite the presence of DNA damage caused by MMC. Excess origin firing increases the number of RPA foci and exhausts the nuclear RPA pool. Ultimately, this leads to massive chromosome breakage and a type of cell death known as replication catastrophe.[23]

This study provides insights into the mechanism of action of ATR inhibition in combination with a standard chemotherapy used in HIPEC. Understanding how a drug combination works before it enters the clinical setting is important as it can increase the chance of success. It can yield biomarkers for monitoring therapeutic response as well as predictive biomarkers for trial stratification. Of note, all organoids in this cohort have a mutation in *TP53*. ATR inhibition is particularly potent in tumors with deficiencies in the ATM pathway, such as *TP53*-mutant cancers.[25] An important future goal is to further optimize organoid establishment and long-term expansion, in order to create an organoid panel of PMs from colorectal cancer that completely reflects the diversity of mutational and histological subtypes. Further research is also required to find the optimal timing, dose and route of administration (intraperitoneal or systemic) of ATR inhibitors in the clinical HIPEC setting. By modelling the effects of sequential or concomitant treatment, the *in vitro* model could aid in rational trial design for ATR inhibition in HIPEC.

Several factors could potentially limit the predictive value of the present model. First, the culture matrix used in the model is an abstraction of the microenvironment of the peritoneum, which includes fibroblasts and other stromal and immune cells. These components potentially influence drug response. Second, HIPEC is nearly always preceded by CRS which induces cytokine production[26] that could also influence drug response. Third, intrapatient interlesion heterogeneity may provide an additional level of complexity that is not modelled in the present organoid collection.[27, 28] Despite these limitations, this model of PM from colorectal cancer is a robust *in vitro* system that allows rapid evaluation of existing and novel HIPEC strategies in a biologically relevant setting.

Acknowledgements

The authors thank O. Imhof for the HIPEC perfusion reports, J. Laoukili and E. Küçükköse for help with organoid transfection, L. Wijler and J. Laoukili for setting up high-throughput drug screening in the authors' laboratory, and C. Huysentruyt for the microscopic image of p02-1. This work was supported by the Dutch Cancer Society (UU2014–6617 to I.U.), and the Marie Curie Network Ploidynet which is funded by the European Union Seventh Framework Programme (FP7/2007-2013) under Grant Agreement number 607722 (to A.C.F.B.). The sponsors had no influence on the study design, or collection, analysis and interpretation of data.

REFERENCES

1. Segelman J, Akre O, Gustafsson UO, et al. External validation of models predicting the individual risk of metachronous peritoneal carcinomatosis from colon and rectal cancer. *Colorectal disease : the official journal of the Association of Coloproctology of Great Britain and Ireland*. 2016;**18**(4):378-85.
2. Koppe MJ, Boerman OC, Oyen WJ, et al. Peritoneal carcinomatosis of colorectal origin: incidence and current treatment strategies. *Ann Surg*. 2006;**243**(2):212-22.
3. Bushati M, Rovers KP, Sommariva A, et al. The current practice of cytoreductive surgery and HIPEC for colorectal peritoneal metastases: Results of a worldwide web-based survey of the Peritoneal Surface Oncology Group International (PSOGI). *Eur J Surg Oncol*. 2018;**44**(12):1942-8.
4. Franko J, Ibrahim Z, Gusani NJ, et al. Cytoreductive surgery and hyperthermic intraperitoneal chemoperfusion versus systemic chemotherapy alone for colorectal peritoneal carcinomatosis. *Cancer*. 2010;**116**(16):3756-62.
5. Elias D, Gilly F, Boutitie F, et al. Peritoneal colorectal carcinomatosis treated with surgery and perioperative intraperitoneal chemotherapy: retrospective analysis of 523 patients from a multicentric French study. *J Clin Oncol*. 2010;**28**(1):63-8.
6. Verwaal VJ, Bruin S, Boot H, et al. 8-Year Follow-Up of Randomized Trial: Cytoreduction and Hyperthermic Intraperitoneal Chemotherapy Versus Systemic Chemotherapy in Patients with Peritoneal Carcinomatosis of Colorectal Cancer. *Ann Surg Oncol*. 2008;**15**(9):2426-32.
7. van Eden WJ, Kok NFM, Woensdregt K, et al. Safety of intraperitoneal Mitomycin C versus intraperitoneal oxaliplatin in patients with peritoneal carcinomatosis of colorectal cancer undergoing cytoreductive surgery and HIPEC. *Eur J Surg Oncol*. 2018;**44**(2):220-7.
8. Prada-Villaverde A, Esquivel J, Lowy AM, et al. The American Society of Peritoneal Surface Malignancies evaluation of HIPEC with Mitomycin C versus Oxaliplatin in 539 patients with colon cancer undergoing a complete cytoreductive surgery. *J Surg Oncol*. 2014;**110**(7):779-85.
9. Leung V, Huo YR, Liauw W, et al. Oxaliplatin versus Mitomycin C for HIPEC in colorectal cancer peritoneal carcinomatosis. *Eur J Surg Oncol*. 2017;**43**(1):144-9.
10. Hompes D, D'Hoore A, Wolthuis A, et al. The use of Oxaliplatin or Mitomycin C in HIPEC treatment for peritoneal carcinomatosis from colorectal cancer: a comparative study. *J Surg Oncol*. 2014;**109**(6):527-32.
11. Kuijpers AM, Mirck B, Aalbers AG, et al. Cytoreduction and HIPEC in the Netherlands: nationwide long-term outcome following the Dutch protocol. *Ann Surg Oncol*. 2013;**20**(13):4224-30.
12. Quenet F, Elias D, Roca L, et al. A UNICANCER phase III trial of hyperthermic intra-peritoneal chemotherapy (HIPEC) for colorectal peritoneal carcinomatosis (PC): PRODIGE 7. *J Clin Oncol*. 2018;**36**(18_suppl):LBA3503-LBA.
13. van Driel WJ, Koole SN, Sikorska K, et al. Hyperthermic Intraperitoneal Chemotherapy in Ovarian Cancer. *N Engl J Med*. 2018;**378**(3):230-40.
14. Kemmel V, Mercoli HA, Meyer N, et al. Mitomycin C Pharmacokinetics as Predictor of Severe Neutropenia in Hyperthermic Intraperitoneal Therapy. *Ann Surg Oncol*. 2015;**22 Suppl 3**:S873-S9.
15. Lecona E, Fernandez-Capetillo O. Targeting ATR in cancer. *Nat Rev Cancer*. 2018;**18**(9):586-95.
16. Gargiulo D, Kumar GS, Musser SS, et al. Structural and function modification of DNA by mitomycin C. Mechanism of the DNA sequence specificity of mitomycins. *Nucleic Acids Symp Ser*. 1995(34):169-70.
17. Toledo L, Neelsen KJ, Lukas J. Replication Catastrophe: When a Checkpoint Fails because of Exhaustion. *Mol Cell*. 2017;**66**(6):735-49.
18. van de Wetering M, Francies HE, Francis JM, et al. Prospective derivation of a living organoid biobank of colorectal cancer patients. *Cell*. 2015;**161**(4):933-45.
19. Vlachogiannis G, Hedayat S, Vatsiou A, et al. Patient-derived organoids model treatment response of metastatic gastrointestinal cancers. *Science*. 2018;**359**(6378):920-6.
20. Verissimo CS, Overmeer RM, Ponsioen B, et al. Targeting mutant RAS in patient-derived colorectal cancer organoids by combinatorial drug screening. *Elife*. 2016;**5**.
21. van Ruth S, Mathot RA, Sparidans RW, et al. Population pharmacokinetics and pharmacodynamics of mitomycin during intraoperative hyperthermic intraperitoneal chemotherapy. *Clin Pharmacokinet*. 2004;**43**(2):131-43.
22. Mehta AM, Van den Hoven JM, Rosing H, et al. Stability of oxaliplatin in chloride-containing carrier solutions used in hyperthermic intraperitoneal chemotherapy. *Int J Pharm*. 2015;**479**(1):23-7.

23. Toledo LI, Altmeyer M, Rask MB, et al. ATR prohibits replication catastrophe by preventing global exhaustion of RPA. *Cell*. 2013;**155**(5):1088-103.
24. Byrne BM, Oakley GG. Replication protein A, the laxative that keeps DNA regular: The importance of RPA phosphorylation in maintaining genome stability. *Semin Cell Dev Biol*. 2019;**86**:112-20.
25. Reaper PM, Griffiths MR, Long JM, et al. Selective killing of ATM- or p53-deficient cancer cells through inhibition of ATR. *Nat Chem Biol*. 2011;**7**(7):428-30.
26. Leijte GP, Custers H, Gerretsen J, et al. Increased Plasma Levels of Danger-Associated Molecular Patterns Are Associated With Immune Suppression and Postoperative Infections in Patients Undergoing Cytoreductive Surgery and Hyperthermic Intraperitoneal Chemotherapy. *Front Immunol*. 2018;**9**:663.
27. Ubink I, van Eden WJ, Snaebjornsson P, et al. Histopathological and molecular classification of colorectal cancer and corresponding peritoneal metastases. *Br J Surg*. 2018;**105**(2):e204-e11.
28. Roerink SF, Sasaki N, Lee-Six H, et al. Intra-tumour diversification in colorectal cancer at the single-cell level. *Nature*. 2018;**556**(7702):457-62.

SUPPLEMENTARY MATERIALS AND METHODS

Organoid culture

Thirteen tissue samples of colorectal peritoneal metastases from nine patients were collected for organoid derivation. From these samples four different organoid lines were established from three patients. From the colorectal cancer organoids already established by the HUB foundation, we identified HUB-02-B2-040 (TOR10), which had been derived from a primary mucinous adenocarcinoma of a patient with synchronous PM-CRC. TOR10MII was generated from a peritoneal metastasis that developed upon orthotopic implantation of TOR10 organoids into the caecal wall of a mouse. We selected this organoid for our cohort, rather than the original TOR10 primary tumor organoid, because PM might respond differently to HIPEC than primary cancers. In addition to the five lines generated from solid peritoneal metastases, we included an organoid line that was established from malignant ascites (p02-1).

Organoids were established from solid lesions according to methods described by Fujii *et al.*[1] Tissue specimens were cut into small pieces, washed ten times with cold PBS and digested with 0.1mg/ml Liberase™ TH research grade (Roche, REF 05401135001, Mannheim, Germany) for 60 min at 37°C, with vortexing every 15 minutes. The cell suspension was collected, centrifuged and embedded in Basement Membrane Matrix (BME, Cultrex PathClear Reduced Growth Factor BME Type 2, R&D Systems, Minneapolis, MN, USA) mixed with basal culture medium in a 7:3 ratio. Ascites was collected intraoperatively through one of the laparoscopic trocar openings. With a gastro-nasal tube and a syringe, 40 ml of ascites was aspirated. The ascites fluid was washed five times with cold PBS, centrifuged at 400g for 5 minutes and the cell pellet was resuspended in Matrigel® (Corning, 356231, New York, USA) mixed with basal culture medium in a 7:3 ratio. Drops of 10 µl cell suspension were allowed to solidify for 30 minutes in an incubator at 37°C and 5% CO_2, after which they were overlaid with basal culture medium. Fresh medium was added once to twice a week. Outgrowing organoids were passaged by mechanical and enzymatic disruption with TrypLE™ express enzyme (Gibco, Thermo Scientific).

Basal culture medium consisted of Advanced DMEM/F12 (Gibco, Life Technologies Corporation, 12634-010, Grand Island, NY, USA), supplemented with penicillin (100 U/ml) and streptomycin (100 µg/ml; PAA), 10mM Hepes (Lonza, BE17-737E, Basel, Switzerland), 400 µM Glutamax (Life Technologies, 35050038), 1X B27 (Life Technologies, 17504044) and 1mM N-Acetyl-L-cysteine (Sigma-Aldrich, A9165-5G, St Louis, MO, USA). The following niche factors were used: 50ng/ml Noggin, 500nM A83-01 (Biovision, 1725-1, Zurich, Switzerland) and 10 µM SB202190 (Sigma-Aldrich, S7067).

Animal experiments

To study recapitulation of tumor histology and metastatic potential of organoids, collagen drops containing ~150,000 organoids of TOR14, TOR17 and TOR10 each were surgically implanted below the serosa of the caecal wall of NOD.Cg-PrkdcscidIl2rgtm1Wjl/SzJ (NSG) mice, as described by Fumagalli et al.[2] Five months after implantation, one of the TOR10 caecal tumors had spread extensively to the peritoneum. One PM was harvested and organoids were established which resulted in PM-CRC organoid line TOR10MII.

The project proposals for studies involving laboratory animals (104816-4 and 500-16-614-01-004) were approved by Utrecht University's Animal Welfare Body and the Animal Ethics Committee, and licensed by the Central Authority for Scientific Procedures on Animals (license number AVD115002016614). All experiments were conducted in accordance with the Dutch Experiments on Animals Act and in line with European Directive 2010/63/EU, and by licensed personnel.

Next generation sequencing

Sequencing of original cancer tissues and organoids was performed by the Molecular Pathology Laboratory of the UMC Utrecht on the IonTorrent platform with the Ion Ampliseq™ Cancer Hotspot Panel v2Plus. From TOR14, the same peritoneal metastasis was sequenced, from TOR17, TOR21/22 and TOR10MII the primary tumors were sequenced.

Analysis of HIPEC in vitro drug screens

To estimate the 50% inhibitory concentration (IC50), data points from repeated experiments were combined, using non-linear mixed-effect models, taking between-batch heterogeneity into account by random effects. Curves were fit using a two-parameter model including ln(IC50) and slope as fixed effects. To show the fit of these curves, the mean viability of each organoid per concentration was estimated and plotted onto the dose-response curves. The mean viabilities were estimated using concentration as a categorical variable in linear-mixed effects models, while again correcting for random batch effects. Data analyses were performed with the packages *nlme* (version 3.1-124) and *lme4* (version 1.1-11) for R (version 3.2.1 for macOS).

Cell cycle analysis

Organoids (three days old) were collected in 15 ml falcon tubes, centrifuged (400g, 5min) and resuspended in pre-heated (42°C) basal growth medium without niche factors, with MMC, 1μM VE-821, a combination of both, or plain medium (control) for 90 minutes. For each organoid, the MMC concentration was equal to its estimated IC50 based on multiple in vitro HIPEC experiments. Organoids were treated in suspension for 90 minutes in a water bath at 42°C; the tubes were shaken every 15 minutes. After treatment the organoids

were centrifuged, the chemotherapy was removed, and the organoids were washed one time with PBS. The organoids were replated in matrigel and cultured for 24 hours. VE-821 (1μM) was added to the medium of corresponding organoids during this period. After 24 hours cell cycle profiles were generated by flow cytometric analysis of propidium iodide staining.[3] TOR14 and TOR17 were directly dissolved in Nicoletti buffer (0.1% sodium citrate (wt/v), 0.1% Triton X-100 (v/v) in deionized distilled water) + 20μg/ml propidium iodide (PI). The nuclei were incubated for 4-16 hours prior to analysis by flow cytometry on BD FASC Celesta (BD Biosciences, San Jose, CA, USA). TOR22, TOR10MII and p02-1 were enzymatically dissociated to single cells with trypsin, washed with PBS and fixed by suspension in 4,5 mL ice-cold 70% ethanol in a drop-wise fashion while vortexing. After at least two hours, cells were centrifuged, washed in PBS and incubated with 300 μl staining solution (0.1% Triton-X, 0.2 mg/ml RNase A and 0.5 mg/ml PI) for 15 minutes at 37°C. The cells were transferred to ice and measured immediately with flow cytometry.

Live cell imaging

TOR14 organoids were infected with lentivirus encoding mNeon-tagged histone 2B and a puromycin-resistance cassette (pLV-H2B-mNeon-ires-Puro). Single cells were sorted based on H2B-mNeon expression. ~2000 organoids (two days old) were plated on a bottom layer of 70μl BME in the four central wells of a μ-Slide 8 Well plate (Ibidi). After two days, organoids were incubated with 200 μl of either basal culture medium, 1 μM VE821, 0.5 μM MMC, or 0.5μM MMC + 1 μM VE821 for 90 minutes at 42°C. After chemotherapy was washed away, the plate was mounted on an inverted confocal microscope (Nikon TiE-based CSU-W1 Spinning Disk) equipped with a culture chamber at 37 °C and 5% CO2. Over 72 h, selected organoids were imaged simultaneously in XYZT-mode using a ×30 silicon objective (N.A. 1.05), with minimal amounts of 3% power of a 448 mW laser with 50 nm pinhole. Time interval was 15 min. For post-acquisition analyses of cell fate, data sets were converted into manageable and maximally informative videos, combining z-projection and depth color-coding. Cell fate was scored, assessed and counted manually.

Western blot

Organoids were collected from BME with dispase at the indicated time points and lysed in laemmli lysis buffer (2.5% SDS, 20% glycerol, 120 mM Tris pH 6.8). Equal amounts of protein were run on SDS-PAA gels and were analyzed by western blot (Trans-Blot Turbo, Bio-Rad, Hercules, CA, USA). The following antibodies were used: Chk1 (2G1D5, #2630 Cell Signaling Technology, Danvers, MA, USA), Phospho-Chk1 (Ser345) (133D3, #2348 Cell Signaling Technology) and β-Actin (AC-15, #NB600-501, Novus Biologicals, Littleton, CO, USA).

Analysis and quantification of RPA foci

Quantification of replication protein A (RPA) attachment to single-stranded DNA (RPA foci) was performed according to the protocol developed by Forment and Jackson.[4] Organoids were treated in suspension as described for the cell cycle analyses. After treatment, organoids were dissociated with TrypLE™. Unbound proteins were extracted from the nucleus with 0.2% (v/v) Triton-X 100 in PBS for 10 minutes on ice. Cells were washed with 1mg/ml BSA (Acros organics, Thermo Scientific #240401000) in PBS at 4C and fixed in 2% paraformaldehyde for 20 minutes at room temperature. DB Perm/wash buffer (BD #51-2091KZ) was used to wash the cells from this point on. Cells were incubated with RPA70/RPA1 antibody (#2267 Cell Signaling, 1:25) or phospho-RPA32 (S4/S8) antibody (A300-245A, Bethyl Laboratories, Montgomery, TX, USA, 1:250) for one hour at room temperature. After washing, the cells were incubated for 30 minutes at room temperature in the dark with goat anti-rabbit AlexaFluor 568 (Invitrogen, Thermo Fisher Scientific, #A11036, 1:600) as a secondary antibody for both. After washing, the cells were resuspended in analysis buffer containing 0,02% (w/v) sodium azide, 250 µg/ml RNase A (Sigma #R4875) and 0,5 µg/ml Dapi in PBS-BSA 1 mg/ml, and incubated at 37C for 20 minutes. Immunofluorescence intensity was immediately analyzed by flow cytometry on BD FASC Celesta. RPA70 or p-RPA32 fluorescence was measured in a logarithmic PE-CF594 area histogram plot; 10000 events per sample were acquired and the mean 561 nm fluorescence was measured for analysis. Just prior to FACS analysis, a fraction of the samples was taken to spin on a glass slide by CytoSpin and mounted with ProLong Gold antifade reagent (Cell Signaling #9071S) and a cover slip. The fluorescence signal of RPA70 and p-RPA32 was visualized with a Zeiss LSM 550 confocal laser microscope, with a 60x objective. Maximum intensity projections were created from z-stacks zoomed in 4x with Zeiss Zen Software.

REFERENCES

1. Fujii M, Shimokawa M, Date S, et al. A Colorectal Tumor Organoid Library Demonstrates Progressive Loss of Niche Factor Requirements during Tumorigenesis. *Cell Stem Cell*. 2016;**18**(6):827-38.
2. Fumagalli A, Suijkerbuijk SJE, Begthel H, et al. A surgical orthotopic organoid transplantation approach in mice to visualize and study colorectal cancer progression. *Nat Protoc*. 2018;**13**(2):235-47.
3. Riccardi C, Nicoletti I. Analysis of apoptosis by propidium iodide staining and flow cytometry. *Nat Protoc*. 2006;**1**(3):1458-61.
4. Forment JV, Jackson SP. A flow cytometry-based method to simplify the analysis and quantification of protein association to chromatin in mammalian cells. *Nat Protoc*. 2015;**10**(9):1297-307.

SUPPLEMENTARY FIGURES AND TABLES

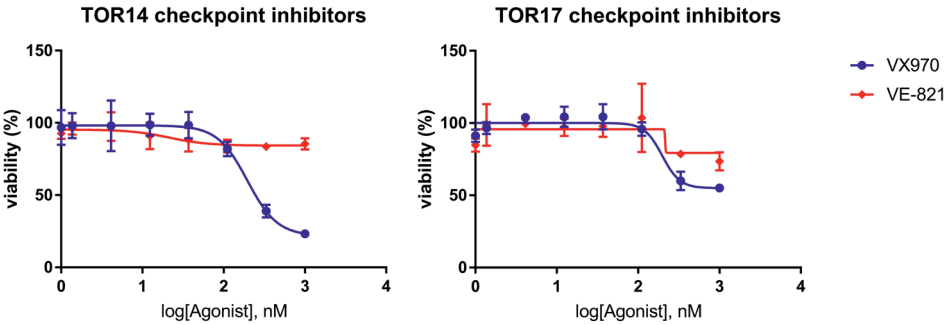

Supplementary Figure 1. Toxicity of 72 hours monotherapy with VE-821 or VX-970 in TOR14 & TOR17.

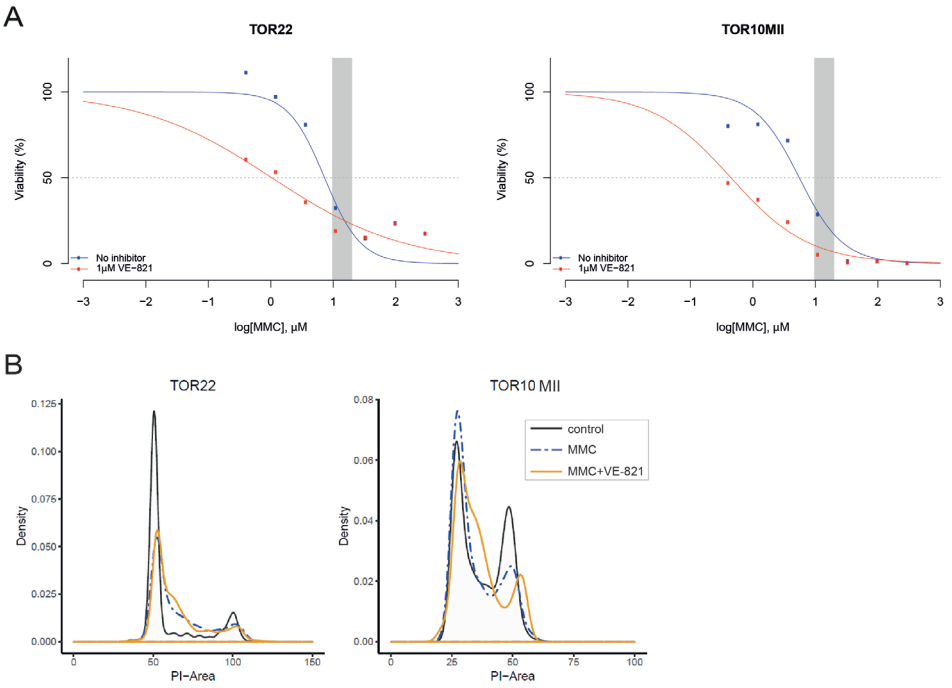

Supplementary Figure 2. Effects of mitomycin C and ATR inhibition on organoid viability and cell cycle distribution.
(a) Dose–response curves comparing mitomycin C (MMC) monotherapy and the combination of MMC and ATR inhibitor VE-821 in TOR22 and TOR10MII. The shaded area represents the clinically relevant concentration ranges determined in the clinical cohort. The dashed line crosses the individual curves at the concentration required to eliminate 50 per cent of the tumor cells. (b) Cell cycle profiles of the different organoids 24 h after treatment (90 min at 42°C) with either no drugs (control), MMC (TOR14, 3 µmol/l; TOR17, 20 µmol/l; p02-1, 24 µmol/l), or MMC followed by 24 h of treatment with 1 µmol/l VE-821. The DNA content of individual cells was measured by propidium iodide (PI) intensity.

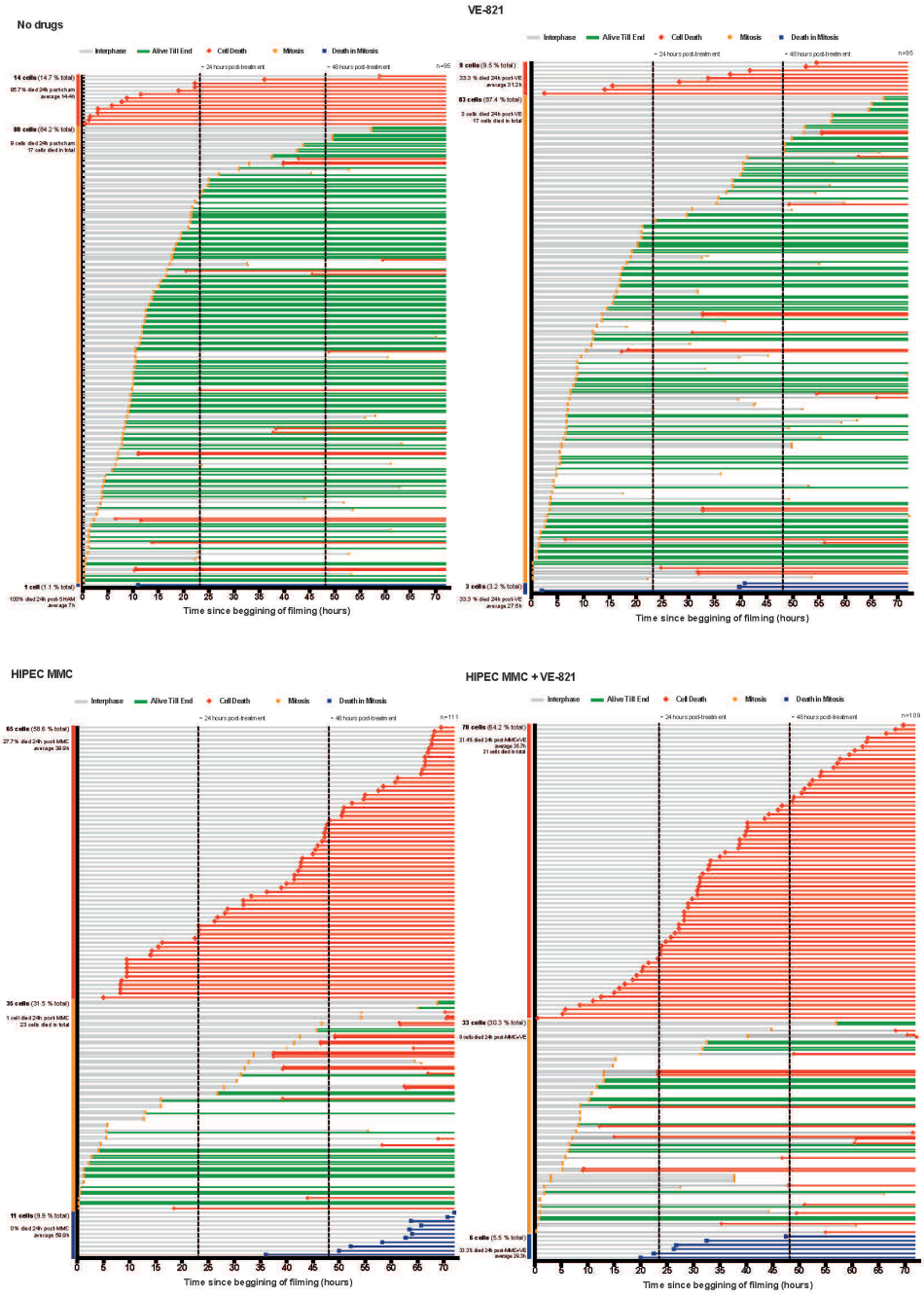

Supplementary Figure 3. Live-cell imaging fate profiles of individual cells in TOR14 organoids treated with no drugs, MMC, ATR inhibitor VE-821 or both.

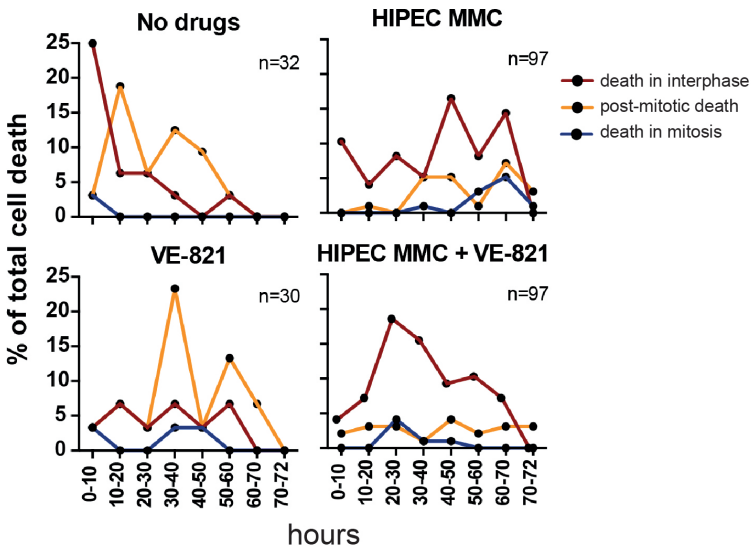

Supplementary Figure 4. Percentage of all cell deaths that occurred in each 10-hour interval after HIPEC, to compare timing of death in interphase, in mitosis and post-mitotic death in the four treatment conditions. The peak of cell death in interphase occurs earlier in co-treatment of MMC + VE-821, compared with MMC alone. N = total number of cell death events

Supplementary Table 1. Clinical and tumor characteristics of the patient-derived PM organoids.

Organoid ID	Location PM	Gender	Age	TNM stage at diagnosis	Location primary tumor	Histology	MSI-status	Neoadjuvant systemic chemotherapy
TOR14	Diaphragm	F	76	T4N2M0	Sigmoid	AC	MMR+	No
TOR17	Omentum	M	83	T4N2M1	Sigmoid	AC	MMR+	No
TOR22	Serosa sigmoid	M	82	T4N2M1	Sigmoid	AC	MMR+	No
TOR10MII	Ventral abdominal wall (mouse model)	F	55	T4N2M1	Sigmoid	MAC	MMR+	No
P02-1	Ascites	M	58	T3N1M0	Hepatic flexure	AC	MMR+	No

AC=adenocarcinoma; MAC=mucinous adenocarcinoma, MMR = mismatch repair, MSI = microsatellite instability, PM=peritoneal metastasis

Supplementary Table 2. Decrease in IC50 by combining MMC with ATR inhibitors.
Estimated fold-decrease in IC50 values across organoids given inhibitor compared to MMC only - MMC-only-reference non-linear mixed models

MMC + 1 uM VE-821		**95% CI**		
	fold decrease in IC50	**lower limit**	**upper limit**	***P* value**
p02-1	2.58	2.07	3.22	<0.0001
TOR10MII	12.39	9.09	16.90	<0.0001
TOR14	8.09	7.10	9.21	<0.0001
TOR17	6.44	5.06	8.19	<0.0001
TOR22	6.96	3.67	13.20	<0.0001
overall	6.38	4.05	10.05	<0.0001

MMC + 100 nM VX-970		**95% CI**		
	fold decrease in IC50	**lower limit**	**upper limit**	***P* value**
TOR14	2.94	2.50	3.47	<0.0001
TOR17	6.89	4.78	9.93	<0.0001
TOR10MII	5.35	3.65	7.84	<0.0001
overall	4.39	2.98	6.48	<0.0001

MMC + 500 nM VX-970		**95% CI**		
	fold decrease in IC50	**lower limit**	**upper limit**	***P* value**
TOR14	16.30	11.55	23.00	<0.0001
TOR17	95.02	27.54	327.80	<0.0001
TOR10MII	40.06	14.43	111.24	<0.0001
overall	36.06	16.78	77.50	<0.0001

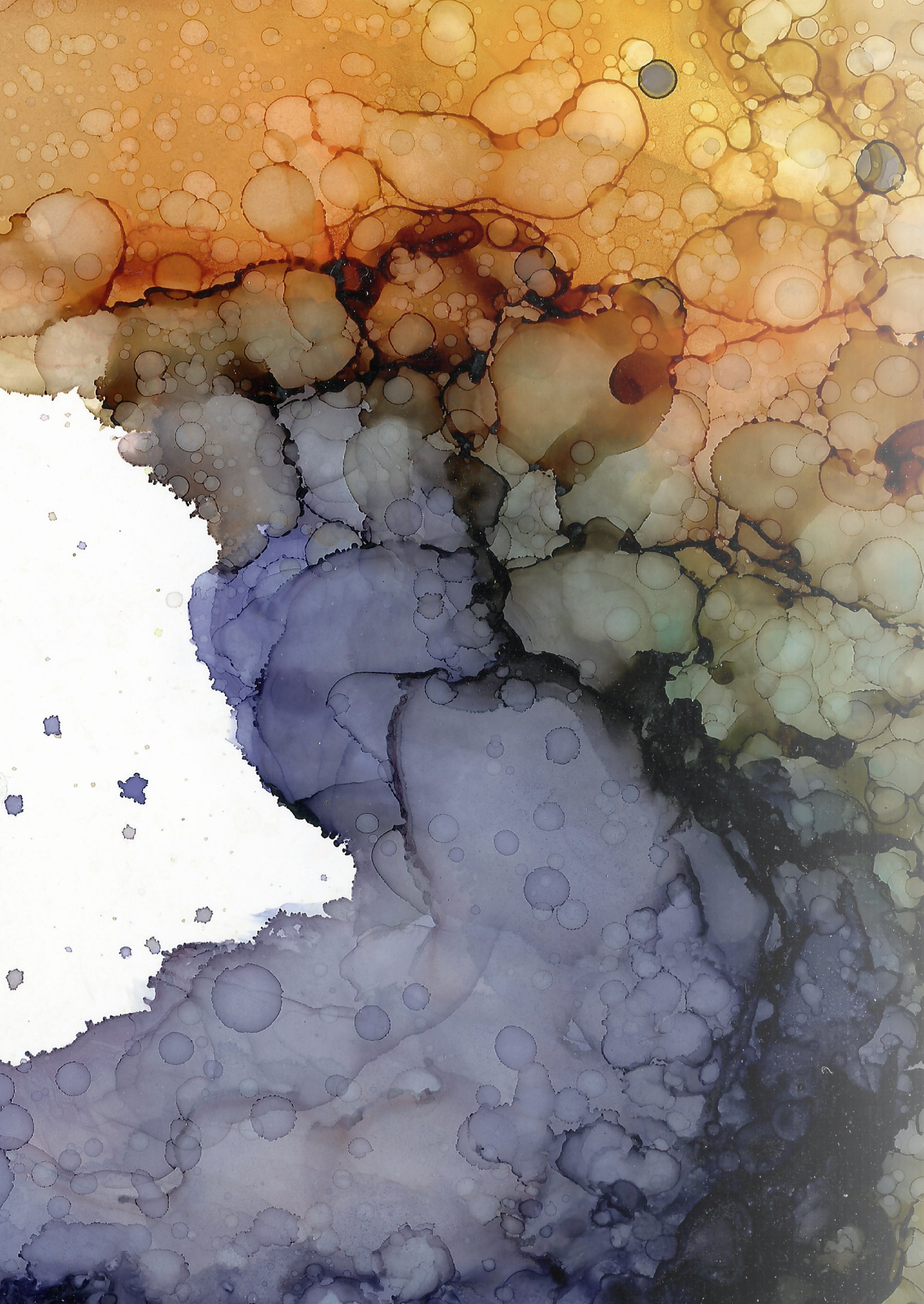

7

Neoadjuvant chemotherapy affects molecular classification of colorectal tumors

Kari Trumpi, Inge Ubink, Anne Trinh, Melika Djafarihamedani, Jennifer M.J. Jongen, Klaas M. Govaert, Sjoerd G. Elias, Sander R. van Hooff, Jan Paul Medema, Miangela M. Lacle, Louis Vermeulen, Inne H.M. Borel Rinkes and Onno Kranenburg

Oncogenesis 2017;6(7):e357

ABSTRACT

The recent discovery of 'molecular subtypes' in human primary colorectal cancer has revealed correlations between subtype, propensity to metastasize and response to therapy. It is currently not known whether the molecular tumor subtype is maintained after distant spread. If this is the case, molecular subtyping of the primary tumor could guide subtype-targeted therapy of metastatic disease. In this study, we classified paired samples of primary colorectal carcinomas and their corresponding liver metastases (n=129) as epithelial-like or mesenchymal-like, using a recently developed immunohistochemistry-based classification tool. We observed considerable discordance (45%) in the classification of primary tumors and their liver metastases. Discordant classification was significantly associated with the use of neoadjuvant chemotherapy. Furthermore, gene expression analysis of chemotherapy-exposed versus chemotherapy naive liver metastases revealed expression of a mesenchymal program in pre-treated tumors. To explore whether chemotherapy could cause gene expression changes influencing molecular subtyping, we exposed patient-derived colonospheres to six short cycles of 5-fluorouracil. Gene expression profiling and signature enrichment analysis subsequently revealed that the expression of signatures identifying mesenchymal-like tumors was strongly increased in chemotherapy-exposed tumor cultures. Unsupervised clustering of large cohorts of human colon tumors with the chemotherapy-induced gene expression program identified a poor prognosis mesenchymal-like subgroup. We conclude that neoadjuvant chemotherapy induces a mesenchymal phenotype in residual tumor cells and that this may influence the molecular classification of colorectal tumors.

INTRODUCTION

Colorectal cancer (CRC) is one of the leading causes of cancer-related mortality. The vast majority of CRC patients die from metastatic disease. At the time of presentation 20–25% of CRC patients already have metastatic disease and an additional ~35% will develop metastases during follow-up.[1-3]

The currently used clinical and pathological parameters have insufficient predictive power to identify the patients who are at risk of developing metastases. Recently, gene expression-based molecular classification studies have identified subgroups of human colon cancer.[4-10] Cross-comparison of these studies subsequently revealed the existence of four consensus molecular subtypes (CMS), which are characterized by differential activity of various signaling pathways.[11] Interestingly, the molecular subtypes also differ in terms of prognosis. Notably, tumors of the 'mesenchymal-like' subtype (CMS4) have a shorter disease-free and overall survival due to higher metastatic potential and relative resistance to chemotherapy- and EGFR-targeted therapy.[11-13] To enable implementation of the novel classification system in clinical practice, we recently developed an immunohistochemistry-based diagnostic test that distinguishes mesenchymal-like cancers from epithelial-like subtypes based on the expression of five markers in tumor cells (HTR2B, FRMD6, ZEB1, CDX2 and pancytokeratin).[12] This test can be used for patient stratification and the development of subtype-directed therapies.

The molecular classification system and the novel diagnostic test are based on the analysis of primary colorectal tumors. It is currently unknown whether molecular subtypes are preserved in metastatic cancer, and whether classification of primary colorectal tumors can guide subtype-targeted therapy for metastatic disease. Dissemination and homing to a different organ environment requires adaptations by cancer cells to survive and proliferate, which could result in altered gene expression patterns. Moreover, neoadjuvant therapy is frequently used to downsize primary (rectal) tumors and liver metastases, and may change the constitution of the tumor bulk and affect gene expression in residual cancer cells.

RESULTS AND DISCUSSION

Neoadjuvant therapy of primary colorectal tumors is associated with a mesenchymal tumor subtype

Paraffin-embedded tissue samples of the resection specimens of paired primary colorectal tumors and corresponding liver metastases were available of 129 patients, and were assembled into a tissue microarray. This cohort solely consists of patients with operable colorectal liver metastases. The tissue microarray is created of the resection specimens of

both tumors of these patients. All patient characteristics are described in Table 1. In brief, the majority was male, had synchronous metastases and a moderately differentiated colon tumor. Tissue microarray sections were subsequently used for analysis of the expression of HTR2B, FRMD6, ZEB1, CDX2 and pancytokeratin by immunohistochemistry, as described previously.[12] After digital analysis of the staining patterns of the primary tumors, 61 tumors were scored as epithelial-like (47.3%) and 68 were scored as mesenchymal-like (52.7%) (Figure 1a). In the current cohort—consisting exclusively of metastasized tumors—the percentage of mesenchymal-like tumors is approximately two-fold higher compared to studies on stage I–IV primary colorectal tumors.[11] This is in line with previous analyses of the mesenchymal phenotype in two large cohorts of metastasized primary colorectal tumors.[12, 14, 15] Mesenchymal-like tumors have a higher risk of recurrence, which explains their enrichment in these cohorts.

Patient and tumor characteristics (including age, gender, onset of disease, invasion depth, lymph node status, Dukes classification and differentiation status) were equally distributed between the two groups of patients with epithelial-like and mesenchymal-like tumors. However, univariate analysis showed differences in tumor localization: mesenchymal-like tumors were more often located in the rectum, whereas epithelial-like tumors were predominantly located in the sigmoid (P=0.020). Furthermore, we found that patients with mesenchymal-like tumors had more frequently received neoadjuvant radiotherapy (P=0.009) and neoadjuvant chemotherapy (P=0.013) compared to patients with epithelial-like tumors (Figure 1b; Table 1). Multivariate analysis identified neoadjuvant chemotherapy as an independent predictor (P=0.012).

As neoadjuvant chemoradiation is mainly administered to patients with rectal cancer, tumor localization could be a confounding factor in the association between chemoradiation and the mesenchymal phenotype. However, rectal cancers treated with neoadjuvant chemo- and/or radiotherapy more often had a mesenchymal phenotype than untreated rectal cancers (71% versus 30%, respectively; P=0.027), indicating that neoadjuvant therapy is a predictor of the mesenchymal phenotype, independent of tumor localization. These findings are in line with previous results showing that posttreatment rectal tumors were mostly classified to the stroma-rich subtype, although that classification was based on stromal parameters.[16]

Mesenchymal-like colorectal tumors (CMS4) have a poorer prognosis compared to the other three CMS.[11] In this cohort, which consists solely of patients with operable metastatic colorectal tumors, a trend of survival disadvantage for mesenchymal-like tumors could be observed (P=0.276, Figure 1c). The hazard ratio after multivariate analysis is 1.441 (95% confidence interval (CI) 0.893–2.325, P=0.134).

Table 1. Patient characteristics.

	all tumors		epithelial-like		mesenchymal-like		
	n=129	(%)	n=61	(%)	n=68	(%)	*p*-value
Age	61.9	(37-83)	62.4	(42-83)	61.5	(37-82)	
Gender							
Female	43	33.3	21	34.4	22	32.4	0.835
Male	86	66.7	40	65.6	46	67.6	
Onset of metastasis							
Synchronous	76	58.9	37	60.7	39	57.4	0.703
Metachronous	53	41.1	24	39.3	29	42.6	
Site of primary tumor							
Right colon	28	21.7	11	18	17	25	0.119
Transverse colon	4	3.1	0	0	4	5.9	
Left colon	13	10.1	7	11.5	6	8.8	
Sigmoid	39	30.2	25	41	14	20.6	
Rectosigmoid	4	3.1	1	1.6	2	2.9	
Rectum	41	31.8	16	26.2	25	36.8	
Unknown	1	0.8	1	1.6	0	0	
Invasion depth							
T2	9	7	6	9.8	3	4.4	0.506
T3	96	74.4	45	73.8	51	75	
T4	22	17.3	10	16.4	12	17.6	
unknown	2	1.6	0	0	2	2.9	
Lymph node status							
N0	49	38	28	45.9	21	30.9	0.206
N1	48	37.2	21	34.4	27	39.7	
N2	29	22.5	11	18	18	26.5	
Unknown	3	2.3	1	1.6	2	2.9	
Dukes classification							
B1	5	3.9	3	4.9	2	2.9	0.733
B2	20	15.5	8	13.1	12	17.6	
C1	1	0.8	0	0	1	1.5	
C2	27	20.9	14	23	13	19.1	
D	75	58.1	36	59	39	57.4	
Unknown	1	0.8	0	0	1	1.5	
Differentiation							
Well	7	5.4	2	3.3	5	7.4	0.752
Well-moderate	2	1.6	1	1.6	1	1.5	
Moderate	78	60.5	37	60.7	41	60.3	
Moderate-poor	8	6.2	3	4.9	5	7.4	
Poor	11	8.5	7	11.5	4	5.9	
Unknown	23	17.9	11	18	11	16.2	
Neoadjuvant Radiotherapy							
Yes	32	24.8	9	14.8	23	33.8	0.009
No	95	73.6	52	85.2	43	63.2	

Table 1. Continued

	all tumors		epithelial-like		mesenchymal-like		
	n=129	(%)	n=61	(%)	n=68	(%)	*p*-value
Neoadjuvant chemotherapy							
Yes	13	10.1	2	3.3	11	16.2	0.013
No	114	88.4	59	96.7	55	80.9	
Unknown	2	1.6	0	0	2	2.9	
Adjuvant chemotherapy							
Yes	45	34.9	20	32.8	25	36.8	0.506
No	81	62.8	41	67.2	40	58.8	
Unknown	3	2.3	0	0	3	4.4	

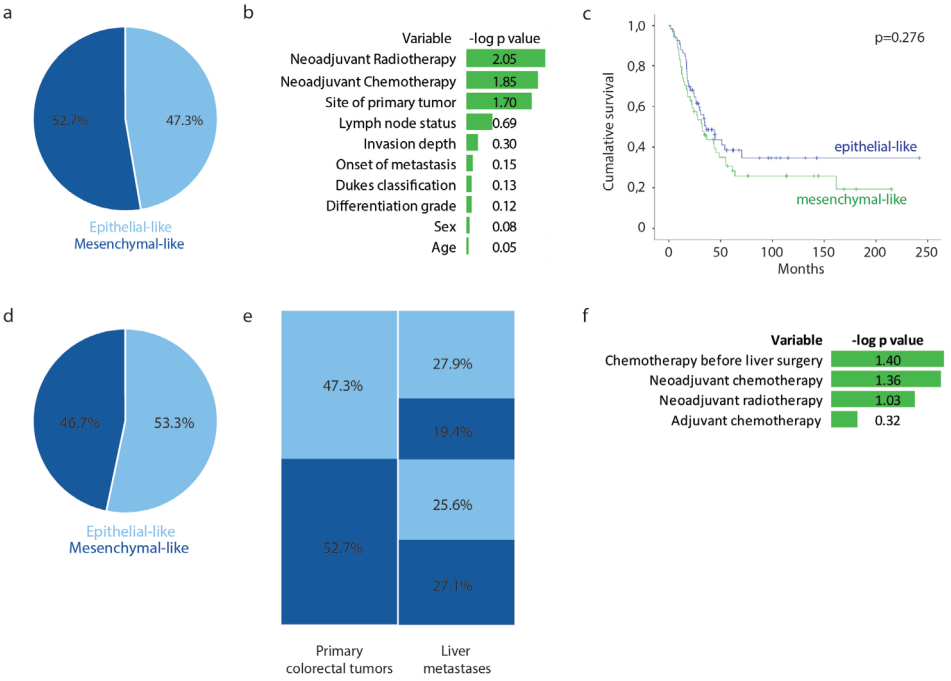

Figure 1. Molecular classification of primary colorectal tumors and corresponding liver metastases.
A tissue microarray (TMA) was constructed from the resection specimens of primary colorectal tumors and liver metastases of 129 patients. Tumor-rich areas were identified via haemotoxylin and eosin stainings and three cores of 0.6 mm were obtained per tumor type. Digital images of immunohistochemically stained TMA slides were created with an Aperio Scanscope XT system (Leica Biosystems, Wetzlar, Germany). Images were automatically analyzed as described previously.[12] Cores with a random forest probability of 60% were scored as 'mesenchymal-like'. Patient subtypes were determined using majority consensus.
(a) Pie chart showing the distribution of epithelial-like and mesenchymal-like classification of the primary colorectal tumors from the paired cohort. (b) Clinical and histopathological characteristics (Table 1) of patients with epithelial-like primary tumors were compared to those of patients with mesenchymal-like tumors. Age was compared using the Wilcoxon rank sum test, for all other variables the Pearson's chi-squared test was used. (c) Kaplan–Meier survival curves showing overall survival after liver resection, calculated with a log- ▶

▶ rank test (P=0.276). The blue line represents the patients with epithelial-like primary colorectal tumors and the green line represents patients with mesenchymal-like primary colorectal tumors. (d) Pie chart showing the distribution of molecular classification of the liver metastases from the paired cohort. (e) Correlation between the classification of primary colorectal tumors and their corresponding liver metastases. (f) Univariate analysis of the influence of various kinds of chemotherapy on discordancy in classification of tumor pairs. Neoadjuvant chemotherapy is treatment given to downsize the tumor, primary or metastases, prior to surgery. Adjuvant chemotherapy is treatment given following resection of the primary colorectal tumor, to prevent outgrowth of metastases. Three groups were compared using Pearson's chi-squared test: concordant classification, discordant with a switch from epithelial-like to mesenchymal-like, and discordant with a switch from mesenchymal-like to epithelial-like; results are depicted as minus log10 P-values.

Discordant molecular classification of primary colorectal tumors and their corresponding liver metastases is associated with neoadjuvant chemotherapy

The immunohistochemical diagnostic test was also applied to the liver metastases of the same patients: 69 metastases were scored as epithelial-like (53.3%) and 60 metastases were scored as mesenchymal-like (46.5%), which roughly corresponds to the subtype distribution of the primary tumors (Figure 1d). However, the classification of primary tumors and the corresponding liver metastases was concordant in only 71 pairs (55% (95% CI 46.3–63.7)), of which 36 were epithelial-like tumors (27.9% (95% CI 20.1–35.8)) and 35 were mesenchymal-like tumors (27.1% (95% CI 19.4–34.9)). Of the 58 discordant tumor pairs (45% (95% CI 36.3–53.7)), 25 primary colorectal tumors that were classified as epithelial-like (19.4% (95% CI 12.5–26.3)) gave rise to liver metastases that were classified as mesenchymal-like, and 33 mesenchymal-like colorectal tumors (25.6% (95% CI 18.0–33.2)) gave rise to epithelial-like liver metastases (Figure 1e). This frequently discordant molecular classification is in contrast with the high concordance that has been reported for mutations in driver genes in primary tumors and the corresponding metastases, for example, *KRAS*, *BRAF* and *PIK3CA*.[17, 18] This finding is important as it indicates that molecular subtyping via immunohistochemistry of primary colorectal tumors cannot simply be extrapolated to classify metastatic disease.

We observed a significant correlation between the administration of chemotherapy prior to tumor resection (neoadjuvant chemotherapy) and discordant classification. More than half of the primary tumors that were exposed to neoadjuvant chemotherapy showed discordant classification of the tumor pairs. In the majority of the cases, this was a switch from a mesenchymal-like primary colorectal tumor, to an epithelial-like liver metastasis, rather than vice versa (P=0.044). Similarly, discordant classification was more common in patients who received chemotherapy prior to resection of liver metastasis compared to those who did not. In these cases a switch from an epithelial-like primary colorectal tumor (not exposed to chemotherapy) to a mesenchymal-like liver metastasis (exposed to chemotherapy) was predominant (P=0.040) (Figure 1f; Supplementary Table 1). These findings suggest that neoadjuvant chemotherapy influences cancer cell biology and drives colorectal tumors toward a more mesenchymal-like phenotype.

Molecular changes in response to chemotherapy have been described for other types of cancer. For example, neoadjuvant treatment in breast cancer is associated with gene expression changes and discordant molecular subtype classification in 38% of the cases.[19, 20] Chemotherapy-induced changes in HER2 status are also frequently observed in breast cancer and have a potential impact on clinical management.[21] Besides chemotherapy, the molecular subtype could also be influenced by the organ microenvironment and/or intra-tumor heterogeneity, and/or heterogeneity between distinct metastases. Indeed, we have recently found that there is extensive subtype heterogeneity among different regions of the same tumor in approximately half of the colorectal tumors analyzed.[22] When selecting patients for subtype-targeted therapies, all factors influencing the tumor subtype should be taken into consideration.

Chemotherapy-surviving tumor cells express a mesenchymal gene signature that identifies aggressive CMS4-like tumors.

To further explore the relationship between neoadjuvant therapy and the mesenchymal phenotype, we classified liver metastases from a previously published data set[23] with the CMS classifier[11]. In this set of liver metastases, we compared chemotherapy-exposed liver metastases to (n=64) chemotherapy naive liver metastases (n=55). Chemotherapy-exposed metastases were more frequently classified as mesenchymal-like compared to the chemotherapy naive liver metastases (33% versus 16%, P=0.06, Figure 2a). In comparison, ~32% of liver metastases exposed to prior treatment in the Khambata-Ford *et al.*[24] cohort were classified as the mesenchymal subtype.[5] In an unbiased approach, we identified all genes that were higher expressed in chemotherapy-exposed liver metastases compared to chemotherapy naive liver metastases (Supplementary Table 2). These genes were used to cluster the primary tumors of two large cohorts into high and low subgroups. The tumor group expressing high levels of these genes was strongly enriched for mesenchymal-type tumors (CMS4) in the CMS-3232 cohort[11] (Figure 2b). These patients had a significantly reduced relapse-free survival probability (Figure 2c).

The vast majority of patients receiving neoadjuvant therapy prior to primary tumor resection are patients with rectal cancer. According to the Dutch guidelines, neoadjuvant chemotherapy in this patient category consists of oral capecitabine, a 5-fluorouracil (5-FU) prodrug, in combination with radiation therapy.[25, 26] To study a potential causal relationship between chemotherapy and mesenchymal gene expression we exposed patient-derived colonospheres to six cycles of 5-FU. RNA was isolated from colonospheres prior to treatment (n=5) and from the surviving tumor cells after the last cycle (n=5). Gene expression profiling revealed that 5-FU treatment resulted in drastic changes in gene expression (Supplementary Table 3), with 68 significantly upregulated genes and 36 significantly downregulated genes ($P<e^{-6}$; Figure 3a). Additionally, we found that expression of the 68

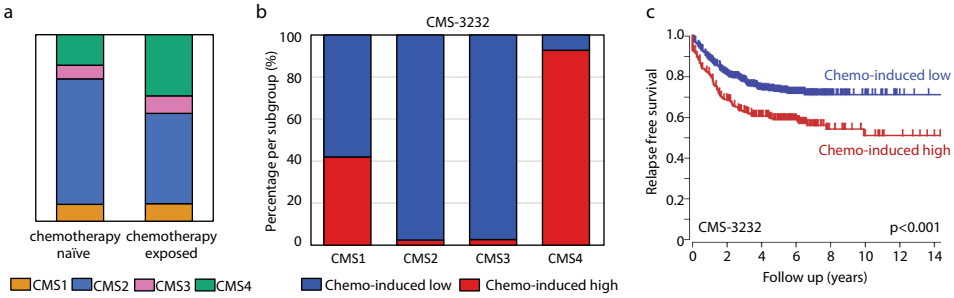

Figure 2. Chemotherapeutic treatment is associated with a mesenchymal tumor phenotype.
(a) Comparison of Consensus Molecular Classification between chemotherapy naïve and chemotherapy exposed colorectal liver metastases from[23]. (b) Genes that were upregulated in chemotherapy exposed liver metastases compared with chemotherapy naïve metastases (chemo-induced genes) were used to cluster the primary tumors of the CMS-3232 cohort into chemo-induced high and low subgroups (K-means option in R2, using a two group separation) based on single gene P-values. These tumors have previously been classified into molecular subtypes.[11] The graphs show the distribution of the CMS subtypes within the chemo-induced high and low subgroups. The chemo-induced high subgroup is enriched for mesenchymal subtypes (CMS4). (c) Kaplan–Meier curves showing the differences in relapse-free survival between the chemo-induced high and low subgroups in the CMS-3232 cohort.

5-FU-induced genes was strongly correlated with the expression of previously published gene sets reflecting a mesenchymal tumor phenotype. These include (i) the core drivers of epithelial–mesenchymal transition, (ii) genes that are upregulated in liver metastases that have previously been exposed to chemotherapy, (iii) genes that are highly expressed in the tumor cell compartment of mesenchymal-like tumors[27] and (iv) genes that are highly expressed in mesenchymal-like colorectal cancer cell lines *in vitro*.[27] By contrast, the 68 5-FU-induced genes showed a strong negative correlation with (i) a gene set reflecting epithelial differentiation, (ii) genes that are highly expressed in the tumor cell compartment of epithelial-like tumors, (iii) genes that are highly expressed in epithelial-like colorectal cancer cell lines *in vitro,* and (iv) the target genes of HNF4a, a master inducer of epithelial differentiation and suppressor of mesenchymal genes[27] (Figure 3b).

To address this further, we used the 68 5-FU-induced genes to cluster the primary colorectal tumors of two large cohorts into two subgroups with high and low expression of the 5-FU-induced genes (K-means). The 5-FU-high groups were strongly enriched for mesenchymal-type tumors (CMS4) in the CMS-3232 cohort[11] (Figure 3c) and had a significantly reduced relapse-free survival probability (Figure 3d). To further assess the relevance of the 5-FU-induced gene set derived from the *in vitro* experiments, we compared its expression to the genes that are upregulated in liver metastases of patients who were exposed to neoadjuvant chemotherapy (Supplementary Table 2). This revealed a strong correlation (R=0.80, P=2.0e^{-110}) between the expression of both independently generated gene sets (Figure 3e). The tumors expressing the highest levels of 5-FU-induced genes (both

the *in vitro*-derived and patient-derived signatures) were enriched in CMS4 (right upper quadrant), indicating that chemotherapy-induced genes are already highly expressed in treatment-naive mesenchymal-like primary colorectal tumors. There are three genes positively identifying mesenchymal tumor in the IHC test: HTR2B, FRMD6 and ZEB1. ZEB1 was not present on the arrays used and could thus not be evaluated. HTR2B and FRMD6 were both expressed to very low levels in this cohort (2log values lower than 4), for which we have no logical explanation. Indeed, in the CMS-3232 data set we observed a strong positive correlation between the chemotherapy-induced gene set and ZEB1, HTR2B and FRMD6, as expected, with ANOVA *P*-values of $3.2e^{-193}$, $6.8e^{-149}$ and $8.8e^{-315}$, respectively.

In this report we show that neoadjuvant therapy can influence molecular classification of primary colorectal tumors and liver metastases. Chemotherapy induces a shift toward a more mesenchymal-like phenotype. These results are in line with previous reports showing the treatment-resistant nature of mesenchymal-like tumors both in colon cancer[13, 28, 29] and other types of cancer.[30] Although chemotherapy has prolonged median overall survival of patients with metastatic CRC from ~6 months to over 2 years, tumor recurrence (almost) always ensues.[14, 31] An in-depth analysis of the phenotype of residual tumor cells following chemotherapy will provide novel targets for therapy targeting residual disease. The results in the present study suggest that CMS4-targeted therapy may not only be effective in the treatment of CMS4-diagnosed tumors, but also in the adjuvant treatment of chemotherapy-surviving tumor residue of other CRC subtypes that gained a mesenchymal-like phenotype.

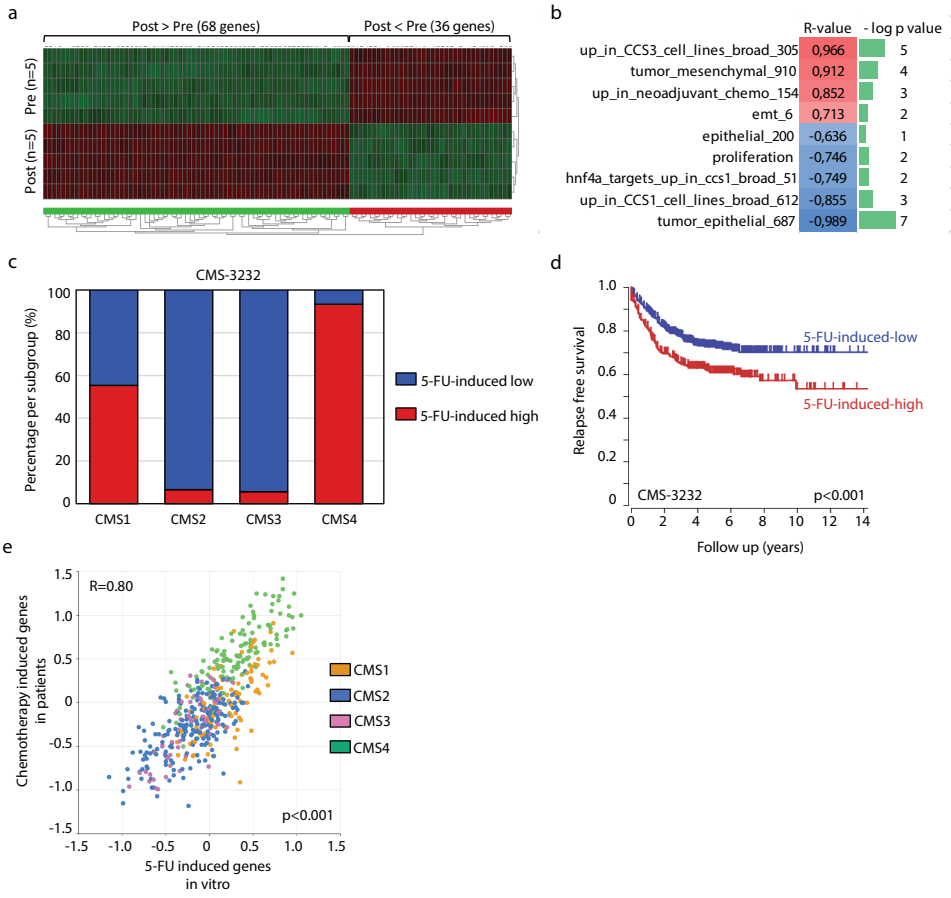

Figure 3. Chemotherapy induces mesenchymal gene expression in patient-derived colonospheres.
(a) Liver metastasis-derived colonospheres were treated with 5-FU for six cycles. RNA was isolated from control (n=5) and 5-FU-treated cells (n=5), and were analyzed by gene expression profiling. The heat map shows all genes that were significantly ($P<e^{-6}$) upregulated (68) or downregulated (36) in post-treatment tumor cells. See Supplementary Table 3 for a full list of genes. (b) Expression of the 5-FU-induced gene set (68 genes) was correlated with gene sets reflecting either an epithelial or a mesenchymal tumor phenotype in the data set of the same experiment. Correlations were assessed by using the 'gene set versus gene sets' option in the R2 genomics analysis and visualization platform. Gene sets reflecting a mesenchymal tumor cell phenotype positively correlate with the 5-FU-induced gene set (indicated in red), while gene sets reflecting an epithelial phenotype show a negative correlation (in blue). The P-values of the correlations are given as minus log10 P-values in green bars. (c) The 68 5-FU-induced genes were used to cluster the tumors of the CMS-3232 cohort into 5-FU-induced high and low subgroups (K-means option in R2, using a two group separation) based on single gene P-values. The graphs show the distribution of the CMS subtypes within the 5-FU-induced high and low subgroups. The 5-FU-induced high subgroup is enriched for mesenchymal subtypes (CMS4). (d) Kaplan–Meier curves showing the differences in relapse-free survival between the 5-FU-high and 5-FU-low subgroups in both cohorts. (e) Expression of the experimental-derived gene set of 5-FU-induced genes was compared to expression of genes upregulated in chemotherapy-exposed liver metastases by using the 'relate 2 tracks' option in the R2 genomics analysis and visualization platform. The XY-plot shows the correlation of the expression of both gene sets (R=0.80, P=2.0e^{-110}) in the CIT subset of the CMS cohort. The CMS subgroups are CMS1: orange, CMS2: blue, CMS3 pink, CMS4: green.

REFERENCES

1. Chau I, Cunningham D. Treatment in advanced colorectal cancer: what, when and how? *Br J Cancer*. 2009;**100**(11):1704-19.
2. Andre T, Boni C, Navarro M, et al. Improved overall survival with oxaliplatin, fluorouracil, and leucovorin as adjuvant treatment in stage II or III colon cancer in the MOSAIC trial. *J Clin Oncol*. 2009;**27**(19):3109-16.
3. Midgley R, Kerr D. Colorectal cancer. *Lancet*. 1999;**353**(9150):391-9.
4. Sadanandam A, Lyssiotis CA, Homicsko K, et al. A colorectal cancer classification system that associates cellular phenotype and responses to therapy. *Nat Med*. 2013;**19**(5):619-25.
5. De Sousa EMF, Wang X, Jansen M, et al. Poor-prognosis colon cancer is defined by a molecularly distinct subtype and develops from serrated precursor lesions. *Nat Med*. 2013;**19**(5):614-8.
6. Oh SC, Park Y-Y, Park ES, et al. Prognostic gene expression signature associated with two molecularly distinct subtypes of colorectal cancer. *Gut*. 2012;**61**(9):1291-8.
7. Marisa L, de Reynies A, Duval A, et al. Gene expression classification of colon cancer into molecular subtypes: characterization, validation, and prognostic value. *PLoS Med*. 2013;**10**(5):e1001453.
8. Roepman P, Schlicker A, Tabernero J, et al. Colorectal cancer intrinsic subtypes predict chemotherapy benefit, deficient mismatch repair and epithelial-to-mesenchymal transition. *Int J Cancer*. 2014;**134**(3):552-62.
9. Schlicker A, Beran G, Chresta CM, et al. Subtypes of primary colorectal tumors correlate with response to targeted treatment in colorectal cell lines. *BMC Med Genomics*. 2012;**5**:66.
10. Budinska E, Popovici V, Tejpar S, et al. Gene expression patterns unveil a new level of molecular heterogeneity in colorectal cancer. *J Pathol*. 2013;**231**(1):63-76.
11. Guinney J, Dienstmann R, Wang X, et al. The consensus molecular subtypes of colorectal cancer. *Nat Med*. 2015;**21**(11):1350-6.
12. Trinh A, Trumpi K, De Sousa EMF, et al. Practical and Robust Identification of Molecular Subtypes in Colorectal Cancer by Immunohistochemistry. *Clin Cancer Res*. 2017;**23**(2):387-98.
13. Song N, Pogue-Geile KL, Gavin PG, et al. Clinical Outcome From Oxaliplatin Treatment in Stage II/III Colon Cancer According to Intrinsic Subtypes: Secondary Analysis of NSABP C-07/NRG Oncology Randomized Clinical Trial. *JAMA Oncol*. 2016;**2**(9):1162-9.
14. Koopman M, Antonini NF, Douma J, et al. Sequential versus combination chemotherapy with capecitabine, irinotecan, and oxaliplatin in advanced colorectal cancer (CAIRO): a phase III randomised controlled trial. *Lancet*. 2007;**370**(9582):135-42.
15. Tol J, Koopman M, Cats A, et al. Chemotherapy, bevacizumab, and cetuximab in metastatic colorectal cancer. *N Engl J Med*. 2009;**360**(6):563-72.
16. Isella C, Terrasi A, Bellomo SE, et al. Stromal contribution to the colorectal cancer transcriptome. *Nat Genet*. 2015;**47**(4):312-9.
17. Mao C, Wu XY, Yang ZY, et al. Concordant analysis of KRAS, BRAF, PIK3CA mutations, and PTEN expression between primary colorectal cancer and matched metastases. *Sci Rep*. 2015;**5**:8065.
18. Han CB, Li F, Ma JT, et al. Concordant KRAS mutations in primary and metastatic colorectal cancer tissue specimens: a meta-analysis and systematic review. *Cancer Invest*. 2012;**30**(10):741-7.
19. Magbanua MJ, Wolf DM, Yau C, et al. Serial expression analysis of breast tumors during neoadjuvant chemotherapy reveals changes in cell cycle and immune pathways associated with recurrence and response. *Breast Cancer Res*. 2015;**17**:73.
20. Klintman M, Buus R, Cheang MC, et al. Changes in Expression of Genes Representing Key Biologic Processes after Neoadjuvant Chemotherapy in Breast Cancer, and Prognostic Implications in Residual Disease. *Clin Cancer Res*. 2016;**22**(10):2405-16.
21. Valent A, Penault-Llorca F, Cayre A, et al. Change in HER2 (ERBB2) gene status after taxane-based chemotherapy for breast cancer: polyploidization can lead to diagnostic pitfalls with potential impact for clinical management. *Cancer Genet*. 2013;**206**(1-2):37-41.
22. Ubink I, Elias SG, Moelans CB, et al. A Novel Diagnostic Tool for Selecting Patients With Mesenchymal-Type Colon Cancer Reveals Intratumor Subtype Heterogeneity. *J Natl Cancer Inst*. 2017;**109**(8).
23. Snoeren N, van Hooff SR, Adam R, et al. Exploring gene expression signatures for predicting disease free survival after resection of colorectal cancer liver metastases. *PLoS One*. 2012;**7**(11):e49442.

24. Khambata-Ford S, Garrett CR, Meropol NJ, et al. Expression of epiregulin and amphiregulin and K-ras mutation status predict disease control in metastatic colorectal cancer patients treated with cetuximab. *J Clin Oncol*. 2007;**25**(22):3230-7.
25. Kacar S, Varilsuha C, Gurkan A, et al. Pre-operative radiochemotherapy for rectal cancer. A prospective randomized trial comparing pre-operative vs. postoperative radiochemotherapy in rectal cancer patients. *Acta Chir Belg*. 2009;**109**(6):701-7.
26. Sauer R, Liersch T, Merkel S, et al. Preoperative versus postoperative chemoradiotherapy for locally advanced rectal cancer: results of the German CAO/ARO/AIO-94 randomized phase III trial after a median follow-up of 11 years. *J Clin Oncol*. 2012;**30**(16):1926-33.
27. Vellinga TT, den Uil S, Rinkes IH, et al. Collagen-rich stroma in aggressive colon tumors induces mesenchymal gene expression and tumor cell invasion. *Oncogene*. 2016;**35**(40):5263-71.
28. Yang AD, Fan F, Camp ER, et al. Chronic oxaliplatin resistance induces epithelial-to-mesenchymal transition in colorectal cancer cell lines. *Clin Cancer Res*. 2006;**12**(14 Pt 1):4147-53.
29. Tato-Costa J, Casimiro S, Pacheco T, et al. Therapy-Induced Cellular Senescence Induces Epithelial-to-Mesenchymal Transition and Increases Invasiveness in Rectal Cancer. *Clin Colorectal Cancer*. 2015.
30. Creighton CJ, Li X, Landis M, et al. Residual breast cancers after conventional therapy display mesenchymal as well as tumor-initiating features. *Proc Natl Acad Sci U S A*. 2009;**106**(33):13820-5.
31. Bendell JC, Bekaii-Saab TS, Cohn AL, et al. Treatment patterns and clinical outcomes in patients with metastatic colorectal cancer initially treated with FOLFOX-bevacizumab or FOLFIRI-bevacizumab: results from ARIES, a bevacizumab observational cohort study. *Oncologist*. 2012;**17**(12):1486-95.

Supplementary Table 1. The influence of (neo-)adjuvant therapy on the classification of paired tumors.

		Concordant n=71	epithelial - mesenchymal n=25	mesenchymal - epithelial n=33	p-value
Primary tumor - Liver metastatis					
Chemotherapy before liver surgery					
	yes	11	10	8	0.04
	no	60	15	25	
Neoadjuvant chemotherapy					
	yes	5	1	7	0.044
	no	66	24	26	
Neoadjuvant radiotherapy					
	yes	21	2	9	0.093
	no	50	23	24	
Adjuvant chemotherapy					
	yes	9	3	7	0.475
	no	62	22	26	

Supplementary Table 2. Differential gene expression (p<0.01) between chemotherapy exposed and chemotherapy naïve liver metastases.

UP in chemotherapy exposed		
Gene	**R-value**	**P-value**
THAP1	0.53	9.57E-06
SEC22A	0.457	7.00E-04
NDUFA13	0.445	1.31E-03
SAR1A	0.444	1.15E-03
PLCD3	0.442	1.12E-03
DHX29	0.442	8.81E-04
CASC4	0.439	9.14E-04
MAS1	0.43	1.23E-03
BCL2L10	0.426	1.40E-03
COQ10B	0.42	1.68E-03
CMTM6	0.418	1.68E-03
MYL6	0.417	1.67E-03
ENY2	0.416	1.71E-03
RP11-884K10,5	0.414	1.71E-03
CANX	0.412	1.76E-03
BLOC1S2	0.411	1.82E-03
KBTBD8	0.41	1.88E-03
TRMT112	0.409	1.88E-03
HPS6	0.408	1.83E-03
MYADM	0.408	1.86E-03
FCER1G	0.406	1.80E-03
TNFAIP8	0.406	1.83E-03
EHD4	0.406	1.78E-03
MRPS16	0.406	1.81E-03
TRAM1	0.405	1.82E-03
MED31	0.405	1.78E-03
SIRT1	0.404	1.79E-03
C1QC	0.403	1.85E-03
RBP2	0.401	1.98E-03
TIGD5	0.4	2.05E-03
DPH3	0.4	2.08E-03
PLEKHO2	0.399	2.10E-03
AC174470,1	0.399	2.08E-03
POP4	0.398	2.11E-03
TMED3	0.398	2.12E-03
DCBLD2	0.395	2.37E-03
C18orf32	0.395	2.32E-03
FEM1B	0.394	2.41E-03
ATP6V0E1	0.391	2.75E-03
ABLIM3	0.391	2.74E-03
MAML1	0.391	2.78E-03
C3orf58	0.388	2.95E-03
TYROBP	0.387	3.10E-03
PEF1	0.387	3.07E-03
ISLR	0.386	3.12E-03
TLR5	0.385	3.17E-03
C8orf83	0.384	3.20E-03
SSPN	0.383	3.22E-03
ZNF432	0.382	3.46E-03
CACNA2D3	0.381	3.48E-03

DOWN in chemotherapy exposed		
Gene	**R-value**	**P-value**
XXbac-BPG154L12,4	-0.468	6.42E-04
AGPAT5	-0.463	6.33E-04
ZNF91	-0.442	9.82E-04
PLA2G6	-0.441	8.35E-04
KBTBD6	-0.437	8.99E-04
RBM11	-0.437	8.53E-04
NPIP	-0.426	1.46E-03
UBAP2L	-0.421	1.77E-03
RHOD	-0.42	1.75E-03
LGTN	-0.42	1.81E-03
AC002115,6	-0.419	1.64E-03
AC068288,1	-0.417	1.66E-03
PNN	-0.415	1.74E-03
SEC16A	-0.413	1.76E-03
RP11-111G23,1	-0.413	1.78E-03
WASF2	-0.413	1.73E-03
D2HGDH	-0.409	1.87E-03
EXOC7	-0.408	1.90E-03
FOXK1	-0.407	1.84E-03
ATG9B	-0.407	1.84E-03
CCDC144A	-0.403	1.85E-03
ZNF202	-0.402	1.94E-03
GPR84	-0.4	2.05E-03
GANAB	-0.398	2.12E-03
PMS2L2	-0.397	2.21E-03
LOXL2	-0.394	2.46E-03
C2orf29	-0.392	2.69E-03
C16orf70	-0.39	2.77E-03
POLE	-0.389	2.86E-03
NCAPD2	-0.388	2.97E-03
SNORD107	-0.388	2.99E-03
ASRGL1	-0.387	3.06E-03
DUSP7	-0.386	3.13E-03
DZIP1L	-0.386	3.13E-03
FNBP4	-0.385	3.14E-03
MAN1A1	-0.384	3.25E-03
SFRS16	-0.384	3.22E-03
CMTM8	-0.384	3.21E-03
MRPL37	-0.382	3.40E-03
SMCR8	-0.382	3.37E-03
ZNF85	-0.381	3.50E-03
UPK3B	-0.38	3.66E-03
DHX15	-0.38	3.60E-03
CCL25	-0.379	3.66E-03
KIAA0907	-0.378	3.73E-03
AC008073,1	-0.377	3.89E-03
CYLC2	-0.376	3.91E-03
PDCL	-0.376	3.93E-03
SNORA48	-0.376	3.95E-03
PRPF4	-0.375	4.08E-03

Supplementary Table 2. Continued

UP in chemotherapy exposed		
Gene	**R-value**	**P-value**
UBE2D2	0.38	3.62E-03
ORMDL2	0.379	3.65E-03
LMOD1	0.379	3.66E-03
SNX11	0.378	3.75E-03
SCYL3	0.378	3.75E-03
PHF23	0.378	3.73E-03
ICOSLG	0.377	3.88E-03
OSGIN2	0.376	3.93E-03
TCEB1	0.375	4.07E-03
C18orf21	0.374	4.11E-03
CCDC90B	0.374	4.12E-03
RNASEH2C	0.374	4.11E-03
DDX50	0.373	4.25E-03
ARRB2	0.373	4.24E-03
DYNLT1	0.373	4.20E-03
ACTR10	0.373	4.21E-03
SCAMP1	0.37	4.39E-03
EHD1	0.37	4.43E-03
PJA2	0.37	4.41E-03
BCL7C	0.369	4.56E-03
MGP	0.368	4.74E-03
CST3	0.367	4.89E-03
SLC15A3	0.367	4.87E-03
SLC17A6	0.367	4.96E-03
CEBPD	0.366	4.96E-03
C11orf10	0.366	4.93E-03
AC138655,6	0.366	4.99E-03
KRT76	0.365	4.98E-03
ELANE	0.365	5.02E-03
C1orf54	0.364	5.11E-03
DCUN1D1	0.364	5.08E-03
ANAPC13	0.364	5.13E-03
PURA	0.363	5.25E-03
SERTAD3	0.363	5.25E-03
TIMM8B	0.363	5.24E-03
MAF1	0.362	5.32E-03
MFSD5	0.361	5.52E-03
MGAT2	0.361	5.61E-03
XRCC3	0.361	5.64E-03
SPG21	0.36	5.76E-03
MGST3	0.36	5.73E-03
COX7A1	0.36	5.75E-03
AARSD1	0.36	5.72E-03
TNS1	0.359	5.90E-03
NDUFB1	0.359	5.89E-03
KPNA4	0.359	5.81E-03
UBTD2	0.358	5.94E-03
CNBP	0.358	5.95E-03
ATP5H	0.358	6.09E-03
GPR52	0.357	6.09E-03
CCNJ	0.357	6.13E-03
SERTAD1	0.356	6.28E-03

DOWN in chemotherapy exposed		
Gene	**R-value**	**P-value**
DNASE1	-0.375	4.06E-03
RAB3GAP2	-0.374	4.08E-03
SLC25A3	-0.373	4.26E-03
DNMBP	-0.372	4.23E-03
CHCHD3	-0.372	4.20E-03
NNT	-0.371	4.40E-03
AC139530,1	-0.371	4.41E-03
CAMP	-0.371	4.41E-03
AC020915,1	-0.371	4.41E-03
HMBOX1	-0.371	4.41E-03
TMEM212	-0.37	4.43E-03
ERAL1	-0.369	4.62E-03
RP1-90K10,3	-0.368	4.76E-03
XXyac-R12DG2,2	-0.367	4.94E-03
LUC7L	-0.366	4.95E-03
TNFRSF10B	-0.366	5.00E-03
C3orf49	-0.366	4.93E-03
CLC	-0.365	5.05E-03
CELSR3	-0.365	5.01E-03
UBE2I	-0.365	5.00E-03
CWC25	-0.364	5.09E-03
PITRM1	-0.364	5.11E-03
AC015871,1	-0.364	5.07E-03
SNAPC4	-0.363	5.25E-03
CPT2	-0.362	5.37E-03
AC018696,2	-0.361	5.60E-03
AL669831,1	-0.36	5.76E-03
EXOSC5	-0.358	5.98E-03
POLD2	-0.358	5.96E-03
ATP4A	-0.357	6.09E-03
SRSF1	-0.357	6.17E-03
XRCC2	-0.357	6.11E-03
GMNN	-0.357	6.07E-03
ZFP42	-0.357	6.07E-03
TMEM8B	-0.356	6.26E-03
OGFOD2	-0.356	6.12E-03
INSL3	-0.356	6.15E-03
YTHDC1	-0.356	6.28E-03
TUBE1	-0.355	6.31E-03
C8B	-0.355	6.27E-03
PARP6	-0.355	6.32E-03
AC008268,3	-0.355	6.29E-03
SUGP2	-0.354	6.31E-03
RP11-163O17,1	-0.353	6.53E-03
TIA1	-0.353	6.51E-03
RBP5	-0.353	6.52E-03
KIAA0556	-0.352	6.85E-03
AMPD2	-0.352	6.88E-03
KARS	-0.351	6.91E-03
GABRE	-0.351	7.12E-03
SFRS18	-0.35	7.30E-03
SLC30A5	-0.349	7.28E-03

Supplementary Table 2. Continued

UP in chemotherapy exposed		
Gene	**R-value**	**P-value**
RAF1	0.356	6.26E-03
HNRNPF	0.355	6.28E-03
RRAS	0.355	6.29E-03
THAP11	0.355	6.30E-03
NOL6	0.355	6.27E-03
NDUFB8	0.355	6.28E-03
ARF6	0.354	6.49E-03
ZBBX	0.354	6.31E-03
EXOSC4	0.354	6.33E-03
NDUFA2	0.353	6.66E-03
TMEM176B	0.353	6.54E-03
PTPN18	0.352	6.65E-03
RP11-187C18,3	0.352	6.64E-03
HK1	0.351	7.10E-03
CORO1B	0.35	7.24E-03
RABAC1	0.35	7.32E-03
MRPS28	0.35	7.19E-03
STAT2	0.35	7.28E-03
LHFPL2	0.35	7.27E-03
DUSP4	0.349	7.26E-03
DYNC1H1	0.349	7.30E-03
SNAP23	0.349	7.42E-03
GLIS2	0.348	7.44E-03
SKP1	0.348	7.48E-03
TNKS1BP1	0.346	7.98E-03
RP4-761I2,2	0.346	7.88E-03
GLIPR1	0.346	7.92E-03
TMEM50B	0.345	8.33E-03
SOX18	0.345	8.34E-03
AC091196,1	0.344	8.55E-03
SSR3	0.343	8.66E-03
RBP7	0.343	8.66E-03
CESK1	0.343	8.61E-03
C6orf72	0.343	8.62E-03
EXOC6	0.342	9.00E-03
PTPRA	0.341	9.32E-03
TBCB	0.341	9.27E-03
VPS4B	0.341	9.31E-03
CR2	0.34	9.37E-03
U47924,1	0.34	9.32E-03
TRMT61A	0.34	9.54E-03
STARD3NL	0.339	9.77E-03
THTPA	0.339	9.77E-03
RASSF8	0.339	9.75E-03
FBXO8	0.339	9.70E-03
MARK2	0.339	9.78E-03
ADAM29	0.339	9.70E-03
C11orf73	0.339	9.73E-03
DARC	0.338	9.76E-03
EPB41L1	0.338	9.79E-03
GMFB	0.338	9.81E-03
CYP1B1	0.338	9.78E-03

DOWN in chemotherapy exposed		
Gene	**R-value**	**P-value**
TIGD1L	-0.349	7.28E-03
OR8D1	-0.349	7.30E-03
ASCL1	-0.348	7.51E-03
NR0B2	-0.348	7.47E-03
CIDEB	-0.348	7.48E-03
XRCC5	-0.348	7.41E-03
USP24	-0.347	7.77E-03
NOP2	-0.347	7.65E-03
LHB	-0.347	7.74E-03
KNTC1	-0.346	7.93E-03
ACTR2	-0.346	7.89E-03
SIN3B	-0.345	8.13E-03
TCP11L1	-0.345	8.35E-03
RRP1B	-0.345	8.29E-03
CEACAM3	-0.344	8.45E-03
TRIM56	-0.344	8.50E-03
C3orf30	-0.344	8.50E-03
SNAPC1	-0.343	8.58E-03
GNAZ	-0.343	8.59E-03
TRMT2B	-0.343	8.64E-03
ACO1	-0.342	8.91E-03
HSPA8	-0.342	8.91E-03
C9	-0.341	9.26E-03
MYSM1	-0.341	9.24E-03
PAN2	-0.341	9.27E-03
AC145146,1	-0.34	9.55E-03
WASH4P	-0.34	9.35E-03
TAOK1	-0.339	9.67E-03
TMTC2	-0.339	9.73E-03
LYL1	-0.338	9.79E-03
ARGLU1	-0.338	9.78E-03
WDR85	-0.338	9.78E-03
GALNT3	-0.338	9.76E-03
LARP1	-0.338	9.80E-03
KRT15	-0.337	9.96E-03
AL133153,1	-0.337	9.95E-03
PSG8	-0.337	9.98E-03

Supplementary Table 3. Differential gene expression (p<e^-6) between 5-FU treated colonospheres and untreated colonospheres.

UP after 5-FU		
Gene	**R-value**	**p-value**
APOBEC3B	-0.999	4.95E-08
BECN1	-0.999	5.53E-08
HIST1H2BD	-0.999	3.93E-08
HIST1H2AC	-0.999	3.23E-08
KRT23	-0.999	6.05E-08
ATL3	-0.999	6.02E-08
DNTTIP1	-0.999	3.80E-08
IFRD1	-0.998	9.21E-08
HDAC9	-0.998	5.61E-08
HIST1H4H	-0.998	2.01E-07
UCA1	-0.998	2.01E-07
RUNX2	-0.998	1.21E-07
LINC00525	-0.997	2.46E-07
ANXA1	-0.997	3.33E-07
RANBP9	-0.997	3.97E-07
GULP1	-0.997	3.42E-07
SCGB2A1	-0.997	3.86E-07
HIST1H2BE	-0.997	2.81E-07
DEGS1	-0.997	4.03E-07
PHLDA1	-0.997	4.08E-07
HSPB8	-0.997	4.06E-07
TBC1D23	-0.997	4.06E-07
MAP3K2	-0.997	3.92E-07
SAMD9	-0.997	3.57E-07
GJA3	-0.997	3.20E-07
PEA15	-0.996	5.12E-07
GPNMB	-0.996	5.83E-07
SLC20A1	-0.996	5.99E-07
TJP1	-0.996	6.11E-07
ARL4C	-0.996	5.44E-07
GEM	-0.996	4.44E-07
C10orf10	-0.996	5.15E-07
AKAP12	-0.996	5.10E-07
BIRC3	-0.996	4.50E-07
CAV1	-0.996	4.96E-07
LYZ	-0.996	5.21E-07
MOSPD1	-0.996	4.96E-07
PDP1	-0.996	4.59E-07
ETS1	-0.996	4.92E-07
CREBRF	-0.996	5.58E-07
TNFRSF10D	-0.996	4.76E-07
SDR16C5	-0.996	5.79E-07
EPAS1	-0.995	8.12E-07
CYR61	-0.995	7.51E-07
PLK2	-0.995	6.55E-07
KLF10	-0.995	7.53E-07
CXCL8	-0.995	9.15E-07
FAM50A	-0.995	7.43E-07

DOWN after 5-FU		
Gene	**R-value**	**p-value**
PHB2	0.994	9.79E-07
PDXK	0.994	9.60E-07
FAH	0.994	9.51E-07
GMDS	0.994	9.55E-07
SLCO1B3	0.994	9.63E-07
PIR	0.994	9.60E-07
HIBCH	0.994	9.63E-07
DCPS	0.994	9.69E-07
GALNT12	0.994	9.44E-07
EBPL	0.994	9.68E-07
HSD17B4	0.995	8.27E-07
AKR1A1	0.995	9.07E-07
SNRPD1	0.995	8.02E-07
ABCB6	0.995	7.46E-07
ATP2C2	0.995	9.14E-07
NDUFAF3	0.995	8.26E-07
SUCLG1	0.995	7.35E-07
ECI2	0.995	6.43E-07
SSR3	0.995	8.17E-07
ST6GALNAC1	0.995	7.93E-07
CYC1	0.996	5.53E-07
GBAS	0.996	5.60E-07
ASL	0.996	4.98E-07
CLNS1A	0.996	4.39E-07
NDUFS4	0.996	5.45E-07
REG4	0.996	4.46E-07
C8orf59	0.996	5.02E-07
MVB12A	0.996	5.98E-07
UGT1A6	0.996	4.89E-07
ETHE1	0.997	3.41E-07
ACAT1	0.997	3.69E-07
AGR2	0.997	3.91E-07
SLC18B1	0.997	4.04E-07
AKR1B10	0.998	5.44E-08
ADH5	0.998	1.04E-07
RNPEP	0.999	3.77E-08

Supplementary Table 3. Continued

UP after 5-FU		
Gene	**R-value**	**p-value**
EMP3	-0.995	7.60E-07
MMP7	-0.995	7.46E-07
SPINK1	-0.995	8.56E-07
MDK	-0.995	7.86E-07
MAX	-0.995	7.45E-07
FEM1C	-0.995	8.99E-07
SELENBP1	-0.995	6.63E-07
FGD6	-0.995	6.61E-07
ELK3	-0.995	8.10E-07
PMEPA1	-0.995	6.45E-07
CARD6	-0.995	8.06E-07
ZFAND2A	-0.995	8.17E-07
RAB30	-0.995	7.57E-07
TNFSF15	-0.995	8.18E-07
ALDH1A3	-0.994	9.74E-07
CREM	-0.994	9.99E-07
RRAGC	-0.994	9.44E-07
RNF111	-0.994	9.11E-07
PGM2L1	-0.994	9.87E-07
KRT80	-0.994	9.16E-07

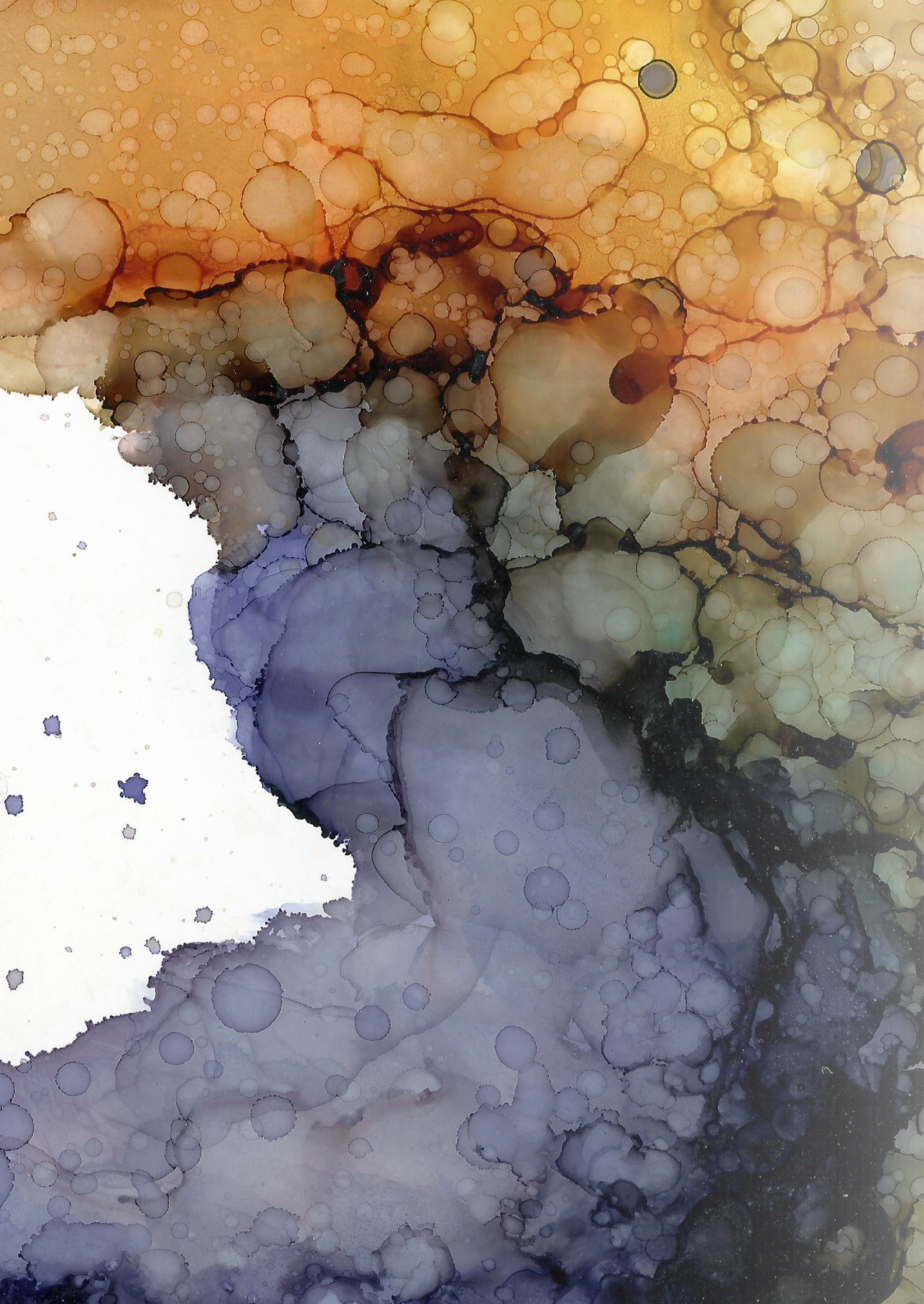

8

Resection of colorectal liver metastases after long-term chemotherapy

Inge Ubink, Boris Galjart, Mara Z. Meulendijks, Jan Willem van Wijnbergen, I. Quintus Molenaar, Onno Kranenburg, Cornelis Verhoef, Inne H.M. Borel Rinkes, Dirk J. Grünhagen and Jeroen Hagendoorn

Submitted

ABSTRACT

Background

Induction chemotherapy followed by liver resection improves the prognosis of metastatic colorectal cancer patients. The aim of this study was to determine whether patients with stable disease or partial response to long-term chemotherapy without downsizing intent, benefit from hepatectomy.

Methods

From prospective databases, 101 patients were identified who underwent surgery after long-term chemotherapy (defined as >6 cycles of CAPOX or irinotecan, >8 cycles of FOLFOX, or >6 months of chemotherapy) from 2000-2016.

Results: Ten patients proved to be inoperable during surgery and 23 patients had residual intra- or extrahepatic disease after surgery. Median disease-free survival (DFS) of the 68 patients without signs of residual disease after resection was 7.6 months (95% confidence interval [CI] 4.5-10.7 months). A subset of these patients (11/68) showed DFS exceeding 3 years. Median overall survival (OS) after surgery was 32.6 months (95% CI 24.7-40.4 months). Patients with residual disease after liver surgery had a significantly shorter median OS (17.1 months versus 41.5 months, $p<0.001$).

Discussion

Although DFS was generally short, a subgroup of patients seemed to benefit from surgery. Based on OS results, liver resection should not be performed if not all macroscopic disease can be resected.

INTRODUCTION

Liver resection extends survival for patients with colorectal liver metastases (CRLM), and offers a chance of cure.[1, 2] Unfortunately, the majority of patients with CRLM are not direct candidates for resection. Preoperative induction chemotherapy can result in downsizing of metastases, rendering 20-40% of initially irresectable metastases resectable, depending on the treatment regimen.[3-5] Although survival of patients after conversion chemotherapy is worse compared with survival of patients with primarily resectable disease, it surpasses outcome after chemotherapy alone.[6] Short intensive induction chemotherapy is recommended for downsizing, since maximal response is expected within four months of therapy.[5, 7, 8] Even if first-line chemotherapy fails due to lack of response or toxicity, second-line chemotherapy and subsequent resection of CRLM can yield a significant survival benefit.[9] If disease is considered too extensive and resection is deemed unachievable, the chemotherapeutic treatment goal shifts from maximum tumor shrinkage to disease control.[7] Yet some patients show partial response after a prolonged period of chemotherapeutic treatment and could be candidates for surgery. Furthermore, patients with substantial extrahepatic disease are often considered inoperable, but if the lesions remain stable in the long run, liver surgery might be considered.[10] These patients are occasionally referred to tertiary hepatobiliary surgery centers for evaluation of treatment options. Hepatectomy is considered in these scenario's because it would allow discontinuation of chemotherapy. The risk of this strategy is that chemotherapy withdrawal might cause (earlier) reactivation of dormant metastases elsewhere. In this study, we describe outcomes of hepatectomy in a Dutch patient population who had undergone previous long-term systemic therapy. The aim of this retrospective study was to determine whether patients who received such long-term systemic therapy (defined as >8 cycles of FOLFOX or >6 cycles CAPOX/Irinotecan) benefited from liver surgery.

METHODS

Patient selection

Patients were identified from prospective databases at University Medical Center Utrecht and Erasmus MC Rotterdam, two tertiary oncological referral centers in the Netherlands. Patients who underwent liver resection after long-term chemotherapy from January 2000 to December 2016 were selected for this study. "Long-term chemotherapy" was defined as more than six cycles of CAPOX or irinotecan, or more than eight cycles of FOLFOX therapy. If the exact number of treatment cycles was unknown, chemotherapy for a duration exceeding 6 months was considered long-term. Chemotherapy was mostly administered

at other hospitals before referral to tertiary centers, and treatment decisions were made there. Referring hospitals were contacted for any missing data on the type of treatment or number of cycles. Response to chemotherapy was evaluated with computed tomography according to Response Evaluation Criteria in Solid Tumors (RECIST) [10].

Hepatic resection

Prior to surgery, all patients were discussed in multidisciplinary team (MDT) meetings at the tertiary centers, involving surgeons, medical oncologists, radiologists and pathologists. Resectability was defined as the ability to surgically remove all visible liver metastases with tumor-free margins while preserving adequate future liver remnant volume (FLRV) with sufficient vascular supply and biliary drainage.[1] Hepatic resection was performed as described previously.[11] Major hepatectomy was defined as resection of 4 or more liver segments.[12] Resection margins were assessed by a pathologist, with R0 denoting that all resection surfaces were free of tumor, R1 that there was microscopic invasion of the resection margin, and R2 that the resection was macroscopically not radical. Postoperative complications were graded according to the Clavien-Dindo classification[13]; only complications that occurred before first hospital discharge were recorded. Postoperative mortality rate was assessed at 90 days after surgery.

Survival

Disease-free survival (DFS) was calculated from date of hepatic resection to date of first recurrence detected with radiological imaging or death. Overall survival (OS) was calculated from start of chemotherapy and from hepatic resection to death. Post-recurrence survival (PRS) was calculated from date of first recurrence to date of death. If there were no events, patients were censored at last follow-up. Hepatectomy was considered 'not globally curative' if not all intrahepatic lesions were resected or ablated, if extrahepatic disease was not resected or if the primary tumor was still in situ. Patients for whom hepatectomy was not globally curative were excluded from the DFS analyses but included in the OS analyses.

Statistics

Statistical analyses were performed with SPSS 24 (IBM SPSS, Chicago, IL). Discrete or categorical data were compared with Pearson chi-square test. DFS and OS curves were generated using the Kaplan-Meier method; differences between survival curves were assessed by log rank test. A level of $P < .05$ was considered statistically significant.

RESULTS

Patient and Oncologic Characteristics

In the study period, 101 patients were considered for surgery after long-term chemotherapy. Clinical characteristics of the study population are presented in Table 1. Patients received a median of 10 cycles of chemotherapy during a median of 8 months. Most patients were treated with a single line of therapy, but 18% received two or more lines of therapy due to toxicity or lack of response to first-line treatment. In the first line, doublet regimens were most commonly (87%) administered. These were often oxaliplatin-based (90%) rather than irinotecan-based (10%). Monotherapy with capecitabine or 5-FU/LV was given to 7% of patients, and only 2% of patients received triplet regimens in the first line. A detailed description of treatment regimens can be found in Table 2. Objective response to upfront chemotherapy was observed in 75% of patients.

Surgical outcomes

Median time from the last chemotherapy cycle to surgery was 1.9 months (interquartile range (IQR) 1.2-2.7). Of the 101 patients who went for surgery, ten patients proved to be inoperable during exploratory surgery, either due to the unanticipated presence of extrahepatic metastases (peritoneal metastases or lymph node metastases in hepatoduodenal ligament), or due to more extensive intra-hepatic disease than judged pre-operatively, or both. These patients were excluded from further analyses (Figure 1).

Details on surgical procedures are shown in Table 3. Cancer resection was not complete in 23 of the 91 operated patients (25%) (Figure 1). Of the fourteen patients scheduled for two-stage liver resection, nine patients could not undergo a second procedure, either due to development of lung metastases (n=3), progression of intrahepatic disease (n=4), or both (n=2). In eight patients who underwent a liver-first procedure, the primary tumor was eventually not resected due to disease progression in the meantime. Six patients had extrahepatic disease at other sites that was not resected (Figure 1). Major postoperative complications (Clavien-Dindo grades III to V) occurred in 14% of patients, and were more common after major resection (27% vs. 5% after minor resection, Pearson Chi-Square p=0.007). Postoperative mortality was 1%.

Table 1. Oncologic details.

Patient and tumor characteristics	**n=101**
Age in years, median [IQR]	61 [54-67]
Sex ratio (M:F)	55:46
Physical status[a]	
ASA 1, n (%)	32 (35)
ASA 2, n (%)	54 (59)
ASA 3, n (%)	6 (7)
Location primary tumor	
Right colon, n (%)	20 (20)
Left colon, n (%)	37 (37)
Rectum, n (%)	43 (43)
Double tumor, n (%)	1 (1)
pT category[b]	
pyT0, n (%)	5 (6)
pT1, n (%)	0 (0)
pT2, n (%)	6 (7)
pT3, n (%)	60 (74)
pT4, n (%)	10 (12)
pN category[c]	
pN0, n (%)	20 (25)
pN1, n (%)	34 (43)
pN2, n (%)	26 (33)
Metastases	
Synchronous, n (%)	85 (84)
Metachronous, n (%)	16 (16)
Number of liver metastases, median [IQR][d]	4 [2-5]
Chemotherapy	
Duration of chemotherapy in months, median [IQR][e]	8.1 [5.7-13.7]
Lines of chemotherapy	
One line, n (%)	83 (82)
Two lines, n (%)	10 (10)
Three or more lines, n (%)	8 (8)
Response to last line of chemotherapy[f]	
Complete response, n (%)	1 (1)
Partial response, n (%)	72 (74)
Stable disease, n (%)	18 (19)
Progressive disease, n (%)	6 (6)

IQR = interquartile range. a) data available from 92/101 patients. b) data available from 81/86 patients (primary tumor not resected n=15). c) data available from 80/86 patients (primary tumor not resected n=15). d) data available from 99/101 patients. e) start and stop date of chemotherapy available from 85/101 patients. f) data available from 97/101 patients.

Table 2. Chemotherapy regimens.

	1st line (n=101)	2nd line (n=18)	3rd line (n=8)
5-FU+LV or capecitabine single	7	1	0
Oxaliplatin-based	81	1	3
Irinotecan-based	10	15	0
Oxaliplatin + irinotecan-based	2	0	0
Anti-VEGFR or anti-EGFR antibody monotherapy	1	0	3
Other chemotherapy	0	1	2
Anti-VEGFR antibody in combination with chemotherapy	52	4	0
Anti-EGFR antibody in combination with chemotherapy	2	0	1

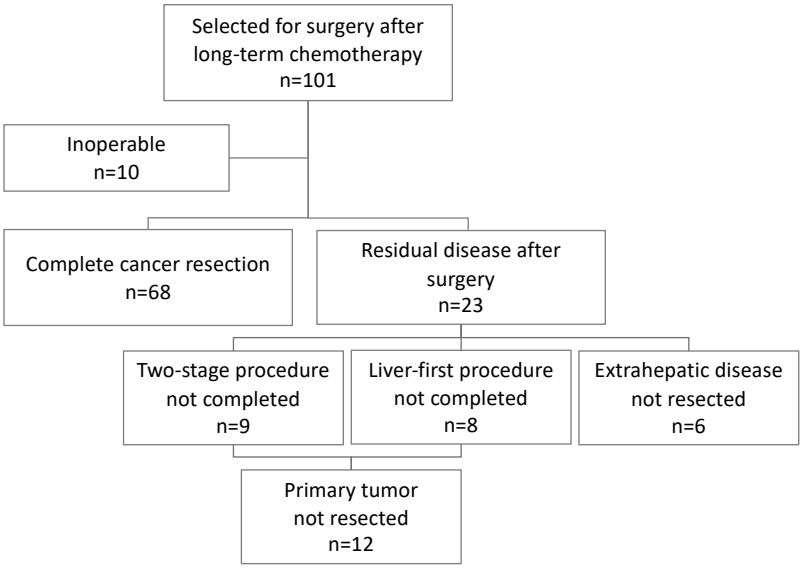

Figure1. Flow chart of surgical outcomes.

Oncological outcomes

Median follow-up after start of chemotherapy was 41.2 months (IQR 29.0-74.2 months), median follow-up after hepatectomy was 28.6 months (IQR 15.6-56.1 months). Median DFS of patients without signs of residual disease (n=68) was 7.6 months (95% confidence interval [CI] 4.9-10.3 months). A subset of patients (11/68) showed prolonged DFS exceeding 3 years (Figure 2a). Of the 56 patients with recurrence during follow-up, the first location of recurrence was intrahepatic in 23 patients, extrahepatic in 20 patients, and 13

Table 3. Surgical details.

Surgical characteristics	**n=91**	
Portal vein embolization, n (%)	9 (10)	
Combined primary + liver resection, n (%)	8 (9)	
Liver-first procedure, n (%)	24 (26)	
Local ablation only, n (%)	5 (5)	
Hepatectomy, n (%)	86 (95)	
Major liver resection, n (%)		30 (35)
Concomitant radiofrequent ablation, n (%)		30 (35)
Resection margins R0, n (%)		66 (77)
Resection margins R1, n (%)		20 (23)
Incomplete cancer resection, n (%)	23 (25)	
Primary tumor not resected, n (%)		12 (52)
Residual intrahepatic disease, n (%)		9 (39)
Extra-hepatic disease not resected, n (%)		12 (52)
Hospital stay in days, median [IQR]	8 [5-10]	
Postoperative complications grade ≥3, n (%)[a]	11 (14)	
90-day postoperative morbidity, n (%)	1 (1)	

a) data available from 78/91 patients, IQR = interquartile range

patients showed both intra- and extrahepatic disease. Patients with both intra- and extrahepatic disease had poorer PRS compared with the other two groups (Figure 2b).

Median OS from the start of upfront chemotherapy was 45 months (95% confidence interval [CI] 35.9-54.2 months, Figure 2c). After hepatectomy, median OS was 32.6 months (95% CI 24.7-40.4 months), with 1-year OS of 89%, 3-year OS of 45%, and 5-year OS of 27%. Patients who did not undergo complete resection of all tumor lesions (i.e. intra- or extrahepatic residual disease, or primary tumor in situ) had a significantly shorter median OS (17.1 months; 95% CI 8.2-26.0 months) compared with patients without signs of residual disease (41.5 months; 95% CI 27.0-55.9 months), as shown in Figure 2d.

DISCUSSION

The patient population presented here consists largely of patients who were treated with palliative intent but who achieved response or stable disease after long-term chemotherapy. This patient group includes patients who were initially deemed to have irresectable disease, either due to extensive liver involvement that later partially responded, or due to extrahepatic disease that was considered a contraindication for

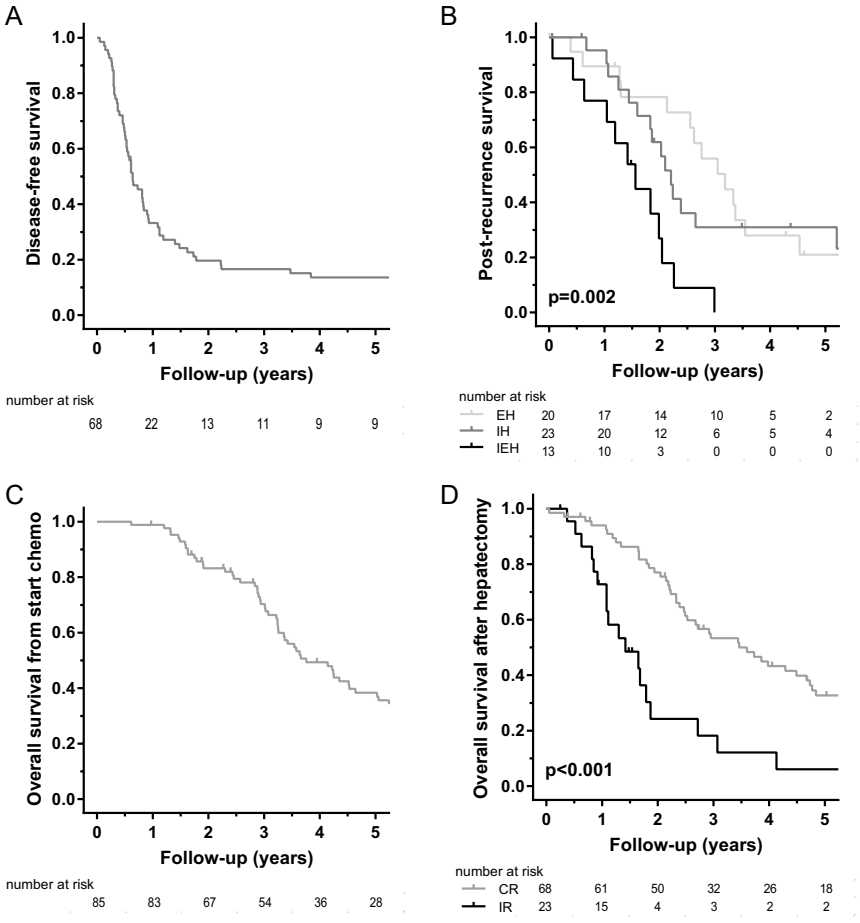

Figure 2. Oncologic outcomes.
(a) Disease-free survival of patients with no clinical signs of residual disease after hepatectomy. (b) Post-recurrence survival of patients with recurrent disease after clinically complete resection (EH=extrahepatic, IH = intrahepatic, IEH=intra- and extrahepatic disease as first recurrence location). (c) Overall survival from start of upfront chemotherapy (start date available from 85/91 patients). (d) Overall survival of patients with no signs of residual disease after hepartectomy compared with patients with incomplete cancer resection (CR=complete resection, IR=incomplete resection).

hepatectomy but which remained stable in the long run. The cohort further includes patients whose disease was deemed resectable only after eventual referral to tertiary institutions. These subgroups have in common that metastatic disease was treated systemically for a long time, theoretically predisposing these patients to high risk of (distant) recurrence, due to continuous dissemination of tumor cells, or enrichment of unfavorable molecular CRC subtypes.[14] Previous studies have shown a survival benefit

from resection of CRLM primarily after treatment schedules with downsizing intent, even after second-line chemotherapy.[3, 4, 9] For the overarching patient group presented here, it needs to be determined whether surgery can still provide clinical benefit.

Despite the high number of pre-operative chemotherapy cycles, post-operative outcomes were favorable in this study, with 14% major morbidity and 1% mortality. DFS was generally short, and disease recurrence in the remaining liver lobes was common. In a subset of patients, however, long-term recurrence-free survival was observed. Furthermore, despite the short DFS, resection resulted in a positive median OS of 41 months in patients who had undergone complete cancer resection. This was comparable to the outcome of patients who underwent hepatectomy after second-line chemotherapy with downsizing intent.[9] In contrast, this study also contained a considerable subgroup of patients with residual disease after surgery. These patients had a significantly worse OS compared to patients without residual disease, suggesting that hepatectomy might not be the preferred treatment option in these patients. Worse survival after failed two-stage liver resection and liver-first procedures was also observed in recent studies.[15, 16]

Furthermore, 10% of patients initially selected for hepatectomy proved inoperable during exploration. Although this percentage might have been reduced in recent years by improved imaging modalities, identification of patients who can undergo complete cancer resection remains a key challenge for physicians, and patient counseling on the risk of residual disease or inoperability is particularly important in this patient group.

Overall survival from the start of chemotherapy of the entire group that underwent hepatectomy (45 months) compares favorably to outcomes reported from trials with first-line palliative chemotherapy with intensive treatment schedules (OS 25 to 30 months[17, 18]). When comparing these studies, it should be taken into account that there is selection bias in our cohort, since only patients who responded to chemotherapy or remained stable for a long time were considered for surgery. Possibly these patients had more indolent cancers than the majority enrolled in the chemotherapy trials, which could also explain the long period from disease recurrence to death. Even if survival benefit cannot be definitively shown in the absence of randomized or matched comparisons, our data show that the surgical approach affords a considerable group of patients a period off of systemic therapy – in several instances even up to 3 years.

Liver metastases of 25 patients included in this study were considered resectable at the tertiary referral centers in the absence of radiological evidence of response to chemotherapy. This means that the decision of the MDT differed from the original assessment at the referring centers. This problem was also recently remarked by Engstrand et al.[19], who found that 13% of patients who were not discussed by a hepatobiliary MDT were potential candidates for liver resection. It has been shown that assessment of resectability and need for downsizing chemotherapy differs between surgeons and oncologists.[20] These and our

findings, combined with the favorable prognosis of surgery after long-term chemotherapy in selected patients, underscore the importance of all patients being evaluated at a dedicated hepatobiliary MDT meeting.

The current study is limited by retrospective analysis of prospectively maintained databases. The intent of upfront chemotherapy (downsizing or palliation) was often difficult to trace back. Furthermore, the considerations for (initial) irresectability were diverse, resulting in a highly heterogeneous patient population. Although this accurately reflects the patient population at tertiary oncological centers, it hampers translation of the results to the individual patient. Finally, to truly determine whether there is a benefit from surgery on survival outcome, OS data from patients in this cohort should be compared with outcome of matched patients who did not undergo liver resection.

In conclusion, even after long-term (palliative) chemotherapy, hepatectomy for CRLM can result in a favorable prognosis if all cancer lesions can be resected. Patients with CRLM should therefore always be presented at a multidisciplinary hepatobiliary conference before initiating a palliative treatment course.

REFERENCES

1. Kopetz S, Chang GJ, Overman MJ, et al. Improved survival in metastatic colorectal cancer is associated with adoption of hepatic resection and improved chemotherapy. *J Clin Oncol*. 2009;**27**(22):3677-83.
2. Hackl C, Neumann P, Gerken M, et al. Treatment of colorectal liver metastases in Germany: a ten-year population-based analysis of 5772 cases of primary colorectal adenocarcinoma. *BMC Cancer*. 2014;**14**(1):810.
3. Adam R, Delvart V, Pascal G, et al. Rescue surgery for unresectable colorectal liver metastases downstaged by chemotherapy: a model to predict long-term survival. *Ann Surg*. 2004;**240**(4):644-57; discussion 57-8.
4. Lam VWT, Spiro C, Laurence JM, et al. A systematic review of clinical response and survival outcomes of downsizing systemic chemotherapy and rescue liver surgery in patients with initially unresectable colorectal liver metastases. *Ann Surg Oncol*. 2012;**19**(4):1292-301.
5. Tomasello G, Petrelli F, Ghidini M, et al. FOLFOXIRI Plus Bevacizumab as Conversion Therapy for Patients With Initially Unresectable Metastatic Colorectal Cancer: A Systematic Review and Pooled Analysis. *JAMA Oncol*. 2017;**3**(7):e170278.
6. Kataoka K, Kanazawa A, Iwamoto S, et al. Does "Conversion Chemotherapy" Really Improve Survival in Metastatic Colorectal Cancer Patients with Liver-Limited Disease? *World J Surg*. 2014;**38**(4):936-46.
7. Van Cutsem E, Cervantes A, Adam R, et al. ESMO consensus guidelines for the management of patients with metastatic colorectal cancer. *Ann Oncol*. 2016;**27**(8):1386-422.
8. Folprecht G, Grothey A, Alberts S, et al. Neoadjuvant treatment of unresectable colorectal liver metastases: correlation between tumour response and resection rates. *Ann Oncol*. 2005;**16**(8):1311-9.
9. Adam R, Yi B, Innominato PF, et al. Resection of colorectal liver metastases after second-line chemotherapy: is it worthwhile? A LiverMetSurvey analysis of 6415 patients. *Eur J Cancer*. 2017;**78**:7-15.
10. Mise Y, Kopetz S, Mehran RJ, et al. Is complete liver resection without resection of synchronous lung metastases justified? *Ann Surg Oncol*. 2015;**22**(5):1585-92.
11. Ubink I, Jongen JMJ, Nijkamp MW, et al. Surgical and Oncologic Outcomes After Major Liver Surgery and Extended Hemihepatectomy for Colorectal Liver Metastases. *Clin Colorectal Cancer*. 2016;**15**(4):e193-e8.
12. Reddy SK, Barbas AS, Turley RS, et al. A standard definition of major hepatectomy: resection of four or more liver segments. *HPB (Oxford)*. 2011;**13**(7):494-502.
13. Dindo D, Demartines N, Clavien PA. Classification of surgical complications: a new proposal with evaluation in a cohort of 6336 patients and results of a survey. *Ann Surg*. 2004;**240**(2):205-13.
14. Trumpi K, Ubink I, Trinh A, et al. Neoadjuvant chemotherapy affects molecular classification of colorectal tumors. *Oncogenesis*. 2017;**6**(7):e357.
15. Jouffret L, Ewald J, Marchese U, et al. Is progression in the future liver remnant a contraindication for second-stage hepatectomy? *HPB (Oxford)*. 2019.
16. de Jong MC, Beckers RCJ, van Woerden V, et al. The liver-first approach for synchronous colorectal liver metastases: more than a decade of experience in a single centre. *HPB (Oxford)*. 2018;**20**(7):631-40.
17. Heinemann V, von Weikersthal LF, Decker T, et al. FOLFIRI plus cetuximab versus FOLFIRI plus bevacizumab as first-line treatment for patients with metastatic colorectal cancer (FIRE-3): a randomised, open-label, phase 3 trial. *Lancet Oncol*. 2014;**15**(10):1065-75.
18. Cremolini C, Loupakis F, Antoniotti C, et al. FOLFOXIRI plus bevacizumab versus FOLFIRI plus bevacizumab as first-line treatment of patients with metastatic colorectal cancer: updated overall survival and molecular subgroup analyses of the open-label, phase 3 TRIBE study. *Lancet Oncol*. 2015;**16**(13):1306-15.
19. Engstrand J, Kartalis N, Stromberg C, et al. The Impact of a Hepatobiliary Multidisciplinary Team Assessment in Patients with Colorectal Cancer Liver Metastases: A Population-Based Study. *Oncologist*. 2017;**22**(9):1067-74.
20. Homayounfar K, Bleckmann A, Helms HJ, et al. Discrepancies between medical oncologists and surgeons in assessment of resectability and indication for chemotherapy in patients with colorectal liver metastases. *Br J Surg*. 2014;**101**(5):550-7.

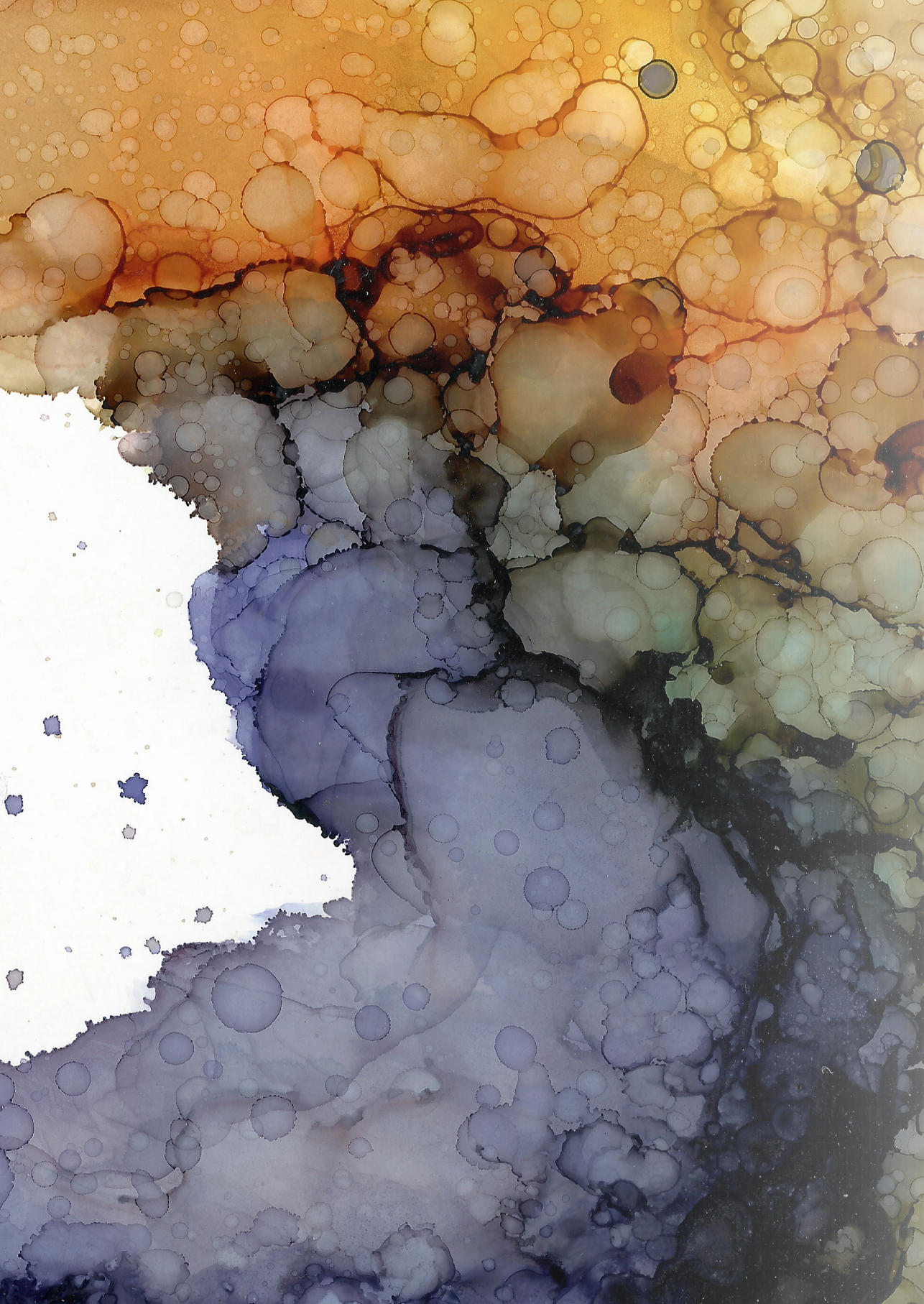

9

Surgical and oncologic outcomes after major liver surgery and extended hemihepatectomy for colorectal liver metastases

Inge Ubink, Jennifer M.J. Jongen, Maarten W. Nijkamp, Eelco F.J. Meijer, Thomas T. Vellinga, Richard van Hillegersberg, I. Quintus Molenaar, Inne H.M. Borel Rinkes and Jeroen Hagendoorn

Clinical Colorectal Cancer 2016;15(4):e193-e198

ABSTRACT

Purpose

To determine the surgical and oncologic outcomes after major liver surgery for colorectal liver metastases (CRLM) at a Dutch University Hospital.

Patients and Methods

Consecutive patients with CRLM who had undergone major liver resection, defined as ≥ 4 liver segments, between January 2000 and December 2015 were identified from a prospectively maintained database.

Results

Major liver surgery was performed in 117 patients. Of these, 26 patients had undergone formal extended left or right hemihepatectomy. Ninety-day postoperative mortality was 8%. Major postoperative complications occurred in 27% of patients; these adverse events were more common in the extended hemihepatectomy group. Median disease-free survival was 11 months and median overall survival 44 months.

Conclusion

Major liver surgery, including formal extended hemihepatectomy, is associated with significant operative morbidity and mortality but can confer prolonged overall survival for patients with CRLM.

INTRODUCTION

Complete surgical resection is the only curative treatment option for patients with colorectal liver metastases (CRLM). If left untreated, median survival after diagnosis of CRLM is less than 1 year.[1] With a 5-year survival rate of up to 50%, surgical resection significantly improves the prognosis of these patients.[2, 3] The limited criteria for partial liver resection (presence of a maximum of 3 metastases, absence of additional extrahepatic disease, and resection margin > 10 mm[4]) have largely been abandoned. Resectability is now defined as the ability to surgically remove all visible liver metastases with tumor-free margins while preserving adequate future liver remnant volume (FLRV) with sufficient vascular supply and biliary drainage.[3] Advances in surgical technique, use of preoperative portal vein embolization (PVE) to induce compensatory hypertrophy for improvement of FLRV, and effectiveness of neoadjuvant chemotherapeutic regimens have increased the number of patients eligible for resection.[5-7] Nevertheless, only 20% to 30% of patients with liver metastases are potential candidates for resection.[3, 8]

With the expanding indications for liver resection in patients with CRLM, major hepatectomy, defined as resection of 4 or more liver segments[9] and extended hemihepatectomies (ie, right or left trisectionectomy[10]), are executed in most hepatobiliary tertiary referral centers. Major liver resection remains a high-risk procedure, however. The incidence of complications has been correlated to the extent of liver surgery, with severe complications reported in up to 40% of patients undergoing major liver resection for CRLM.[11-13] Despite improvement in perioperative management, the mortality associated with extensive liver surgery has remained unchanged over the past 20 years.[14] Careful appraisal of the benefits is therefore essential. Data on the long-term outcomes of major liver surgery are scarce, however, with only a few available reports from high-volume centers that specialize in liver surgery.

Here we present the surgical and oncologic outcomes of major liver resections, including extended hemihepatectomies, in patients with CRLM from a large single-center cohort.

PATIENTS AND METHODS

Study Population

From a prospective database, we identified patients undergoing major liver surgery for CRLM with curative intent between January 2000 and December 2015 at the University Medical Center Utrecht, the Netherlands. Major liver surgery is defined as resection of 4 or more liver segments.[9]

Data Collection

Demographic and clinicopathologic characteristics, including age, sex, primary tumor characteristics, chemotherapeutic treatment, PVE, number of CRLMs, type of liver surgery, resection margins, postoperative mortality, disease-free survival (DFS), and overall survival (OS) were collected prospectively.

Synchronous liver metastases were defined as metastases detected before or during primary tumor resection. The postoperative mortality rate was assessed at 90 days after surgery. DFS and OS were calculated from the date of hepatic resection to the date of first recurrence detected with radiologic imaging and death. If there were no events, patients were censored at last follow-up. Patients whose extrahepatic disease was not resected or who had a primary tumor still in situ were excluded from the DFS analyses but included in the OS analyses.

Data on duration of surgery, amount of blood loss, duration of hospital and intensive care unit stay, and postoperative morbidity were collected retrospectively. Postoperative complications were independently graded according to the Clavien-Dindo classification[15] by 2 researchers (I.U. and J.J.) on the basis of information available from electronic medical records. In case of disagreement, a third opinion (J.H.) was decisive. Only major complications (Clavien-Dindo grades III to V) that occurred before first hospital discharge were recorded.

Hepatic Resection

Routine preoperative imaging included liver contrast-enhanced 3-phase computed tomography and thoracoabdominal spiral computed tomographic scan to assess resectability, FLRV, and extrahepatic metastases. Magnetic resonance imaging of the liver or positron emission tomography were performed as indicated. Portal vein embolization was carried out before surgery to improve FLRV if indicated.

All resections were performed with curative intent by 4 expert hepatic surgeons. After laparotomy, the abdomen was explored, and intraoperative ultrasound was performed to determine the extent and resectability of the metastases. Parenchymal transection was performed with an ultrasonic dissector. To minimize blood loss, central venous pressure was maintained below 5 mm Hg. Intermittent portal triad clamping (Pringle maneuver) was applied if the surgeons expected excessive blood loss.[16] Hemostasis and biliostasis were achieved with bipolar cautery coagulation, clips, or ligation.

The Brisbane 2000 terminology[10] was used to describe the type of liver resections. Extended right hemihepatectomy (or right trisectionectomy) requires en bloc resection of segment IV (a, b, or both) in addition to right hemihepatectomy with or without caudate resection. Extended left hemihepatectomy (or left trisectionectomy) is defined as left hepatectomy (segments I, II, III, and IV) plus segments V and VIII. The resection specimen was analyzed by an experienced pathologist to assess resection margins. A resection is

denoted R0 if all margins are free of tumor, R1 if there is microscopic invasion of the resection surface, and R2 if the resection is macroscopically not radical.

Statistical Analysis

Statistical analyses were performed by SPSS 20 (IBM SPSS, Chicago, IL). The Pearson chi-square test was used to compare differences in discrete or categorical data, whereas continuous data were analyzed with the Mann-Whitney *U* test. DFS and OS curves were generated using the Kaplan-Meier method; differences between survival curves were assessed by log rank test. A level of $P < .05$ was considered statistically significant.

RESULTS

Patients and Oncologic Characteristics

Between January 2000 and December 2015, a total of 543 partial hepatectomies were performed, of which 312 were performed for CRLM. Repeat hepatectomies (n = 33), 2-stage hepatectomies (n = 8), and resections in combination with hyperthermic intraperitoneal chemotherapy (n = 1) were excluded from this analysis, resulting in a cohort of 270 liver resections for CRLM. Of these, 117 (43%) were major hepatic resections. Patient and tumor characteristics are listed in Table 1. The median age at time of liver surgery was 63 years; 66% of patients were male. The majority of primary tumors were located in the sigmoid and rectum. Half of the patients presented with synchronous CRLM; 23 patients (9%) had simultaneous extrahepatic disease. Neoadjuvant chemotherapy was administered to 29% of all patients, more often before major resection than minor hepatectomy ($P = .014$). Patients with synchronous CRLM had more often received neoadjuvant chemotherapy ($P < .001$). PVE to increase FLRV before liver resection was performed in 12 patients.

Surgical Outcomes of Major Hepatectomy for CRLM

Of the 117 major liver resections, 26 procedures were formal extended hemihepatectomies (right, n = 22; left, n = 4; Table 2). Radiofrequency ablation in addition to major surgery was performed in 9 patients, and liver surgery was combined with resection of extrahepatic disease in 3 of 8 patients. The majority of patients with synchronous CRLM were treated in the traditional (primary tumor first) order; the reversed, or liver-first, procedure, in which CRLM are resected before the primary tumor, was used in 9 patients, of whom 5 underwent an extended hemihepatectomy. The R0 resection rate was 90% (Table 2).

Major postoperative complications (Clavien-Dindo grades III to V) occurred in 27% of patients who underwent major resection. An overview of these complications is shown in Table 3. The most common adverse event was pleural effusion requiring thoracocentesis. Major complications were more common after formal extended hemihepatectomy

compared to other major resections (46% vs. 21% complication rate, respectively, $P = .01$). Patients treated with neoadjuvant chemotherapy more often experienced major complications, but this difference was not statistically significant (36% vs. 21% respectively, $P = .08$). The occurrence of major complications significantly prolonged median intensive care unit and hospital stay. Of the discharged patients, 15% were readmitted to the hospital for unresolved or new complications.

The 90-day postoperative mortality rate after major liver surgery was 8% compared to 2% in the minor resection group ($P = .02$). Causes of death after major resection were as follows: hepatic failure (n = 2), multiorgan failure (n = 2), pancreatitis (n = 1), acute respiratory distress syndrome (n = 2), pulmonary embolism (n = 1), and intra-abdominal hemorrhage (n = 1).

Table 1. Patient and Oncologic Characteristics.

Characteristic	All resections (n=270)	Minor resections (n=153)	Major resections (n=117)
Age, years	63 (32-85)	64 (37-85)	62 (32-83)
Male gender	177 (66)	98 (65)	79 (67)
Primary tumor			
Location[a]			
Cecum + right hemicolon	56 (21)	37 (24)	19 (17)
Left hemicolon	19 (7)	6 (4)	13 (11)
(Recto)sigmoid	93 (35)	55 (36)	38 (33)
Rectum	97 (37)	52 (34)	45 (39)
T stage T3/4[b]	215 (88)	122 (89)	93 (88)
N status N1/N2[c]	155 (63)	84 (61)	71 (65)
Hepatic Metastases			
Number	2 (1-20)	1 (1-10)	2 (1-20)
Synchronous metastases	136 (50)	71 (46)	65 (56)
Concomittant extrahepatic disease[d]	23 (9)	15 (10)	8 (7)
Neoadjuvant chemotherapy[e]	78 (29)	33 (22)	45 (39)
Portal Vein Embolisation	12 (4)	2 (1)	10 (9)
ASA Physical Status Classification[f]			
ASA 1	45 (25)	27 (27)	18 (23)
ASA 2	119 (67)	66 (65)	53 (69)
ASA 3	15 (8)	9 (9)	6 (8)

Data are presented as median (range) or n (%). Data are available for: a) 265, b) 243, c) 247, d) 266, e) 254, and f) 179 patients. ASA = American Society of Anesthesiologists.

Recurrence and Overall Survival

Median follow-up after major hepatectomy was 22.5 months (range, 0.3-132 months). The median DFS was 11 months (95% confidence interval [CI], 7.3-15.3 months). One- and 3-year DFS were 49% and 21%, respectively. Median OS was 44 months (95% CI, 28.2-60.3 months). One-, 3-, and 5-year OS rates were 87%, 59%, and 40%, respectively. Patients who had received neoadjuvant therapy had a shorter median OS (35 months; 95% CI, 24-46 months), versus 73 months (95% CI, 32-114 months) without chemotherapy (P = .02). There were no significant differences in DFS and OS between minor and major liver resections (Figure 1).

Table 2. Perioperative characteristics.

Characteristic	All resections (n=270)	Minor resections (n=153)	Major resections (n=117)
Type of liver resection			
Extended left hepatectomy	4 (2)	0 (0)	4 (3)
Extended right hepatectomy	22 (8)	0 (0)	22 (19)
Left hemihepatectomy	24 (9)	0 (0)	24 (21)
Right hemihepatectomy	64 (24)	0 (0)	64 (55)
Multisegmentectomy (≥4)	3 (1)	0 (0)	3 (3)
Three segments	16 (6)	16 (11)	0 (0)
Two segments	42 (16)	42 (28)	0 (0)
One segment	43 (16)	43 (28)	0 (0)
Wedge resection	52 (19)	52 (34)	0 (0)
Combined primary + liver resection	5 (2)	5 (3)	0 (0)
Liver-first procedure	13 (5)	4 (3)	9 (8)
Concomitant radiofrequency ablation	29 (11)	20 (13)	9 (8)
Surgery duration, minutes[a]	220 (70-540)	180 (70-420)	250 (120-540)
Pringle maneuver[b]	139 (52)	77 (63)	62 (55)
Blood loss, mL[c]	600 (0-12,150)	475 (0-11,000)	900 (100-12,150)
Postoperative course			
Hospital stay, days	9 (3-74)	8 (3-74)	12 (4-67)
ICU stay, days	1 (0-55)	1 (0-54)	1 (0-55)
Postoperative deaths	12 (4)	3 (2)	9 (8)
Readmissions	30 (11)	13 (8)	17 (15)
Resection Margins			
R0	243 (90)	138 (90)	105 (90)
R1	26 (10)	15 (10)	11 (9)
R2	1 (0)	0 (0)	1 (1)

Data are presented as median (range) or n (%). Data are available for: a265, b235, and c183 patients. ICU = intensive care unit.

Table 3. Specification Grade 3 or Higher Postoperative Complications.

Complication	Incidence Grade III-V
Hepatic complications	
Hepatic failure	6
Hepatic hemorrhage	1
Hepatic necrosis	1
Perforation bile duct	4
Bile duct stenosis	1
Pulmonary complications	
Pleural effusion	15
Respiratory insufficiency	5
Lung infection	1
Pneumothorax	2
Other complications	
Intra-abdominal abscess	4
Peritoneal infection	3
Thromboembolic event	4
Wound complication	3
Multiorgan failure	2
Acute renal failure	1
Sepsis e causa ignota	1
Intra-abdominal hemorrhage	1
Pancreatitis	1
Gastric ulcer bleeding	1
Pericardial tamponade	1
Procedural complication: colon perforation	1

DISCUSSION

Extensive liver resections are frequently being performed for CRLM; however, data on the short- and long-term oncologic outcomes of these highly complex surgical procedures are scarce and are almost exclusively reported by a few high-volume centers. This leaves several vital questions regarding the potential risks and benefits of these procedures unanswered, encumbering patient counseling and clinical decision making. Here we present data on surgical and oncologic outcomes for 117 patients with metastatic CRLM who underwent major liver resection (4 or more liver segments) at a Dutch tertiary referral center.

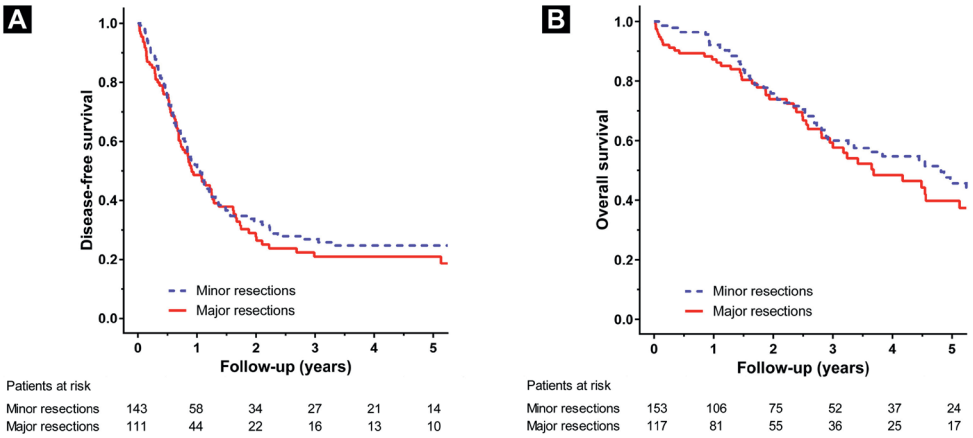

Figure 1. Disease-Free (**A**) and Overall Survival (**B**) After Minor or Major Hepatectomy for Colorectal Liver Metastases.

Short-Term Outcomes

It has been shown that resection of 4 or more segments significantly increases the risk of postoperative morbidity and mortality compared to less extensive resections.[9, 11, 14] High complication rates of major liver surgery have been reported by, eg, Konopke et al[11] (37%) and van Dam et al[12] (33%). In our cohort, 27% of the patients experienced grade III or higher postoperative complications. The distribution of the observed complications corresponds well with the complications found in a recent study on predictors for complications after hemihepatectomy.[17] Patients who underwent extended hemihepatectomy had significantly more complications than patient undergoing other major resections, which should be taken into account when selecting patients for resection. Postoperative complications led to death in 9 patients (8%) in this cohort, which is comparable with other studies on major liver surgery for CRLM, with reported mortality rates between 0% and 10%[9, 13, 18-21] Over the past 2 decades, Kingham et al[14] noted a remarkable decline in postoperative complications and deaths coinciding with a decrease in the number of major resections performed. Preservation of hepatic parenchyma, by combining resection with radiofrequency ablation or by expanding FLRV with PVE, could thus limit postoperative morbidity and mortality.

Long-Term Outcomes

Few studies have presented survival data on major liver surgery for CRLM, defined as resection of 4 or more liver segments. Five-year DFS ranged from 4% to 25.5%; 5-year OS was reported between 25% and 38.7%.[18, 19, 22-24] Our survival results (3-year DFS 21% and

5-year OS 40%) are in line with these reports. In previous studies, major hepatectomy patients appear to have a shorter survival compared to patients undergoing minor resection for CRLM.[18, 22] Presumably this is due to a higher tumor burden, considering that the number of metastases significantly influences OS.[1] We did not observe differences in DFS or OS between minor and major resections in our cohort; however, we did see a correlation between the number of metastases and survival outcomes (data not shown). The improvement in OS compared to palliative chemotherapy (median OS, 20-24 months[25]) indicates that surgical resection, even if major or extended hepatectomy is required, is the preferred treatment option for CRLM if possible. Despite the fairly positive OS rate, DFS remains low in this study, even though R0 resection was achieved in the majority of patients.

Preoperative Chemotherapy

Neoadjuvant chemotherapy is considered for downsizing initially unresectable CRLM; up to 23% of patients with initially unresectable metastases can undergo macroscopic curative resection after neoadjuvant therapy.[6] Preoperative chemotherapy is also used in patients with resectable disease to reduce the chances of postoperative relapse, although recently no significant survival benefit was found with the addition of perioperative chemotherapy (FOLFOX4) compared to surgery alone for patients with resectable liver metastases.[2] Unfortunately, preoperative chemotherapy comes at a cost: chemotherapy-induced hepatic injury increases the risk of postoperative complications.[26] In our cohort, we observed a trend toward increased morbidity associated with neoadjuvant chemotherapy, but this was not statistically significant. We did notice a shorter OS in patients who had received preoperative chemotherapy. Cases were not matched, however, and we did not correct for potential confounding variables. A possible explanation for the shorter OS is that these patients presented with initially unresectable metastases, reflecting a more extensive tumor spread compared to patients who did not require neoadjuvant chemotherapy. Indeed, patients with primarily resectable disease had better OS than patients with down-staged metastases in a large series of CRLM.[27] Nevertheless, survival outcome of resection after conversion chemotherapy is better compared to survival after chemotherapy alone.[28]

Even though this study is limited by the relatively small sample size with patients from a single institution, and even though our findings are from retrospective analysis of prospectively collected data, the results of this study confirm that major hepatic resection and formal extended hemihepatectomy for the treatment of CRLM can provide significant long-term survival. As a result of the complexity of the procedure, major liver surgery is associated with relatively high postoperative morbidity and mortality. Determination of the appropriate treatment sequence for synchronous liver metastases, increasing efforts to perform parenchymal-sparing resections, and further improvement in selection of patients

suitable for major hepatic resection should reduce the complication rate and ameliorate DFS and OS.

Acknowledgements

We are grateful to Charlotte van Kessel, Klaas Govaert, and Morsal Samim for their efforts in the maintenance of the prospective liver surgery database. I.U., J.M.J.J., T.T.V., and J.H. were supported by grants from the Dutch Cancer Society (KWF): UU2014-6617, UU2013-5865, UU2011-5226, and UU2014-6904, respectively.

REFERENCES

1. Hackl C, Neumann P, Gerken M, et al. Treatment of colorectal liver metastases in Germany: a ten-year population-based analysis of 5772 cases of primary colorectal adenocarcinoma. *BMC Cancer*. 2014;**14**(1):810.
2. Nordlinger B, Sorbye H, Glimelius B, et al. Perioperative FOLFOX4 chemotherapy and surgery versus surgery alone for resectable liver metastases from colorectal cancer (EORTC 40983): long-term results of a randomised, controlled, phase 3 trial. *The lancet oncology*. 2013;**14**(12):1208-15.
3. Kopetz S, Chang GJ, Overman MJ, et al. Improved survival in metastatic colorectal cancer is associated with adoption of hepatic resection and improved chemotherapy. *J Clin Oncol*. 2009;**27**(22):3677-83.
4. Ekberg H, Tranberg KG, Andersson R, et al. Determinants of survival in liver resection for colorectal secondaries. *The British journal of surgery*. 1986;**73**(9):727-31.
5. Shindoh J, Tzeng CWD, Aloia TA, et al. Portal vein embolization improves rate of resection of extensive colorectal liver metastases without worsening survival. *The British journal of surgery*. 2013;**100**(13):1777-83.
6. Lam VWT, Spiro C, Laurence JM, et al. A systematic review of clinical response and survival outcomes of downsizing systemic chemotherapy and rescue liver surgery in patients with initially unresectable colorectal liver metastases. *Ann Surg Oncol*. 2012;**19**(4):1292-301.
7. Wicherts DA, de Haas RJ, Andreani P, et al. Impact of portal vein embolization on long-term survival of patients with primarily unresectable colorectal liver metastases. *The British journal of surgery*. 2010;**97**(2):240-50.
8. Manfredi S, Lepage C, Hatem C, et al. Epidemiology and management of liver metastases from colorectal cancer. *Ann Surg*. 2006;**244**(2):254-9.
9. Reddy SK, Barbas AS, Turley RS, et al. A standard definition of major hepatectomy: resection of four or more liver segments. *HPB (Oxford)*. 2011;**13**(7):494-502.
10. Strasberg SM. Nomenclature of hepatic anatomy and resections: a review of the Brisbane 2000 system. *J Hepatobiliary Pancreat Surg*. 2005;**12**(5):351-5.
11. Konopke R, Kersting S, Bunk A, et al. Colorectal liver metastasis surgery: analysis of risk factors predicting postoperative complications in relation to the extent of resection. *Int J Colorectal Dis*. 2009;**24**(6):687-97.
12. van Dam RM, Lodewick TM, van den Broek MAJ, et al. Outcomes of extended versus limited indications for patients undergoing a liver resection for colorectal cancer liver metastases. *HPB: the official journal of the International Hepato Pancreato Biliary Association*. 2014;**16**(6):550-9.
13. Cauchy F, Aussilhou B, Dokmak S, et al. Reappraisal of the risks and benefits of major liver resection in patients with initially unresectable colorectal liver metastases. *Ann Surg*. 2012;**256**(5):746-52; discussion 52-4.
14. Kingham TP, Correa-Gallego C, D'Angelica MI, et al. Hepatic parenchymal preservation surgery: decreasing morbidity and mortality rates in 4,152 resections for malignancy. *J Am Coll Surg*. 2015;**220**(4):471-9.
15. Dindo D, Demartines N, Clavien PA. Classification of surgical complications: a new proposal with evaluation in a cohort of 6336 patients and results of a survey. *Ann Surg*. 2004;**240**(2):205-13.
16. Nijkamp MW, van der Bilt JDW, Snoeren N, et al. Prolonged portal triad clamping during liver surgery for colorectal liver metastases is associated with decreased time to hepatic tumour recurrence. *European journal of surgical oncology: the journal of the European Society of Surgical Oncology and the British Association of Surgical Oncology*. 2010;**36**(2):182-8.
17. Alghamdi T, Abdel-Fattah M, Zautner A, et al. Preoperative model for end-stage liver disease score as a predictor for posthemihepatectomy complications. *Eur J Gastroenterol Hepatol*. 2014;**26**(6):668-75.
18. Karanjia ND, Lordan JT, Quiney N, et al. A comparison of right and extended right hepatectomy with all other hepatic resections for colorectal liver metastases: a ten-year study. *European journal of surgical oncology: the journal of the European Society of Surgical Oncology and the British Association of Surgical Oncology*. 2009;**35**(1):65-70.
19. Wicherts DA, de Haas RJ, Andreani P, et al. Short- and long-term results of extended left hepatectomy for colorectal metastases. *HPB: the official journal of the International Hepato Pancreato Biliary Association*. 2011;**13**(8):536-43.
20. Grąt M, Hołówko W, Lewandowski Z, et al. Early post-operative prediction of morbidity and mortality after a major liver resection for colorectal metastases. *HPB: the official journal of the International Hepato Pancreato Biliary Association*. 2013;**15**(5):352-8.

21. Mayo SC, Shore AD, Nathan H, et al. Refining the definition of perioperative mortality following hepatectomy using death within 90 days as the standard criterion. *HPB: the official journal of the International Hepato Pancreato Biliary Association*. 2011;**13**(7):473-82.
22. Stewart GD, O'Súilleabháin CB, Madhavan KK, et al. The extent of resection influences outcome following hepatectomy for colorectal liver metastases. *European journal of surgical oncology: the journal of the European Society of Surgical Oncology and the British Association of Surgical Oncology*. 2004;**30**(4):370-6.
23. Halazun KJ, Al-Mukhtar A, Aldouri A, et al. Right hepatic trisectionectomy for hepatobiliary diseases: results and an appraisal of its current role. *Ann Surg*. 2007;**246**(6):1065-74.
24. Ardito F, Vellone M, Barbaro B, et al. Right and extended-right hepatectomies for unilobar colorectal metastases: impact of portal vein embolization on long-term outcome and liver recurrence. *Surgery*. 2013;**153**(6):801-10.
25. Lehmann K, Rickenbacher A, Weber A, et al. Chemotherapy before liver resection of colorectal metastases: friend or foe? *Ann Surg*. 2012;**255**(2):237-47.
26. Robinson SM, Wilson CH, Burt AD, et al. Chemotherapy-associated liver injury in patients with colorectal liver metastases: a systematic review and meta-analysis. *Ann Surg Oncol*. 2012;**19**(13):4287-99.
27. Adam R, Delvart V, Pascal G, et al. Rescue surgery for unresectable colorectal liver metastases downstaged by chemotherapy: a model to predict long-term survival. *Ann Surg*. 2004;**240**(4):644-57; discussion 57-8.
28. Kataoka K, Kanazawa A, Iwamoto S, et al. Does "Conversion Chemotherapy" Really Improve Survival in Metastatic Colorectal Cancer Patients with Liver-Limited Disease? *World J Surg*. 2014;**38**(4):936-46.

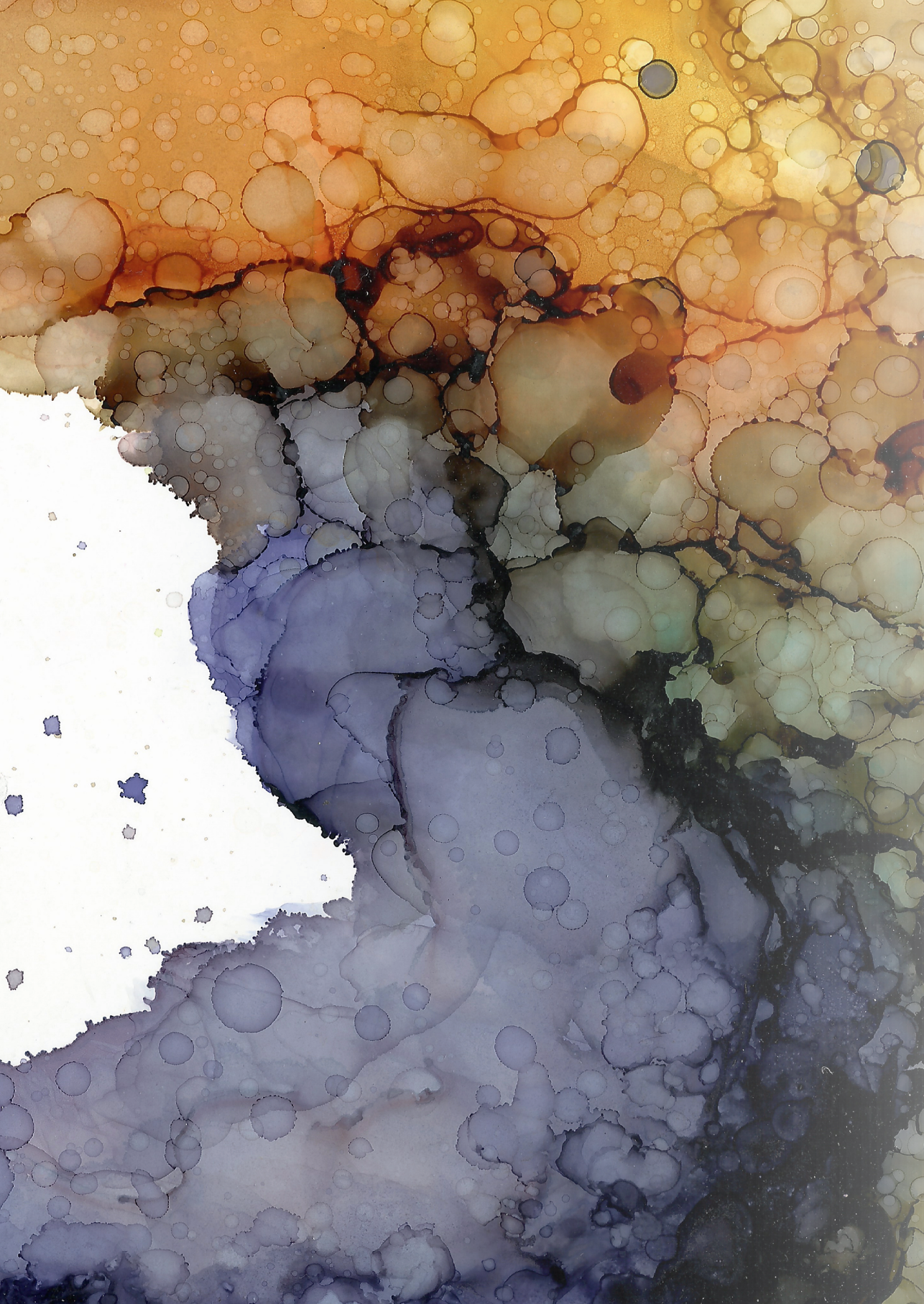

10

Discussion and future perspectives

Patient selection for subtype-targeted therapy

The Consensus Molecular Subtypes (CMS) classification holds great potential for improvement of colorectal cancer (CRC) therapy. Besides predicting response to conventional chemotherapy, it provides leads for novel subtype-specific therapeutic targets. Subtype-targeted therapy could benefit selected patients, while sparing others from ineffective and potentially toxic treatment. Molecular subtyping is based on genome-wide expression data, which is rather expensive and requires bioinformatical processing. This hampers widespread implementation of the CMS classifier in clinical practice. There is a need for a diagnostic assay that can be easily performed at molecular pathology labs, and that identifies subtypes quickly, reliably and at a relatively low cost. In **chapter 2**, we introduced such a diagnostic test. This RT-qPCR test identifies CMS4 tumors based on the expression of *PDGFC*, *PDGFRA*, *PDGFRB* and *KIT*. These genes were chosen based on preclinical work demonstrating that PDGFR and KIT are upregulated in CMS4 and contribute to the aggressive behavior of tumor cells.[1, 2] These receptors are the targets of the receptor tyrosine kinase (RTK) inhibitor imatinib, and as such, the test should identify CMS4 tumors that are most likely to respond to imatinib therapy. The developed pipeline for the generation of a companion diagnostic tool – starting with selection of a small set of subtype-specific therapeutic targets in Affymetrix data, and resulting in an RT-qPCR algorithm – could be applied to the other subtypes as well.

The RT-qPCR test was developed in the context of the ImPACCT trial (**chapter 3**), to enable prospective CMS4 classification on endoscopic CRC biopsies. We demonstrated the feasibility of obtaining high quality fresh-frozen biopsy samples in this multicenter trial, which allowed CMS4 classification of each included tumor. The requirement for fresh-frozen tissue is a major drawback of the RT-qPCR test because additional biopsies need to be obtained. As this is not part of standard diagnostic procedure, informed consent to obtain these extra biopsies is required prior to colonoscopy. In addition, liquid nitrogen must be available at endoscopy centers for snap-freezing, which can be logistically challenging. Furthermore, it precludes application of the test on historical cohorts, from which often only formalin-fixed paraffin-embedded (FFPE) tissue is available. Translation of the RT-qPCR test to FFPE material is not straightforward. Formalin fixation causes RNA crosslinking and degradation, which leads to gene-to-gene variations in RT-qPCR efficiency.[3]

Trinh *et al.* developed an assay that distinguishes mesenchymal-type tumors (CMS4) from epithelial-like tumors (CMS2/3), based on a small panel of tumor cell markers that can be assessed by immunohistochemistry (IHC) on FFPE material. The IHC test was trained in a relatively small cohort of 70 stage II CRC samples, but its prognostic value was confirmed in three large patient series.[4] The test is ideally suited for historical cohorts, and by making use of tissue microarrays, a large number of samples can be analyzed simultaneously. We therefore used this test in **chapter 7** to classify paired primary tumors

and CRLMs on archival FFPE tissue. The IHC test has several limitations however. If used on a per-patient basis in a non-automated fashion, staining intensity may vary from day-to-day and interobserver variation in stain scoring might influence the result. Besides these technical issues, there are also limitations in subtyping. In this test, MSI tumors are per definition classified as CMS1. In reality, not all MSI tumors are CMS1 (in the original series a subset of CMS3 tumors were also MSI), and not all CMS1 tumors are MSI.[5] Moreover, the test cannot distinguish between the two epithelial subtypes CMS2 and 3.

Several groups are working with NanoString nCounter technology to develop an RNA-based test on FFPE material. This relatively new technology measures gene expression by labeling isolated mRNA with barcoded reporter probes, and then counting the number of hybridized barcodes. The nCounter platform does not require an amplification step, which limits the effect of formalin-fixation on quantitative RNA analysis. Comparison of gene expression in fresh-frozen tissue measured with Affymetrix microarray and in FFPE tissue measured with NanoString showed only moderate correlations.[6] However, when measuring both fresh-frozen and FFPE material on the NanoString platform, Ragulan *et al.* found a high correlation in median gene expression between 24 matched fresh frozen and FFPE colorectal cancer samples.[7] Piskol *et al.* reached 86% concordance between RNA-sequencing and NanoString CMS classification of FFPE samples.[8] In the metastatic setting, CMS1 assigned based on NanoString testing was associated with the worst prognosis[8, 9], in line with the original CMS publication.[5] These data suggest that classification is possible on FFPE tissue with NanoString technology, but this requires further validation and optimization. Our group is working on a direct comparison of RT-qPCR on FFPE and fresh-frozen tissue, the IHC test and NanoString analysis, against the gold standard CMS classifier applied to RNA-sequencing data.

Intratumor subtype heterogeneity

No two cancers are identical, but the cells within a single tumor also differ, a phenomenon called intratumor heterogeneity (ITH). By studying tumor sections under a microscope one can already appreciate that the morphology of each cancer cell is slightly different. Often, fields of cancer cells with different growth patterns can be seen in a single CRC.[10] On a genetic level, numerous subclones exist that have private mutations not present in other subclones.[11] Furthermore, one genotype can give rise to multiple distinct phenotypes. In the cancer stem cell (CSC) model, stem-like cells that drive tumor growth and differentiated cells co-exist, similar to normal tissue organization.[12] A recent study suggests that cells with CSC functionality are often located at the edges of the tumor, in close contact with stromal cells, leading to spatial variation in stem cell activity.[13] Non-malignant cells in the tumor microenvironment (TME) have a major influence of cancer cell phenotype, and the variable distribution of stromal cells throughout the tumor as well as the resulting

variations in microenvironmental conditions (e.g. uneven vascularization leading to variable oxygen and nutrient supply) further contribute to phenotypic ITH.[14, 15]

In this thesis we demonstrated the presence of molecular subtype ITH. In **chapter 2**, we performed CMS testing on multiple regions of twenty primary colorectal cancers and found that one CRC could test both positive and negative for CMS4. These findings were supported by analysis of pretreatment biopsies within the ImPACCT trial **(chapter 3)**. Microarray profiling of a subset of samples from the BOSS cohort confirmed that multiple CMSs can be present within one tumor.[16]

The observed subtype ITH could be partly caused by genetic differences between tumor regions. Indeed, private mutations are frequently confined to separate tumor regions.[11, 17] However, subtype ITH is probably largely due to differences in stromal composition between tumor areas. Spatial heterogeneity of the TME, with regional differences in blood vessel density, fibrosis and immune cells, is commonly observed in histological sections of CRC.[18, 19] The CMS classifier was created using unsegregated tumor samples which contain both cancer cells and non-neoplastic cells, including CAFs, immune cells and endothelial cells. These stromal cells contribute to the CMS gene expression profiles, particularly in CMS4 tumors where the majority of genes in the classifier are derived from fibroblasts.[5, 20-22] Spatial variation in TME composition is therefore likely to influence subtype assignment.

Isella *et al.* argued that these stromal genes might obscure more subtle gene expression differences in CRC cells and developed a molecular classifier based solely on tumor cell-intrinsic gene expression patters (colorectal cancer intrinsic subtypes, CRIS).[23] This classifier was developed using patient-derived xenografts, in which human stromal cells are replaced by murine cells and therefore not detected by human-specific microarray analysis. Five CRIS are distinguished (A-E) with different genetic and phenotypic characteristics. Some of these subtypes are reminiscent of the CMS subtypes, with an MSI-like subtype with inflammatory traits (CRIS-A), a group of poorly differentiated tumors with TGFβ signaling and EMT features (CRIS-B), and a subtype with high WNT-signaling (CRIS-D). However, the overlap between CMS and CRIS subtyping is limited. The cell-intrinsic classifier allows a more refined classification of the largest and most heterogeneous epithelial-like subtype CMS2, which was dispersed among CRIS-C,-D and -E. Furthermore, CMS4 was distributed across all five CRIS groups, suggesting that CMS4 tumors are bound by the presence of stromal cells rather than by cell-intrinsic features.

Interestingly, CRIS were far less heterogeneous within a single tumor than CMS.[24] Only 1/7 tumors from our multiregional BOSS study (**chapter 2**) demonstrated 100% subtype concordance with CMS, compared with 5/7 tumors analyzed with CRIS.[16] Stromal heterogeneity is therefore sometimes perceived as 'confounding' ITH, with stromal genes only obscuring relevant cancer cell-intrinsic signals (Figure 1, left panel). However, CMS-ITH is likely biologically relevant, considering that the TME has a major influence on cancer

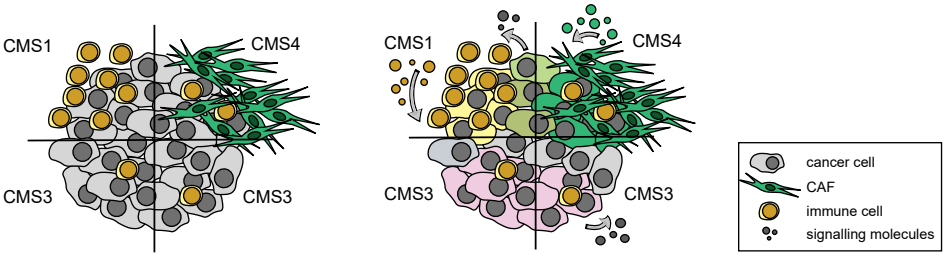

Figure 1. Stromal heterogeneity causes molecular subtype ITH.
Gene transcripts derived from stromal cells contribute to CMS classification (left panel), but these stromal cells also influence the cancer cells in close proximity through paracrine signaling by cytokines, growth factors, and ECM deposition (right panel). Figure depicts CMS classification of biopsy samples from BOSS13, and is based on figure 6 from Alderdice *et al.* J Pathol 2018.

cell phenotype and vice versa (Figure 1, right panel). Enrichment of CMS4 at the invasive front is probably due to the increased number of transcripts from recruited CAFs[25], but also reflects phenotypic differences in invading cancer cells. Microdissection and RNA-sequencing of tumor bulk and budding tumor cells revealed that budding regions underwent EMT and showed enrichment of CMS4 compared to CMS2 in the tumor bulk.[26] This would explain why epithelial cell enrichment by laser-capture microdissection did not overcome CMS subtype ITH in the study of Alderdice et al.[16] It further explains why CMS can be assigned by merely analyzing cancer cell markers, as in the CMS-IHC test and CMScaller (a modified CMS classifier based on epithelial cell-intrinsic features to assign CMS in preclinical models).[4, 27]

Conflicting CMS assignment of multiple biopsy samples from a single patient complicates patient stratification, and CRIS classification might therefore be more feasible in the clinical setting. Yet, this would dismiss the biological and prognostic significance of the TME that is captured by the CMS classifier. Although CRIS was an independent predictor of prognosis in CRC, integration of high CAF presence in the CRIS classifier improved its prognostic value. Bramsen *et al.* also developed a cancer cell-intrinsic classifier by making use of epithelial cell-derived transcripts. However, their three 'cancer cell archetypes' were not associated with survival differences. Only when including stroma-derived transcripts in the classifier, prognostic differences were observed, related to antitumor immune cell and fibroblast activity.[28] Indeed, the prognostic significance of the CMS classification is largely explained by the presence of CAFs and lymphocyte infiltrate.[29]

Thus, rather than dismissing stromal ITH as a disturbing feature in patient stratification, we must find a way to deal with this added level of complexity. In **chapter 2** we suggest to combine CMS classification of several tumor regions. To ensure that tumors included in the ImPACCT trial are predominantly CMS4, we selected only tumors from which multiple

biopsies combined reached the threshold of CMS4-positivity. Using this approach we hoped to find more pronounced differences in gene expression after treatment with imatinib. However, this approach may not reflect the biological significance of CMS4. It is currently unknown whether a tumor with a small CMS4 component has a similarly poor prognosis as a tumor dominated by CMS4. Our strategy of combining multiple biopsies is clinically relevant if the chance of metastasis increases with the abundance of CMS4 positive areas. However, if the presence of a single region of CMS4 determines metastatic potential of a tumor, the biopsy with the highest CMS4 chance should be leading. In this latter scenario sampling issues with regard to subtype ITH become more important. Positron Emission Tomography tracers that specifically bind stromal surface proteins, such as PDGFR and fibroblast activation protein (FAP) in case of CAFs, could be used to visualize stromal ITH and overcome sampling errors. With this strategy, we can also start to address the questions raised above about clinical relevance of subtype ITH. Eventually these tracers could be linked to stroma-directed targeted therapeutics, a treatment strategy termed theranostics. Our research group is currently exploring the correlation between PDGFR/FAP tracer binding and CMS4 classification in *in vivo* CRC models.

Molecular classification of metastatic disease

In **chapters 5 and 7** we studied molecular classification of colorectal liver metastases (CRLM) and peritoneal metastases (PM) from CRC in relation to their primary tumors. Given the profound subtype-ITH that we found by examining multiple regions within primary tumors, it is perhaps not surprising that there is also substantial subtype heterogeneity between primary tumors and corresponding metastases. In our paired analysis of primary tumors and CRLM we found that 45% of paired tumors were classified discordantly into epithelial/mesenchymal subtypes with the CMS-IHC test (**chapter 7**). This is in line with a recent study using NanoString, in which CMS assignment of 40% of paired primary cancers and CRLM were discordant.[8] This high level of discordance indicates that CMS classification of primary tumors cannot be used to infer the subtype of the corresponding metastasis.

There are several possible explanations for the subtype heterogeneity between cancer lesions from the same patient. Firstly, since subtype ITH is abundant in primary cancers, it is possible that the tumor region that gave rise to the metastasis was not sampled from the primary tumor.

Secondly, neo-adjuvant therapy can influence molecular subtyping. We found that rectal tumors treated with (chemo)radiation were more often classified as mesenchymal compared with treatment-naive rectal cancers. Chemoradiation causes cancer cell death and extensive fibrosis within rectal cancers.[30] Upregulation of stromal gene transcripts combined with loss of epithelial cell content is consistent with the stroma-rich CMS4 subtype.[20] CRLM

treated with neo-adjuvant chemotherapy were also more frequently classified as mesenchymal. Confirming our results, acquired resistance to cetuximab therapy has recently been linked to a switch from the CMS2/transit-amplifying cell subtype to the CMS4/stem-cell subtype.[31] Moreover, EMT, hypoxia and angiogenesis pathways were upregulated in chemotherapy-treated metastases, whereas treatment-naive samples showed high MYC-activation and proliferation.[32] Stromal remodeling in response to chemotherapy and targeted therapy plays a major role in resistance. However, given that the IHC test measures tumor cell-intrinsic markers, chemotherapy must also influence cancer cell behavior. Indeed, we and others found a clear shift towards mesenchymal gene expression after chemotherapy in colorectal cancer cells *in vitro*.[33]

Thirdly, the metastatic niche might influence cancer cell phenotype and molecular classification. We found that the majority (75%) of peritoneal lesions were CMS4-positive (**chapter 5**). In a more recent RNA-sequencing analysis of 26 samples from 9 primary tumors and 39 paired PMs, even 92% of all samples were found to be CMS4 (*unpublished data, E. Wassenaar*). This could either mean that CMS4 tumors are more fit to disseminate to the peritoneum compared with other subtypes, or that the stroma-rich peritoneal microenvironment induces the CMS4 subtype in metastases. Cancer cells are thought to attach to areas in the peritoneum where the underlying collagen-rich stromal matrix is exposed. Activated by TGF-β signaling from cancer cells and inflammatory cells, peritoneal mesothelial cells and fibroblasts can function as CAFs and secrete numerous cytokines, growth factors and extracellular matrix (ECM) components.[34, 35] Moreover, peritoneal macrophages that normally protect against tumor invasion, can become tumor-promoting by cytokines secreted by CRC cells.[36] These features (CAFs, collagen type I, TGF-β and pro-tumorigenic macrophages) have all been linked to CMS4.

Finally, CMS was developed using primary CRC and it is not yet established whether it can also be applied to metastatic lesions. Several studies reported that ~30% of CRLM could not be classified into CMS, which is higher than the percentage of indeterminate samples in primary CRC (13%[5]). Furthermore, the majority of CRLM that can be classified were assigned to CMS2, whereas CMS3 CRLM were almost absent in all analyses.[32, 37-39] Perhaps the stromal constitution is different or less pronounced in liver metastases, thus limiting CMS1/4 assignment. Survival within the liver microenvironmental niche might require alternative metabolic pathways for survival, which may not be included in the CMS3 gene signature. *De novo* molecular classification of CRLM could result in the discovery of new subtypes with different activated pathways, or in different gene sets identifying the same CMS groups. Pitroda *et al.* used miRNA and mRNA data from 93 CRLM to create such a new classifier, and distinguished three CRLM subtypes with variable prognoses. Interestingly, the biological features of the subtypes showed some overlap with the CMS groups: subtype 1 displayed low stromal and immune infiltrate and

high MYC signaling (CMS2), subtype 2 showed high immune infiltration (CMS1) but also enrichment KRAS pathways (CMS3), and subtype 3 exhibited high stromal infiltration, EMT, ECM remodeling, angiogenesis and inflammation (CMS4). Similarly, unsupervised clustering of 119 CRLM from our institution revealed three liver metastases subtypes, including one subtype with a poorer prognosis that was correlated with CMS4 genes, and with stromal and macrophage gene transcripts.[40] The specific gene sets of the CMS classifier and those CRLM classifiers hardly overlap however, suggesting that a modified CMS classifier might be needed for CRLM.

Molecular classification of colorectal metastases might improve risk stratification for surgical treatment. In **chapters 8 and 9**, we studied short-term surgical outcomes and long-term oncologic outcomes after major hepatectomy and after hepatectomy following prolonged preoperative chemotherapy. Given the considerable morbidity associated with extended liver surgery, careful appraisal of the survival benefit of these procedures is necessary. In both studies we found a subset of patients with long-term disease-free survival following these somewhat exceptional liver surgeries, but no means of identifying these patients was provided. Integration of molecular subtyping with the validated Clinical Risk Score[41] allowed identification of patients with a favorable prognoses after resection of CRLM.[37] It would therefore be highly interesting to study molecular subtypes and clinical risk scores in patients included in the prospective databases and biobanks of CRLM that were used for these studies.

Preclinical development of targeted therapies against poor prognosis CRC

Targeting tumor-stroma interactions in mesenchymal-type CRC

In this thesis we made use of organoid technology to identify and test novel therapies against aggressive CRC. Organoids are thought to resemble patient's tumors more closely than two-dimensional adherent cell cultures, due to cell-matrix interactions and cellular hierarchy within a multicellular three-dimensional (3D) culture. Morphologic and genetic features of original tumors are well preserved in organoids.[42-44] Furthermore, *in vitro* drug response tests on organoids accurately predict clinical therapeutic effects.[45-47] These features make organoids a valuable tool in preclinical drug development.

In **chapter 4** we used organoid models to search for an alternative CMS4-targeted therapy. It has been argued that CMS cannot be recapitulated in patient-derived organoids. In particular, when applying the CMS classifier to 55 patient-derived organoids, Fujii *et al.* found no CMS4 organoids due to a lack of stromal cells in the culture.[42] By modification of the CMS classifier through exclusion of stromal gene contribution, all CMSs can in fact be identified in cell lines and patient-derived xenografts.[48, 49] This confirms that cancer cells in stroma-rich CMS4 tumors have a specific phenotype.[22] Furthermore, it implies that organoids can be used for development of subtype-targeted therapy. We studied the effects

of ECM composition on cancer cell behavior, and showed that exposure to collagen type I induces mesenchymal-type gene expression and interface migration of tumor cells. Introduction of fibroblasts in co-culture enabled organoid invasion in a 3D collagen matrix. This model of organoids in a CMS4-like tumor microenvironment can be used for the discovery of novel therapeutic targets. We found that interaction with collagen type I activates Src pathway signaling in organoids. This non-receptor tyrosine kinase can be inhibited with dasatinib, and dasatinib further targets a number of RTKs that are highly expressed by cancer cells and/or stromal cells in CMS4 CRC (including PDGFRs and c-KIT). Dasatinib is therefore a promising drug to target tumor-stroma and tumor-ECM interactions in CMS4.

In our model, dasatinib inhibited colony formation and sheet-invasion in mono-culture, and 3D invasion and fibroblast proliferation in the co-culture model. By interfering with these tumor-microenvironment interactions, dasatinib could render tumors less aggressive. Yet, the effects of dasatinib monotherapy in terms of patient survival are expected to be limited, since the clinically attainable concentrations are insufficient to inhibit cancer cell proliferation.[50, 51] Dasatinib did have an anti-metastatic effect in an *in vivo* model of pancreatic adenocarcinoma[50], suggesting that the tumor-stroma interactions driving invasion and metastasis that we observed in our organoid model can be effectively blocked at clinical dosage. Combined treatment with dasatinib and chemotherapy might therefore be more effective, with chemotherapy targeting the actively proliferating tumor bulk, and dasatinib targeting both the stromal fibroblasts and the invasive tumor cells. Two early clinical trials showed that addition of dasatinib to current standard chemotherapeutic regimens is safe.[52, 53] Dasatinib might also further enhance the efficacy of chemotherapy; oxaliplatin treatment leads to upregulation of Src activity in liver metastases, and this is correlated with shorter relapse-free survival.[54]

Improvement of HIPEC treatment

In **chapter 6**, organoid technology was employed to establish a panel of organoids from peritoneal metastases (PMs) from CRC. With these PM organoids we developed a model system for testing of HIPEC regimens *in vitro*. Mitomycin-C (MMC) and oxaliplatin are both being used in HIPEC for CRC, but there is currently no consensus on the optimal drug or dosage.[55] With our organoid model of PM, head-to-head comparisons between treatment regimens were possible. Chemotherapy sensitivity differed significantly between organoids, but ninety-minute treatment with hyperthermic MMC was invariably more effective at clinical dosage than thirty-minute heated oxaliplatin treatment. Interestingly, oxaliplatin-based HIPEC was administered in the Prodige 7, COLOPEC and PROPHYLOCHIP trials, which may explain the negative outcomes of these studies.[56-58] With both MMC and oxaliplatin however, a substantial fraction of tumor cells survived,

stressing the need for improvement of HIPEC efficacy. We identified ATR inhibition as a powerful strategy to improve MMC cytotoxicity.

Ataxia telangiectasia and Rad3-related protein (ATR) is part of the DNA damage response. Its main function is to maintain genomic stability during replication by preventing collapse of stalled replication forks. Shortage of nucleotides, excessive origin firing and interstrand crosslinks (ICLs) can each cause replication fork stalling. Accumulation of stalled forks causes replication stress (RS). RS induces ATR activation, which in turn phosphorylates Chk1, to slow down DNA replication in S-phase and to prevent entry into mitosis.[59] Cancer cells generally have higher baseline levels of RS compared with normal cells due to oncogene activity, and are therefore reliant on a functioning ATR pathway to prevent disproportionate genomic instability.[60] Cancer cells might therefore be particularly vulnerable to ATR inhibition. Certain chemotherapies, such as MMC, cause further RS by inducing ICLs. Combining these therapies with ATR inhibition is therefore promising.[61, 62] Several clinical trials combining chemotherapy with ATR inhibition are underway. The first reported phase I trial (systemic topotecan plus ATR inhibitor M6620 in patients with advanced solid malignancies) suggested that the combination was well tolerated and preliminary efficacy data were promising.[63]

In the PM organoid model we found that ATR inhibition at low concentrations significantly improved efficacy of MMC. ATR inhibition might also enhance efficacy of HIPEC with oxaliplatin. ATR activity was recently identified as an important mechanism of oxaliplatin resistance through a loss-of-function genetic screen. Treatment with ATR inhibitors increased sensitivity towards oxaliplatin in multiple CRC cell lines and *in vivo*, by augmenting replication stress.[64] These findings warrant clinical evaluation of HIPEC combined with ATR inhibitors. A trial protocol similar to the recently completed CRC-PIPAC trial would be ideal to test this combination. In this trial patients received repetitive intraperitoneal treatment with pressurized oxaliplatin aerosols at six-weeks intervals.[65] Tissue and blood samples were collected prior to each treatment cycle, and disease progression was monitored four weeks after each cycle. Besides assessing the safety of combining HIPEC with ATR inhibition, such as trial would allow investigation of the mechanism of action in the clinical setting by obtaining pre- and posttreatment biopsies.

Limitations of organoids as preclinical models for drug development

Organoids are valuable models for drug discovery and drug testing. If we could grow organoids from every patient's tumor, and test a range of known and novel anticancer drugs to determine the most effective treatment, we could truly personalize anti-cancer treatment. Unfortunately, not all cancers give rise to viable organoids, and some organoids fail to expand sufficiently within a clinically relevant time frame to allow drug testing. Moreover, by sampling from a single tumor region, intratumor (subtype) heterogeneity is lost in organoid

models. Studies in which organoids were cultured from multiple tumor regions from the same patient showed genetic and transcriptomic heterogeneity.[66-68] This heterogeneity caused (corresponding) differences in drug responses, suggesting that anticipated clinical treatment effects might be over- or underestimated if organoids are created from a single region. In this light, malignant ascites is an interesting source of cells for organoid culturing. It presumably contains a mixture of tumor cells shed from different peritoneal metastases and the resulting organoids may therefore reflect intratumor heterogeneity.

Organoid models cannot accurately capture the complexity of the TME. The profound changes in gene expression and cytokine production that we observed upon merely changing the culture matrix from laminin-rich Matrigel to collagen type I (**chapter 4**) illustrate the major influence of the TME on organoid behavior. Stromal cells, matrix components, pH, and oxygen and nutrient concentrations have each been shown to influence therapeutic efficacy.[14] Although culture conditions can be manipulated to some extent, and various co-culture systems can be envisioned, the TME will remain an abstraction which limits extrapolation of results from organoid models to the clinic.

Proof-of-concept studies for subtype-targeted therapy

Since the addition of oxaliplatin to 5-FU and leucovorin more than 15 years ago, no drug has been identified that further improved the results of adjuvant therapy in CRC. Development of adjuvant therapy is a slow process, as only therapies proven effective in metastatic CRC eventually reach clinical testing in the adjuvant setting. Patients with mCRC included in drug trials have often received multiple lines of standard chemotherapy, which likely makes their tumors more resistant to novel drugs. As a result, many promising drugs are being discarded, while they could be potentially effective in untreated patients or in the adjuvant setting. Furthermore, targeted therapies that were proven effective in mCRC, such as vascular endothelial growth factor receptor (VEGFR)-inhibitors and epidermal growth factor receptor (EGFR)-inhibitors, showed no benefit in the adjuvant setting.[69, 70]

The CMS classification provides novel leads for subtype-specific therapeutic targets in early-stage CRC. To allow rapid translation of preclinical findings to patient studies, alternative trial designs and study endpoints are needed. Randomized controlled trials (RCTs) in stage II/III CRC require a large number of subjects, due to the relatively low recurrence rate, and at least two years of follow-up for the majority of these recurrences to occur. Molecular stratification is not often part of classical RCTs, even when testing targeted therapies. Before initiating these costly and time-consuming trials, it would be useful to confirm a novel drug's mechanism-of-action observed in preclinical models in the clinical setting. 'Window-of-opportunity trials' (WOTs) are ideally suited for this purpose. In this type of trial, the time period between cancer diagnosis and planned surgical treatment (the window of opportunity) is utilized to test a novel therapy in treatment-naive patients, to

observe changes in tumor biology. By comparing pretreatment biopsies with the resection specimen posttreatment, treatment effects can be studied on a molecular level. The study endpoint for each patient is reached within several weeks, leading to rapid assessment of the mechanism-of-action. Unlike neo-adjuvant therapy trials, the goal of WOTs is not to demonstrate treatment advantage, but rather to inform the subsequent phases of drug development and subject stratification.[71]

In this thesis we proposed to target tumor-stroma interactions in CMS4 tumors with RTKs. We designed a proof-of-concept study within the pre-operative window period, to test the effects of imatinib treatment on CMS4 CRC (ImPACCT, **chapter 3**). The primary endpoint of this study is the change in gene expression profiles, while taking subtype ITH into account by analyzing multiple tumor regions. Imatinib treatment might lead to partial stromal depletion, which could influence gene expression in both the tumor and stromal compartments, and might even lead to subtype switching. The ImPACCT trial was unfortunately terminated prematurely, due to a low accrual rate. Ultimately, five patients were treated with imatinib within the trial. We are currently analyzing gene expression profiles and proteomics of the pre- and posttreatment samples of these patients, to study whether any of the anticipated treatment effects can be observed in this small cohort.

Conducting a WOT requires a large multidisciplinary effort to ensure that patients are informed, included and treated within the short time frame before surgery. With the ImPACCT trial we have demonstrated that these logistic hurdles can be overcome with dedicated research teams in multiple hospitals. In spite of intense efforts of many collaborators, subject accrual was too slow, due to problems with pre-screening informed consent, exclusion criteria for drug treatment, and lack of willingness to participate in a WOT, as discussed in **chapter 3**. Nevertheless, we still believe in the potential of WOTs to expedite CMS-targeted therapy for early-stage CRC. We have shown that rapid testing of CMS4 status on multi-region endoscopic biopsies by RT-qPCR is technically and logistically possible alongside routine histopathological diagnostics within a WOT. Sufficient and high quality RNA can be derived from the vast majority of fresh-frozen endoscopic biopsies. Indeed, CMS4 status could be assessed in all 62 CRCs that were included in the prescreening part of the ImPACCT trial. A change in ethical guidelines that allows obtaining additional biopsies for molecular diagnostic tests without upfront informed consent is needed to improve accrual rates for subtype-targeted therapy studies immediately after diagnosis of CRC. Since the risk of complications from colonoscopy, such as bowel perforation or bleeding, is very low, and is mainly associated with performance of endoscopic interventions such as polypectomy (0.016-0.2%[72]), this seems justifiable. To further improve subject enrollment, patients should be educated on the necessity of patient participation in clinical trials to advance cancer treatment. Finally, we could develop an umbrella protocol of WOTs for each subtype, so that participation in a subtype-specific clinical trial can be offered to all early-stage CRC patients.

Risk stratification and targeted therapy - beyond CMS

To improve outcome of CRC, the major challenges remain to identify patients at risk for developing metastases, and to assign these patients to the appropriate adjuvant treatments. The CMS classification is a first step towards stratification of this highly heterogeneous disease and it offers clues to development of subtype-targeted therapy. However, its prognostic value is limited. Patients with CMS4 CRC have an increased chance of progression to metastatic disease, but not all patients with CMS4 tumors develop metastases, while some patients with CMS1-3 tumors do develop metastases. In fact, when CMS1 tumors metastasize, they even have a worse prognosis compared with the other subtypes.[5, 73]

Further substratification within CMS and combinations with other classification systems are likely to improve the prognostic value of CMS. Various markers, such as genetic mutations, microsatellite stability, Immunoscore[74] and stroma score[75] might carry variable prognostic information within different molecular subtypes. For example, low expression of CDX2 is only found in CMS1 and CMS4. In CMS4 it identifies a subgroup with particularly poor prognosis, but low CDX2 expression is not prognostic in CMS1.[76, 77] As another example, BRAF-mutated MSS tumours have a high risk of metastasis, but are mostly found within the context of CMS1, and may therefore be less relevant in other subtypes.[78] A recent study combined CMS, CRIS and (modified) Immunoscore to identify a CRIS-C subgroup within CMS2 with low levels CD8+ lymphocytes that would benefit most from adjuvant chemotherapy without excess overtreatment.[79] Thus, by establishing rather homogeneous molecular subtypes, CMS may provide a starting point for validation of subtype-specific biomarkers and substratification, to find the right treatment strategy for each patient (Figure 2).

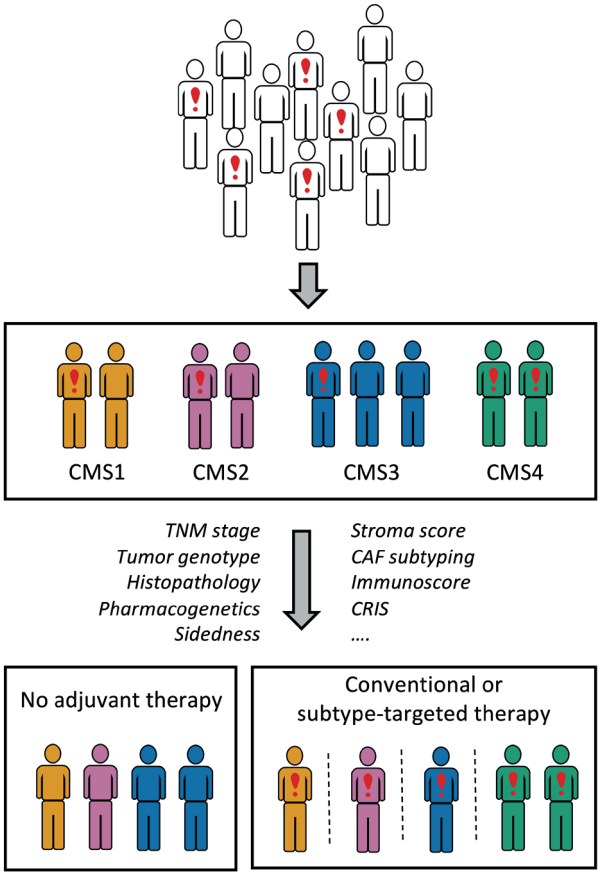

Figure 2. Future perspective on patient stratification in CRC.
Substratification of patients within CMS groups, based on additional histological, genetic and phenotypic markers, could help to identify those patients at risk of developing metastases (depicted by red exclamation marks), who require adjuvant therapy. The CMS could provide leads for alternative targeted therapies in subtypes that respond poorly to conventional therapy.

REFERENCES

1. Steller EJA, Raats DA, Koster J, et al. PDGFRB promotes liver metastasis formation of mesenchymal-like colorectal tumor cells. *Neoplasia*. 2013;**15**(2):204-17.
2. Fatrai S, van Schelven SJ, Ubink I, et al. Maintenance of Clonogenic KIT(+) Human Colon Tumor Cells Requires Secretion of Stem Cell Factor by Differentiated Tumor Cells. *Gastroenterology*. 2015;**149**(3):692-704.
3. Kashofer K, Viertler C, Pichler M, et al. Quality control of RNA preservation and extraction from paraffin-embedded tissue: implications for RT-PCR and microarray analysis. *PLoS One*. 2013;**8**(7):e70714.
4. Trinh A, Trumpi K, De Sousa EMF, et al. Practical and Robust Identification of Molecular Subtypes in Colorectal Cancer by Immunohistochemistry. *Clin Cancer Res*. 2017;**23**(2):387-98.
5. Guinney J, Dienstmann R, Wang X, et al. The consensus molecular subtypes of colorectal cancer. *Nat Med*. 2015;**21**(11):1350-6.
6. Chen X, Deane NG, Lewis KB, et al. Comparison of Nanostring nCounter(R) Data on FFPE Colon Cancer Samples and Affymetrix Microarray Data on Matched Frozen Tissues. *PLoS One*. 2016;**11**(5):e0153784.
7. Ragulan C, Eason K, Fontana E, et al. Analytical Validation of Multiplex Biomarker Assay to Stratify Colorectal Cancer into Molecular Subtypes. *Sci Rep*. 2019;**9**(1):7665.
8. Piskol R, Huw L, Sergin I, et al. A Clinically Applicable Gene-Expression Classifier Reveals Intrinsic and Extrinsic Contributions to Consensus Molecular Subtypes in Primary and Metastatic Colon Cancer. *Clin Cancer Res*. 2019;**25**(14):4431-42.
9. Lenz HJ, Ou FS, Venook AP, et al. Impact of Consensus Molecular Subtype on Survival in Patients With Metastatic Colorectal Cancer: Results From CALGB/SWOG 80405 (Alliance). *J Clin Oncol*. 2019;**37**(22):1876-85.
10. De Smedt L, Lemahieu J, Palmans S, et al. Microsatellite instable vs stable colon carcinomas: analysis of tumour heterogeneity, inflammation and angiogenesis. *Br J Cancer*. 2015;**113**(3):500-9.
11. Sottoriva A, Kang H, Ma Z, et al. A Big Bang model of human colorectal tumor growth. *Nat Genet*. 2015;**47**(3):209-16.
12. Kreso A, Dick JE. Evolution of the cancer stem cell model. *Cell Stem Cell*. 2014;**14**(3):275-91.
13. Lenos KJ, Miedema DM, Lodestijn SC, et al. Stem cell functionality is microenvironmentally defined during tumour expansion and therapy response in colon cancer. *Nat Cell Biol*. 2018;**20**(10):1193-202.
14. Junttila MR, de Sauvage FJ. Influence of tumour micro-environment heterogeneity on therapeutic response. *Nature*. 2013;**501**(7467):346-54.
15. Alfarouk KO, Ibrahim ME, Gatenby RA, et al. Riparian ecosystems in human cancers. *Evol Appl*. 2013;**6**(1):46-53.
16. Alderdice M, Richman SD, Gollins S, et al. Prospective patient stratification into robust cancer-cell intrinsic subtypes from colorectal cancer biopsies. *J Pathol*. 2018;**245**(1):19-28.
17. van der Heijden M, Miedema DM, Waclaw B, et al. Spatiotemporal regulation of clonogenicity in colorectal cancer xenografts. *Proc Natl Acad Sci U S A*. 2019;**116**(13):6140-5.
18. Galon J, Costes A, Sanchez-Cabo F, et al. Type, density, and location of immune cells within human colorectal tumors predict clinical outcome. *Science*. 2006;**313**(5795):1960-4.
19. Heindl A, Nawaz S, Yuan Y. Mapping spatial heterogeneity in the tumor microenvironment: a new era for digital pathology. *Lab Invest*. 2015;**95**(4):377-84.
20. Isella C, Terrasi A, Bellomo SE, et al. Stromal contribution to the colorectal cancer transcriptome. *Nat Genet*. 2015;**47**(4):312-9.
21. Calon A, Lonardo E, Berenguer-Llergo A, et al. Stromal gene expression defines poor-prognosis subtypes in colorectal cancer. *Nat Genet*. 2015;**47**(4):320-9.
22. Vellinga TT, den Uil S, Rinkes IH, et al. Collagen-rich stroma in aggressive colon tumors induces mesenchymal gene expression and tumor cell invasion. *Oncogene*. 2016;**35**(40):5263-71.
23. Isella C, Brundu F, Bellomo SE, et al. Selective analysis of cancer-cell intrinsic transcriptional traits defines novel clinically relevant subtypes of colorectal cancer. *Nat Commun*. 2017;**8**:15107.
24. Dunne PD, Alderdice M, O'Reilly PG, et al. Cancer-cell intrinsic gene expression signatures overcome intratumoural heterogeneity bias in colorectal cancer patient classification. *Nat Commun*. 2017;**8**:15657.
25. Dunne PD, McArt DG, Bradley CA, et al. Challenging the Cancer Molecular Stratification Dogma: Intratumoral Heterogeneity Undermines Consensus Molecular Subtypes and Potential Diagnostic Value in Colorectal Cancer. *Clin Cancer Res*. 2016;**22**(16):4095-104.

26. De Smedt L, Palmans S, Andel D, et al. Expression profiling of budding cells in colorectal cancer reveals an EMT-like phenotype and molecular subtype switching. *Br J Cancer*. 2017;**116**(1):58-65.
27. Eide PW, Bruun J, Lothe RA, et al. CMScaller: an R package for consensus molecular subtyping of colorectal cancer pre-clinical models. *Sci Rep*. 2017;**7**(1):16618.
28. Bramsen JB, Rasmussen MH, Ongen H, et al. Molecular-Subtype-Specific Biomarkers Improve Prediction of Prognosis in Colorectal Cancer. *Cell Rep*. 2017;**19**(6):1268-80.
29. Dienstmann R, Villacampa G, Sveen A, et al. Relative contribution of clinicopathological variables, genomic markers, transcriptomic subtyping and microenvironment features for outcome prediction in stage II/III colorectal cancer. *Ann Oncol*. 2019.
30. Tanaka S, Martling A, Lindholm J, et al. Remaining cancer cells within the fibrosis after neo-adjuvant treatment for locally advanced rectal cancer. *Eur J Surg Oncol*. 2015;**41**(9):1204-9.
31. Woolston A, Khan K, Spain G, et al. Genomic and Transcriptomic Determinants of Therapy Resistance and Immune Landscape Evolution during Anti-EGFR Treatment in Colorectal Cancer. *Cancer Cell*. 2019;**36**(1):35-50 e9.
32. Kamal Y, Schmit SL, Hoehn HJ, et al. Transcriptomic Differences between Primary Colorectal Adenocarcinomas and Distant Metastases Reveal Metastatic Colorectal Cancer Subtypes. *Cancer Res*. 2019;**79**(16):4227-41.
33. Yang AD, Fan F, Camp ER, et al. Chronic oxaliplatin resistance induces epithelial-to-mesenchymal transition in colorectal cancer cell lines. *Clin Cancer Res*. 2006;**12**(14 Pt 1):4147-53.
34. Yao Q, Qu X, Yang Q, et al. CLIC4 mediates TGF-beta1-induced fibroblast-to-myofibroblast transdifferentiation in ovarian cancer. *Oncol Rep*. 2009;**22**(3):541-8.
35. Sodek KL, Murphy KJ, Brown TJ, et al. Cell-cell and cell-matrix dynamics in intraperitoneal cancer metastasis. *Cancer Metastasis Rev*. 2012;**31**(1-2):397-414.
36. Pretzsch E, Bosch F, Neumann J, et al. Mechanisms of Metastasis in Colorectal Cancer and Metastatic Organotropism: Hematogenous versus Peritoneal Spread. *J Oncol*. 2019;**2019**:7407190.
37. Pitroda SP, Khodarev NN, Huang L, et al. Integrated molecular subtyping defines a curable oligometastatic state in colorectal liver metastasis. *Nat Commun*. 2018;**9**(1):1793.
38. Ostrup O, Dagenborg VJ, Rodland EA, et al. Molecular signatures reflecting microenvironmental metabolism and chemotherapy-induced immunogenic cell death in colorectal liver metastases. *Oncotarget*. 2017;**8**(44):76290-304.
39. Fontana E, Eason K, Cervantes A, et al. Context matters-consensus molecular subtypes of colorectal cancer as biomarkers for clinical trials. *Ann Oncol*. 2019;**30**(4):520-7.
40. Trumpi K, Frenkel N, Peters T, et al. Macrophages induce "budding" in aggressive human colon cancer subtypes by protease-mediated disruption of tight junctions. *Oncotarget*. 2018;**9**(28):19490-507.
41. Fong Y, Fortner J, Sun RL, et al. Clinical score for predicting recurrence after hepatic resection for metastatic colorectal cancer: analysis of 1001 consecutive cases. *Ann Surg*. 1999;**230**(3):309-18; discussion 18-21.
42. Fujii M, Shimokawa M, Date S, et al. A Colorectal Tumor Organoid Library Demonstrates Progressive Loss of Niche Factor Requirements during Tumorigenesis. *Cell Stem Cell*. 2016;**18**(6):827-38.
43. van de Wetering M, Francies HE, Francis JM, et al. Prospective derivation of a living organoid biobank of colorectal cancer patients. *Cell*. 2015;**161**(4):933-45.
44. Weeber F, van de Wetering M, Hoogstraat M, et al. Preserved genetic diversity in organoids cultured from biopsies of human colorectal cancer metastases. *Proc Natl Acad Sci U S A*. 2015;**112**(43):13308-11.
45. Vlachogiannis G, Hedayat S, Vatsiou A, et al. Patient-derived organoids model treatment response of metastatic gastrointestinal cancers. *Science*. 2018;**359**(6378):920-6.
46. Sachs N, de Ligt J, Kopper O, et al. A Living Biobank of Breast Cancer Organoids Captures Disease Heterogeneity. *Cell*. 2018;**172**(1-2):373-86 e10.
47. Verissimo CS, Overmeer RM, Ponsioen B, et al. Targeting mutant RAS in patient-derived colorectal cancer organoids by combinatorial drug screening. *Elife*. 2016;**5**.
48. Linnekamp JF, Hooff SRV, Prasetyanti PR, et al. Consensus molecular subtypes of colorectal cancer are recapitulated in in vitro and in vivo models. *Cell Death Differ*. 2018.
49. Sveen A, Bruun J, Eide PW, et al. Colorectal Cancer Consensus Molecular Subtypes Translated to Preclinical Models Uncover Potentially Targetable Cancer Cell Dependencies. *Clin Cancer Res*. 2018;**24**(4):794-806.
50. Morton JP, Karim SA, Graham K, et al. Dasatinib inhibits the development of metastases in a mouse model of pancreatic ductal adenocarcinoma. *Gastroenterology*. 2010;**139**(1):292-303.

51. Scott AJ, Song EK, Bagby S, et al. Evaluation of the efficacy of dasatinib, a Src/Abl inhibitor, in colorectal cancer cell lines and explant mouse model. *PLoS One*. 2017;**12**(11):e0187173.
52. Parseghian CM, Parikh NU, Wu JY, et al. Dual Inhibition of EGFR and c-Src by Cetuximab and Dasatinib Combined with FOLFOX Chemotherapy in Patients with Metastatic Colorectal Cancer. *Clin Cancer Res*. 2017;**23**(15):4146-54.
53. Strickler JH, McCall S, Nixon AB, et al. Phase I study of dasatinib in combination with capecitabine, oxaliplatin and bevacizumab followed by an expanded cohort in previously untreated metastatic colorectal cancer. *Invest New Drugs*. 2014;**32**(2):330-9.
54. Kopetz S, Morris VK, Parikh N, et al. Src activity is modulated by oxaliplatin and correlates with outcomes after hepatectomy for metastatic colorectal cancer. *BMC Cancer*. 2014;**14**:660.
55. Bushati M, Rovers KP, Sommariva A, et al. The current practice of cytoreductive surgery and HIPEC for colorectal peritoneal metastases: Results of a worldwide web-based survey of the Peritoneal Surface Oncology Group International (PSOGI). *Eur J Surg Oncol*. 2018;**44**(12):1942-8.
56. Quenet F, Elias D, Roca L, et al. A UNICANCER phase III trial of hyperthermic intra-peritoneal chemotherapy (HIPEC) for colorectal peritoneal carcinomatosis (PC): PRODIGE 7. *J Clin Oncol*. 2018;**36**(18_suppl):LBA3503-LBA.
57. Klaver CEL, Wisselink DD, Punt CJA, et al. Adjuvant hyperthermic intraperitoneal chemotherapy in patients with locally advanced colon cancer (COLOPEC): a multicentre, open-label, randomised trial. *Lancet Gastroenterol Hepatol*. 2019;**4**(10):761-70.
58. Goere D, Glehen O, Quenet F, et al. Results of a randomized phase 3 study evaluating the potential benefit of a second-look surgery plus HIPEC in patients at high risk of developing colorectal peritoneal metastases (PROPHYLOCHIP- NTC01226394). *J Clin Oncol*. 2018;**36**(15_suppl):3531.
59. Toledo LI, Altmeyer M, Rask MB, et al. ATR prohibits replication catastrophe by preventing global exhaustion of RPA. *Cell*. 2013;**155**(5):1088-103.
60. Macheret M, Halazonetis TD. DNA replication stress as a hallmark of cancer. *Annu Rev Pathol*. 2015;**10**:425-48.
61. Lecona E, Fernandez-Capetillo O. Targeting ATR in cancer. *Nat Rev Cancer*. 2018;**18**(9):586-95.
62. Karnitz LM, Zou L. Molecular Pathways: Targeting ATR in Cancer Therapy. *Clin Cancer Res*. 2015;**21**(21):4780-5.
63. Thomas A, Redon CE, Sciuto L, et al. Phase I Study of ATR Inhibitor M6620 in Combination With Topotecan in Patients With Advanced Solid Tumors. *J Clin Oncol*. 2018;**36**(16):1594-602.
64. Combes E, Andrade AF, Tosi D, et al. Inhibition of Ataxia-Telangiectasia Mutated and RAD3-related (ATR) overcomes oxaliplatin resistance and promotes anti-tumor immunity in colorectal cancer. *Cancer Res*. 2019.
65. Rovers KP, Lurvink RJ, Wassenaar EC, et al. Repetitive electrostatic pressurised intraperitoneal aerosol chemotherapy (ePIPAC) with oxaliplatin as a palliative monotherapy for isolated unresectable colorectal peritoneal metastases: protocol of a Dutch, multicentre, open-label, single-arm, phase II study (CRC-PIPAC). *BMJ Open*. 2019;**9**(7):e030408.
66. Roerink SF, Sasaki N, Lee-Six H, et al. Intra-tumour diversification in colorectal cancer at the single-cell level. *Nature*. 2018;**556**(7702):457-62.
67. Schumacher D, Andrieux G, Boehnke K, et al. Heterogeneous pathway activation and drug response modelled in colorectal-tumor-derived 3D cultures. *PLoS Genet*. 2019;**15**(3):e1008076.
68. Arnadottir SS, Jeppesen M, Lamy P, et al. Characterization of genetic intratumor heterogeneity in colorectal cancer and matching patient-derived spheroid cultures. *Mol Oncol*. 2018;**12**(1):132-47.
69. Allegra CJ, Yothers G, O'Connell MJ, et al. Phase III trial assessing bevacizumab in stages II and III carcinoma of the colon: results of NSABP protocol C-08. *J Clin Oncol*. 2011;**29**(1):11-6.
70. Huang J, Nair SG, Mahoney MR, et al. Comparison of FOLFIRI with or without cetuximab in patients with resected stage III colon cancer; NCCTG (Alliance) intergroup trial N0147. *Clin Colorectal Cancer*. 2014;**13**(2):100-9.
71. Maugeri-Sacca M, Barba M, Vici P, et al. Presurgical window of opportunity trial design as a platform for testing anticancer drugs: Pros, cons and a focus on breast cancer. *Crit Rev Oncol Hematol*. 2016;**106**:132-42.
72. Lohsiriwat V. Colonoscopic perforation: incidence, risk factors, management and outcome. *World journal of gastroenterology: WJG*. 2010;**16**(4):425-30.
73. Mooi JK, Wirapati P, Asher R, et al. The prognostic impact of consensus molecular subtypes (CMS) and its predictive effects for bevacizumab benefit in metastatic colorectal cancer: molecular analysis of the AGITG MAX clinical trial. *Ann Oncol*. 2018;**29**(11):2240-6.

74. Pages F, Mlecnik B, Marliot F, et al. International validation of the consensus Immunoscore for the classification of colon cancer: a prognostic and accuracy study. *Lancet*. 2018;**391**(10135):2128-39.
75. Huijbers A, Tollenaar RA, v Pelt GW, et al. The proportion of tumor-stroma as a strong prognosticator for stage II and III colon cancer patients: validation in the VICTOR trial. *Ann Oncol*. 2013;**24**(1):179-85.
76. Pilati C, Taieb J, Balogoun R, et al. CDX2 prognostic value in stage II/III resected colon cancer is related to CMS classification. *Ann Oncol*. 2017;**28**(5):1032-5.
77. Sandberg TP, Sweere I, van Pelt GW, et al. Prognostic value of low CDX2 expression in colorectal cancers with a high stromal content - a short report. *Cell Oncol (Dordr)*. 2019.
78. Smeby J, Sveen A, Merok MA, et al. CMS-dependent prognostic impact of KRAS and BRAFV600E mutations in primary colorectal cancer. *Ann Oncol*. 2018;**29**(5):1227-34.
79. Allen WL, Dunne PD, McDade S, et al. Transcriptional subtyping and CD8 immunohistochemistry identifies poor prognosis stage II/III colorectal cancer patients who benefit from adjuvant chemotherapy. *JCO Precis Oncol*. 2018;**2018**.

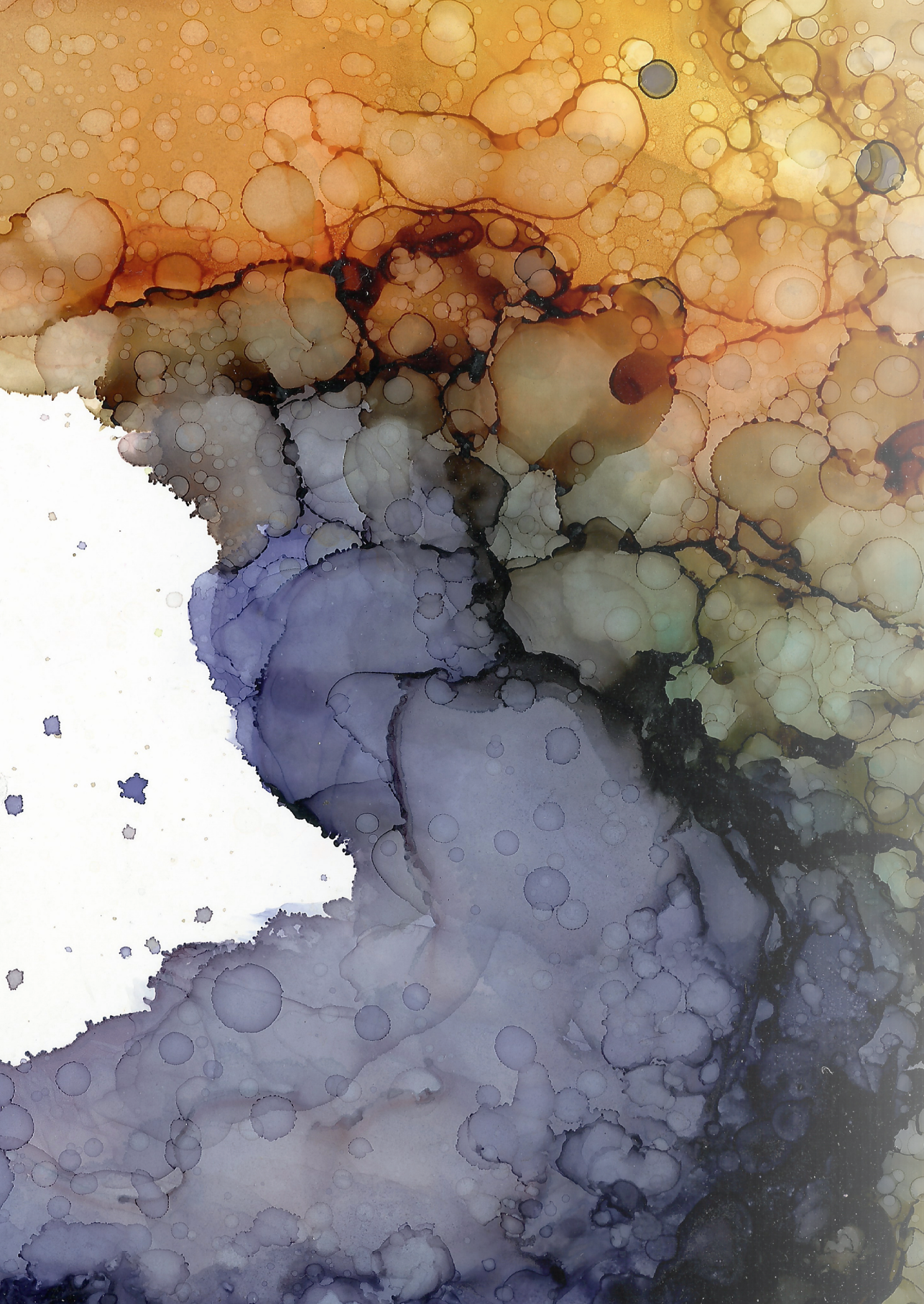

11

Summary in Dutch
Samenvatting in het Nederlands

SAMENVATTING IN HET NEDERLANDS

Jaarlijks krijgen ruim 14.000 Nederlanders de diagnose dikke darmkanker en overlijden er ongeveer 5000 patiënten aan deze ziekte. Uitgezaaide ziekte is de voornaamste oorzaak van sterfte door darmkanker. Ongeveer een kwart van de patiënten heeft al afstandsmetastasen ten tijde van de initiële diagnose, en nog eens 15% van de patiënten ontwikkelt metastasen op een later moment. Het voorkomen van de uitgroei van metastasen zou de prognose van patiënten met darmkanker in een vroeg stadium aanmerkelijk verbeteren. Momenteel kunnen we echter niet goed voorspellen welke patiënten afstandsmetastasen zullen krijgen. We weten dat bepaalde pathologische kenmerken, zoals uitzaaiingen in locoregionale lymfeklieren en doorgroei van de darmtumor in omliggende organen, het risico op metastasen verhogen. Deze patiënten krijgen daarom na operatieve verwijdering van de darmkanker adjuvante chemotherapie aangeboden. Maar lang niet alle patiënten met deze risicofactoren zullen daadwerkelijk metastasen ontwikkelen, en met de huidige chemotherapieën kan terugkeer van ziekte niet bij iedereen worden voorkomen. Er is dus sprake van zowel over- als onderbehandeling, en behoefte aan betere risicostratificatie om patiënten die baat hebben bij adjuvante chemotherapie te identificeren. Bovendien zijn er alternatieve behandelingen nodig voor patiënten met een hoog risico op metastasen die niet op de huidige adjuvante therapie reageren. Onderzoek naar de moleculaire eigenschappen van tumoren kan hierin een rol spelen. Door middel van genexpressieprofielen kunnen darmkankers onderverdeeld worden in moleculaire subgroepen. De Consensus Molecular Subtype (CMS) classificatie onderscheidt vier subtypen. Deze groepen verschillen in activiteit van cellulaire signaleringsroutes. Daarnaast zijn er verschillen in de samenstelling van de tumor micro-omgeving die bestaat uit diverse niet-neoplastische cellen en extracellulaire matrix. De CMSs hebben bovendien een heel verschillende prognose en wisselende gevoeligheid voor huidige chemotherapieën. De CMSs bieden hiermee aanknopingspunten voor patiëntselectie en voor het ontdekken van nieuwe therapieën.

Op dit moment wordt de CMS classificatie echter nog niet toegepast in de behandeling van darmkanker. Een van de redenen hiervoor is dat de classificatie niet eenvoudig geïmplementeerd kan worden in de dagelijkse praktijk. Genexpressie-analyse met behulp van microarray of RNA-sequencing is kostbaar en vergt verwerking en interpretatie door bio-informatici. In **hoofdstuk 2** hebben we de CMS classificatie gereduceerd tot een kleine set van vier genen die samen CMS4 tumoren kunnen identificeren bij individuele patiënten. De test is specifiek gericht op CMS4, omdat dit subtype van de vier de slechtste prognose heeft en omdat dit type ongevoelig is voor standaard adjuvante chemotherapie met oxaliplatine. Identificatie van deze groep en ontwikkeling van nieuwe behandelingen tegen CMS4 zijn dus van groot belang. Door gebruik te maken van de RT-qPCR techniek kan de

test in elk modern pathologie lab uitgevoerd worden. Uit de eerste resultaten van de ImPACCT studie, gepresenteerd in **hoofdstuk 3**, bleek dat het bovendien goed haalbaar is om endoscopische biopten van darmkanker in verschillende ziekenhuizen te verzamelen en gelijktijdig met standaard histopathologische diagnostiek te testen met de RT-qPCR test, om zo de subtypering al te bepalen voordat de tumor verwijderd is.

In **hoofdstuk 2** werd de nieuwe RT-qPCR test voor CMS4 toegepast op meerdere samples van dezelfde tumor. Hieruit bleek dat verschillende gebieden in één tumor tot een ander moleculair subtype kunnen behoren. Deze observatie werd bevestigd door analyse van de ImPACCT biopten in **hoofdstuk 3**. Vermoedelijk heeft deze intratumorale heterogeniteit in subtype grotendeels te maken met verschillen in samenstelling van het stroma tussen de tumorregio's. De CMS classificatie is gebaseerd op genexpressie van de gehele tumor, waarbij zowel genexpressie in de tumorcellen als die in de stromale cellen (zoals fibroblasten en immuuncellen) is meegenomen. Bovendien beïnvloeden tumorcellen en stromale cellen elkaar waardoor de genexpressie in beide compartimenten kan veranderen door interactie. Verschillen in de hoeveelheid en het type stromale cellen kunnen dus leiden tot andere subtypering. Het is nog onduidelijk wat de biologische significantie van deze heterogeniteit is, maar het heeft in ieder geval gevolgen voor patiëntselectie. In **hoofdstuk 2** lieten we zien dat subtypering van een enkel biopt vaak niet representatief is voor de classificatie van het merendeel van de tumor.

De onderliggende signaleringsroutes in de verschillende CMSs bieden gelegenheid voor subtype-gerichte therapie. CMS4 wordt gekenmerkt door expressie van genen die verband houden met epitheliale-naar-mesenchymale transitie en met stamcel eigenschappen, en de micro-omgeving is rijk aan fibroblasten en collageen; dit type wordt daarom ook wel het mesenchymale subtype genoemd. Het agressieve gedrag van CMS4 tumoren wordt vaak toegeschreven aan de interactie tussen tumorcellen en de stroma-rijke omgeving. Met name de aanwezigheid van fibroblasten is vaak gerelateerd aan een slechte prognose, therapie-resistentie en metastasering. Het blokkeren van de interactie tussen tumorcellen en de micro-omgeving zou daarom effectief kunnen zijn in de behandeling van CMS4 tumoren.

Uit eerder werk van onze onderzoeksgroep kwam naar voren dat de platelet-derived growth factor receptoren (PDGFR) en de c-KIT receptor en rol spelen in het agressieve karakter van CMS4. Deze receptoren kunnen zowel op tumorcellen als op stromale cellen aanwezig zijn, en inhibitie ervan leidde tot minder tumorgroei en metastasering in preklinische modellen. In de ImPACCT studie (**hoofdstuk 3**) wilden we onderzoeken of behandeling met imatinib deze receptoren ook in de patiënt zou kunnen remmen en of dit effect heeft op het genexpressieprofiel van CMS4 tumoren. Helaas is deze studie voortijdig beëindigd vanwege te langzame proefpersoneninclusie. Om een dergelijke studie in de toekomst haalbaar te maken zijn er ofwel aanpassingen in regelgeving omtrent informed

consent voor afname van extra studiebiopten nodig, ofwel moeten er alternatieve CMS(4) testen ontwikkeld worden die op paraffinemateriaal werken.

Bij de verdere zoektocht naar nieuwe therapeutische doelwitten in CMS4 werd in **hoofdstuk 4** gekeken naar de effecten van collageen en fibroblasten op genexpressie en invasief gedrag van darmkanker organoïden. Blootstelling aan collageen induceerde een mesenchymaal genexpressieprofiel in de tumorcellen, en leidde tot activatie van Src signalering. Dasatinib, een potente inhibitor van Src en van meerdere receptor tyrosine kinases die tot expressie komen in CMS4 tumoren, remde de uitgroei van organoïden in collageen en de migratie van tumorcellen over een collageen bodemlaag. Wanneer de organoïden samen met fibroblasten werden gekweekt in collageen vormden de organoïden invasieve strengen door de driedimensionale matrix. Ook dit invasieve effect kon geremd worden door behandeling met dasatinib, waarschijnlijk deels door het cytotoxische effect op fibroblasten en deels door een direct effect op de organoïden. Door deze eerste stap in metastasering te remmen, zou dasatinib effectief kunnen zijn tegen CMS4 darmkanker.

In vervolg van dit proefschrift werd gekeken naar moleculaire typering van metastasen van darmkanker en naar nieuwe behandelmogelijkheden hiervoor. Peritoneale metastasen (PM) staan bekend om hun infauste prognose. Histologisch worden PM vaak gekenmerkt door een grote hoeveelheid stroma. Tezamen leidde dit tot de hypothese dat PM mogelijk verrijkt zijn in CMS4. In **hoofdstuk 5** werd deze hypothese getest door de CMS4 RT-qPCR test toe te passen op gepaarde darmkankers en PM. Zowel de primaire tumoren als de PM bleken veel vaker CMS4 te zijn dan de primaire tumoren uit de oorspronkelijke CMS studie. CMS4-gerichte therapie zou mogelijk een plaats kunnen krijgen in de behandeling van peritoneale metastasen van darmkanker.

Een klein deel van de patiënten met PM komt in aanmerking voor behandeling met cytoreductie (een operatie waarbij alle zichtbare metastasen uit de buikholte verwijderd worden) in combinatie met spoeling van de buikholte met verwarmde chemotherapie (hypertherme intraperitoneale chemotherapie (HIPEC)). Er is wereldwijd discussie over de keuze van chemotherapie, de duur van de spoeling en de temperatuur ervan. In Nederland wordt zowel Mitomycine C (MMC) als oxaliplatine gebruikt voor HIPEC bij darmkanker. Met MMC wordt 90 minuten lang gespoeld, met oxaliplatine maar 30 minuten. In **hoofdstuk 6** hebben we deze twee behandelingen vergeleken in een organoïdenmodel van PM. Behandeling met MMC was in dit model effectiever dan oxaliplatine. Mogelijk heeft dit te maken met de relatieve ongevoeligheid van CMS4 tumoren voor oxaliplatine, of komt het door de kortere blootstellingstijd. Hoewel MMC bij klinische dosering in de meeste gevallen voor celdood zorgde, was na behandeling nog een aanzienlijk deel van de tumorcellen in leven. Vervolgens hebben we daarom onderzocht of we de behandeling effectiever konden maken door in te spelen op het werkingsmechanisme van MMC. MMC

veroorzaakt DNA schade door verbindingen te maken tussen DNA strengen, waardoor DNA synthese en celdeling niet goed mogelijk zijn. Het eiwit ATR is verantwoordelijk voor het herstel van deze MMC-geïnduceerde DNA schade. Door dit eiwit te remmen na behandeling met MMC zagen we een significante toename van celdood, waarmee alle organoïdelijnen gevoeliger werden voor HIPEC met MMC.

In de laatste drie hoofdstukken van dit proefschrift is gekeken naar de moleculaire classificatie en de chirurgische behandeling van levermetastasen (LM). De lever is de meest voorkomende lokalisatie voor uitzaaiingen van darmkanker. In **hoofdstuk 7** werd onderzocht of LM tot hetzelfde moleculaire subtype behoren als de primaire tumoren waaruit zij zijn ontstaan. Er werd aanzienlijke discordantie gezien in classificatie van gepaarde tumoren. Subtype-gerichte therapie voor gemetastaseerde ziekte kan daarom niet gebaseerd worden op classificatie van de primaire tumor. Er zijn meerdere verklaringen te bedenken voor de gevonden discordantie, zoals intratumor heterogeniteit en niche factoren. In dit hoofdstuk werd bovendien aangetoond dat behandeling met chemo- en/of radiotherapie gevolgen kan hebben voor de moleculaire subtypering. Door toename van fibrose en genexpressieveranderingen in de kankercellen krijgen tumoren na behandeling vaker een mesenchymaal fenotype. CMS4-gerichte therapie zou daarom ook effectief kunnen zijn tegen resterende tumorcellen na eerdere chemotherapeutische behandeling.

Chirurgie is de enige curatieve behandeling voor LM. Chirurgen zijn daarom geneigd om, indien technisch haalbaar, alle patiënten met LM te opereren. Grote leverresecties gaan echter gepaard met aanzienlijke morbiditeit. Het is daarom van belang om te weten of de ingreep daadwerkelijk overlevingswinst zal bieden. In **hoofdstuk 8** onderzochten we of resectie na langdurige (palliatieve) chemotherapie meerwaarde had. Over het algemeen was de ziektevrije overleving in deze groep patiënten maar kort. Een kleine groep patiënten bleef echter langdurig ziektevrij. Patiënten bij wie niet alle metastasen operatief verwijderd konden worden hadden een beduidend slechtere prognose. In **hoofdstuk 9** vergeleken we korte- en lange termijnuitkomsten van majeure leverchirurgie met die van kleinere resecties. Uitgebreide resectie zorgde voor meer complicaties, maar er werden geen verschillen gezien in ziektevrije of algehele overleving. Bij een fitte patiënt is uitgebreide resectie, ook na langdurige chemotherapie, dus zeker te overwegen. Er zijn echter betere selectiecriteria nodig om te bepalen wie werkelijk baat hebben bij deze hoog-risico ingrepen. Wellicht kunnen moleculaire eigenschappen van de metastasen hier in de toekomst een rol in spelen.

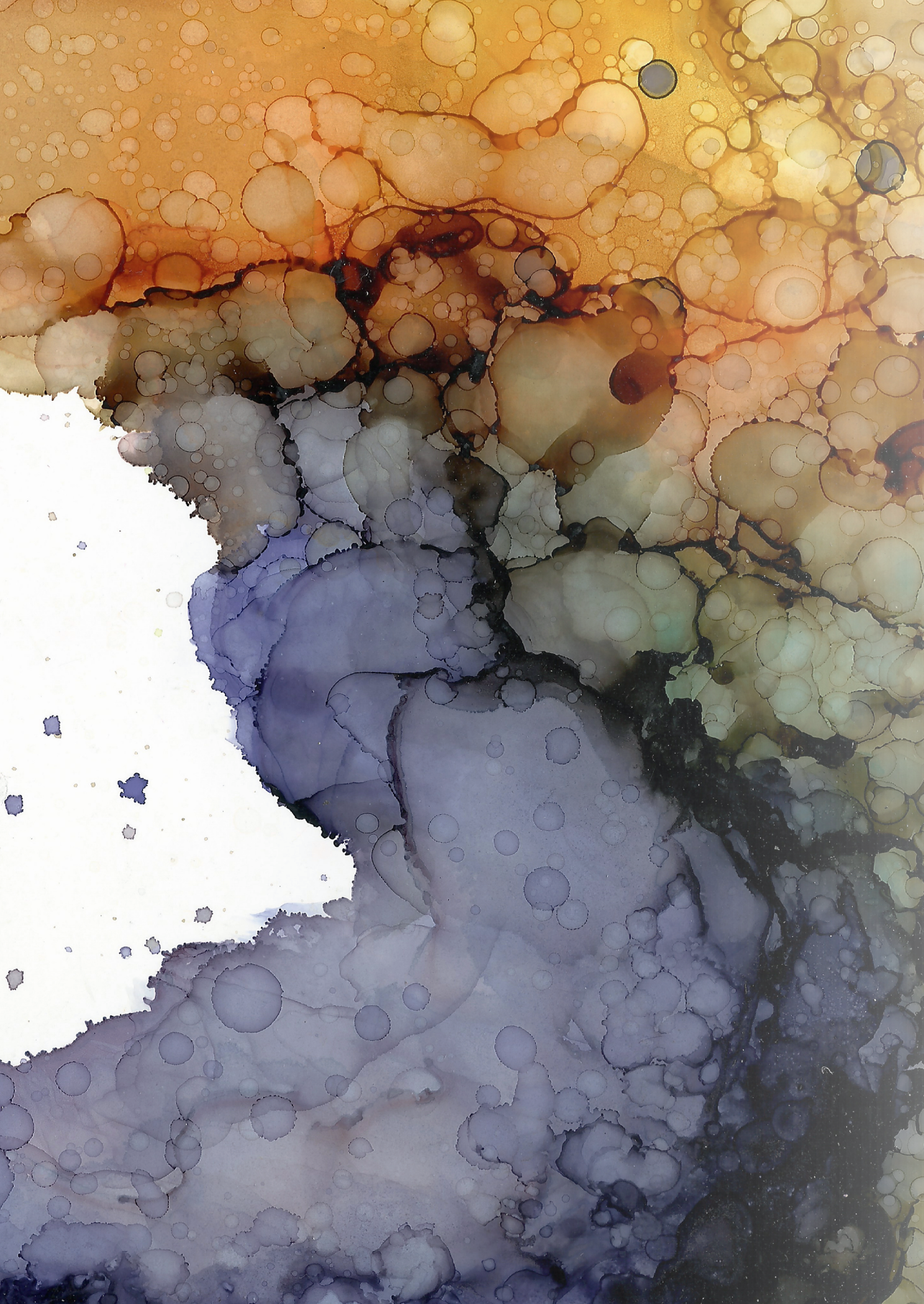

Annexes

Authors and affiliations

Assessment Committee

List of Publications

Acknowledgements

Curriculum Vitae Auctoris

AUTHORS AND AFFILIATIONS

Arend G.J. Aalbers, MD, PhD
Department of Surgical Oncology
Netherlands Cancer Institute -
Antoni van Leeuwenhoek
Amsterdam, the Netherlands

Haiko J. Bloemendal, MD, PhD
Department of Medical Oncology
Meander MC
Amersfoort, the Netherlands
Department of Medical Oncology
Radboud University Medical Center
Nijmegen, the Netherlands

Anneroos W. Boerman, MD
Department of Medical Oncology
Meander MC
Amersfoort, the Netherlands

Ana C.F. Bolhaqueiro, PhD
Oncode Institute, Hubrecht Institute –
Royal Academy of Arts and Sciences
Utrecht, the Netherlands

Inne H.M. Borel Rinkes, MD, PhD
Department of Surgical Oncology
UMC Utrecht Cancer Center
Utrecht, the Netherlands

Menno A. Brink, MD, PhD
Department of Gastroenterology
Meander MC
Amersfoort, the Netherlands

Alexander Constantinides, MD
Department of Surgical Oncology,
UMC Utrecht Cancer Center,
Utrecht, the Netherlands

Paul J. van Diest, MD, PhD
Department of Pathology
UMC Utrecht
Utrecht, the Netherlands

Melika Djafarihamedani
Department of Surgical Oncology
UMC Utrecht Cancer Center
Utrecht, the Netherlands

Wijntje J. van Eden, MD, PhD
Department of Surgical Oncology
Netherlands Cancer Institute -
Antoni van Leeuwenhoek
Amsterdam, the Netherlands

Sjoerd G.Elias, MD, PhD
Julius Center for Health Sciences and
Primary Care
UMC Utrecht
Utrecht, the Netherlands

Remond J.A. Fijneman, PhD
Department of Pathology
Netherlands Cancer Institute -
Antoni van Leeuwenhoek
Amsterdam, the Netherlands

Peter Friedl, PhD
Institute for Molecular Life Sciences,
Department of Cell Biology,
Radboud University Medical Center,
Nijmegen, the Netherlands

Boris Galjart
Department of Surgical Oncology,
Erasmus MC Cancer Institute
Rotterdam, the Netherlands

Klaas M. Govaert, MD, PhD
Department of Surgical Oncology
UMC Utrecht Cancer Center
Utrecht, the Netherlands

Wilhelmina M.U. van Grevenstein, MD, PhD
Department of Surgical Oncology
UMC Utrecht Cancer Center
Utrecht, the Netherlands

Dirk J. Grünhagen, MD, PhD
Department of Surgical Oncology
Erasmus MC Cancer Institute
Rotterdam, the Netherlands

Jeroen Hagendoorn, MD, PhD
Department of Surgical Oncology
UMC Utrecht Cancer Center
Utrecht, the Netherlands

Richard van Hillegersberg, MD, PhD
Department of Surgical Oncology
UMC Utrecht Cancer Center
Utrecht, the Netherlands

Ignace H.J.T. de Hingh, MD, PhD
Department of Surgery
Catharina Ziekenhuis
Eindhoven, the Netherlands
GROW - School for Oncology and
Developmental Biology
Maastricht University
Maastricht, the Netherlands

Yvon C.W. Holierhoek
Department of Gastroenterology
Meander MC
Amersfoort, the Netherlands

Sander R. van Hooff
Center for Experimental Molecular
Medicine
Amsterdam UMC
Amsterdam, the Netherlands

Jennifer M.J. Jongen, MD, PhD
Department of Surgical Oncology
UMC Utrecht Cancer Center
Utrecht, the Netherlands

Niels F.M. Kok, MD, PhD
Department of Surgical Oncology
Netherlands Cancer Institute -
Antoni van Leeuwenhoek
Amsterdam, the Netherlands

Miriam Koopman, MD, PhD
Department of Medical Oncology
UMC Utrecht Cancer Center
Utrecht, the Netherlands

Geert J.P.L. Kops, PhD
Oncode Institute, Hubrecht Institute –
Royal Academy of Arts and Sciences
Utrecht, the Netherlands

Onno Kranenburg, PhD
Department of Surgical Oncology
UMC Utrecht Cancer Center
Utrecht, the Netherlands

Joyce van Kuik
Department of Pathology
UMC Utrecht
Utrecht, the Netherlands

Miangela M. Laclé, MD, PhD
Department of Pathology
UMC Utrecht
Utrecht, the Netherlands

Wendy W.J. de Leng, PhD
Department of Pathology
UMC Utrecht
Utrecht, the Netherlands

Martijn P. Lolkema, MD, PhD
Department of Medical Oncology
Erasmus MC Cancer Institute
Rotterdam, the Netherlands

Ron H.J. Mathijssen, MD, PhD
Department of Medical Oncology
Erasmus MC Cancer Institute
Rotterdam, the Netherlands

Jan Paul Medema, PhD
Center for Experimental Molecular Medicine
Amsterdam UMC
Amsterdam, the Netherlands

Eelco F.J. Meijer, MD, PhD
Department of Surgical Oncology
UMC Utrecht Cancer Center
Utrecht, the Netherlands

Mara Z. Meulendijks
Department of Surgical Oncology
UMC Utrecht Cancer Center
Utrecht, the Netherlands

Cathy B. Moelans, PhD
Department of Pathology
UMC Utrecht
Utrecht, the Netherlands

I. Quintus Molenaar, MD, PhD
Department of Surgical Oncology
UMC Utrecht Cancer Center
Utrecht, the Netherlands

Leon M.G. Moons, MD, PhD
Department of Gastroenterology
UMC Utrecht
Utrecht, the Netherlands

Maarten W. Nijkamp, MD, PhD
Department of Surgical Oncology
UMC Utrecht Cancer Center
Utrecht, the Netherlands

Niek A. Peters, MD
Department of Surgical Oncology
UMC Utrecht Cancer Center
Utrecht, the Netherlands

Daniëlle A.E. Raats
Department of Surgical Oncology
UMC Utrecht Cancer Center
Utrecht, the Netherlands

Koen P. Rovers, MD
Department of Surgery
Catharina Ziekenhuis
Eindhoven, the Netherlands

Joyce Sanders
Department of Pathology
Netherlands Cancer Institute - Antoni van Leeuwenhoek
Amsterdam, the Netherlands

Susanne J. van Schelven
Department of Surgical Oncology
UMC Utrecht Cancer Center
Utrecht, the Netherlands

Matthijs P. Schwartz, MD, PhD
Department of Gastroenterology
Meander MC
Amersfoort, the Netherlands

Petur Snaebjornsson, MD, PhD
Department of Pathology
Netherlands Cancer Institute -
Antoni van Leeuwenhoek
Amsterdam, the Netherlands

Anne Trinh, PhD
Department of Medical Oncology
Dana-Farber Cancer Institute
Boston, MA, United States of America

Kari Trumpi, MD, PhD
Department of Surgical Oncology
UMC Utrecht Cancer Center
Utrecht, the Netherlands

Cornelia Veelken, PhD
Institute for Molecular Life Sciences
Department of Cell Biology
Radboud University Medical Center
Nijmegen, the Netherlands

Thomas T. Vellinga, MD, PhD
Department of Surgical Oncology
UMC Utrecht Cancer Center
Utrecht, the Netherlands

André Verheem
Department of Surgical Oncology
UMC Utrecht Cancer Center
Utrecht, the Netherlands

Kirsten K.J. Verheij, MD
Department of Surgical Oncology
UMC Utrecht Cancer Center
Utrecht, the Netherlands

Paul M. Verheijen, MD, PhD
Department of Surgery
Meander MC
Amersfoort, the Netherlands

Cornelis Verhoef, MD, PhD
Department of Surgical Oncology
Erasmus MC Cancer Institute
Rotterdam, the Netherlands

Louis Vermeulen, MD, PhD
Center for Experimental Molecular
Medicine, Amsterdam UMC
Amsterdam, the Netherlands

Emma C.E. Wassenaar, MD
Department of Surgical Oncology
UMC Utrecht Cancer Center
Utrecht, the Netherlands

Roel A. de Weger, PhD
Department of Pathology
UMC Utrecht
Utrecht, the Netherlands

Jan Willem van Wijnbergen, MD
Department of Surgical Oncology
UMC Utrecht Cancer Center,
Utrecht, the Netherlands

ASSESSMENT COMMITTEE

Prof. dr. G.J.A. Offerhaus
Pathologist, Professor of Gastro-Intestinal Pathology
University Medical Center Utrecht, the Netherlands

Prof. dr. C. Verhoef
Surgeon, Professor of Surgical Oncology
Erasmus Medical Center, Rotterdam, the Netherlands

Prof. dr. M. Koopman
Medical oncologist, Professor of Medical Oncology - Colorectal Cancer
University Medical Center Utrecht, the Netherlands

Prof. dr. I.Q. Molenaar
Surgeon, Professor of Hepato-Pancreatico-Biliary Surgery
University Medical Center Utrecht, the Netherlands

Prof. dr. G.J.P.L. Kops
Professor of Molecular Tumor Cell Biology
University Medical Center Utrecht, the Netherlands
Hubrecht Institute, Utrecht, the Netherlands

LIST OF PUBLICATIONS

Ubink I, Bolhaqueiro ACF, Elias SG, Raats DAE, Constantinides A, Peters NA, Wassenaar ECE, de Hingh I, Rovers KP, van Grevenstein WMU, Lacle MM, Kops G, Borel Rinkes IHM, Kranenburg O. Organoids from colorectal peritoneal metastases as a platform for improving hyperthermic intraperitoneal chemotherapy. *Br J Surg*. 2019;**106**(10):1404-14.

Backes Y, Seerden TCJ, van Gestel R, Kranenburg O, **Ubink I**, Schiffelers RM, van Straten D, van der Capellen MS, van de Weerd S, de Leng WWJ, Siersema PD, Offerhaus GJA, Morsink FH, Ramphal W, Terhaar Sive Droste J, van Lent AUG, Geesing JMJ, Vleggaar FP, Elias SG, Lacle MM, Moons LMG. Tumor Seeding During Colonoscopy as a Possible Cause for Metachronous Colorectal Cancer. *Gastroenterology*. 2019;**157**(5):1222-32.e4.

van der Waals LM, Jongen JMJ, Elias SG, Veremiyenko K, Trumpi K, Trinh A, Laoukili J, **Ubink I**, Schenning-van Schelven SJ, van Diest PJ, Borel Rinkes IHM, Kranenburg O. Increased Levels of Oxidative Damage in Liver Metastases Compared with Corresponding Primary Colorectal Tumors: Association with Molecular Subtype and Prior Treatment. *Am J Pathol*. 2018;**188**(10):2369-77.

Ubink I, van Eden WJ, Snaebjornsson P, Kok NFM, van Kuik J, van Grevenstein WMU, Lacle MM, Sanders J, Fijneman RJA, Elias SG, Borel Rinkes IHM, Aalbers AGJ, Kranenburg O. Histopathological and molecular classification of colorectal cancer and corresponding peritoneal metastases. *Br J Surg*. 2018;**105**(2):e204-e11.

Vellinga TT, Kranenburg O, Frenkel N, **Ubink I**, Marvin D, Govaert K, van Schelven S, Hagendoorn J, Borel Rinkes IH. Lymphangiogenic Gene Expression Is Associated With Lymph Node Recurrence and Poor Prognosis After Partial Hepatectomy for Colorectal Liver Metastasis. *Ann Surg*. 2017;**266**(5):765-71.

Ubink I, Elias SG, Moelans CB, Lacle MM, van Grevenstein WMU, van Diest PJ, Borel Rinkes IHM, Kranenburg O. A Novel Diagnostic Tool for Selecting Patients With Mesenchymal-Type Colon Cancer Reveals Intratumor Subtype Heterogeneity. *J Natl Cancer Inst*. 2017;**109**(8).

Ubink I, Bloemendal HJ, Elias SG, Brink MA, Schwartz MP, Holierhoek YCW, Verheijen PM, Boerman AW, Mathijssen RHJ, de Leng WWJ, de Weger RA, van Grevenstein WMU, Koopman M, Lolkema MP, Kranenburg O, Borel Rinkes IHM. Imatinib treatment of poor prognosis mesenchymal-type primary colon cancer: a proof-of-concept study in the preoperative window period (ImPACCT). *BMC Cancer*. 2017;**17**(1):282.

Trumpi K, **Ubink I**, Trinh A, Djafarihamedani M, Jongen JM, Govaert KM, Elias SG, van Hooff SR, Medema JP, Lacle MM, Vermeulen L, Borel Rinkes IHM, Kranenburg O. Neoadjuvant chemotherapy affects molecular classification of colorectal tumors. *Oncogenesis*. 2017;**6**(7):e357.

Borovski T, Vellinga TT, Laoukili J, Santo EE, Fatrai S, van Schelven S, Verheem A, Marvin DL, **Ubink I**, Borel Rinkes IHM, Kranenburg O. Inhibition of RAF1 kinase activity restores apicobasal polarity and impairs tumour growth in human colorectal cancer. *Gut*. 2017;**66**(6):1106-15.

Ubink I, Verhaar ER, Kranenburg O, Goldschmeding R. A potential role for CCN2/CTGF in aggressive colorectal cancer. *J Cell Commun Signal*. 2016;**10**(3):223-7.

Ubink I, Jongen JMJ, Nijkamp MW, Meijer EFJ, Vellinga TT, van Hillegersberg R, Molenaar IQ, Borel Rinkes IHM, Hagendoorn J. Surgical and Oncologic Outcomes After Major Liver Surgery and Extended Hemihepatectomy for Colorectal Liver Metastases. *Clin Colorectal Cancer*. 2016;**15**(4):e193-e8.

Cirkel GA, Weeber F, Bins S, Gadellaa-van Hooijdonk CG, van Werkhoven E, Willems SM, van Stralen M, Veldhuis WB, **Ubink I**, Steeghs N, de Jonge MJ, Langenberg MH, Schellens JH, Sleijfer S, Lolkema MP, Voest EE. The time to progression ratio: a new individualized volumetric parameter for the early detection of clinical benefit of targeted therapies. *Ann Oncol*. 2016;**27**(8):1638-43.

van der Sluis PC, **Ubink I**, van der Horst S, Boonstra JJ, Voest EE, Ruurda JP, Borel Rinkes IH, Wiezer MJ, Schipper ME, Siersema PD, Los M, Lolkema MP, van Hillegersberg R. Safety, efficacy, and long-term follow-up evaluation of perioperative epirubicin, cisplatin, and capecitabine chemotherapy in esophageal resection for adenocarcinoma. *Ann Surg Oncol*. 2015;**22**(5):1555-63.

Hoogstraat M, Gadellaa-van Hooijdonk CG, **Ubink I**, Besselink NJ, Pieterse M, Veldhuis W, van Stralen M, Meijer EF, Willems SM, Hadders MA, Kuilman T, Krijgsman O, Peeper DS, Koudijs MJ, Cuppen E, Voest EE, Lolkema MP. Detailed imaging and genetic analysis reveal a secondary BRAF(L505H) resistance mutation and extensive intrapatient heterogeneity in metastatic BRAF mutant melanoma patients treated with vemurafenib. *Pigment Cell Melanoma Res*. 2015;**28**(3):318-23.

Fatrai S, van Schelven SJ, **Ubink I**, Govaert KM, Raats D, Koster J, Verheem A, Borel Rinkes IH, Kranenburg O. Maintenance of Clonogenic KIT(+) Human Colon Tumor Cells Requires Secretion of Stem Cell Factor by Differentiated Tumor Cells. *Gastroenterology*. 2015;**149**(3):692-704.

Ubink I, van der Sluis P, Schipper M, Reerink O, Voest E, Borel-Rinkes I, Wijrdeman H, Vleggaar F, Agterof M, Overkleeft E, Siersema P, van Hillegersberg R, Lolkema MP. Adding preoperative radiotherapy plus cetuximab to perioperative chemotherapy for resectable esophageal adenocarcinoma: a single-center prospective phase II trial. *Oncologist*. 2014;**19**(1):32-3.

ACKNOWLEDGEMENTS / DANKWOORD

In dit promotieonderzoek heb ik met veel toewijding gezocht naar nieuwe behandelstrategieën voor dikke darmkanker. Het begon met het bedenken en opzetten van de ImPACCT studie, gebaseerd op werk van voorgangers uit onze onderzoeksgroep. Gaandeweg leidden nieuwe ideeën en inzichten, evenals interessante samenwerkingen met collega's binnen en buiten het UMC Utrecht, tot dit bredere proefschrift over de identificatie, gerichte therapie en chirurgische behandeling van darmkanker met een slechte prognose. Aan het onderzoek en de totstandkoming van deze dissertatie hebben veel mensen bijgedragen. Veel dank aan alle co-auteurs voor hun bijdragen, en aan eenieder die mij heeft geholpen met experimenten of administratieve zaken. Dank ook aan iedereen die gedurende de afgelopen jaren interesse heeft getoond in mijn onderzoek, of die juist gezorgd heeft voor de nodige afleiding en ontspanning. Een aantal mensen wil ik in het bijzonder bedanken.

Prof. dr. Kranenburg, beste Onno, ik bewonder je tomeloze wetenschappelijke inspiratie. Eén foto van een invasieve organoïde en jij ziet gelijk een heel nieuw project voor je. Na onze wekelijkse besprekingen verliet ik je kamer steevast vol nieuwe ideeën en (meestal) goede moed. Veel dank voor de fijne samenwerking, de vrijheid die je me gegund hebt in de diverse projecten, en de kans om mijn promotietraject af te sluiten in Boston.

Prof. dr. Borel Rinkes, beste Inne, waar Onno steeds met nieuwe ideeën kwam, wist jij de nodige focus aan te brengen in mijn PhD traject en minder succesvolle projecten tijdig te schrappen. Je pikt uit elk project feilloos de essentie, en weet artikelen altijd aan te scherpen. Ook nu mijn promotietijd erop zit kan ik bij je terecht voor carrière advies. Hartelijk dank voor de goede gesprekken en je wijze raad.

Dr. Elias, beste Sjoerd, we begonnen samen aan de ontwikkeling van een CMS4 test, en vanaf dat moment ben je bij alle projecten nauw betrokken gebleven. Maar je had niet alleen aandacht voor de statistiek, je had ook oog voor mijn persoonlijke ontwikkeling en mijn gemoedstoestand, waarvoor dank.

Dr. Hagendoorn, beste Jeroen, bedankt voor je begeleiding bij de artikelen uit de leverdatabase, en voor de goede tips voor Boston. Jouw ambitie om een chirurgische carrière te combineren met basaal wetenschappelijk onderzoek is inspirerend.

Geachte leden van de lees- en promotiecommissie, prof. dr. Offerhaus, prof. dr. Verhoef, prof. dr. Koopman, prof. dr. Molenaar, prof. dr. Kops en dr. van Grevenstein, hartelijk dank voor uw tijd om mijn proefschrift te beoordelen, en om zitting te nemen in de oppositie.

Dr. Lolkema, beste Martijn, tijdens de SUMMA opleiding liet jij me kennis maken met alle facetten van oncologisch onderzoek. Ik heb mee mogen werken aan mooie klinische, translationele en basale lab-projecten, welke resulteerden in mijn eerste publicaties. Toen mijn hart bij de chirurgie bleek te liggen, heb jij me, ondanks je aanvankelijk teleurstelling, ook hierbij op weg geholpen.

Dr. Naxerova, dear Kamila, thank you for the warm welcome to Boston and the excellent introduction to cancer genomics. Your love for science and your drive to unravel cancer evolution are truly inspiring.

Laboratory of Translational Oncology, to all previous and current members, I would like to thank you all for your help with experiments, for your knowledge and the work discussions, but mostly for the great atmosphere and the good times we shared both within and outside the lab.
Kari en Thomas, bedankt dat ik aan mocht haken bij jullie mooie projecten, die nu ook deel uitmaken van dit proefschrift. Emma, dank voor je inbreng in de projecten over peritoneale metastasen en voor de goede tijd in Boston. Emre, bedankt voor je inzet als student, mooi om te zien dat je nu als PhD kandidaat in onze groep je eigen veelbelovende projecten hebt.

ImPACCT studie team, aan iedereen die betrokken was bij de opzet en uitvoering van dit onderzoek in het Meander MC en het UMC Utrecht, veel dank voor jullie inzet. In het bijzonder Haiko Bloemendal en Yvon Holierhoek, zonder jullie was de studie nooit van de grond gekomen. Niek en Alexander, waarde opvolgers, ik weet dat jullie er alles aan gedaan hebben om de studie vol te krijgen maar het mocht niet zo zijn. Aan de studiedeelnemers, bedankt voor het vertrouwen in ons onderzoek.

Chirurgen en arts-assistenten in het Jeroen Bosch Ziekenhuis en het UMC Utrecht, dank voor de leerzame en gezellige tijd!

Jeroen, we hebben vaak van gedachten gewisseld over mijn onderzoek en wetenschap in het algemeen. Je wist me te motiveren als ik het doel van mijn projecten even niet meer inzag. Dank voor je betrokkenheid.

Lieve Nicola, we hebben veel gedeeld in ons kantoortje G02.626; onderzoeksfrustraties, onverwachte resultaten (e.g. unicorn phenomena), toekomstplannen, en meer. Ik vind het heel bijzonder dat je tijdens de verdediging naast me staat.

Lieve Frank, grote broer, ik ben zo trots dat jij mijn andere paranimf bent. Onze (wetenschappelijke) interesses en onze opvattingen komen niet altijd overeen, maar ondanks deze verschillen is het altijd fijn om elkaar te zien en kunnen we op elkaar bouwen.

Lieve pap en mam, jullie steun en trots zijn voor mij onmisbaar. Ik ben jullie enorm dankbaar voor de ruimte en ondersteuning die jullie me gaven om te studeren, te reizen en alles te doen wat ik leuk vond. Ongeacht hoe ver of hoe lang ik weg ben geweest (Middelburg, Utrecht, Chili, Uppsala, Boston…), bij jullie is het altijd weer heerlijk thuiskomen.

CURRICULUM VITAE AUCTORIS

Inge Ubink (June 9, 1988) grew up in Ter Aar. In 2006, she graduated *cum laude* from Gymnasium and moved to Middelburg to start her academic career at Roosevelt Academy. Within the Liberal Arts & Sciences program, she discovered her enthusiasm for biomedical research and medicine, and focused on courses in the premedical track. She obtained her Bachelor of Science degree *summa cum laude* in 2009, and continued her studies with the Selective Utrecht Medical Master (SUMMA) program at Utrecht University, to become a medical doctor and clinical researcher. Her major research internship performed at the Center for Personalized Cancer Therapy (CPCT) focused on intratumor heterogeneity and dynamics of response to targeted therapy in melanoma, under supervision of prof. dr. Voest, dr. Lolkema and dr. Cirkel.

To prepare for her PhD project, she studied the fundamentals of PDGFR signaling during an extracurricular internship at the Ludwig Institute in Uppsala, Sweden, under guidance of prof. dr. Heldin and dr. Lennartsson. After having graduated *cum laude* from SUMMA in 2014, she started as a PhD student within the Laboratory of Translational Oncology, supervised by prof. dr. Borel Rinkes and prof. dr. Kranenburg. During the final months of her PhD period, she worked at Massachusetts General Hospital in Boston, U.S.A., to contribute to the Tumor Phylogenetics Consortium led by dr. Naxerova.

Inge has started her clinical career in 2019 as a surgical resident not in training, first at Jeroen Bosch Ziekenhuis, and currently at University Medical Center Utrecht.